FACTORS THAT INFLUENCE END ZONE CRACKING IN PRE-TENSIONED PRESTRESSED CONCRETE BRIDGE BEAMS – A FINITE ELEMENT ANALYSIS

By

GORAN RADINOVIC

Bachelor of Science in Civil Engineering
University of Oklahoma
Norman, Oklahoma
2004

Master of Science in Civil Engineering
University of Oklahoma
Norman, Oklahoma
2010

Submitted to the Faculty of the
Graduate College of the
Oklahoma State University
in partial fulfillment of
the requirements for
the Degree of
MASTER OF SCIENCE
May, 2021

FACTORS THAT INFLUENCE END ZONE

CRACKING IN PRE-TENSIONED PRESTRESSED

CONCRETE BRIDGE BEAMS – A FINITE ELEMENT

ANALYSIS

Thesis Approved:

Dr. Bruce W. Russell

Thesis Adviser

Dr. Mohamed Soliman

Dr. Robert N. Emerson

ACKNOWLEDGEMENTS

Special thank you for the work accomplished goes to my advisor and instructor Dr. Bruce Russell, without whom no work would be accomplished. No work is perfect, but Dr. Russell made it better and more complete than I could ever do it on my own.

Special respect and appreciation to all of my instructors in the School of Civil Engineering at the Oklahoma State. I admire the brave hearts, bright souls and friendly hands of you all, even in the times of doubts and challenges.

I dedicate this work to friends and family.

Name: GORAN RADINOVIC

Date of Degree: MAY, 2021

Title of Study: FACTORS THAT INFLUENCE END ZONE CRACKING IN PRE-TENSIONED PRESTRESSED CONCRETE BRIDGE BEAMS – A FINITE ELEMENT ANALYSIS

Major Field: CIVIL ENGINEERING

Abstract: The basic problem studied as part of this master's thesis work consists of two main parts.
The first part investigates the incidence of cracking in end regions and potential methods and means to help mitigate the incidence of cracking through changes in prestress force and eccentricity. Previous experimental testing revealed that cracking in the regions may come from a number of different causes, some of which may be more studied and better understood than the others. Under loading, failures in end regions of prestressed concrete beams generally occur due to combinations of shear and bond failure. Interaction with flexural cracking is also observed. Historically the interpretation of these failures has been confused. Based on the past experience, a number of variables used in the design and study of prestressed concrete beams may affect the end regions of beams when the prestressing is initially applied as well as during the loading of the beams.

The second part uses finite elements analysis (FEA) to examine results from experimental testing programs, and uses FEA to help develop rational design methods to help prevent shear failures in the end regions of precast/prestressed beams. Beams developed through experimental testing programs described in John Jacob (1998) thesis work from the University of Oklahoma, Norman, and Amol Ganpatye (2006) thesis work from the Oklahoma State University, Stillwater, are selected to be analyzed with FEA. Commercially available software FEA package called ANSYS 17.0 contains suitable finite elements or block elements that are used to analyze stresses in the concrete after applying prestressing forces at the ends of the prestressed concrete beams that mimic the transfer of prestressing forces into the concrete. FEA model is used to observe the behavior in the end regions of beams by comparing and contrasting changes in the potential flexural, shear and bond stresses in the beam as the number of variables is modified.

This research paper describes the methods and means to help mitigate cracking and addresses potential gaps or limitations in the existing knowledge and current design practices, and provides the results of the linear elastic static finite elements analysis. It is believed that this work will provide summary of the current state-of-the-art and point direction for future studies and research.

TABLE OF CONTENTS

LIST OF TABLES

Table Page

LIST OF FIGURES

Figure Page

Figure Page

Figure Page

Figure Page

Figure Page

Figure Page

Figure Page

Figure Page

Figure Page

Figure Page

CHAPTER I

INTRODUCTION

This research paper presents the results from finite element analyses in end regions, and FEA testing regions of pre-tensioned, prestressed concrete bridge beams. Research variables included the (a) size of prestressing strands, (b) the bond quality of prestressing strands as represented by the ASTM A1081 Standard Tests for Bond, (c) the effects of changing eccentricity by adding fully tensioned top strands and (d) the effects of reducing prestressing forces in end regions through the use of shielded or debonding of a small percentage of prestressing forces, where the modeling approach uses finite element model of the concrete beam with the prestressing force applied in the nodes representing transfer zone of the prestressing strands. Reasonable agreement with the experimental testing program demonstrates advantage and practicality of the finite element model with respect to the cost and efficiency in obtaining results for prestressed concrete beams.

The finite element model was constructed for a 24-inch deep I-shaped 3/8 scale AASHTO Type IV beam with a composite deck. The beam model having same geometry was already tested previously through the experimental destructive testing and was described in papers by Jacob (1998) and Ganpatye (2006) and further analyzed in the paper by Tanasap (2015). Number of variables were examined through the experimental testing by Jacob (1998) and Ganpatye (2006). Jacob's work consisted on obtaining the experimental results for each end of four (4) experimentally tested beam specimens, giving the number of tests with different variables to

eight (8). Ganpatye's work consisted in experimentally testing eight (8) beams with each end of the beam tested, resulting in fifteen (15) ends being tested. One beam end was damaged during transportation.

Experimental program results by John Jacob and Ganpatye were used to validate the FEA model addressed in this thesis paper, or in other words, the finite element analysis results were validated by comparing FEA results with the results of the experimental testing. With the FEA modeling, a total of thirty-five (35) results for different prestressing variables was obtained. These results were then compared to one another to determine the effect of changing different prestressing variables.

The goal of the study was accomplished by obtaining sufficient sample size of thirty-five (35) that provided reasonable model results for comparisons for different prestressing variables.

CHAPTER II

BACKGROUND AND LITERATURE REVIEW

Cracking in the end regions of pre-tensioned prestressed bridge beams was addressed by numerous authors from the academia, transportation agencies and the industry.

Field of knowledge in this area is rapidly increasing, and some of the most recent articles are addressed here, with the most notable being by Hasenkamp et al. (2008), Oliva and Okumus (2011), Hasenkamp et al. (2012), Okumus, Oliva & Becker (2012), Okumus and Oliva (2013), Ross et al (2014), Okumus and Oliva (2014), Arab et al. (2014), Okumus et al. (2016), and Steinberg and Semendary (2017). In addition, significant research has historically been done in part by the academia at the Oklahoma State and University of Oklahoma and reported in the graduate research papers by Jacob (1998), Tessema (2000), Chandran (2001), Ganpatye (2006), Jayaseelan (2007), Tanasap (2015) and Mayhorn (2016). In his paper Tessema (2000) discusses the effect of high strength concrete on the bondability of prestressing strands and summarizes the state-of-the-art through the literature review. His finding was that the current code equations governing the bond of strand have been shown to be inaccurate, that the bond test was needed that would help to determine the effects of bond variations, and that concrete strength would affect bond of prestressing strand. Chandran (2001) continues on the topic and continues discussing assessing of the bond quality of prestressing strands using North American Strand Producer's (NASP) bond test and relating the results to the prototype prestressed concrete beams.

Jayaseelan (2007) researches prestress losses in concrete and long-term deflections and camber in prestressed concrete bridges. According to her findings, excessive cracking can reduce bridge's durability, since cracking can be a route for water borne contaminants to cause deterioration of concrete and reinforcement. Her recommendations consisted in adding top presteressing strands and mild steel in prestressed concrete beams to lower the long-term losses and camber and using the proposed AASHTO Time Step method to determine the losses for the prediction of prestress losses and camber and deflections. Tanasap (2015) investigated the effects of additional horizontal web shear reinforcement on shear capacity of the specimens from Jacob's (1998) research by focusing on the shear modulus using shear-stress, shear-strain diagrams and transformations of strains. Mayhorn (2016) continued the discussion of the effects of the water and water borne contaminants by investigating the effects of cracking and end region deterioration in the presteressed concrete bridge girders.

Other authors like Kannel et al. (1997) are known for using linear finite element analysis to investigate debonding strands and changing the order of strand cutting to control cracking at the base of the web and inclined and vertical cracks on the sides of the bottom flange. Burgueño and Sun (2011) used nonlinear finite element analysis to study strand debonding by considering localized damage around the strands. It is also correctly summarized in Okumus and Oliva (2013) that the crack control method investigated and used most commonly by other authors involved adjustments to the end-zone reinforcement patterns, and that recommendations on the design of the end-zone reinforcement cross-sectional area and spacing were developed based on experimental or linear analytical studies.

Hasenkamp et al. (2008) address sources of end zone cracking of prestressed bridge girders with the objectives of establishing procedures for acceptance, repair or rejection of girders with

longitudinal web cracking, and of preparing the user's manual for the application of these procedures. As some of the sources of cracking these authors specify the method of detensioning, release of the top strand or draped strands before the bottom straight strands, order of release of bottom strands with the flame cutting method, length of the free strand in the prestressing bed, lifting of the precast member from the bed, use of 0.6-inch strand and strand distribution. Hasenkamp et al. (2012) continue with further and in more detail addressing the proposed evaluation and repair procedures for prestressed concrete bridge girders with end zone cracking. It was found by Okumus et al. (2016) after further research that the length and width of the end zone cracks depended primarily on the beam depth and the amount of the prestressing force.

2.1 Oliva and Okumus (2011)

As part of the Wisconsin Highway Research Program, Oliva and Okumus (2011) performed nonlinear finite element analysis of deep wide-flanged pre-stressed girders to understand and control end cracking. Finite element analysis utilizing commercially available finite element software Abaqus/CAE was the main method of investigation. The finite element analysis was preferred because full stress and strain field can be obtained on the entire girder end region. The finite element results were verified using the data gathered through experimental testing. Strains were monitored in two girders manufactured by County Materials Corp. during and after prestress release, and these results were used to validate the finite element models. The available literature was also searched for the data to be used for comparison. The results of the experimental testing performed at the University of Texas, Austin as described in O'Callaghan (2008) were also used to validate and evaluate the accuracy of the finite element models.

The main goal of the research was looking for solutions that would control cracking which occurs during or after prestress release in the end zones of deep wide flanged prestressed girders. For the research, Oliva and Okumus (2011) explain that all deep wide flange girders exhibit similar types of cracking. The deepest Wisconsin standard wide flange girders 54W, 72W and 82W experience were reported the most severe cracking, with number of cracks and the crack widths larger for deeper girders and girders with heavier prestressing.

This study was performed to evaluate the impact of changes to the end zone reinforcement, debonding some strands at the girder end, debonding with the in the end zone reinforcement, modifications to the strand cutting order, removing, spreading or lowering the draped strands and coping the top flange of the girders.

Debonding of the strands at the end of the girder was found to lower the stresses transferred to the concrete at the end and controlling all crack types. Debonding of the certain number of bottom flange strands was also found to remove the need for the draped strands, and to completely eliminate the inclined cracking problem. It was found that the number of horizontal web cracks and the size of the cracks can be reduced significantly by debonding, and that for shallower 54W girders 50% debonding could eliminate web cracks, while 25 to 35% debonding can reduce the web strains approximately by 50 to 70%. It appears that the most important finding of the project was that methodically selected debonding could reduce or eliminate the hazardous Y cracking strains, where the strand layout in the bottom flange plays an important role in Y crack formation. Debonded strands at the end should be as close to the exterior face as possible, which would reduce resultant eccentricity of the strands along the width of the bottom flange. This debonded strand pattern would prevent the locations of concentrated compression, that is, debonded strands should be uniformly distributed along the width of the bottom flange.

When possible, the columns of debonded strands should not be adjacent to one another. In addition to these findings, when a girder was analyzed with debonded strands at the girder end with increased size vertical reinforcement bars, the result was a superposed reduction in strains. It was found that increasing the size of the first two pairs of bars from the end was very effective in reducing the web strains, while methodically debonding 35% of the strands, virtually eliminated inclined cracks, and Y strains strains and reduced the web strains on 54W girders. An alternative recommended was to change the first two pairs of bars at the girder end to #10 bars while debonding 35% of the strands at the girder end.

2.2 Okumus, Oliva and Becker (2012)

Linear and nonlinear finite element analysis was used by Okumus, Oliva and Becker (2012) to study the causes of cracks in Wisconsin bridge girders. The model was verified with the experimental data and used to analyze the girder end zone. It was found that using a first order tetrahedral finite element and 2010 FIB model code gave more accurate results.

2.3 Okumus and Oliva (2013)

In their PCI article on evaluation of crack control methods for end zone cracking in prestressed concrete bridge girders, Okumus and Oliva (2013) discuss deep bulb-tee girders exhibiting cracking near the ends during prestress release. From their experience, the cracking is reported to look more severe in deeper sections with slender webs and large amount of prestress. Girder cracks are further reported not to be random, but to exhibit characteristic pattern, among them those studied in the paper on a 54 in. deep bulb-tee girder, and cracks are classified as horizontal

web cracks, inclined cracks with similar widths to web cracks and bottom flange Y cracks (Figure 2.1). The article further talks about the multiple horizontal cracks occurring in the web due to the eccentricity of the strands over the depth of the girder, and the often-longest inclined cracks occurring near the top flange around the draped strands and initiated by tensile strains created by the draped strands. These two types of cracks are expected to close under service loading and are thought to be caused by the strand distribution in the girder or the prestress release procedures. On the other hand, so called Y- or T-shaped cracks formed at the intersection of the web and the bottom flange and propagated down through the bottom flange. Y- or T-shaped cracks are not expected to close under the service loads. The fourth type of cracks, consisting of vertical transverse cracks across the bottom flanges in plane perpendicular to the girder axis and often result of end restraint during prestress transfer, was not observed in girders examined by authors and was not further studied by Okumus and Oliva (2013).

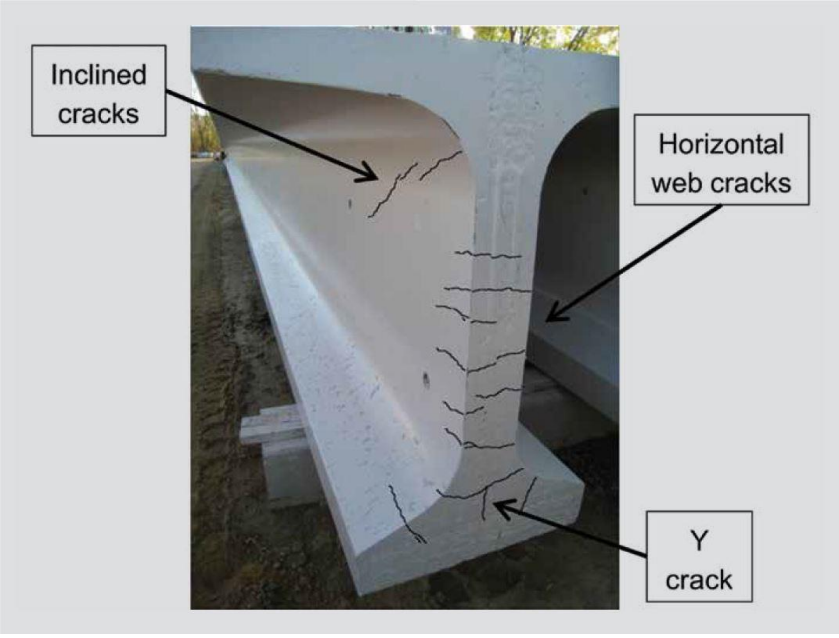

Figure 2.1. Typical Cracking Pattern and Crack Types (Okumus and Oliva, 2013)

The paper by Okumus and Oliva (2013) investigated the following crack control methods: varying the order in which the strands were cut, modifying the draped strand pattern, changing the end zone reinforcement pattern, strand debonding, and varying the locations of the lifting hoops.

The crack control methods were investigated on a standard 54 in. deep flanged bulb-tee girder that was taken as a standard comparison basis. The girder was 129 ft long girder design from a bridge, and examined for cracks immediately after fabrication and exhibited all three types of cracks described previously.

Based on their nonlinear finite element analysis verified by test data, the most effective crack control methods consist in debonding the strands at the ends, locating the lift loops a distance equal to girder depth from each end, and releasing the strands beginning with the innermost ones. Only a quarter of the girder was modeled using symmetry along the girder length and walls. Only the region within the distance equal to the girder depth from the end of the girder was modeled as the nonlinear concrete material. The pretensioned girder end zones were analyzed by finite element analysis once the method was verified by comparison with experimental or test data. The accuracy of the model was achieved by incorporating the nonlinear properties of concrete and redistribution of strains after cracking into the material model. Plasticity model was used which is adequate for simulating the nonlinear behavior of concrete in compression and tension under monotonic loading. The material properties for the plastic range of the stress-strain relationship for concrete under compression, and for stress-crack opening relationship for concrete under tension were defined using the International Federation for Structural Concrete Model Code 2010. For model behavior when the concrete strains were linearly elastic, the modulus of elasticity was determined using the AASHTO LRFD Bridge Design Specifications.

The reinforcing bars were modeled as linearly elastic with the modulus of elasticity given by the AASHTO LRFD specifications.

The only load applied to the girder was the prestressing force, since the goal was to investigate the cracks formed soon after the prestress release. As explained by the authors, the initial prestressing force was applied on the concrete by excluding the strands from the model and applying a surface stress to the concrete along the strand surface over the transfer length which was taken as 60 times strand diameter, with strand stresses assumed to vary linearly, and the bond stresses assumed to be uniform as per AASHTO LRFD specification.

The finite element model was having a dense mesh at the girder end where stress accuracy was important, and the mesh size was gradually increased away from the girder end. Concrete elements in the linear regions, nonlinear regions and reinforcing bar elements were all discretized with four-node tetrahedral, six-node triangular prism, and two-node truss elements.

Based on the research summarized in this research paper, debonding strands at the girder ends was highly recommended for all types of cracks, especially for the more critical Y cracks. The innermost strands of the bottom flange should be fully bonded and the remaining bonded strands should be evenly distributed across the bottom flange. 25% debonding was shown through finite element modeling to be adequate to prevent Y cracking and inclined cracking in a girder, while the complete elimination of web cracks required 50% debonding, which is higher than the AASHTO limit, and was only recommended if the shear capacity is sufficient. Debonding all strands within 12 inches from the ends was also highly recommended to control the web and Y cracking. The effects on shear capacity should also be checked.

2.4 Ross et al (2014)

This paper by Ross et al. (2014) describes the research on four detailing schemes for controlling end region cracking in 63 in. deep Florida I-beams. Detailing schemes included end standard reinforcement per AASHTO LRFD Specifications, large-diameter end reinforcement, vertical end-region posttensioning and partial debonding of 45% of the number of strands. Crack locations, lengths and widths of the cracks in the detailed beams were monitored during the prestress transfer and for several months after the prestress transfer, and crack data were mutually compared to determine the effectiveness of each of these detailing schemes in controlling appearance of web cracks. As described, the beams were then loaded to ultimate capacity to determine influence of each detailing scheme on the ultimate capacity of the beam. It was found that all of the three modified detailing schemes had the reduced web cracking when compared to the standard detail based on AASHTO LRFD Specifications.

It was found that end region reinforcement as per AASHTO LRFD Specifications was the least effective scheme in preventing cracks, even though it limited web cracks to the maximum width of 0.008 in. Strand debonding was found to effective method in controlling web-splitting cracks; however, the effect of strand debonding on bond-shear behavior and service load cracks would have to be considered. Increasing the area of vertical reinforcement in the end regions was found to be effective in controlling the cracks, and this detailing scheme was recommended by the authors in cases where web-splitting resistance is desired beyond the minimum provided in the AASHTO Code. Vertical posttensioning helped with preventing the horizontal cracks in the end surface but made worse the inclined cracks in the web, with the authors concluding that this detailing scheme needs more research.

2.5 Okumus and Oliva (2014)

In their paper about using strand debonding to control end cracking in pretensioned bridge girders, Okumus and Oliva (2014) further researched impacts of strand debonding on cracking in end regions by using nonlinear finite element analysis with analysis including plastic behavior of concrete and observations in plants producing prestressed members. FEA was done for 54 in., 72 in. and 82 in. deep prestressed bulb tee Wisconsin wide flange girders with 25%, 35% and 50% of the strands debonded at the girder end region. The tensile strains were used to determine if cracking would occur.

Based on the results of the nonlinear finite element methods, concrete tension strains that could cause cracking in the critical locations could be completely eliminated if 25% debonding was applied. Other cracks or strains associated with cracking could be significantly reduced with 25-35% debonding or eliminated with 50% debonding. The selection of the strands to be debonded was found to be important and to affect cracking significantly. It was also found that choosing the pattern of strand debonding, so that the interior strands remained bonded, reduced the strains causing the Y cracking.

The model was verified by comparing the predicted strains from the FEA with the measured strain data available in the literature. 124 microstrains theoretical concrete cracking strain as used in the AASHTO LRFD Bridge Design Specifications was used to distinguish in the model between the cases where cracking occurred or did not occur.

It was found by the after further research that the length and width of the end zone cracks depended primarily on the beam depth and the amount of the prestressing force.

2.6 Arab et al. (2014)

Nonlinear finite element methods were used by Arab et al. (2014) to understand the behavior of the end zone in prestressed deep girders. Finite element model was calibrated using the experimental data from testing 100 in. deep and 210 ft. long girders. Stresses in the mid-height of the girder were shown to be within the allowable limit of the AASHTO LRFD Bridge Design Specification (2012), but the tensile stresses in the web reinforcement and the bottom flange to web interface were higher than the allowable stresses by 85%. Arab et al. (2014) concluded that vertical reinforcement is needed to control the width of these cracks.

2.7 Okumus et al. (2016)

In this study, Okumus et al. (2016) looked at different reasons of crack growth in the end regions after detensioning. Using the fully-coupled thermal-mechanical analyses with non-linear concrete properties, as potential reasons these authors studied differential cooling, creep and shrinkage of bulb-tee cross sections shown in Figure 2.2. Analytical calculations as well as the available test data were used to validate the thermal-mechanical model. It was determined that the shrinkage strains were the primary cause for the increase in the crack width and length following the detensioning procedure, whereas temperature changes from curing and creep had favorable and negligible effect on concrete strains.

Figure 2.2. Bulb Tee Cross Sections Studied by Okumus et al. (2016)

2.8 Steinberg and Semendary (2017)

As described in Steinberg and Semendary (2017), in order to understand the behavior and cracking of the end zone of modified 84 in. deep Type 4 bridge I-girders, three dimensional linear and nonlinear finite element models were developed using the ABAQUS/CAE commercial software. The cross-section of the beam was modeled using ABAQUS/CAE and extended to the mid-span of the girder because the girder is symmetrical. The strands were provided in the model to be represented as in the actual girder, and web reinforcement was also provided as in actual girder. For linear finite element model, researchers used Young's Modulus for normal weight concrete as defined in equation from ACI 318-11 and Poisson's Ratio of 0.2 for concrete properties in the elastic range, with the concrete compressive strength defined as 6 ksi. For strands, modulus of elasticity used was 28,500 ksi and Poisson's Ratio was 0.3. For reinforcement, which consisted of welded wires, 70 ksi yield strength was used with the modulus of elasticity of 29,000 ksi, in accordance with AASHTO LRFD Bridge Design Specifications.

The prestressing force of 44 kips was used for each strand, with stress assumed to vary linearly along the transfer length, with transfer length taken as 60 strand diameters. As to the interactions and boundary conditions, the interaction between concrete and reinforcement, as well as between the concrete and the strands was modeled as an embedded constraint, with strands and reinforcement modeled as embedment, non-host elements, while the girder itself was modeled as the host element, with prevented slip between concrete and reinforcement. The vertical movement at one end was restrained, while the girder was free to rotate and deflect in all other directions. The mesh size used was 3 in. mesh with the four node linear tetrahedral elements to model the concrete. For the model of reinforcement and strands, two node linear three dimensional trusses were used. Based on the findings of the linear model, the linear finite element model created using the ABAQUS/CAE was giving the inconsistent results compared with the field observations. The maximum principal tensile stresses were more accurate in predicting cracks, while the maximum principal tensile strains didn't give such good predictions of crack locations.

Nonlinear finite element model verification was performed using a 70 in. deep girder having 48 prestressed strands tested and monitored with strain gauges by O'Callaghan and Bayrak as described in O'Callaghan and Bayrak (2008) at the University of Texas in Austin, Texas. Each strand was prestressed to a force of 43 kips, and concrete strength was 6.7 ksi. For the nonlinear finite element model, the elastic behavior was defined with the Poisson's Ratio and the modulus of elasticity for the concrete, reinforcement and strands, while the inelastic range behavior was defined using the concrete damage plasticity (CDP) model. CDP model had various parameters such as the dilation angle of 31º, flow potential eccentricity (ε) of 0.1, compressive stress ratio of 1.16, stress invariant ratio (k) of 0.667, and viscosity parameter which was equal to zero. For

concrete in compression, modified Hognestad stress-strain curve was used to define the concrete, while the concrete in compression was assumed to be linear elastic until it reached 40% of its compressive strength, after which Hognestad stress-strain curve was used. Tensile stress versus strain curve is linear until cracking. After cracking of reinforced concrete, there would be significant loss in tensile strength but the tensile strength would not fall down to zero. The Vecchio and Collins (1981) model was selected for concrete in tension in nonlinear finite element model because it did not have any analysis convergence issues. Further, as described in the paper, half of the girder was modeled, and the girder was divided in two regions, so that one region up to a distance of 70 in. from the end of the beam was nonlinear and cracking was expected in this region, while the remainder of the girder was considered as a linear region.

The results demonstrated the accuracy of the input parameters. After the non-linear finite element model was verified with the test data available from literature and showed the accuracy of the parameters, the results of the nonlinear finite element analysis were obtained which allowed the prediction of the cracking pattern and locations based on the strains and the stresses in the reinforcement. One of the findings was that the girder had an insignificant effect in lowering the amount of inclined cracking. Among other findings was that the changes in the end reinforcement details based on the new ODOT (Ohio Department of Transportation) Standards relative to the old drawings have improved the end cracking performance of prestressed concrete I-girders. The values of the maximum principal tensile strain were calculated to be significantly less for the new Standards when compared to the old Standards. The new ODOT Standard is now in agreement with the AASHTO LRFD Bridge Design Specifications for the end zone reinforcement. Based on the finite element models the new standard detail resulted in stress

levels lower than 16.5 ksi, while based on the old ODOT design detail model gave stresses of 40 ksi, which was significantly over 20 ksi AASHTO limit.

As the goal for the future, Steinberg and Semendary (2017) explain the need to compare the finite element model results with experimental data by using the instrumentation of the end zones to help better understand the behavior after cracking, as well as using other methods for controlling the cracking in the end zone and to compare them with the standard design.

2.9 Current Practice to Reduce Cracking in End Regions

As described in the PCI Design Handbook for Precast and Prestressed Concrete (2010) by Precast/Prestressed Concrete Institute, the common practice is for primarily economic reasons to use all straight strands, rather than depressing at midspan or at 0.4ℓ from each end. Straight strand patterns are known to cause excessive end release stresses. For these reasons and to improve camber control, producers of precast members may choose to debond some of the strands in the end regions. This is also called shielding, because debonding is usually performed using the plastic tube or shield over the strand to prevent it from bonding to the concrete, even though grease can be used as well.

Some engineers feel that debonding should be avoided whenever possible to maintain the capacity of the member, whereas other engineers place emphasis on the cracking that un-debonded strands may cause in the end regions, which may lead to ingress of water and salts through the cracks and cause deterioration of steel and bond between steel and concrete, and thus also cause the loss of the capacity. Design of the end regions of prestressed members is thus still in many ways a balancing act.

Debonding normally reduces prestress force and can reduce eccentricity.

The following guidelines for debonding are recommended by the PCI (2010):

- Do not debond all strands in the bottom row.
- Stagger debonding at transfer length increments along the length of the component.
- Do not debond more than 50% of the strands below a dapped end.
- Avoid debonding adjacent strands.
- Provide vertical reinforcement (welded wire reinforcement, stirrups, or bearing plate anchorage) at least equal to minimum shear reinforcement in the debonded area.

In addition, here are some of the additional known rules-of-thumb for debonding known in the design industry and academia:

- Do not debond more than 1/3 of the total strands.
- Do not debond more than 2/5 of one row of strands.
- Debond in pairs.

Of interest are currently the standard details used by the Oklahoma Department of Transportation (ODOT), with an example design of 54 in. deep, 100 ft. span, Type IV prestressed concrete beam shown in Figure 2.3. As may be seen from the Figure 2.3, the design uses straight strands with four of the bottom 0.6 in. diameter strands being debonded. Section 503 of the ODOT Specifications (2009) deals with the prestressed concrete bridge members. Based on the findings of this thesis paper, the standard details may be improved by varying the strand size and debonding procedures to better address cracking in the end regions.

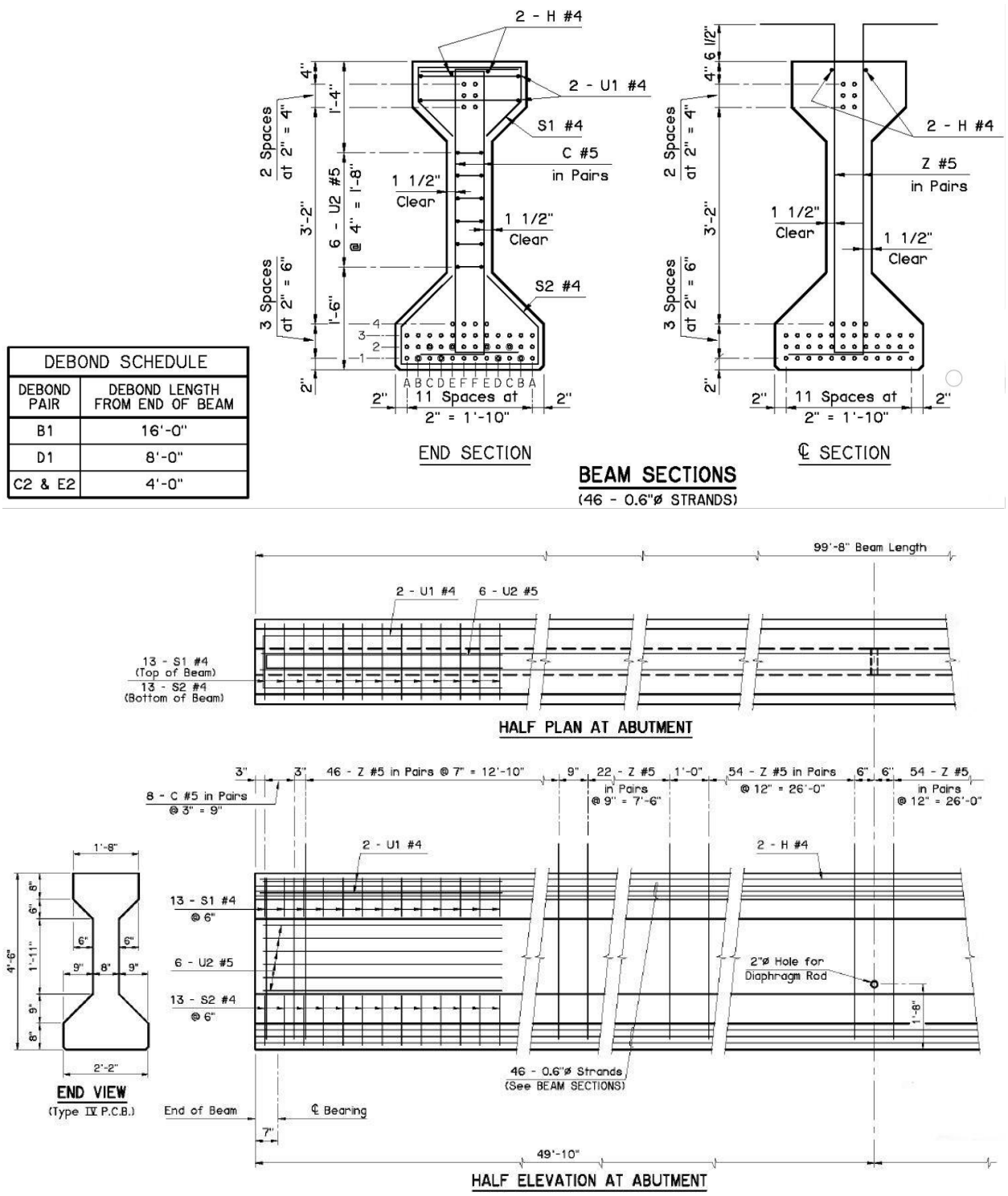

Figure 2.3. Type IV Prestressed Concrete Beam (100 ft. Span) Details by Oklahoma Department of Transportation (2009)

In addition to debonding, AASHTO LRFD Bridge Design Specifications specify that reinforcement should confine the prestressing steel at the ends of the beam; however, fitting the reinforcement into the beam webs and flanges has been shown to be an issue. This procedure has not successfully prevented visible girder end cracks to form in the end regions.

In addition to FEA, other methods have been used to research problem of cracking in the end regions, such as empirical methods, linear analytical, simplified analytical and strut-and-tie methods.

2.10 John Jacob (1998)

Based on John Jacob, the major objective of his research was to determine the effects from the inclusion of horizontal mild steel reinforcement placed within the web in the end-regions of thin webbed prestressed concrete members and compare the effects of horizontal steel with the effect of variations in the amount of vertical shear steel.

As described in his work, John Jacob is providing test results from eight tests for four approximately 3/8 scale AASHTO Type IV prestressed concrete bridge I-beams. Beams were 24-foot long and had a deck cast monolithically as part of the I-beam. Each beam was pretensioned with five 0.5-inch diameter, LOLAX seven wire prestressing strands. In each beam, four strands were placed in the so-called bottom bulb of the beam and the fifth one was placed as fully-tensioned top strand at 22 inches from beam bottom. Five of the eight tests had horizontal mild steel reinforcing within the webs, with the total areas ranging from 0.44 in^2 to 1.24 in^2. Stirrup spacing was also used as a variable. The geometry and components of the beams were set in such a way to ensure that the section would crack in web shear before flexural failure would occur.

Tables provided below provide the summary of data from experimental testing program.

Table 2.1. John Jacob (1998) I-Beam Data Summary

Beam End	Stirrups and Bulb Reinforcement	Horizontal Steel (Longitudinal and Transverse)	1-Day (RLS) Concrete Strength (psi)	Test Day Concrete Strength (psi)
JJ1 North	External hoops @ 6" o.c., 64" from end; Single mesh of reinforcement w/ all cross wires intact	LONG - Deck: (2) #3; Web: No bars; TRANS - Deck: #3 @ 9" c/c	9500	11475
JJ1 South	Single mesh of reinforcement w/ all cross wires intact	LONG - Deck: (2) #3 ; Web Hor: 96" (4) #4 bars; TRANS - Deck: #3 @ 9" c/c	9500	11550
JJ2 North	External hoops @ 6" o.c., 64" from end; Single mesh of reinforcement w/ all cross wires intact	LONG - Deck: (2) #3; Web: 96" (4) #3 bars; TRANS - Deck: #3 @ 9" c/c	8700	11480
JJ2 South		LONG - Deck: (2) #3; Web: 96" (4) #5 bars; TRANS - Deck: #3 @ 9" c/c	8700	11500
JJ3 North	External hoops @ 6" o.c., 64" from end; Single mesh of reinforcement w/ every 3rd cross wire removed	LONG - Deck: (2) #3; Web: No bars; TRANS - Deck: #3 @ 9" c/c	7950	11750
JJ3 South		LONG - Deck: (2) #3; Web: 96" (3) #4 bars + 96" (1) #3 bar; TRANS - Deck: #3 @ 9" c/c	7950	12050
JJ4 North	External hoops @ 6" o.c., 64" from end; (2) meshes of reinforcement w/ every 3rd cross wire removed in each	LONG - Deck: (2) #3; Web: No bars; TRANS - Deck: #3 @ 9" c/c	7950	12400
JJ4 South		LONG - Deck: (2) #3; Web: 96" (3) #4 bars + 96" (1) #3 bar; TRANS - Deck: #3 @ 9" c/c	7950	11680

In the Table 2.2 provided below top strand is Strand A and is 22 inches from beam bottom, middle strand (located in the upper part of bulb) is Strand B and is 4 inches from beam bottom, and Strands C, D and E are bottom strands (located in the lower part of the bulb) and are 2 inches from beam bottom.

Table 2.2. John Jacob (1998) I-Beam Data Summary (Continued)

Beam End	Load (kips) & (End Slip (in)) when Web-Cracking First Occurred	Shear Force V_{cr} when Web-Cracking First Occurred (kips)	Deflection Immediately Prior to Web-Shear Cracking (in)	Load (kips) & (End Slip (in)) when Flexural-Cracking First Occurred	Deflection Immediately Prior to Flexural Cracking (in)	Computed Capacity Against Cracking V_{cw} (kips)
JJ1 North	68.0 (0.015 bottom strands)	43.5	0.26	65.0 (no measured slip)	0.20	41.08
JJ1 South	65.2 (no measured slip)	42.3	0.31	59.6 (no measured slip)	0.20	40.91
JJ2 North	53.1 (0.010 strand C)	40.0	0.22	53.1 (0.010 strand C)	0.22	40.85
JJ2 South	60.1 (no measured slip)	35.4	0.22	60.1 (no measured slip)	0.22	40.74
JJ3 North	55.2 (0.228 strand B, 0.0184 strand C, 0.0218 strand D, 0.0155 strand E)	40.0	0.18	No crack (no measured slip)	No crack	41.33
JJ3 South	60.0 (no measured slip)	37.0	0.21	60.0 (no measured slip)	0.21	40.90
JJ4 North	55.9 (no measured slip)	43.4	0.22	No crack (no measured slip)	No crack	40.74
JJ4 South	65.1 (no measured slip)	38.7	0.26	60.1 (no measured slip)	0.20	41.49

Term V_{cw} shown in the Table 2.2 is the nominal shear strength provided by concrete when diagonal cracking results from excessive principal tensile stress in the web. V_{cw} values were computed based on the Mohr's Circle shown in Figure 2.4.

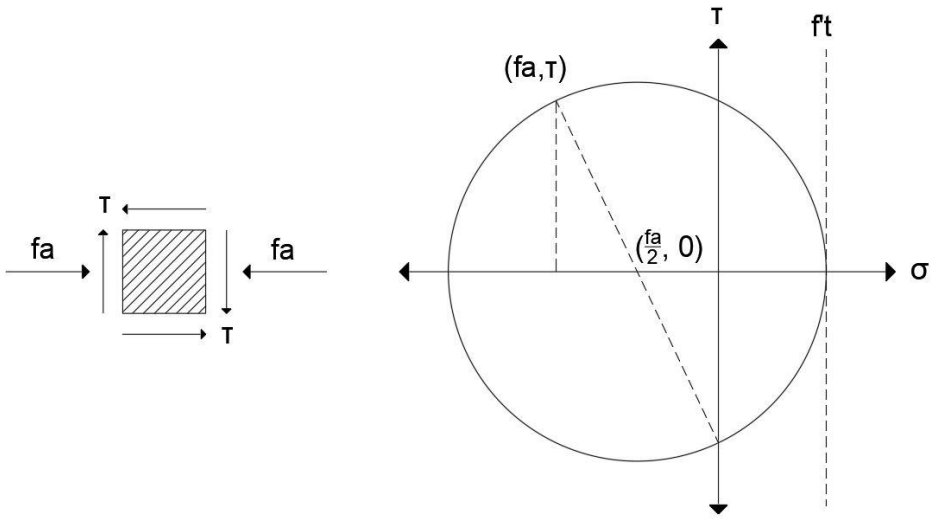

Figure 2.4. Stress Element at Neutral Axis (NA) and Mohr's Circle for Prestressed Concrete

$f_a=F_{se}/A$ is resulting from prestressing where F_{se} is prestress (lbf) and A is beam cross sectional area (163.25 sq.in.). As the Mohr's circle becomes larger, v_{cr} increases in accordance with the following equation $v_{cr} = ft' \left[1 + \frac{fa}{ft'}\right]^{1/2}$, where v_{cr} is shear stress at which cracking occurs. This equation is used to determine v_{cr} (theoretical) For non-prestressed elements cracking occurs when $\tau \geq f_t' \approx 4\sqrt{fc'}$, where f_c' is the compressive concrete strength at testing. v_{cr} (testing) is calculated using the general shear formula $\tau = \frac{VQ}{Ib}$ where Q is equal to 658.25 in^3 and b (web thickness) is equal to 3 inches. Table 2.2 shows the results for the cracking shear, both theoretical and as estimated during testing.

As provided in John Jacob's (1998) work, Figure 2.5 shows the John Jacob's loading setup and deflection and slip measurement configuration for each of the beam ends, meaning it is applicable for both JJ North and JJ South beam ends.

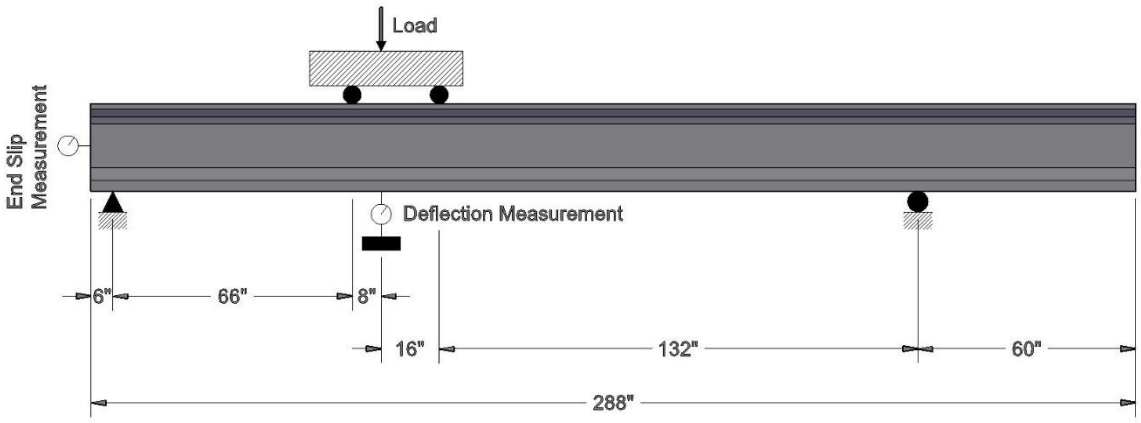

Figure 2.5. Loading Setup and Deflection and Slip Measurement Configuration for All JJ Beams and Ganpatye North End Beams (John Jacob, 1998)

Table 2.3. John Jacob (1998) I-Beam Data Summary (Continued)

Beam End	Transfer at Prestress Release (in)	Transfer at Time Close to Testing (in)	Reported End Slips at Higher than Cracking Loads (in)	Failure Type as Described After Testing
JJ1 North	23.47	30.55	Not reported	Shear / Bond
JJ1 South	21.40	37.40	0.02-0.03 inch end slips at 64.88 kips (deflection less than 1.11 inches)	Bond
JJ2 North	23.03	30.27	Not reported	Bond
JJ2 South	20.33	31.67	B=0.08-in & C,D,E=0.04-in at 69.5 kips (deflection less than 0.55 inches)	Flexure
JJ3 North	21.80	36.56	Not reported	Shear / Bond
JJ3 South	23.90	39.42	B=0.137-in, C=0.0041-in, D=0.0077-in & E=0.0050-in at 63 kips (deflection = 0.282 inches)	Shear
JJ4 North	28.80	44.14	B=0.02-in, C=0.02-in, D=0.03-in & E=0.02-in at 58.4 kips (deflection less than 0.45 inches)	Shear / Bond
JJ4 South	18.42	31.90	B=0.0116-in while other strand slips	Flexure

			negligible at 68 kips (deflection = 0.339 inches)	

Together with Ganpatye's (2006) work, Jacobs's results and data were used to in part validate FEA results described in this thesis work. Our purpose in Jacob's work was to determine whether this FEA adequately predicted V_{cw}, cracking shear force, and overall beam deflections (prior to cracking).

Example of JJ3 North beam end test by Jacob (1998) with shear-bond failure and poorly distributed web cracking occurring without horizontal shear reinforcement is shown in Figure 2.6. One large crack is seen where the shear deformations were not resisted by horizontal web reinforcement.

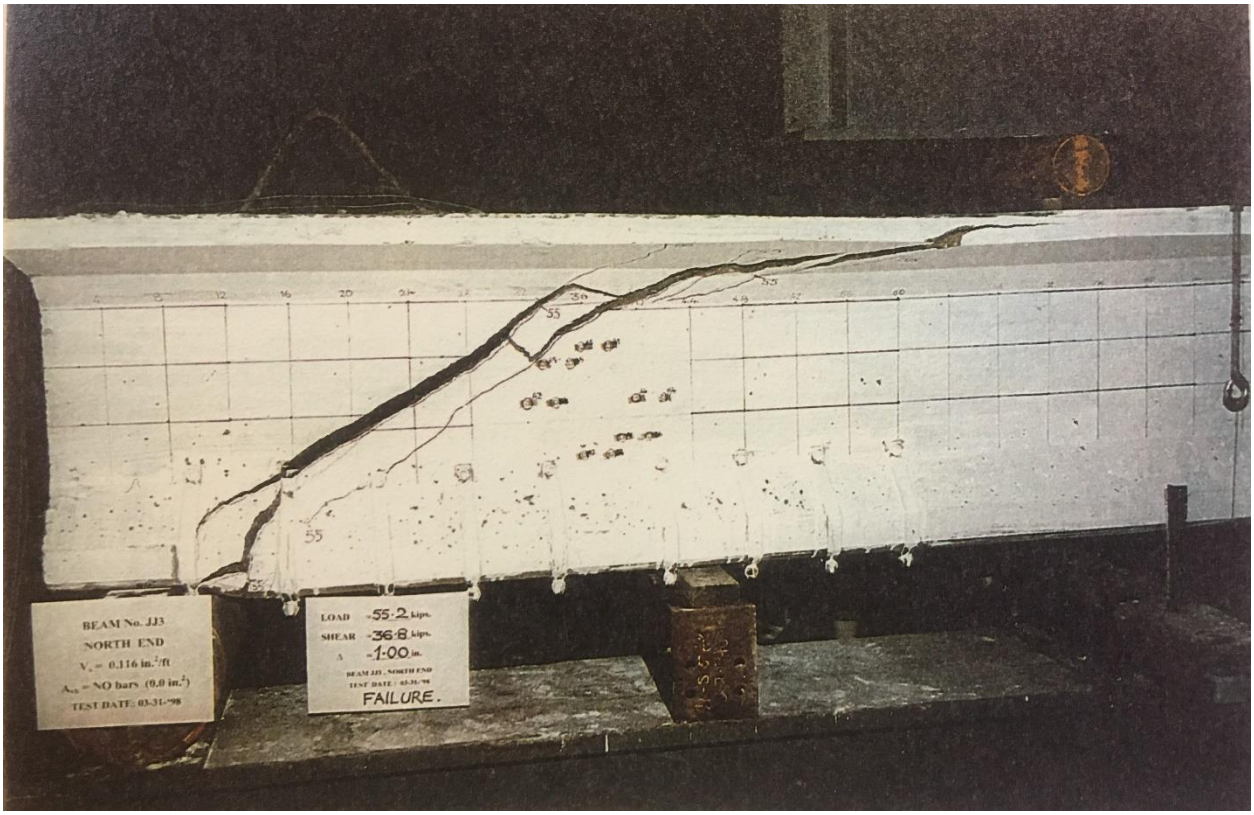

Figure 2.6. JJ3 North Beam End After Testing from Jacob (1998)

Example of JJ3 South beam end test by Jacob (1998) with shear failure and well distributed web cracking occurring with horizontal shear reinforcement is shown in Figure 2.7. One larger crack with multiple smaller cracks is seen where the shear deformations were resisted by horizontal web reinforcement.

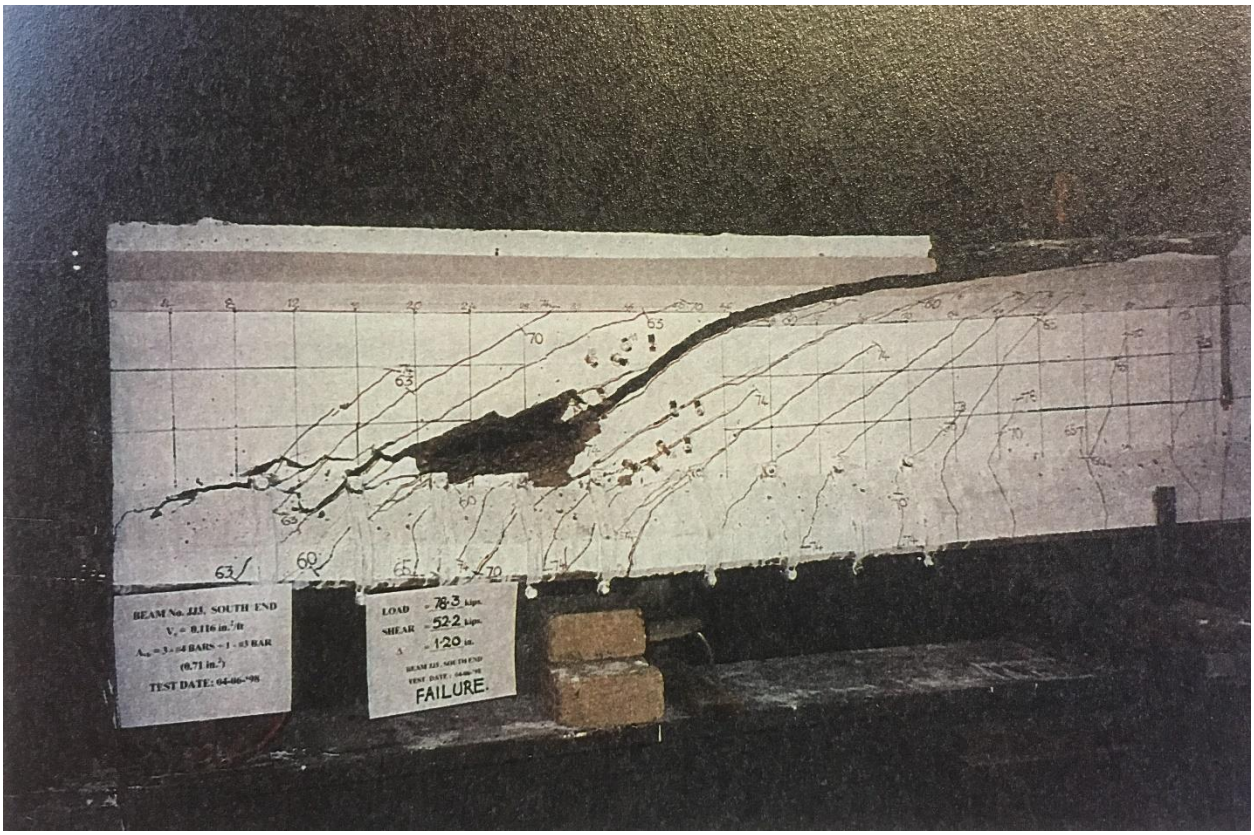

Figure 2.7. JJ3 South Beam End After Testing from Jacob (1998)

The difference that horizontal mild steel can make is also shown in the plots provided in Figures 2.8 and 2.9. At the same time it may be seen from the plots that the first cracking shear is not that much different based on mild steel reinforcement, being approximately 37 kips in both cases of JJ3 North and JJ3 South beam ends.

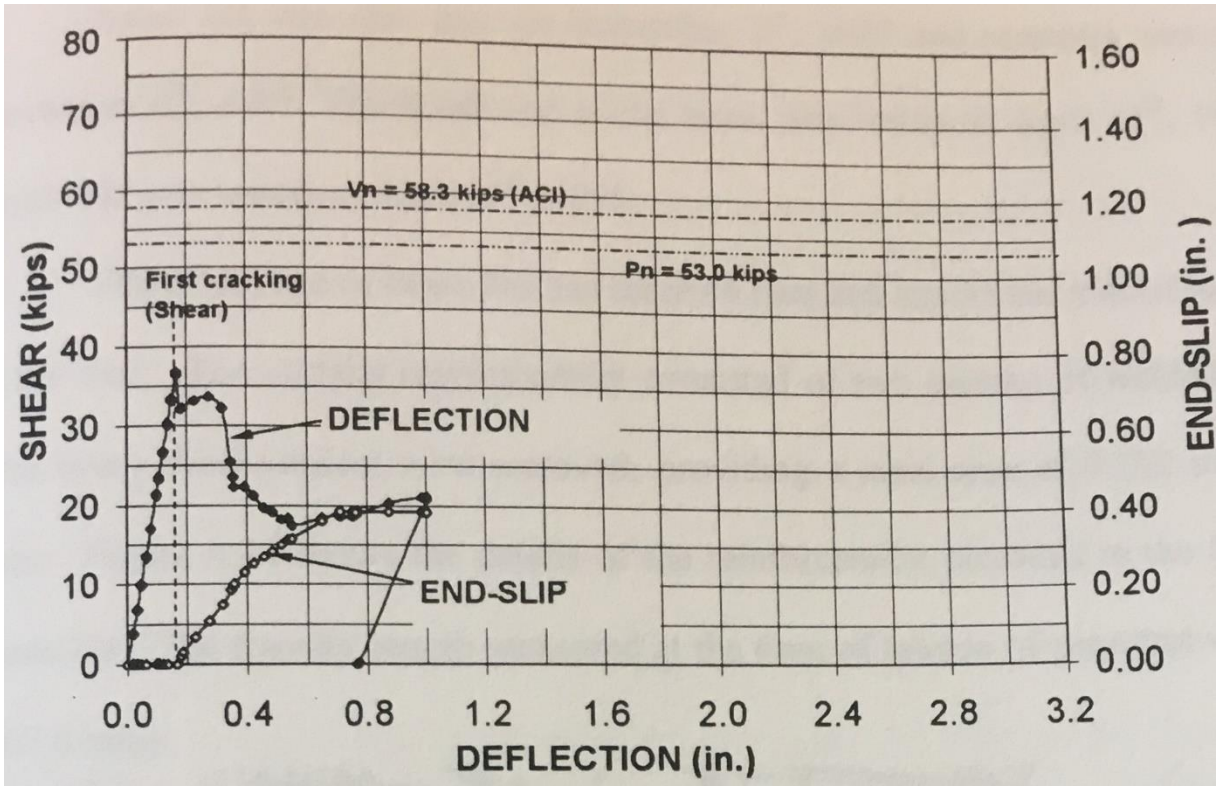

Figure 2.8. Plot Showing Variation of Shear, Deflection and Strand End-Slip for North End of Beam JJ3 without Horizontal Web Reinforcement by Jacob (1998)

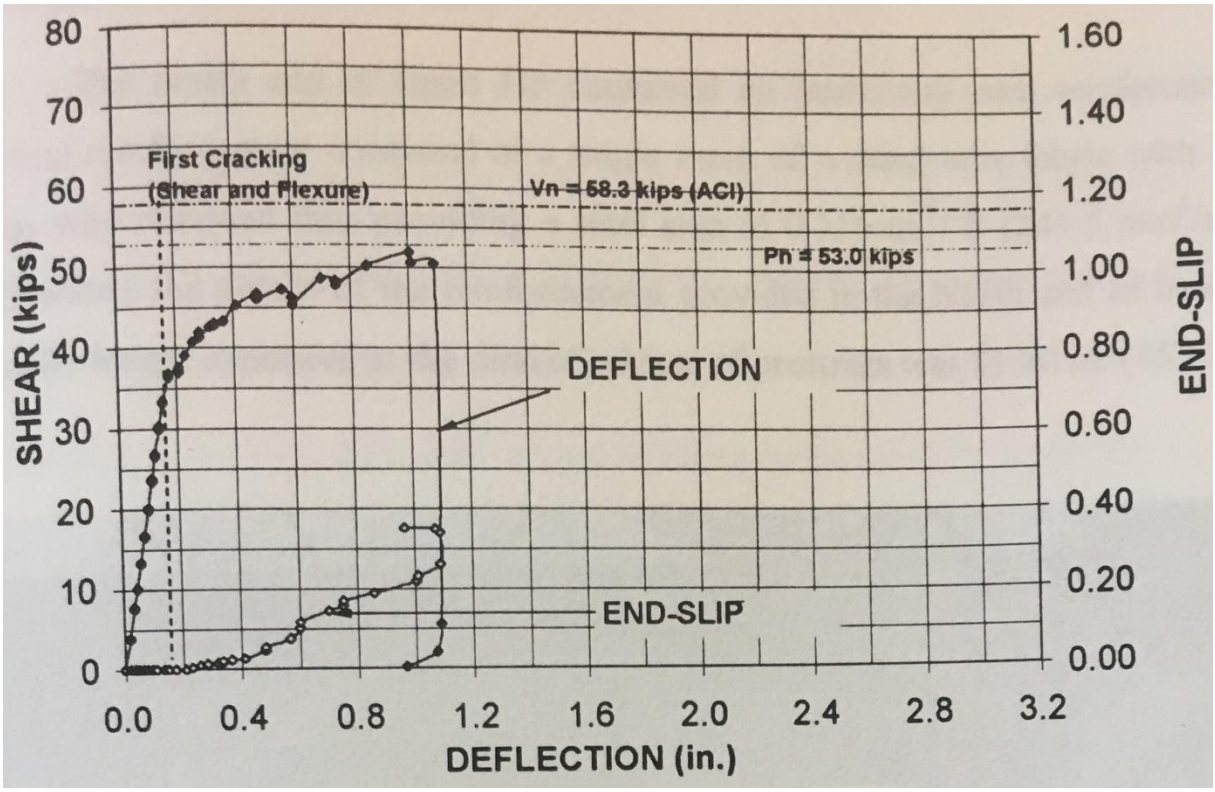

Figure 2.9. Plot Showing Variation of Shear, Deflection and Strand End-Slip for South End of Beam JJ3 with Horizontal Web Reinforcement by Jacob (1998)

2.11 Amol Ganpatye (2006)

Based on Ganpatye (2006) the major purpose of his research project was examining the influence of concrete strength on development lengths of prestressing strands obtained from various sources and having various NASP pull-out strengths, in concrete elements having various compressive strengths. From the obtained flexural test results an attempt was made for introducing the factor of concrete strength in the ACI and AASHTO equations for development length. Another objective of the research was to compare the results from the NASP bond test with the experimental values of development lengths for different strands and suggest minimum

NASP pull-out strengths for adequate anchorage of prestressing strands. All of Ganpatye's I-beams contained horizontal shear reinforcement.

As part of Ganpatye's work he tested the same I-shaped cross section as Jacob (1998). As addressed in Ganpatye (2006), all eight I-beam specimens representing AASHTO Type girders described by John Jacob (1998), were fabricated with goal or target concrete strengths at release ranging from 6,000 psi to 10,000 psi. Four beam specimens consisting of 0.5-inch diameter strands had five strands (one top strand A and four strands B, C, D and E in the bulb), while beam specimens consisting of 0.6-inch diameter strands had 4 strands (one top strand A and three bottom strands C, D and E in the bulb).

For clarification, the nomenclature followed by Ganpatye for naming of the beam ends was as follows: first character in the name is letter "I" to signify I-shaped beam; second character indicating stand source is either one of letters A, B or D for 0.5-inch diameter strands or letter A for 0.6-inch diameter strands; third character is nominal concrete strength number value at release being any one of 4, 6, 8 or 10 ksi; fourth character is the number 5 or 6 where 5 stands for 0.5-inch diameter strands, and 6 stands for 0.6-inch diameter strands; fifth character is the specimen number; and sixth character is the letter indicating North or South tested end of the beams. Beam end IA-6-6-2-S was not addressed in Ganpatye (2006) because it was damaged while handling it after the construction.

Tables provided below provide the summary of data from experimental testing program.

Table 2.4. Amol Ganpatye (2006) I-Beam Data Summary

Beam End	Prestressing Strands	Stirrups and Bulb Reinforcement	Horizontal Steel (Longitudinal and Transverse)	Concrete Strength (psi) at Release	56-Day Concrete Strength (psi)
IB-6-5-1-N	(5) 0.5-inch diameter strands, (4) in	72" #3 bar bulb cage & Stirrups #3 @7" o.c.	LONG - Deck: (2) #3; Web: 96" (4)	5810	9350
IB-6-5-1-S				5810	9350
IB-10-5-1-N				7615	13490

IB-10-5-1-S	bulb, (1) top @ 18" from bottom	alternating orientation	#4; TRANS - Deck: #3 @ 9" c/c	7615	13490
ID-6-5-1-N				5492	9840
ID-6-5-1-S				5492	9840
ID-10-5-1-N				8225	14160
ID-10-5-1-S				8225	14160
IA-6-6-1-N	(4) 0.6 dia. Strands, (3) in bulb, (1) top @ 18" from bottom			4381	8990
IA-6-6-1-S				4381	8990
IA-6-6-2-N				4381	8990
IA-10-6-1-N				10480	14990
IA-10-6-1-S				10480	14990
IA-10-6-2-N				10590	14930
IA-10-6-2-S				10590	14930

For illustrative purposes, locations of I-beam reinforcement including the 72” long bulb beam end reinforcement from the experimental program described by Ganpatye (2006) are illustrated for the ½ beam span shown in Figure 2.10.

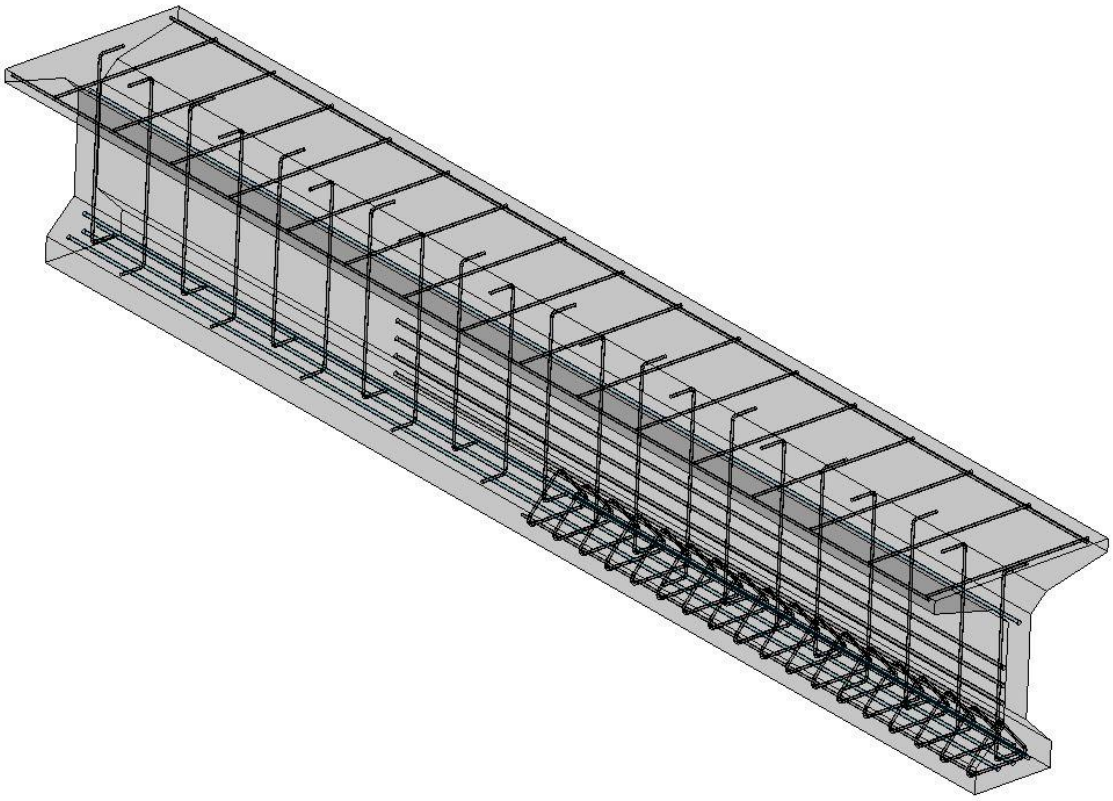

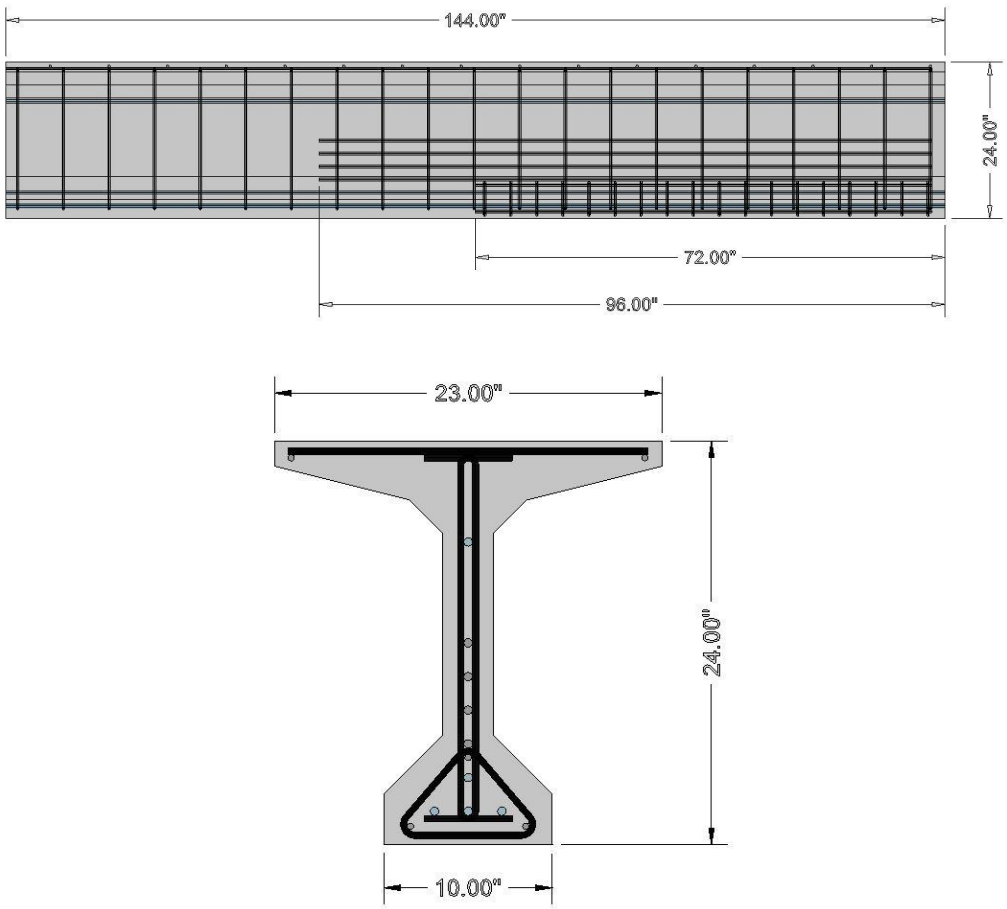

Figure 2.10. Illustration of Reinforcement and Strand Locations from Experimental Program by Ganpatye (2006)

Table 2.5. Amol Ganpatye (2006) I-Beam Data Summary (Continued)

Beam End	Load (kips) & (End Slip (in)) when Web-Cracking First Occurred	Shear Force V_{cr} when Web-Cracking First Occurred (kips)	Deflection Immediately Prior to Web-Shear Cracking (in)	Load (kips) & (End Slip (in)) when Flexural-Cracking First Occurred	Deflection Immediately Prior to Flexural Cracking (in)	Computed Capacity Against Cracking V_{cw} (kips)
IB-6-5-1-N	76.7 (no measured slip)	44.3	0.37	69.1 (no measured slip)	0.34	37.64
IB-6-5-1-S	61.2 (no measured slip)	40.8	0.34	54.1 (no measured slip)	0.26	37.64

IB-10-5-1-N	77.2 (no measured slip)	51.5	0.30	77.2 (no measured slip)	0.30	42.63
IB-10-5-1-S	81.0 (no measured slip)	54.0	0.38	77.5 (no measured slip)	0.33	42.63
ID-6-5-1-N	52.4 (no measured slip)	34.9	0.35	49.0 (no measured slip)	0.30	38.29
ID-6-5-1-S	48.6 (0.01 bottom)	32.4	0.85	41.7 (no measured slip)	0.58	35.68
ID-10-5-1-N	54.6 (no measured slip)	36.4	1.20	48.7 (no measured slip)	0.85	40.58
ID-10-5-1-S	66.3 (0.01 bottom)	44.2	0.48	56.3 (no measured slip)	0.30	43.35
IA-6-6-1-N	66.3 (no measured slip)	33.15	0.33	73.3 (no measured slip)	0.38	21.38
IA-6-6-1-S	79.0 (no measured slip)	39.5	0.70	64.6 (no measured slip)	0.40	31.21
IA-6-6-2-N	44.0 (no measured slip)	29.3	0.50	44.0 (no measured slip)	0.50	35.11
IA-10-6-1-N	85.2 (no measured slip)	54.8	0.35	85.2 (no measured slip)	0.35	27.61
IA-10-6-1-S	81.6 (no measured slip)	54.4	0.58	65.7 (no measured slip)	0.33	27.61
IA-10-6-2-N	55.7 (no measured slip)	37.1	0.63	64.9 (no measured slip)	0.80	45.74
IA-10-6-2-S	73.0 (no measured slip)	48.7	1.20	51.4 (no measured slip)	0.35	37.76

Term V_{cw} shown in the Table 2.5 is the nominal shear strength provided by concrete when diagonal cracking results from excessive principal tensile stress in the web. V_{cw} values were computed as previously described for Jacob (1998).

Figure 2.11 shows the Ganpatye's loading setup and deflection and slip measurement configuration for the South beam ends. Ganpatye's North beam ends are loaded the same way as the John Jacob's North and South beam ends.

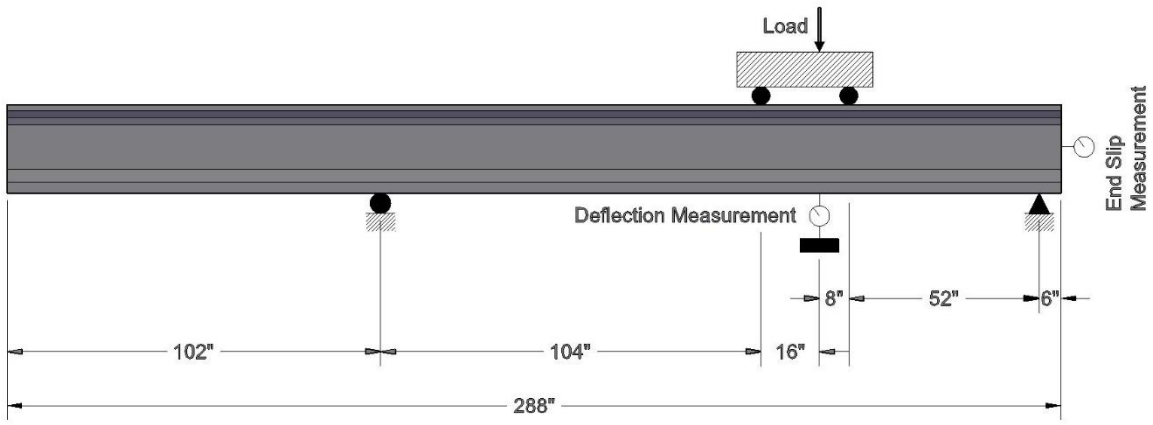

Figure 2.11. Loading Setup and Deflection and Slip Measurement Configuration for Ganpatye (2006) South Beam Ends

Transfers in Table 2.6 are listed in order from top strand (Strand A) to bottom strands (Strands B, C, D, E). For clarification, where it is being specified as 'No failure' by the researcher in the table, failure type was specified based on the researcher's overall visual condition assessment of beam overall exterior geometry after the testing rather than based on the quantitative maximum load and response data during the testing. All beams were tested to their ultimate capacities.

Table 2.6. Amol Ganpatye (2006) I-Beam Data Summary (Continued)

Beam End	Transfers at Prestress Release (in)	Transfers at Time Close to Testing (in)	Reported End Slips at Higher than Cracking Loads (in)	Failure Type as Described After Testing

IB-6-5-1-N	21.43, 16, 16.12, 10.93, 17.82	35.90, 22.63, 21.23, 14.30, 23.76	Bottom 0.01-in end slip at 101.8 kips (deflection 0.7 inches)	No failure
IB-6-5-1-S	6.16, 6.48, 6.42, 9.45, 2.90	23.04, 14.35, 13.11, 16.19, 3.69	Bottom 0.01-in end slip at 85.2 kips (deflection 1.4 inches)	Flexure
IB-10-5-1-N	0, 11.31, 11.14, 11.60, 10.03	23.31, 15.73, 15.73, 24.02, 19.54	Bottom 0.01-in end slip at 113.6 kips (deflection 0.8 inches)	No failure
IB-10-5-1-S	0, 9.90, 12.45, 12.45, 5.80	21.70, 11.59, 30.14, 10.25, 14.26	0-in end slip throughout	No failure
ID-6-5-1-N	36.25, 28.96, 24.47, 26.69, 23.47	73.10, 36.99, 35.34, 55.05, 32.71	Bottom 0.01-in end slip at 54.2 kips (deflection 0.38 inches)	Bond
ID-6-5-1-S	29.99, 11.04, 12.23, NA, 2.56	68.63, 26.67, 46.22, NA, 9.10	Not reported	Bond
ID-10-5-1-N	NA, 23.51, 19.03, 15.99, 23.51	NA, 41.86, 29.63, 38.93, 40.40	0.01-in end slip at 55.4 kips at middle strand (deflection 1.3 inches)	No failure
ID-10-5-1-S	16.86, 23.94, 19.03, 21.13, 23.61	35.81, 53.04, 22.84, 57.00, 30.73	Not applicable	Bond
IA-6-6-1-N	22.84, 0, 18.36, 20.15. 29.83	NA, NA, NA, NA, NA	Bottom 0.01-in end slip at 82.1 kips (deflection 0.48 inches)	Shear failure at opposite end
IA-6-6-1-S	9.36, 0, 16.33, 20.15, 22.21	30.70, 0, 36.72, 0, 0	Bottom 0.01-in end slip at 83.5 kips (deflection 0.8 inches)	Flexure
IA-6-6-2-N	20.22, 0, 9.62, 22.58, 15.48	NA, 0, 27.10, 35.72, 29.95	Bottom 0.01-in end slip at 58.5 kips (deflection 1.1 inches)	Shear
IA-10-6-1-N	0	0	Bottom 0.01-in end slip at 100.9 kips	Shear failure at opposite end

			(deflection 0.45 inches)	
IA-10-6-1-S	0	0	Bottom 0.01-in end slip at 92.7 kips (deflection 0.9 inches)	Strand fracture
IA-10-6-2-N	21.43, 16.00, 16.20, 10.93, 17.82	23.43, 0, 22.51, 50.43, 20.53	Arrangement to prevent end slip	Shear failure at opposite end
IA-10-6-2-S	6.16, 6.48, 6.42, 9.45, 2.90	19.36, 0, 10.64, NA, NA	0-in end slip throughout	No failure

Together with Jacob's (1998) work, Ganpatye's results and data were used to in part validate FEA results described in this thesis work. Our purpose in Ganpatye's work was to determine whether this FEA adequately predicted V_{cw}, cracking shear force, and overall beam deflections (prior to cracking).

CHAPTER III

CONSTRUCTION OF AND VALIDATION OF THE FINITE ELEMENT ANALYSIS

ANSYS® Academic simulation software was used as the finite element program. The software used for this FEA is called ANSYS Workbench Release 17.0 available from ANSYS, Inc. and made available through the Oklahoma State University. Static Structural analysis tool from ANSYS Workbench consisted of inputs such as engineering data, beam geometry, material properties and loading geometry. FEA outputs included strains, deformations, stresses and other results. No software extensions other than the basic academic version of the software were utilized. The bond element was not required in this analysis as the transfer zone was modeled as a linear pick-up of the effective prestressing force in each strand over the whole length of the transfer length. ASTM A1081 Test Results were directly related to applied transfer lengths.

As described in the ANSYS Workbench Simulation Software guidebook reference, FEA which is part of this software is a mathematical representation of a physical system comprising of a model, material properties and boundary conditions, the solution of the mathematical representation, and the study of the results of the solution. Boundary conditions include various forms of physical forces (loads, pressures, moments, etc.), thermal loads and conditions (temperature, conductivity, convection, etc.), and constraints (fixed, pinned, frictionless/symmetrical, etc.). FEA software uses computer-aided design (CAD) representation of the physical model and breaks it down into small pieces called finite elements. This process is called meshing. The higher the quality of the mesh or the collection of elements, the better the

representation of the physical model. The primary purpose of an element is to connect nodes with predictable mathematical equations based on stiffness between nodes. By combining the behaviors of each element using simultaneous equations, it is possible to predict the behavior of shapes that would otherwise not be understood using basic "closed form" calculations. 3D elements represent solid shapes and are usually in two basic shapes: brick (hexahedrons or "hex") and pyramids (tetrahedrons or "tets"). ANSYS Workbench Simulation applies these various element types automatically. The "finite" term used in FEA means that there is a known number of elements in the finite model. Based on the analysis performed on the solids as part of this work, it may be said that the element type used as part of this study is best approximated by 8-noded hexahedral 3D or volume element.

ANSYS Workbench Simulation provides two forms of automated meshing: fully automatic and manually directed automatic. Both forms employ a fault-tolerant philosophy meaning that, if a problem occurs, at least 12 attempts of automatic trouble-shooting are made before the mesher fails and tags the area of difficulty with a label. Manually directed means that the user may specify meshing overrides on specific areas of a part or the baseline mesh density on entire parts.

Structural and thermal material data are defined, modified, and used in Workbench Simulation for structural and thermal analyses. Material properties include Young's modulus, Poisson's ratio, density, coefficient of thermal expansion, and thermal conductivity. ANSYS Workbench among other types of analyses performs linear/static analysis. This type of analysis was performed for this work.

Post-processing or interpretation of results in ANSYS is used to create graphical displays that show the distribution of stresses, strains, deformations, and other aspects of the model.

Interpretation of these post-processed results was the key in identifying areas of potential concern, such as over-stressed areas in the model or areas experiencing significant deflections or movements, or valuable information on model performance characteristics that otherwise would not be known until a physical model were built and tested (so called prototype).

The post-processing phase of FEA is where the most critical thinking must take place, where the user looks at the results (the numbers vs. color contours, movements, etc.) and compares results with what might be expected. It is up to the user to determine if the results make sense, to be able to explain the results based upon engineering "common sense". If the results are other than expected, one must search until an explanation can be found before the results can be fully trusted. The select set of results was available to view and interrogate. The set of results were stresses.

Structural analysis can be either linear or non-linear. Linear model analysis assumes that the material doesn't plastically deform (permanent deformation). Non-linear models consist of separating contact conditions (contact with lift-off), when stressing material past its elastic capabilities into the plastic range, or bending greater than 10% of model length (large deformation). At this point, material properties change and stresses in the material will vary with the amount of deformation. All of the modeling done for this thesis used linear-elastic material models. Cracking can be assumed in concrete where computed stresses are greater than the cracking stress of concrete, and this information is wholly sufficient for the purposes and goals of this paper.

Stress occurs when the beam is subject to loading and is expressed in terms of force per unit area such as pounds per square inch. There are two types of stresses considered, normal and shear. Strain is a dimensionless quantity calculated as the ratio of deformation to the original size of the

body. The first part of the stress-strain curve illustrating Hooke's Law is very linear and the slope of the curve is defined as the Young's Modulus of the material. In this linear range, stresses and strains are proportional and simple to calculate, this is where the linear stress comes from.

Three dimensional stresses and strains build up in many directions. Common way to express these multi-directional stresses is to summarize them into an equivalent stress also known as Von-Mises stress. The materials used in the model have stress limit called material yield. Any stresses above this limit result in some type of permanent deformation. In the stress-strain curve where they start to diverge, it is defined as the yield limit of the material. If a design is not supposed to permanently deform by going beyond yield (true in most cases), then the maximum allowable stress would be equal to yield limit.

Linear elastic analysis was used as solution method as it was supported by a number of successful models together with the plastic analyses of which some of them were addressed in the literature review. ANSYS Workbench makes the following assumptions about the calculated results:

- Linear structure: Calculated displacements are directly proportional to the load applied to a beam. Linear behavior results when the slope of the stress-strain curve in the elastic region (measured as the modulus of elasticity) is constant.
- Elastic Structure: A beam returns to its original shape when the loads are removed. Elastic behavior results when the stress in a beam corresponds to the elastic region of the material's stress strain curve.
- Small Displacements: The calculated displacements are small in comparison to the principal dimensions of the beam. For example, in studying the deflection of a beam, the

calculated displacement must be significantly less than the minimum cross-section of the beam. The small displacements assumption is related to small strain analysis, in which normal strains are required to be very small compared to one.

- Linear Contact: The contact conditions between two or more parts in an assembly (in this case neoprene pad and concrete beam) are treated in a linear fashion. For stress, shape, and modal analyses, only bonded and frictionless (no separation) contact conditions are supported. As such, ANSYS Workbench does not treat nonlinear friction and nonlinear open-close (gaping) contact.

The image below (Figure 3.1) conceptually shows how the beam model is supported, with the block of neoprene pad at one end and a roller guide at the midspan of the beam. Prestressing axial force $\boldsymbol{F_p}$ is applied. The moment from prestressing is applied at the left end of the beam, and is 'negative' in direction. The moment at midspan is the sum of the prestressing moment minus the gravity moment. At the neoprene beam end, we discovered a moment constraint due to modeling that is not present in actual applications. This was corrected in our simulations by making the neoprene shorter in length. Other attempts were made in "softening" the neoprene pad, but these resulted in instabilities in the numerical modeling. In the end, we believe that the neoprene pad imparts a small restraining moment in experimental application, and we are content to allow a small restraint in modeling as well.

Figure 3.1. Conceptual Beam

The support which was built as neoprene has a very low shear modulus but remained stiff in axial directions. As a result, normal rotational deformation at the support caused the neoprene pad to impart an end moment on the beam. This leads us to conclude that there is certain amount of constraint or restraint caused by the support and that the support is placing small amount of end moment on the beam ANSYS model, however insignificant it may be. In the ANSYS model, the neoprene pad was supported with a single roller located under the center of the neoprene pad. As planned during the research work, the effects of the neoprene pad and the roller are so "small" or insignificant, and don't affect the findings of this study. This is supported by the fact that the beam theory holds true at a reasonable distance from the end of the support.

The key was to reduce the amount of the bearing restraint which is rotational in nature as much as we can while not upsetting the other supporting conditions. This influence of the support was minimized and the model made realistic by reducing the length of the neoprene pad to 2 inches. Neoprene was made to be 10-inch wide, 2-inch long and 4-inch thick (Figures 3.2 and 3.3).

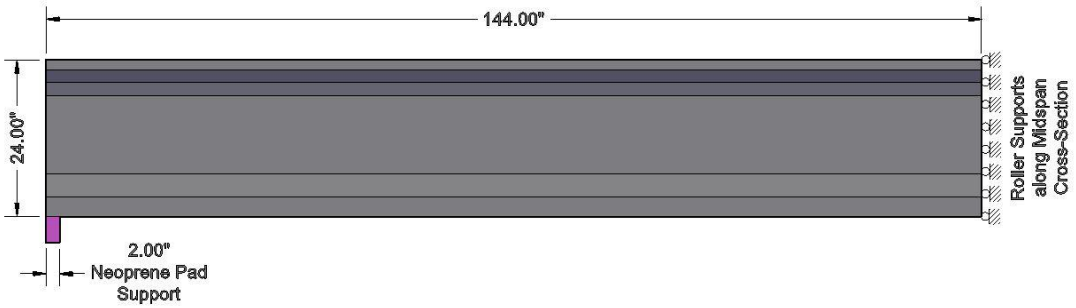

Figure 3.2. 12-foot Long Beam Model Profile with 2-inch Support (FEA Beam at Release and at Testing/Loading)

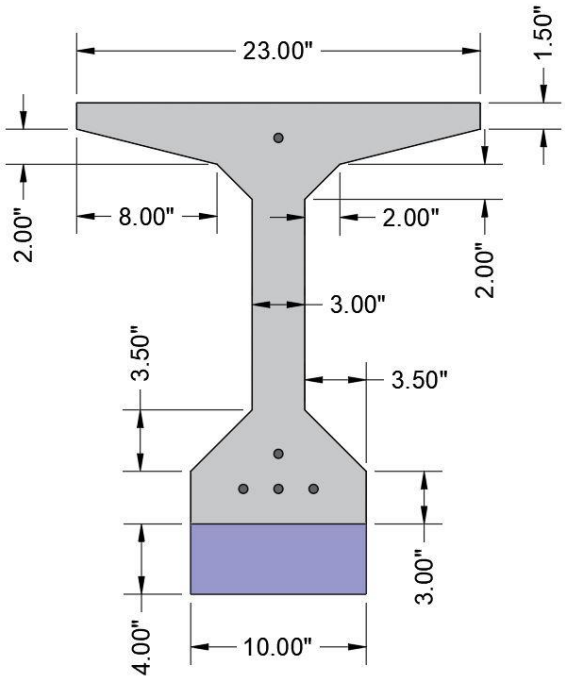

Figure 3.3. 24-Inch Deep Beam Model Cross-Section for Modeling of Prestressing Variables

Figure 3.3 shows the end or cross-section view of the modeled 12 feet (144 inches) long I-beam with the locations where the transfer zone prestressing loads were applied to the I-beams. The full length of each beam was 24 feet, but the end regions were modeled with ½ of the span. Prestressed strands are placed at 2.0 in. center-to-center (c/c) spacing, with distance edge to center of 2.0 in. Top strand is located 22.0 inches from the beam bottom in case of Jacob (1998) experimental program and in the model comparing the prestressing variables, and 18.0 inches from beam bottom in case of Ganpatye (2006) experimental program. Also, where trials were conducted with debonding, strands are debonded 24 inches from end. The beam was modeled as a concrete beam, and the bond transfer was modeled by distributing the prestress force to the nodes located along the transfer length in the location where the prestressing steel strands would be located in the constructed concrete I-beams.

Cross-sectional area of the beam is 163.25 in^2. Neutral axis (NA) is located at 13.75 inches from the bottom. The moment of inertia (I) is 12,371 in^4. Prestress forces were applied along the transfer length of each prestressing strand; 25 kips for 0.5 in. strands and 36 kips for 0.6 in. strands.

Figure 3.4 shows the conceptual computer-aided design (CAD) 12 feet (144 inches) long 3-dimensional (3D) model of the beam showing X-axis in the transverse horizontal (i.e. left and right) direction with respect to the beam, Y-axis in the vertical (i.e. up and down) direction of the beam (direction parallel to gravity and loads applied during experimental testing) and Z-axis in the longitudinal direction along the beam (direction parallel to applied prestress forces).

This model was exported to the ANSYS Workbench, where concrete and neoprene material properties were input as variables, supports were assigned, as well as the loads were applied to mimic those applied during the testing. FEA meshing was performed using the 0.5-inch dominant 8-noded hexahedral block element with defined mechanical behavior. This block element is allowing for 3D volumetric linear strain variation with nodes being able to move in any direction in space. Based on ANSYS, there are six types of degrees of freedom for any given node: three possible translations (one each in the X, Y and Z directions) and three possible rotations (one rotation about each of the X, Y and Z axes). Degrees of freedom are equal to the number of equations of equilibrium for the system, and are defined and restricted by the elements and constraints associated with each node.

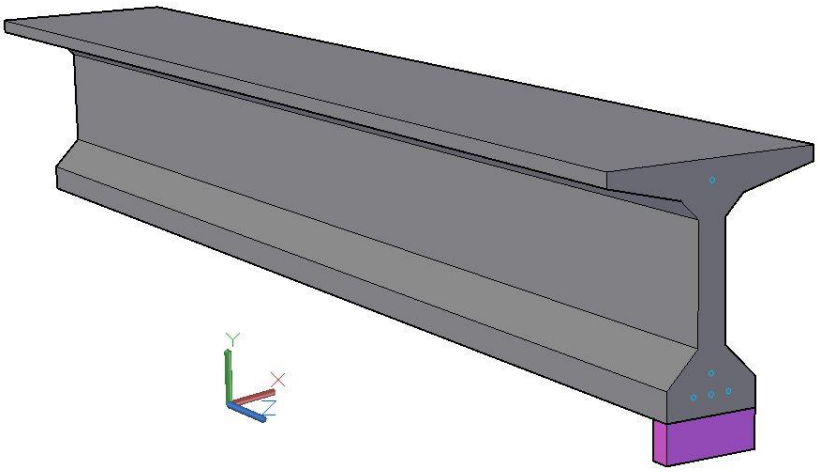

Figure 3.4. Perspective View of CAD I-Beam Model with Defined Coordinate System

Figure 3.5 shows the end view of the model I-beam with the locations where the transfer zone prestressing loads were applied to the I-beams. Horizontal spacing between the bottom row of prestressing strand locations C, D and E is 2 inches center-to-center. The beam was modeled as the plain concrete beam, and the bond transfer was modeled by distributing the prestress force to the nodes located along the transfer length in the location where the steel strands would be located in the constructed concrete I-beams. As shown in Figure 3.5, for John Jacob's beams top strand was located 22 inches from beam bottom, while for Ganpatye's beams top strand was located 18 inches from beam bottom, and top strands were modeled as such in ANSYS.

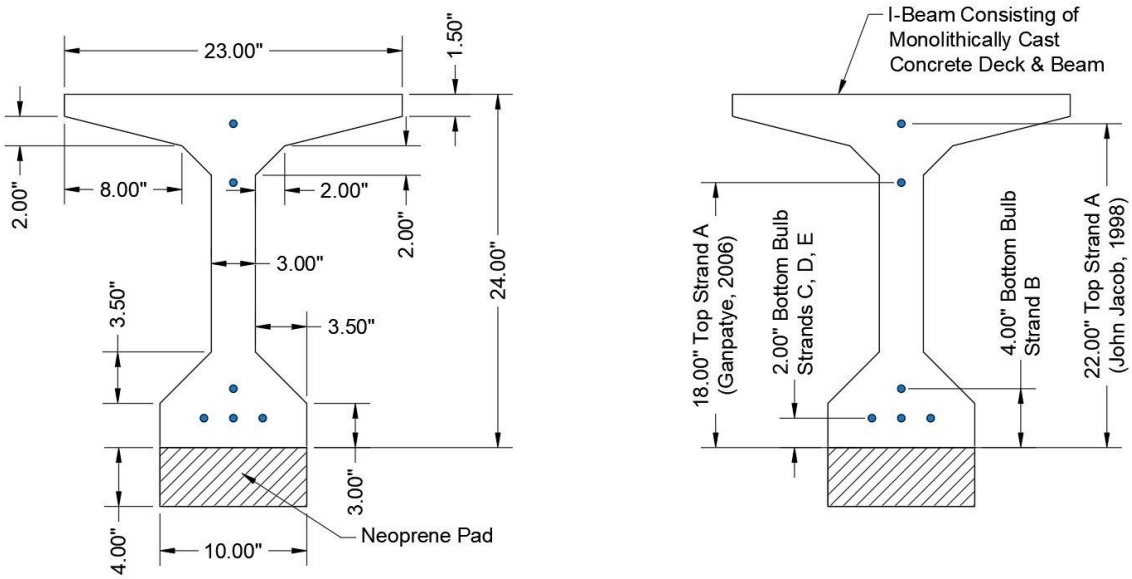

Figure 3.5. End View of Model I-beam with Locations of Strands from Beam Bottom

Cross sectional area of the beam is 163.25 sq.in. Neutral axis (NA) is located at 13.75 inches from the bottom. Second moment of inertia (I) is calculated as 12,371.16 in^4. Forces distributed throughout the transfer length of 0.5-inch and 0.6-inch prestressing strands were 25 kips per strand for 0.5-inch diameter strands and 35 kips per strand for 0.6-inch diameter strands.

The importance of an adequate pad is recognized in the design of the bearings for the prestressed concrete beams. Figure 3.6 shows an example of the elastomeric pad in the beam design drawings by Oklahoma Department of Transportation (ODOT) for Type IV prestressed concrete beam.

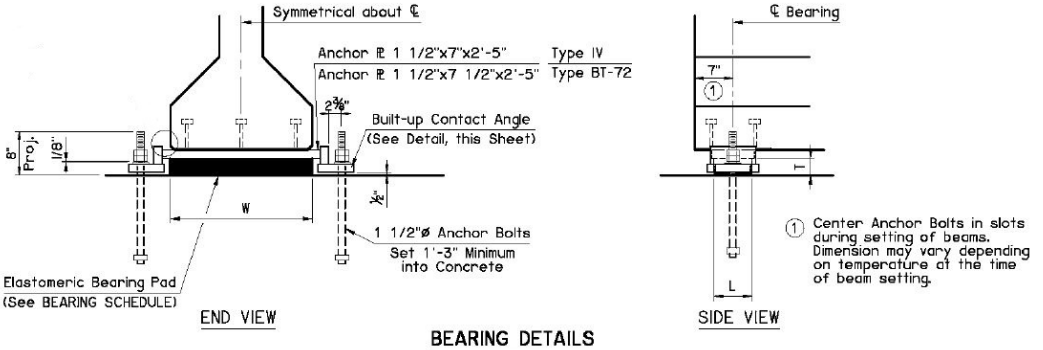

BEARING DETAILS

TYPE IV BEARING SCHEDULE					
SPAN	60 DUROMETER ELASTOMERIC BEARING PAD				MAXIMUM EXPANSION LENGTH ②
	SIZE (T x L x W)	COVER LAYER	INNER LAYER	LAMINATE PLATE	
65'	3 1/8"x6"x2'-2"	2 - 1/4"	5 - 3/8"	6 - 1/8"	205'
70'	3 1/8"x6"x2'-2"	2 - 1/4"	5 - 3/8"	6 - 1/8"	205'
75'	3 1/8"x6"x2'-2"	2 - 1/4"	5 - 3/8"	6 - 1/8"	205'
80'	3 1/8"x6"x2'-2"	2 - 1/4"	5 - 3/8"	6 - 1/8"	205'
85'	3 1/8"x6 1/2"x2'-2"	2 - 1/4"	5 - 3/8"	6 - 1/8"	205'
90'	3 1/8"x6 1/2"x2'-2"	2 - 1/4"	5 - 3/8"	6 - 1/8"	215'
95'	3 1/8"x6 1/2"x2'-2"	2 - 1/4"	5 - 3/8"	6 - 1/8"	215'
100'	3 1/8"x6 1/2"x2'-2"	2 - 1/4"	5 - 3/8"	6 - 1/8"	220'

TYPE BT-72 BEARING SCHEDULE					
SPAN	60 DUROMETER ELASTOMERIC BEARING PAD				MAXIMUM EXPANSION LENGTH ②
	SIZE (T x L x W)	COVER LAYER	INNER LAYER	LAMINATE PLATE	
95'	3 5/8"x6 1/2"x2'-2"	2 - 1/4"	6 - 3/8"	7 - 1/8"	215'
100'	3 5/8"x6 1/2"x2'-2"	2 - 1/4"	6 - 3/8"	7 - 1/8"	220'
105'	3 5/8"x6 1/2"x2'-2"	2 - 1/4"	6 - 3/8"	7 - 1/8"	230'
110'	3 5/8"x6 1/2"x2'-2"	2 - 1/4"	6 - 3/8"	7 - 1/8"	230'
115'	3 5/8"x7"x2'-2"	2 - 1/4"	6 - 3/8"	7 - 1/8"	230'

② Bonding to Anchor Plate not required.

Figure 3.6. Example of Beam Bearing Details for Full-Scale Bridge Beam (ODOT, 2009)

Neoprene pad support for an I-beam from the experimental program was modeled as 4-inches thick, 10-inches wide (to match bottom width of I-beam) and 2-inches long, as shown in Figure 3.7. It was realized that using 2-inch long pad used for FEA models for observing influence of different variables in the beam at release, gives better values and also corresponds better to the beam size constructed in the experimental program and modeled in the FEA study, which is actually 3/8 (0.375) scale model of the Type IV AASHTO Beam. Using such approach 6-inch long pad for full-scale beam multiplied by 0.375 scale factor would give length of 2.25 inches. Different neoprene pad dimensions were initially used for the modeling of beams under loading for looking at shear, flexure and deflections, and for beams under release conditions for looking at web test locations. 2-inch long neoprene pad was found to be significantly better match than initially used 6-inch long pad for comparison with real world results and theory applying to this 3/8 scale beam model.

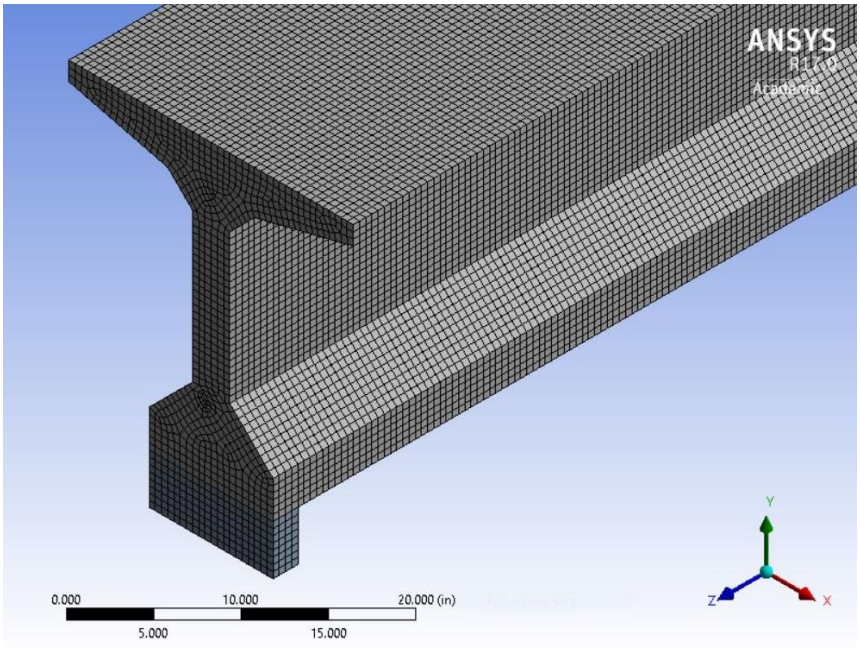

Figure 3.7. Mesh with 0.5-inch Element Size for Neoprene Pad and Model Beam

Neoprene material properties equal to those for study of beam under no loading except prestress were input into the ANSYS finite element model to account for the longitudinal deformation at the support. This also gave the benefit of spreading out the bearing stresses which is also very important, and was believed to benefit future studies regarding the influence of the bearing pad. Modeling inputs and data collection to determine stresses in end regions of beams were slightly different from the modeling and data collection for shear force and deflections to compare to experimental tests and to validate the model, as next described.

In order to collect data, to determine stresses in the end regions of beams and find answers to the five basic questions regarding of influence of different prestressing variables, the test locations where the ANSYS results were obtained for the model were selected as shown in Figures 3.8 and 3.9. For each test location were determined principal stresses and angles and shear stresses in the YZ plane. This part of FEA modeling to determine influence of variables focused on the beam

model with no other external loading applied other than the prestressing force. Self-weight of the beam was included in all FEA models.

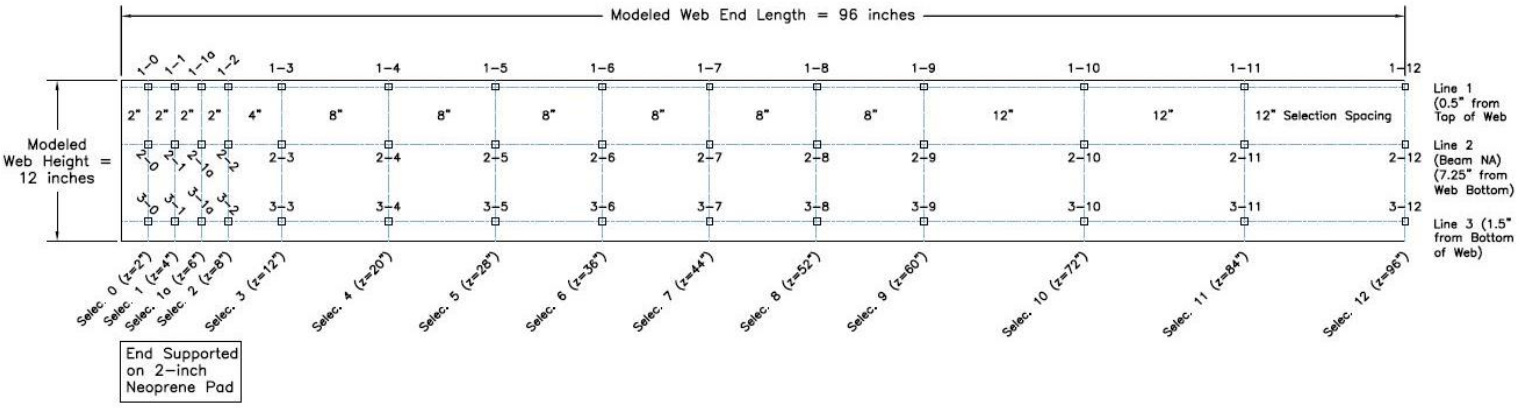

Figure 3.8. Test Locations along Beam Web where FEA Results were Determined for Influence of Prestressing Variables

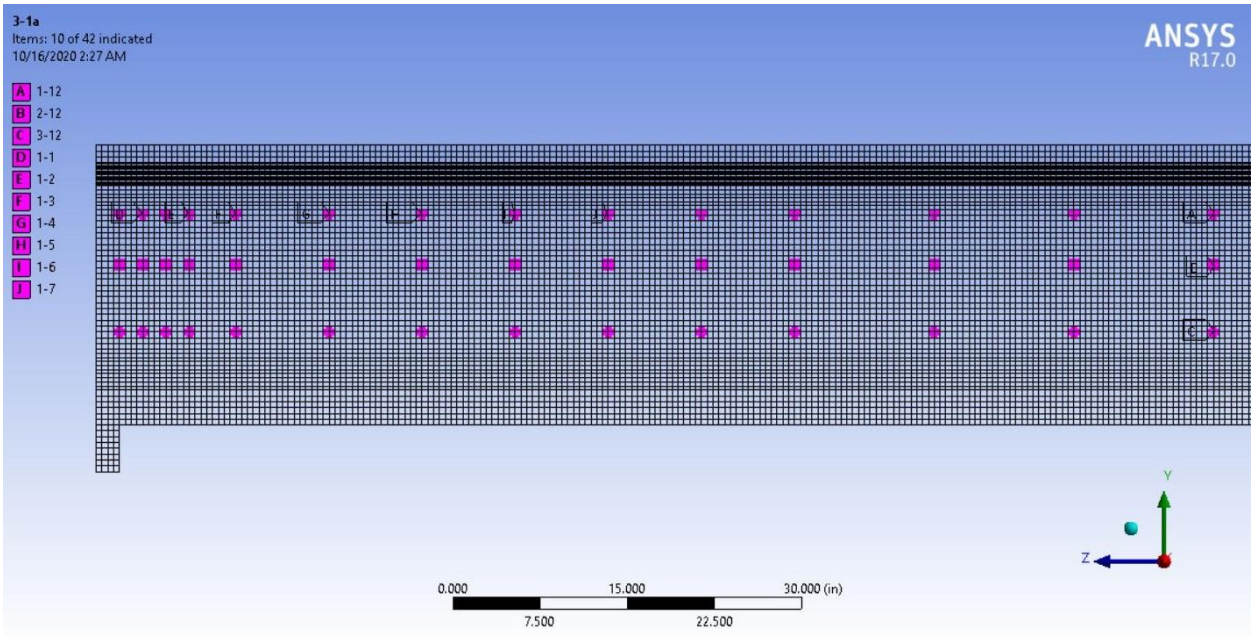

Figure 3.9. Test Locations along Beam Web as Selections in ANSYS FEA Model

The finite element analysis performed was seeking to answer the five (5) basic questions by using different values of the prestressing variables. These five questions were:

1. What are the effects of varying strand bond quality (higher ASTM A1081)?
2. What are the effects of strand size (prestressing force) (0.5 vs. 0.6 in. strand)?
3. What are the effects of concrete strength?
4. What are the effects of including fully-tensioned top strands?
5. What are the effects of the debonding strands?

Basic FEA test matrix was developed to provide test variable inputs and to provide answers to the five basic questions described previously. Table 3.1 with the test matrix is shown below.

Table 3.1. Test Matrix for FEA Test Variables and Answering Five Basic Questions

ANSYS Case No.	ASTM 1081 Bond Test				Strand Force (k)		Concrete Release Strength (ksi)			Top Strand		Debond - One Strand 24 in.		Question it answers				
	9000	12000 (14400)	18000 (21600)	24000 (28800)	25	36	4	6	10	N	Y	N	Y	1	2	3	4	5
1	X				X			X		X		X		1		1		
2		X			X			X		X		X		1	1	1		
3			X		X			X		X		X		1	1	1		
4		X				X		X		X		X		1	1	1	1	1
5			X			X		X		X		X		1	1	1	1	1
6				X		X		X		X		X		1		1	1	1
7	X				X				X	X		X		1		1		
8		X			X				X	X		X		1	1	1		
9			X		X				X	X		X		1	1	1		
10		X				X			X	X		X		1	1	1		
11			X			X			X	X		X		1	1	1		
12				X		X			X	X		X		1		1		
13	X				X		X			X		X		1		1	1	
14		X			X		X			X		X		1		1	1	
15			X		X		X			X		X		1		1		
19	X				X		X				X	X		1		1	1	
20		X			X		X				X	X		1		1	1	
21		X				X		X			X	X		1			1	1
22			X			X		X			X	X		1			1	1
23				X		X		X			X	X		1			1	1
24		X				X		X			X		X	1			1	1
25			X			X		X			X		X	1			1	1
26				X		X		X			X		X	1			1	1
27		X				X		X		X			X	1				1
28			X			X		X		X			X	1				1
29				X		X		X		X			X	1				1

The so-called “test” matrix using the primary variables (bond quality, strand force for 0.5-inch diameter (25 kips per strand) and 0.6-inch diameter (36 kips per strand) strands, concrete strength at release, top strand or no top strand conditions, and debonded strand condition or no

debonding. The test matrix shows 26 separate "tests" or FEA runs conducted with ANSYS software. This number of tests was conservatively selected, even though all of the variables could be evaluated with even fewer tests, the number of which could be reduced to the required number by using Design of Experiments (DOE) techniques in order to analyze the influence of the variables. This is crucially important in experimental testing where creating each new specimen and then conducting laboratory experiments can be incredibly time consuming and expensive. With analytical research additional tests could be added with less expense.

Transfer lengths used in the model are related to the ASTM A1081 Bond Test values for 0.5-inch and 0.6-inch prestressing strands, as shown in Table 3.2. The transfer length (L_t) empirical equation used is shown below, where d_b is the strand diameter in inches, and f'_{ci} is the concrete strength at stress release in ksi units.

$$L_t = \frac{200 * d_b^2}{\sqrt{f'_{ci}}} * \frac{(ASTM\ A1081)}{12{,}000\ lbs}$$

Looking at the Table 3.2, it is important to note here that 12,000 lbs pull-out for 0.5-inch strand is the same bond stress as the 14,400 lbs pull-out for 0.6-inch strand.

Table 3.2. ASTM 1081 Bond Test Values and Resulting Transfer Lengths for ANSYS Model

Concrete Release Strength = 4 ksi					
0.5 in. Strands			0.6 in. Strands		
ASTM Bond Test (lbs)	Bond FLOW (lbs/in)	Transfer Length, Lt	ASTM Bond Test (lbs)	Bond FLOW (lbs/in)	Transfer Length, Lt
9000	750	**33.33**	10,800	900	**40.00**
12000	1000	**25.00**	14,400	1200	**30.00**
18000	1500	**16.67**	21,600	1800	**20.00**
24000	2000	**12.50**	28,800	2400	**15.00**
Concrete Release Strength = 6 ksi					
0.5 in. Strands			0.6 in. Strands		
ASTM Bond Test (lbs)	Bond FLOW (lbs/in)	Transfer Length, Lt	ASTM Bond Test (lbs)	Bond FLOW (lbs/in)	Transfer Length, Lt
9000	919	**27.22**	10,800	1102	**32.66**
12000	1225	**20.41**	14,400	1470	**24.49**
18000	1837	**13.61**	21,600	2205	**16.33**
24000	2449	**10.21**	28,800	2939	**12.25**
Concrete Release Strength = 10 ksi					
0.5 in. Strands			0.6 in. Strands		
ASTM Bond Test (lbs)	Bond FLOW (lbs/in)	Transfer Length, Lt	ASTM Bond Test (lbs)	Bond FLOW (lbs/in)	Transfer Length, Lt
9000	1186	**21.08**	10,800	1423	**25.30**
12000	1581	**15.81**	14,400	1897	**18.97**
18000	2372	**10.54**	21,600	2846	**12.65**
24000	3162	**7.91**	28,800	3795	**9.49**

Example of how transfer lengths were modeled in ANSYS is depicted in Figures 3.10 and 3.11. Rather fine mesh element size of 0.5-inch was selected for the beam element model. Node selections as ANSYS features were used to define transfer zone of each prestressing strand. Prestressing force for either 0.5-inch or 0.6-inch prestressing strands was distributed in the longitudinal (negative z-axis) direction among the number of nodes defining the selected transfer zone. Figure 3.12 shows how applying prestress force results in compressive stresses at the strand locations.

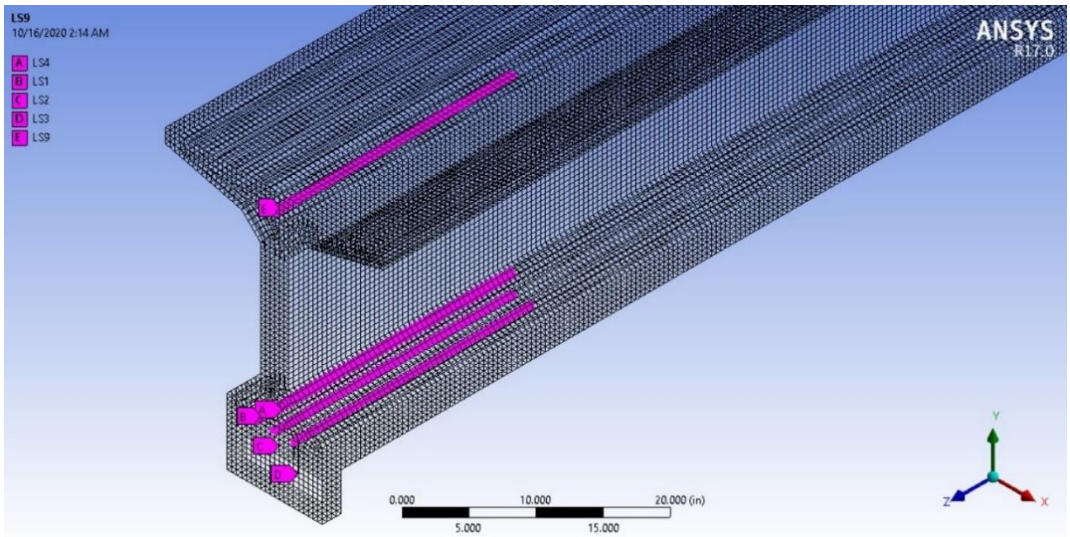

Figure 3.10. Example of Node Selections Defining Transfer Zones of Each Prestressing Strand in ANSYS FEA Model (ANSYS Case 20). Isometric View

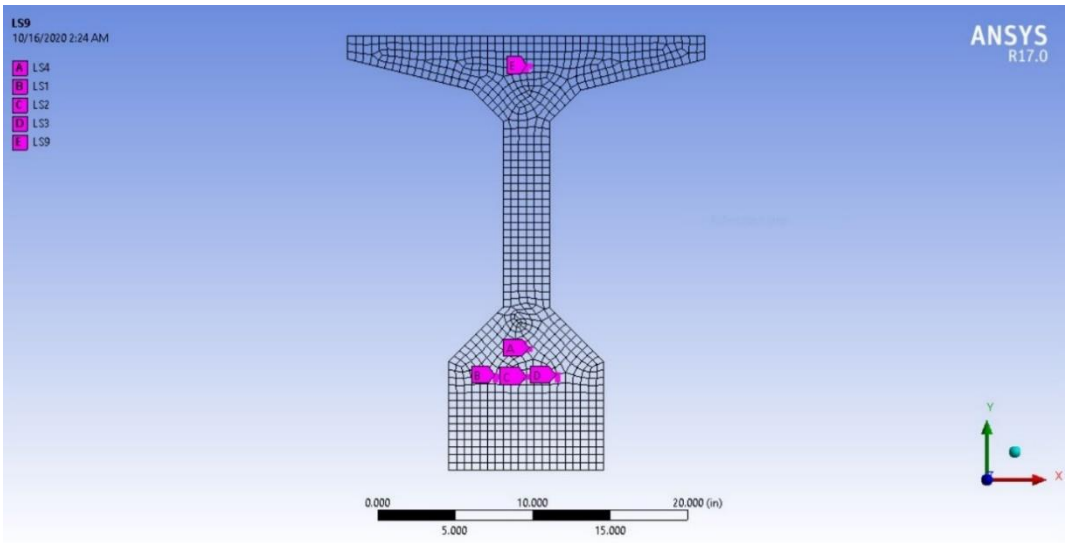

Figure 3.11. Example of Node Selections Defining Transfer Zones of Each Prestressing Strand in ANSYS FEA Model (ANSYS Case 20). End-of-Beam View

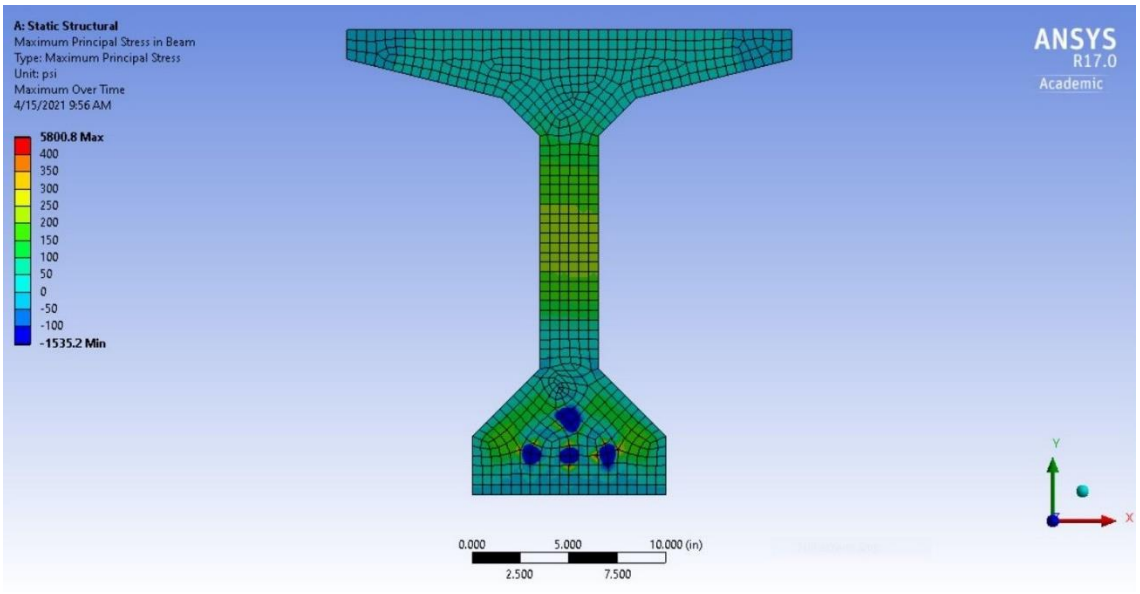

Figure 3.12. End View of Beam ANSYS Case 1

Example of beam geometry and concrete and neoprene pad properties is shown in Figure 3.13. Neoprene pad properties were kept constant for all cases. Elastic modulus of concrete (E_c) was determined from the empirical equation $E_c = 33 * w^{1.5} * \sqrt{f_c'}$ where w which is unit weight of concrete was taken as 144 lb/cu.ft. (f_c'=4,000 psi), 146 lb/cu.ft. (f_c'=6,000 psi) and 150 lb/cu.ft. (f_c'=10,000 psi). Poisson's ratio (ν) was taken as 0.15. Shear modulus (G) was calculated from equation $G = \frac{E}{2*(1+\nu)}$.

Properties

Appearance	
Color	ARGB: 255, 175, 143, 175
Style	By Color, By Style
Material	
Material Name	Concrete Ansys13
Fluid	**False**
Density	**0.0833333163878906 lb/in^3**
Ultimate Strength (Pa)	**27579200 Pa**
Elastic Modulus (Pa)	**2.4866E+10 Pa**
Shear Modulus (Pa)	**1.0811E+10 Pa**
Poisson's Ratio	**0.15**
Thermal Conductivity (W/m-K)	**0.55 W/m-K**
Specific Heat (J/kg-deg C)	**880 J/kg-deg C**

Properties

Appearance	
Color	ARGB: 255, 159, 175, 143
Style	By Color, By Style
Material	
Material Name	Neoprene Ansys1
Fluid	**False**
Density	**0.143999999331056 lb/in^3**
Ultimate Strength (Pa)	**350000000 Pa**
Elastic Modulus (Pa)	**1.0000E+11 Pa**
Shear Modulus (Pa)	**3.6000E+9 Pa**
Poisson's Ratio	**0.4**
Thermal Conductivity (W/m-K)	**0.19 W/m-K**
Specific Heat (J/kg-deg C)	**1500 J/kg-deg C**

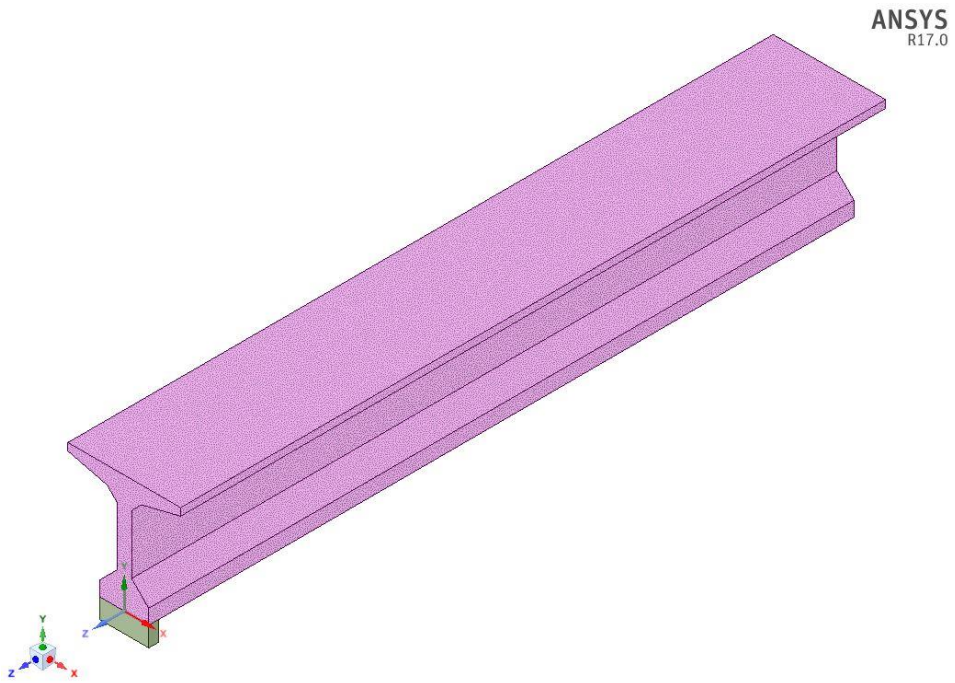

Figure 3.13. Example of Beam Geometry and Concrete and Neoprene Pad Properties (ANSYS Case 20)

Concrete material properties used for the FEA model are given in Table 3.3.

Table 3.3. Concrete Material Properties

Release Concrete Strength (psi)	Unit Weight (lb/ft^3)	Elastic Modulus (psi)	Shear Modulus (psi)	Poisson's Ratio
4000	144	3606514	1568050	0.15
6000	146	4509401	1960609	0.15
10000	150	6062487	2635864	0.15

In all cases that involved debonding, the single strand located 4 inches from bottom was debonded 24 inches from beam end. The inputs and results for the additional ANSYS cases 21A, 21B, 24A, 24B, 25A and 25B, which were added at a later time to better examine effects of debonding, are a variation of cases 21, 24 and 25, respectively, where in 24A and 25A cases all other strands except the one already debonded 24 inches, were debonded 2 inches from the model beam end, and in 24B and 25B cases all other strands were debonded 4 inches from beam end.

As part of looking at experimental programs to validate the FEA model analyzed were prestressed concrete I-beams which were 24-inch deep were developed through experimental testing programs described in Jacob (1998) thesis work from the University of Oklahoma, and Ganpatye (2006) thesis work from the Oklahoma State University. A number of their experimental program beams were analyzed successfully with FEA.

This part of study that considered FEA model comparison with the results of experimental testing by Jacob (1998) and Ganpatye (2006) looked into the cases of end regions of prestressed concrete beams at release and those under the loading causing initial cracking in the prestressed concrete beams. Several variables also considered during the experimental program were looked into to determine their influence on the performance of the end regions. These variables were transfer length, debonding strands to various lengths, concrete strength, using one top stand versus using no top strands, 0.5-inch and 0.6-inch diameter strands, cracking load applied to the

prestressed beam versus no load applied other than the gravity load (dead weight of the beam) and prestress force. Overall, good match was found between the experimental program and the FEA results under loading (at testing) and at release.

The impacts of these different variables were evaluated looking into varying values of stresses and deformations/deflections at different locations throughout the end regions. These locations were at distances D and D/2 from the support of the beam (at neutral axis) for shear, at the bottom part of the beam at location where load was applied and strand length within the transfer zone.

It is common practice in the beam design to use the span length which is understood as the distance from the centerline of the supports. It is important to consider that although the shear computed is the largest immediately adjacent to the reaction, shears that have locations within the width of the support are not physically meaningful. In addition, the compression caused by the reaction caused shear strength to increase in the proximity of the support. Prestressed concrete beam design methods take this increased strength into account by saying that that the region of the prestressed concrete beam from the face of the support to distance D/2 (D = beam depth) or h/2 (h = beam height, where h = D) from the face of the support can be designed for the same shear force that exists at a distance D/2 from the face of the support. For this provision to be valid, the reaction must induce compression in the member, that is, the beam must not be hanging from the support (in which case the critical section would be exactly at the face of the support from which the beam is hanging), the loads must be applied at the top or near the top of the members, and there must be no concentrated loads acting within the distance D or h (in which case the critical section would be exactly at the face of the support).

For these reasons, studying of shear while beam is in the elastic region and at the initiation of cracking by using FEA is an adequate approach, since the area of the beam looked at distance D/2 (or h/2) from the supports is in the end regions where the beam theory doesn't apply. In addition to looking at shear and strand transfer zone bond stresses and deformations, this research also looked at the flexure and deflections at locations where load was applied during experimental testing at testing stage and during prestress release stage as shown in Figure 3.14. FEA model started by analyzing for prestressed beam stresses and deformations at strand prestress transfer regions, D/2 and D distance from support and under the externally applied load for initial comparison of FEA model results with the experimental programs' testing results. In order to look at the incidence of shear cracking in the FEA model, stress data at both D/2 (h/2) and D (h) were collected and compared. ANSYS can determine shear stresses on the whole face of the beam, but since it is difficult to visually quantify and mutually compare the graphical results, it was decided to look at 1-inch square element at the intersection of NA and at D/2 (i.e. h/2) and D (i.e. h) from beam support or neoprene pad.

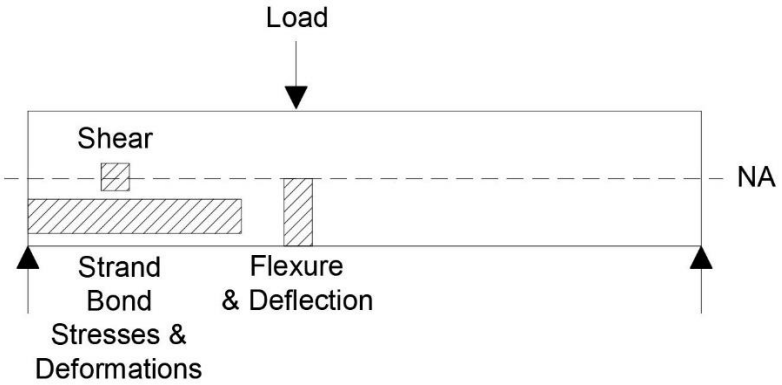

Figure 3.14. Locations of Stresses and Deformations Initially Observed

Concrete material properties input into ANSYS model for several analyzed beam ends from the experimental programs were input into the model as shown in Table 3.4, with different values for the beams at testing and at release.

Table 3.4. Concrete Material Properties for Beams from Experimental Program

Beams from Experimental Program (At Testing)					
Beam End	**Concrete Strength (psi)**	**Elastic Modulus (psi)**	**Shear Modulus (psi)**	**Concrete Density (lbs/ft^3)**	**Poisson's Ratio**
JJ1 South	11550	6125976	2663468	150	0.15
JJ1 North	11475	6106054	2654806	150	0.15
JJ4 South	11680	6160355	2678415	150	0.15
ID-10-5-1-N	14160	6782908	2949091	150	0.15
ID-10-5-1-S	14160	6782908	2949091	150	0.15
IA-6-6-1-N	8990	5404608	2349829	150	0.15
IA-6-6-1-S	8990	5404608	2349829	150	0.15
IA-6-6-2-N	8990	5404608	2349829	150	0.15
IA-10-6-2-S	14930	6964889	3028213	150	0.15
Beams from Experimental Program (At Release)					
Beam End	**Concrete Strength (psi)**	**Elastic Modulus (psi)**	**Shear Modulus (psi)**	**Concrete Density (lbs/ft^3)**	**Poisson's Ratio**
JJ3 North	7950	5082389	2209734	150	0.15
JJ4 South	7950	5082389	2209734	150	0.15
JJ4 North	7950	5082389	2209734	150	0.15
IB-6-5-1-N	5810	4344826	1889055	150	0.15
IB-6-5-1-S	5810	4344826	1889055	150	0.15
ID-6-5-1-N	5492	4224250	1836630	150	0.15
ID-6-5-1-S	5492	4224250	1836630	150	0.15

In order to best model plain concrete and the application of prestress to strands A (top), B (middle row strand, 4" from beam bottom), C, D and E (bottom row strands, 2" from beam bottom) node selections were created in the concrete material and prestressing force was distributed to the nodes representing each transfer zone for each prestressing strand. Within ANSYS Workbench, these selections were arbitrarily called LS9 (Strand A transfer zone node selection), LS4 (Strand B transfer zone node selection), LS3 (Strand C transfer zone node

selection), LS2 (Strand D transfer zone node selection) and LS1 (Strand E transfer zone node selection).

Figure 3.15 shows how loading was applied to the top of the beam end JJ1 South. Load was distributed to the node selection having the extents of the steel plates located under the load beam during testing. Loading on this and other beams was initially applied in ANSYS as was measured during experimental testing to cause initial cracking as shown in Table 3.5. Later, these loads were further reduced to result in shear forces which would cause stresses in the web equal to $f_t' \approx 4\sqrt{fc'}$, where f_c' is the compressive concrete strength at testing.

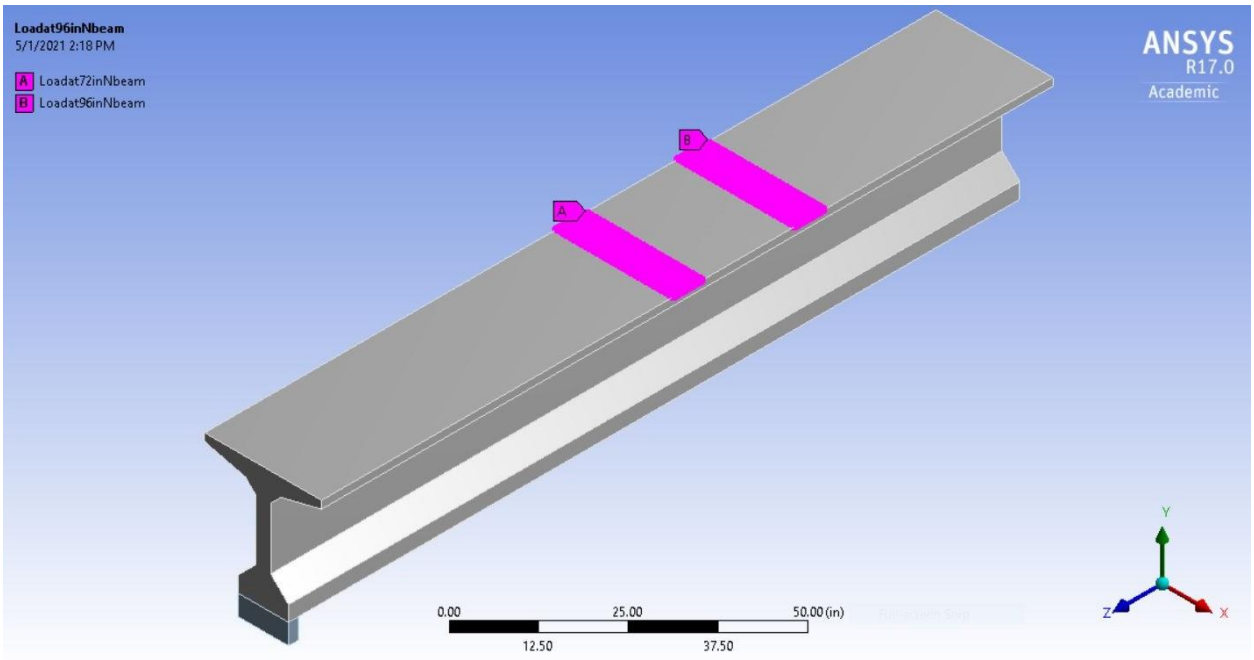

Figure 3.15. Example of Load Application to Beam End JJ1 South at 72-inches and 96-inches from Beam End Supported by Neoprene Pad

Table 3.5. Loads Applied to Experimental Beams Modeled in ANSYS

Beams from Experimental Program (Loads Causing Initial Cracking As Reported During Experimental Testing)				
Beam End	**Load A (lbs)**	**Distance of Load A from Beam End with Neoprene Pad (in)**	**Load B (lbs)**	**Distance of Load B from Beam End with Neoprene Pad (in)**

JJ1 South	39753	72	19847	96
JJ1 North	43355	72	21645	96
JJ4 South	40087	72	20013	96
ID-10-5-1-N	32483	72	16217	96
ID-10-5-1-S	37552	58	18748	82
IA-6-6-1-N	44222	72	22078	96
IA-6-6-1-S	43088	58	21512	82
IA-6-6-2-N	29348	72	14652	96
IA-10-6-2-S	34284	58	17116	82
Beams from Experimental Program (Loads Causing Principal Stresses in Beam Web Equal to $f_t' \approx 4\sqrt{fc'}$)				
Beam End	**Load A (lbs)**	**Distance of Load A from Beam End with Neoprene Pad (in)**	**Load B (lbs)**	**Distance of Load B from Beam End with Neoprene Pad (in)**
JJ1 South	23045	72	11523	96
JJ1 North	24933	72	12467	96
JJ4 South	24304	72	12152	96
ID-10-5-1-N	23660	72	11830	96
ID-10-5-1-S	26741	58	13370	82
IA-6-6-1-N	13039	72	6519	96
IA-6-6-1-S	20540	58	10270	82
IA-6-6-2-N	22880	72	11440	96
IA-10-6-2-S	23360	58	11680	82

Table 3.6 shows the ANSYS Workbench modeled experimental program beam results with values for deflection at the bottom of the beam directly below the location of the loading, shear at D/2 (i.e. h/2) and D (i.e. h) from the support and flexural stress at the bottom of the beam below the loading location. Results were generated in FEA model using the applied loads causing the initial cracking as reported during experimental testing. Positive values of stress indicate tension while negative values of stress indicate compression. In order to determine flexure and deflection observed was 1-inch square element located at the center of the beam bottom below the location of the loading. Positive values of deflection indicate deformation upward, while the negative values of deflection indicate deformation downwards. The results are repeated for purpose of comparison in Table 3.6. This Table also shows the results using the inputs for several of the beam ends at release, with transfer lengths and concrete strengths at

release used in the FEA model as reported by Jacob (1998) and Ganpatye (2006). At Release FEA model results indicate deflection upwards, indicating occurrence of camber, as well as predominantly negative stresses, indicating compression inside the members.

Table 3.6. ANSYS Results for Beams from Experimental Program

Beams from Experimental Program At Testing (Loads Causing Initial Cracking As Reported During Experimental Testing)				
Beam End	**Maximum Deflection (in)**	**Shear Stress at D/2 (psi)**	**Shear Stress at D (psi)**	**Flexure at Beam Bottom (psi)**
JJ1 South	-0.375	1087.60	1058.10	3270.00
JJ1 North	-0.415	1179.50	1162.40	3715.00
JJ4 South	-0.376	1090.90	1072.90	3312.00
ID-10-5-1-N	-0.245	873.35	874.07	2306.30
ID-10-5-1-S	-0.222	967.72	983.73	2013.00
IA-6-6-1-N	-0.588	1259.90	1219.50	5574.40
IA-6-6-1-S	-0.406	978.05	1029.40	3714.90
IA-6-6-2-N	-0.247	756.39	776.29	1712.10
IA-10-6-2-S	-0.249	745.92	887.76	2845.00
Beams from Experimental Program At Release (Only Prestress Force and Self-Weight Loads Applied, No External Loading)				
Beam End	**Maximum Deflection (in)**	**Shear Stress at D/2 (psi)**	**Shear Stress at D (psi)**	**Flexure at Beam Bottom (psi)**
JJ3 North	0.099	-27.72	15.25	-1631.60
JJ4 South	0.100	-22.21	20.21	-1631.10
JJ4 North	0.099	-25.60	-0.11	-1632.50
IB-6-5-1-N	0.131	-65.13	21.23	-1736.00
IB-6-5-1-S	0.116	6.57	28.39	-1751.35
ID-6-5-1-N	0.134	-74.41	-32.29	-1737.25
ID-6-5-1-S	0.080	-44.27	-5.26	-1282.05

Figure 3.16 shows the location at the beam bottom where deflections and flexural stress were determined in ANSYS for beam ends under loading (i.e. at testing). The location is vertically down at the beam bottom under the location where load is applied.

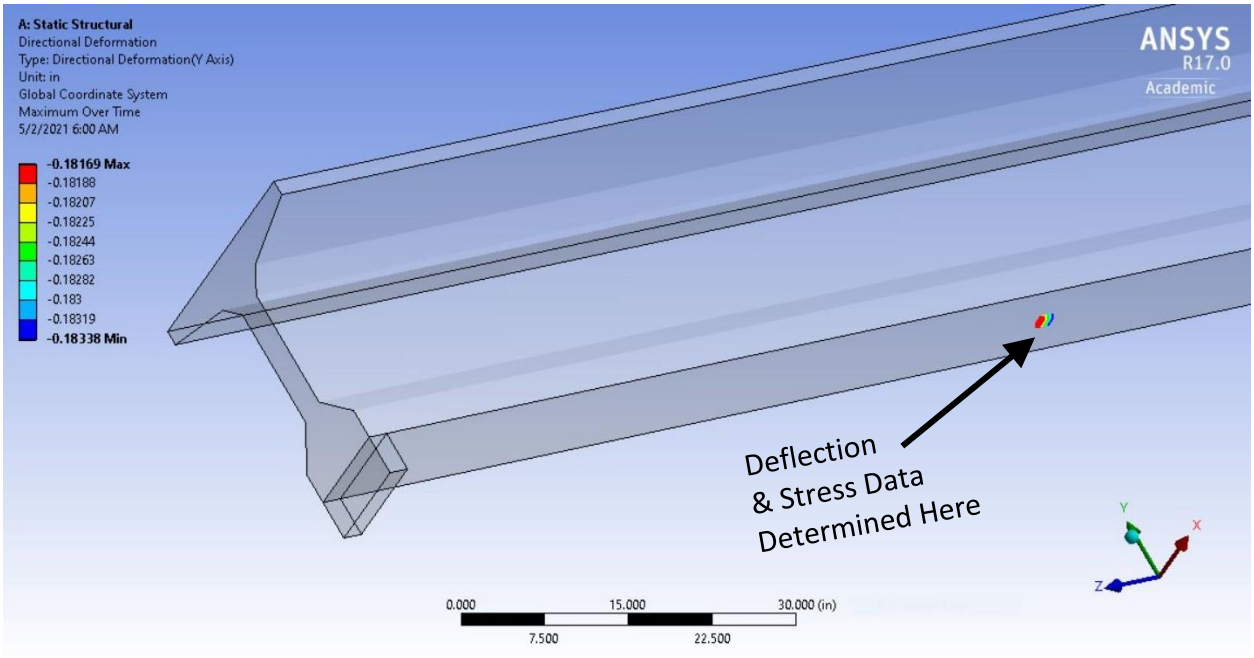

Figure 3.16. Deflection and Flexure Observation Locations at Beam Bottom for Beam Ends under Loading

Previous results shown in the Tables were obtained by considering different design variables as reported in Jacob (1998) and Ganpatye (2006). Transfer lengths used for beams were those reported from these experimental programs. Loading magnitude was used as for their respective beams from the experimental program.

It is possible to approximately adjust values of stresses and deflections calculated in ANSYS Workbench in this study using the adjustment factors defined in Table 3.7. This is because during the experimental programs by John Jacob (1998) and Ganpatye (2006) the beams were supported with an overhang on one end as shown previously and not as simply supported as the ANSYS models are set up. This doesn't affect the study in a significant way since the differences can still be noticed and differentiated between the separate model runs or analyses, including differentiating between the outputs for the models at prestress release and models under loading.

Table 3.7. Deflection and Stress Adjustment Factors

Value Measured	All JJ beams and Ganpatye North End Beams Adjustment Factor	Ganpatye South End Beams Adjustment Factor
Deflection	0.664	0.870
Shear Stress	0.911	0.852
Flexural Stress	0.901	0.833

FEA model results of the incidence of shear cracking under loading conditions compared to the theoretical and experimental data are shown in Figures 3.17 and 3.18. Adjustment factors were applied in this case to the shear stressed calculated by ANSYS. As may be noticed, when these values of shear force were used as the input external loading to the FEA model, the results of FEA under loading conditions overestimated the shear stresses at the time of initial cracking. As described in the last part of this chapter, for verification purposes of the model, these values of load and shear force were reduced to calibrate the stresses in the web to just prior to initial web cracking.

Incidence of Shear Cracking															
Beam End	Comp. Strength (psi)	First shear crack load (kips)	Corresponding Shear (kips)	7.5*SQRT(f_c')	Shear Stress ANSYS (psi) at dist. h from	Shear Stress ANSYS (psi) at dist. h/2 from	Prestress per Strand (lbf)	Number of Strands	Prestress F_{se} (lbf)	f_t' (psi)	Cross-Sectional Area (in^2)	f_a (psi)	v_{cr} (theoretical) (psi)	v_{cr} (testing) (psi)	Beam End
JJ1 South	11,550	65.23	43.50	806.03	959.33	985.57	25,000	5.00	125,000	429.88	163.25	765.70	716.91	771.52	1
JJ1 North	11,475	68.00	42.30	803.41	1,055.26	1,068.65	25,000	5.00	125,000	428.49	163.25	765.70	715.33	750.24	2
JJ4 South	11,680	65.10	43.40	810.56	973.36	987.71	25,000	5.00	125,000	432.30	163.25	765.70	719.64	769.75	3
ID-10-5-1-N	14,160	54.60	36.40	892.47	791.95	792.64	25,000	4.00	100,000	475.98	163.25	612.56	719.81	645.60	4
ID-10-5-1-S	14,160	66.30	44.20	892.47	831.30	822.11	25,000	5.00	125,000	475.98	163.25	765.70	768.78	783.94	5
IA-6-6-1-S	8,990	79.00	39.50	711.12	872.32	831.75	35,000	2.00	70,000	379.26	163.25	428.79	553.59	700.58	6
IA-6-6-2-N	8,990	44.00	29.30	711.12	702.15	684.16	35,000	3.00	105,000	379.26	163.25	643.19	622.72	519.67	7
IA-10-6-2-S	14,930	73.00	48.70	916.41	751.80	626.38	35,000	2.00	70,000	488.75	163.25	428.79	669.67	863.75	8

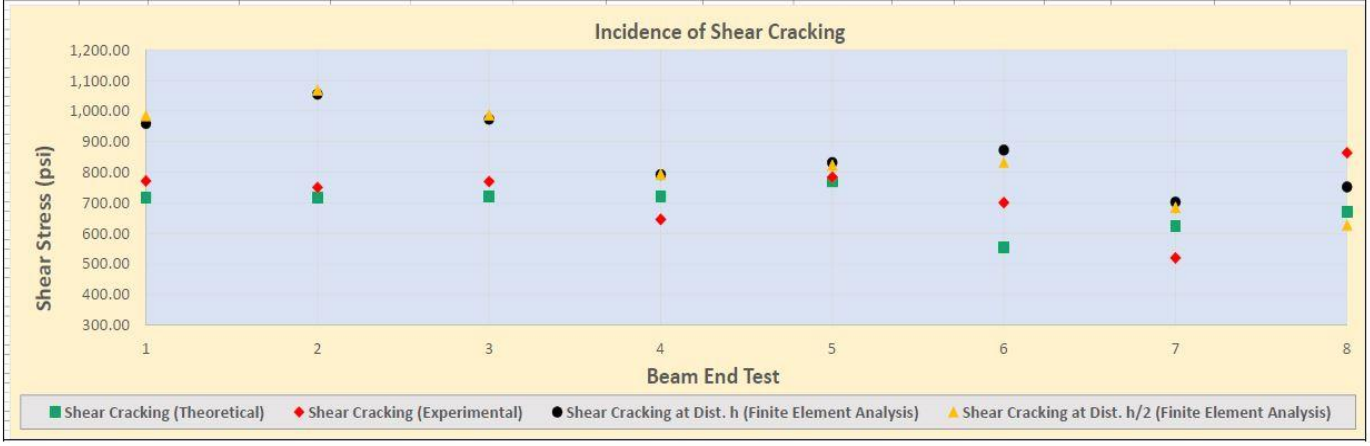

Figure 3.17. Shear Stresses Compared with Results of FEA at Distances h and h/2 from Support

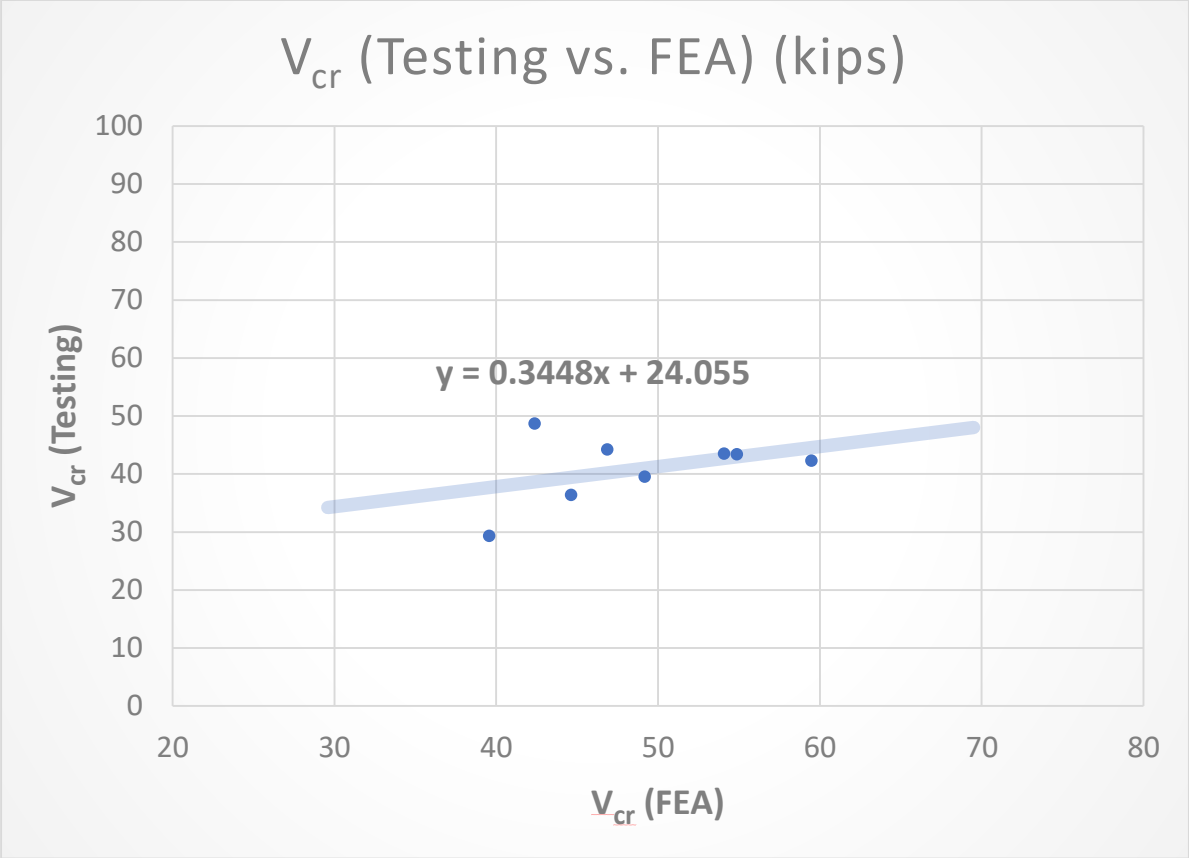

Figure 3.18. FEA Model and Testing Shear Force Comparison

FEA model results (cracking moments) at the incidence of flexural cracking under loading conditions compared to the theoretical and experimental data are shown in Figures 3.19 and 3.20. Adjustment factors were applied in this case to the flexural stressed calculated by ANSYS. In addition, modulus of rupture of concrete and stresses at bottom of beam are shown in Figure 3.21. As described in the last part of this chapter, for verification purposes of the model, these values of load and shear force were reduced to calibrate the stresses in the web to just prior to initial web cracking. Reducing load and shear would also result in reducing the moment in the beam end, which would bring the FEA model results even closer to the testing results.

Incidence of Flexural Cracking											
Beam End	Experimental Cracking Moment M_{cr} (lb-in)	f_r' (psi)	F_{se} (lbf)	A (sq.in.)	e (in)	S_b (in^3)	f_b (psi)	Theoretical M_{cr} (lb-in)	Flexural Stress ANSYS (psi)	M_{cr} (FEA) (lb-in)	Beam End Test
JJ1 South	2,622,400	806	125,000	163.25	3.35	899.71	-1,231.12	1,832,854	2,934.74	3,365,616	1
JJ1 North	2,860,000	803	125,000	163.25	3.35	899.71	-1,231.12	1,830,495	3,334.69	3,723,101	2
JJ4 South	2,644,400	811	125,000	163.25	3.35	899.71	-1,231.12	1,836,923	2,972.49	3,403,651	3
ID-10-5-1-N	2,142,800	892	100,000	163.25	11.25	899.71	-1,862.96	2,479,090	2,068.11	2,663,669	4
ID-10-5-1-S	1,876,667	892	125,000	163.25	4.55	899.71	-1,397.84	2,060,622	1,666.17	2,302,035	5
IA-6-6-1-S	2,153,333	711	70,000	163.25	11.75	899.71	-1,342.97	1,848,089	3,068.98	3,401,000	6
IA-6-6-2-N	1,936,000	711	105,000	163.25	11.75	899.71	-2,014.46	2,452,232	1,534.09	2,020,038	7
IA-10-6-2-S	1,713,333	916	70,000	163.25	11.75	899.71	-1,342.97	2,032,796	2,347.73	2,936,787	8

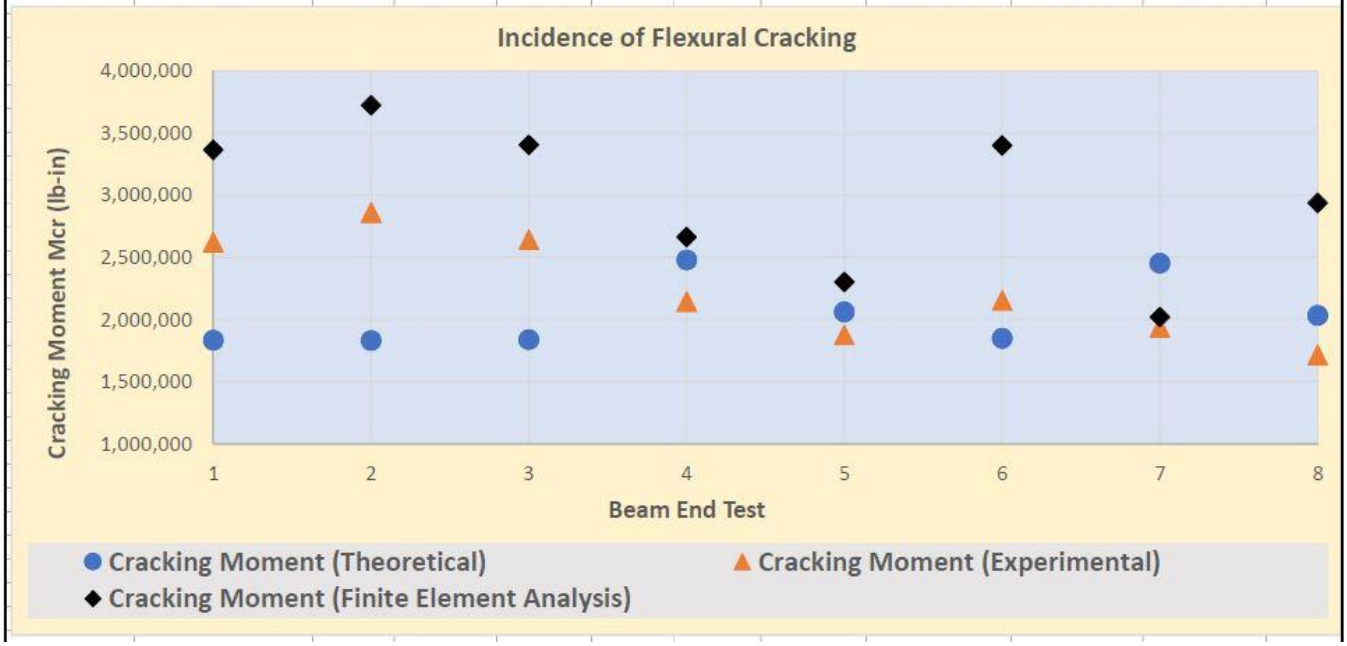

Figure 3.19. Moments Compared with Results of FEA

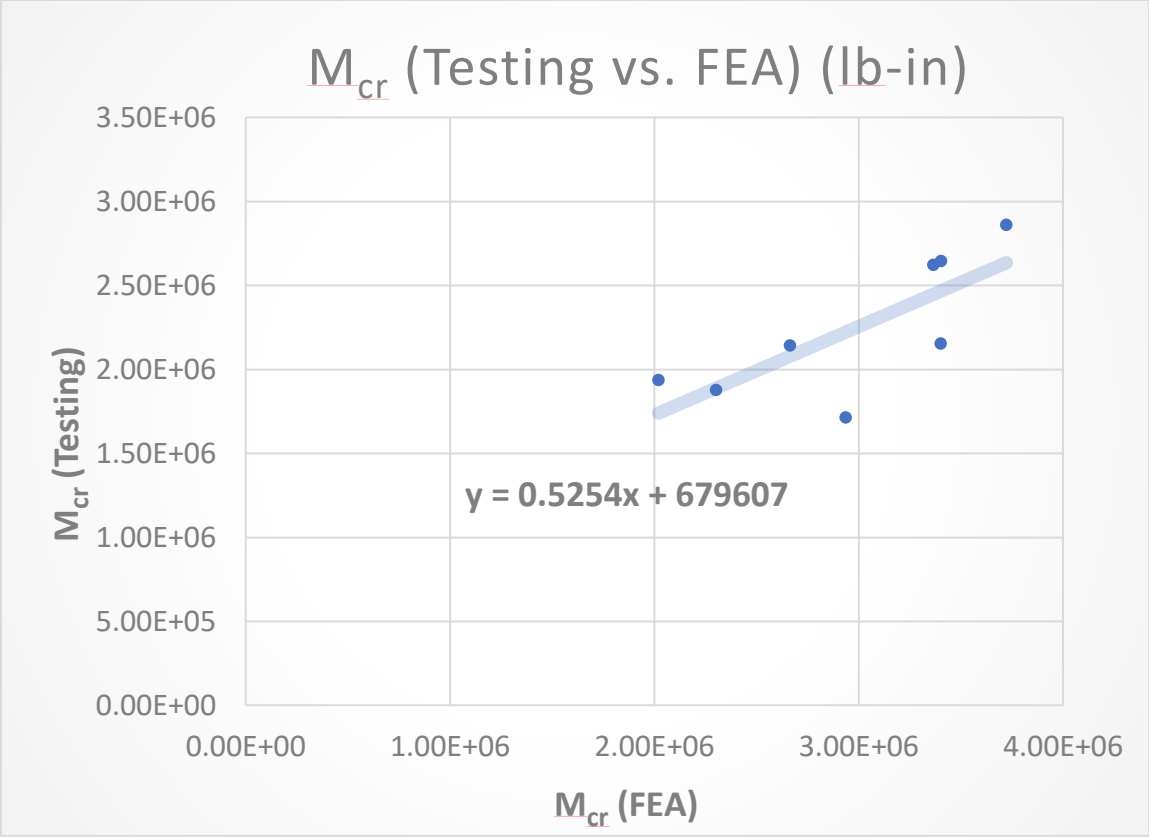

Figure 3.20. FEA Model and Testing Cracking Moment Comparison

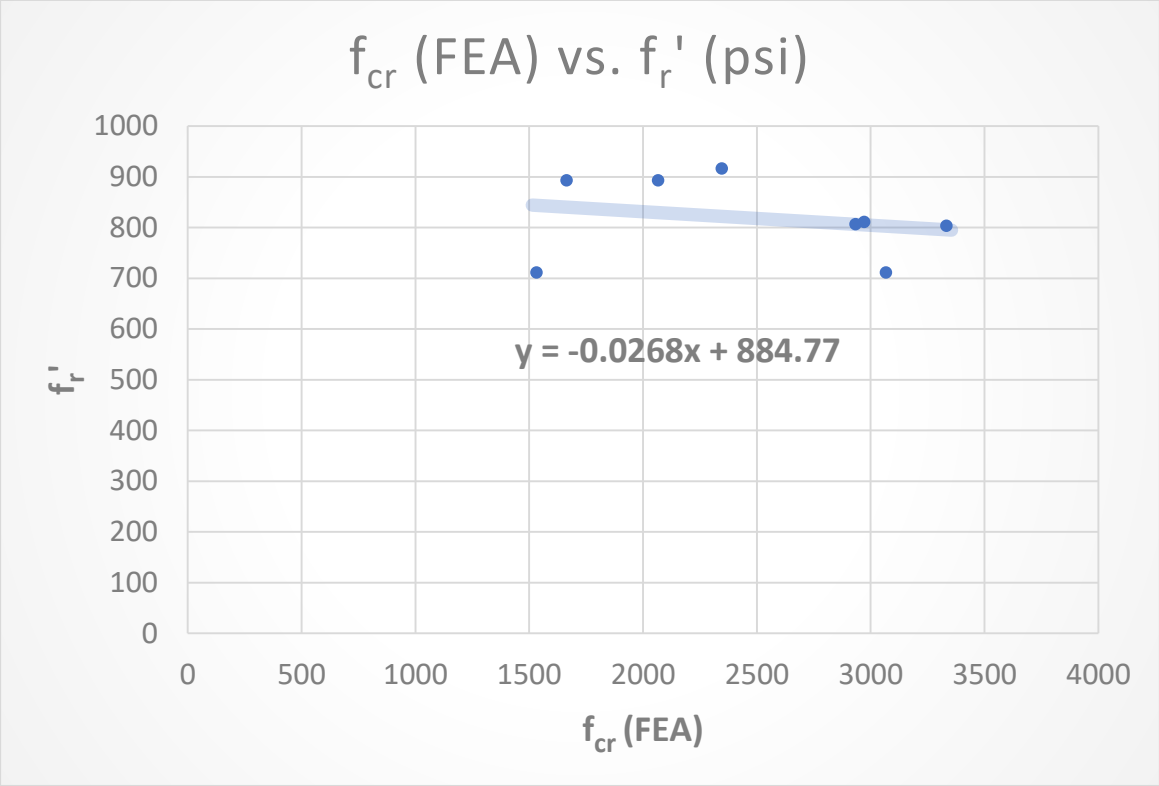

Figure 3.21. FEA Model Stresses at Bottom of Beam and Modulus of Rupture Comparison

Table 3.8 shows average principal S1 (tensile) stresses in 3-dimensional beam space for the strand transfer zone. This and the other tables representing stresses in the transfer zones are generated based on the loads provided in Table 3.5. The experimental testing by Jacob (1998) and Ganpatye (2006) showed there were no strand slips yet occurring at the time when the initial cracking would occur in the beam during load testing. This and the other tables representing stresses in the transfer zones generally show tensile stresses to be less than those that could cause slips in the transfer zones, thus showing the FEA model to provide agreeable results when compared to experimental testing. Blank spaces in the following tables had no transfer lengths reported in the experimental testing program.

Table 3.8. Average Principal S1 (Tensile) Stresses in X, Y, Z Coordinate System for Each Selection (Units: psi)

Beams from Experimental Program (At Testing)					
Beam End	**Strand A**	**Strand B**	**Strand C**	**Strand D**	**Strand E**
JJ1 South	101.74	413.99	434.34	325.30	435.04
JJ1 North	122.88	390.29	409.83	276.14	418.24
JJ4 South	114.01	358.36	365.54	238.06	374.59
ID-10-5-1-N		292.82	274.70	164.95	298.12
ID-10-5-1-S	619.35	456.51	367.25	481.26	381.50
IA-6-6-1-N					
IA-6-6-1-S	762.46				837.58
IA-6-6-2-N			200.12	117.50	208.89
IA-10-6-2-S	557.58		481.89		
Beams from Experimental Program (At Release)					
Beam End	**Strand A**	**Strand B**	**Strand C**	**Strand D**	**Strand E**
JJ3 North	113.97	118.05	120.74	42.42	132.05
JJ4 South	131.79	144.75	146.18	47.56	160.57
JJ4 North	86.91	83.58	86.87	33.55	94.44
IB-6-5-1-N	133.74	156.20	148.30	64.80	185.49
IB-6-5-1-S	298.25	314.48	-141.69	80.99	345.15
ID-6-5-1-N	68.25	78.81	117.56	41.79	118.43
ID-6-5-1-S	97.15	234.08	-180.20		199.24

Figure 3.22 shows the selection nodes for beam end JJ1 South transfer zone under loading modeled as an element and providing results for the 3-dimensional principal S1 (tensile) stresses in X, Y and Z coordinate system.

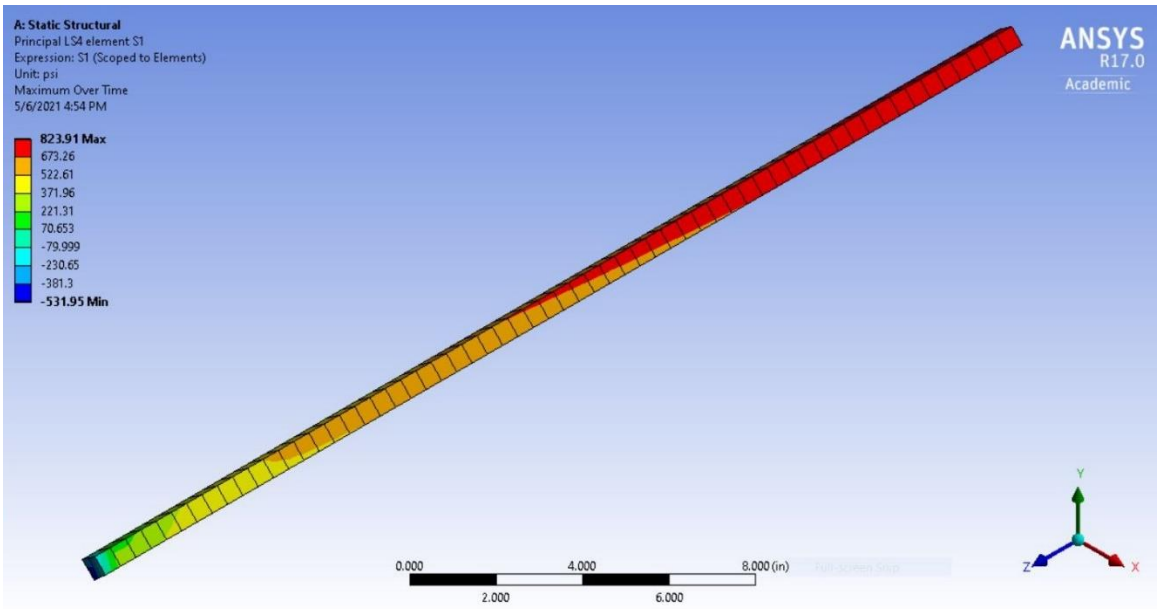

Figure 3.22. Principal S1 (Tensile or Positive Having "+" Sign) Stresses at Strand B Transfer Length for Beam End JJ1 South at Loading

The results for the YZ plane provided in the following Tables relatively closely resemble 3-dimensional principal stress data. Following plane stress equations were used to determine principal stresses from the normal stresses in Y and Z directions and shear stress in the YZ plane computed by ANSYS Workbench for each node in the transfer zone selection.

Maximum principal stress S1 (Tensile)

$$S1 = \frac{S_Y + S_Z}{2} + \sqrt{\left(\frac{S_Y - S_Z}{2}\right)^2 + {\tau_{YZ}}^2}$$

Minimum principal stress S3 (Compressive)

$$S3 = \frac{S_Y + S_Z}{2} - \sqrt{\left(\frac{S_Y - S_Z}{2}\right)^2 + {\tau_{YZ}}^2}$$

Principal angle (ϑp)

$$\theta p = \frac{\arctan\left(\frac{2\tau_{YZ}}{S_Y - S_Z}\right)}{2}$$

Maximum shear stress angle (θs)

$$\theta S = \frac{\arctan\left(-\frac{S_Y - S_Z}{2\tau_{YZ}}\right)}{2}$$

Maximum shear stress (τ_{MAX})

$$\tau_{MAX} = \sqrt{\left(\frac{S_Y - S_Z}{2}\right)^2 + {\tau_{YZ}}^2}$$

Table 3.9. Average Principal S1 (Tensile) Stresses in YZ Plane for Each Selection (Units: psi)

Beams from Experimental Program (At Testing)					
Beam End	**Strand A**	**Strand B**	**Strand C**	**Strand D**	**Strand E**
JJ1 South	67.60	296.70	330.10	216.78	308.17
JJ1 North	84.25	220.38	261.17	104.00	232.38
JJ4 South	76.79	195.64	231.95	74.40	202.30
ID-10-5-1-N		184.14	195.26	45.08	138.37
ID-10-5-1-S	576.91	371.65	263.16	414.91	183.40
IA-6-6-1-N					
IA-6-6-1-S	711.05				714.32
IA-6-6-2-N			19.06	-86.92	9.15
IA-10-6-2-S	470.15		401.94		
Beams from Experimental Program (At Release)					
Beam End	**Strand A**	**Strand B**	**Strand C**	**Strand D**	**Strand E**
JJ3 North	4.24	-6.47	31.03	-46.41	5.31
JJ4 South	1.79	-8.53	40.27	-60.40	7.14
JJ4 North	5.50	-5.21	18.83	-30.82	2.12
IB-6-5-1-N	-2.79	-28.36	25.25	-151.20	-4.08
IB-6-5-1-S	-181.77	-235.37	-668.53	-178.04	-95.75
ID-6-5-1-N	-1.71	-14.22	25.90	-35.58	0.04
ID-6-5-1-S	10.54	-102.14	-761.86		0.78

Table 3.10. Average Principal S3 (Compressive) Stresses in YZ Plane for Each Selection (Units: psi)

Beams from Experimental Program (At Testing)					
Beam End	**Strand A**	**Strand B**	**Strand C**	**Strand D**	**Strand E**
JJ1 South	-834.16	-587.97	-347.76	-276.51	-321.74
JJ1 North	-780.13	-726.61	-463.18	-362.46	-427.71
JJ4 South	-750.05	-681.60	-437.97	-331.98	-403.53

ID-10-5-1-N		-521.95	-327.49	-246.13	-402.21
ID-10-5-1-S	-1305.58	-449.38	-417.71	-178.14	-520.67
IA-6-6-1-N					
IA-6-6-1-S	-1513.69				-291.39
IA-6-6-2-N			-547.04	-476.87	-570.52
IA-10-6-2-S	-1345.61		-213.42		
Beams from Experimental Program (At Release)					
Beam End	**Strand A**	**Strand B**	**Strand C**	**Strand D**	**Strand E**
JJ3 North	-239.91	-843.26	-970.04	-906.21	-935.33
JJ4 South	-290.99	-888.01	-1041.73	-961.18	-997.35
JJ4 North	-187.58	-791.41	-888.49	-846.10	-865.44
IB-6-5-1-N	-361.12	-1005.97	-1190.25	-998.94	-1148.45
IB-6-5-1-S	-1512.06	-1669.29	-5723.02	-1821.33	-2018.91
ID-6-5-1-N	-297.40	-899.22	-902.53	-929.23	-883.82
ID-6-5-1-S	-313.84	-966.55	-6313.39		-1084.36

Table 3.11. Average Principal Shear Stresses in YZ Plane for Each Selection (Units: psi)

Beams from Experimental Program (At Testing)					
Beam End	**Strand A**	**Strand B**	**Strand C**	**Strand D**	**Strand E**
JJ1 South	450.88	442.34	338.93	246.65	314.95
JJ1 North	432.19	473.50	362.18	233.23	330.05
JJ4 South	413.42	438.62	334.96	203.19	302.91
ID-10-5-1-N		353.04	261.38	145.61	270.29
ID-10-5-1-S	941.24	410.52	340.43	296.53	352.04
IA-6-6-1-N					
IA-6-6-1-S	1112.37				502.85
IA-6-6-2-N			283.05	194.98	289.83
IA-10-6-2-S	907.88		307.68		
Beams from Experimental Program (At Release)					
Beam End	**Strand A**	**Strand B**	**Strand C**	**Strand D**	**Strand E**
JJ3 North	122.08	418.39	500.54	429.90	470.32
JJ4 South	146.39	439.74	541.00	450.39	502.24
JJ4 North	96.54	393.10	453.66	407.64	433.78
IB-6-5-1-N	179.16	488.81	607.75	423.87	572.19
IB-6-5-1-S	665.15	716.96	2527.24	821.64	961.58
ID-6-5-1-N	147.84	442.50	464.22	446.83	441.93
ID-6-5-1-S	162.19	432.21	2775.77		542.57

Figure 3.23 shows the selection nodes for beam end JJ1 South transfer zone under loading modeled as an element and providing results for the maximum computed shear stresses in YZ plane.

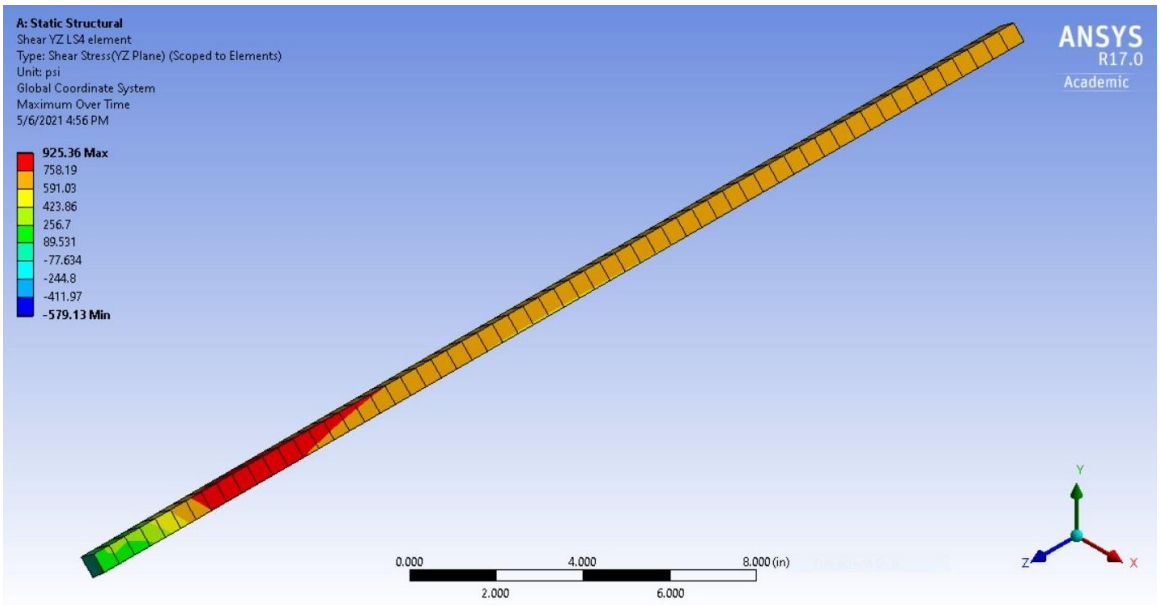

Figure 3.23. Shear Stresses in YZ Plane at Strand B Transfer Length for Beam End JJ1 South at Loading

It is important to emphasize that beams by Jacob (1998) are different from the beams by Ganpatye (2006) in that the beams by John Jacob have external loop while the beams by Ganpatye have bulb reinforcement. This causes the bottom bulb strands in the beams by Ganpatye to be 3-dimensionally more confined than the beams by John Jacob, and ANSYS plain concrete model therefore coincides better with John Jacob beams.

The results regarding the higher concrete strengths, constraint and bottom bulb reinforcement cage all tell us that more confined strands will experience less slip than the beams that have not-so-well confined strands. Bulb reinforcement plays a role in reducing slip even while concrete is still in the elastic and at the end of the elastic region. The fact that potential slips determined in

ANSYS in beams by Ganpatye are equal or exceed those in beams by John Jacob indicate that confining bulb reinforcement plays a significant role even at the incidence of cracking. Reinforcement in the bulb acts similar to using stronger concrete by providing more confinement for the transfer zone of the strands. This is confirmed with the ANSYS FEA model runs using concrete strength as a variable. This was looked into to better understand influences of confinement/constraint.

Orientations of the principal stresses are also found to be different under loading and at release. Bottom central strands are observed to experience shear stresses even in the XY plane (i.e. transverse or plane perpendicular to length of strands) indicating that under certain circumstances torsional effects may also exist that increase the opportunity for strands to slip.

Influence of the beam end support is also recognized in controlling the end slip in the strands. The results indicate and acknowledge that experimental tests are not ideal and not easy to perform due to the cost, variability in the results and time requirements. FEA was determined to be convenient tool to observe, analyze, project, compare and contrast the results obtained through the experimental testing. FEA is more cost efficient and more uniform approach to analyzing different beam configurations with changing variables.

Based on the preliminary results, reducing deflections at the location of the load and reducing slip at the transfer length of the strand (i.e. at the bond) should be good guiding principles when designing prestressed concrete beams. This can be done by considering several variables considered in this study.

Based on the literature reviews, initial results and preliminary findings, there is a number of variables that need to be addressed and researched to determine the influence of each variable on the design of prestressed concrete beams when it comes to controlling cracking in the end

regions of the beams. No single variable alone plays the role in performing the adequate beam design to address the cracking and failures in the end regions. All variables need to be considered, some less and some more.

After validation, the models were later varied for a number of variables to extend through finite element analysis (FEA) the potential results of the beams at release. This model was a plain concrete I-beam model and still gave valuable results with good match to the experimental data. The further value is looked after in constructing the models with steel reinforcement matching that from experimental testing to compare, contract, further project and better quantify the results from the experimental testing.

In order to validate the model, FEA was used to compute the shear force required to cause $f_t' \approx 4\sqrt{fc'}$, where f_c' is the compressive concrete strength at testing, in several successfully analyzed shear spans of Jacob's (1998) and Ganpatye's (2006) experimental programs. Three beam ends were observed from Jacob (1998) and six beam ends were observed from Ganpatye (2006). The values of shear force and f_t', as well as the values of resulting deflections and strains from such shear force at the predicted crack locations are shown in Table 3.12. As may be seen from the Table 3.12, the model is reliable in predicting the values of strains causing the cracking in the beam, as well as correctly predicting the locations where the initial cracking is occurring. Commonly reported values of tensile strain when concrete cracks are generally between 100 and 120 microstrains, whereas the AASHTO LRFD Bridge Design Specifications use 124 microstrains as the theoretical concrete cracking strain.

Table 3.12. Summary of FEA Results for Validation of FEA Model

Beam End	f_t' (psi)	Shear Force in FEA Causing f_t' (kips)	FE Model Deflection (in)	Strain at Predicted Crack Location (microstrains)	Test Locations Where Initial Crack is Predicted	Distance from Beam End Where Initial Crack is Predicted
JJ1 North	428.49	23.27	-0.20	110.7	Line 3, Selec. 3	12
JJ1 South	429.88	25.23	-0.18	103.6	Line 3, Selec. 4	20
JJ4 South	432.30	24.30	-0.20	107.7	Line 3, Selec. 3	12
ID-10-5-1-N	475.98	23.66	-0.15	94.1	Line 3, Selec. 4	20
ID-10-5-1-S	475.98	26.74	-0.14	101.6	Line 3, Selec. 6	36
IA-6-6-1-N	379.26	9.78	-0.18	137.1	Line 3, Selec. 10	72
IA-6-6-1-S	379.26	15.41	-0.18	115.1	Line 3, Selec. 7	44
IA-6-6-2-N	379.26	22.85	-0.16	108.4	Line 3, Selec. 3	12
IA-10-6-2-S	488.75	23.38	-0.16	105.9	Line 3, Selec. 7	44
Average Cracking Strain =				**109.36**	**Average Distance =**	**30.22 in. (2.52 ft)**

Figures 3.24 and 3.25 are shown for illustration purpose and for comparison of the cracking locations. Figure 3.24 representing beam end JJ1 South, shows shear cracking at the bottom of the web (corresponding to Line 3 of FEA model) to start occurring at 20-24 in. from beam end. This agrees well with the maximum shear stress and principal strain determined by FEA at Line 3, Selection 4 which is located at 20 in. from beam end and at 1.5 in. from the bottom of the web. Similarly, Figure 3.25 representing beam end JJ1 North, shows shear cracking at the bottom of the web (corresponding to Line 3 of FEA model) to start occurring at 12-16 in. from beam end. This agrees well with the maximum shear stress and principal strain determined by FEA at Line 3, Selection 3 which is located at 12 in. from beam end and at 1.5 in. from the bottom of the web.

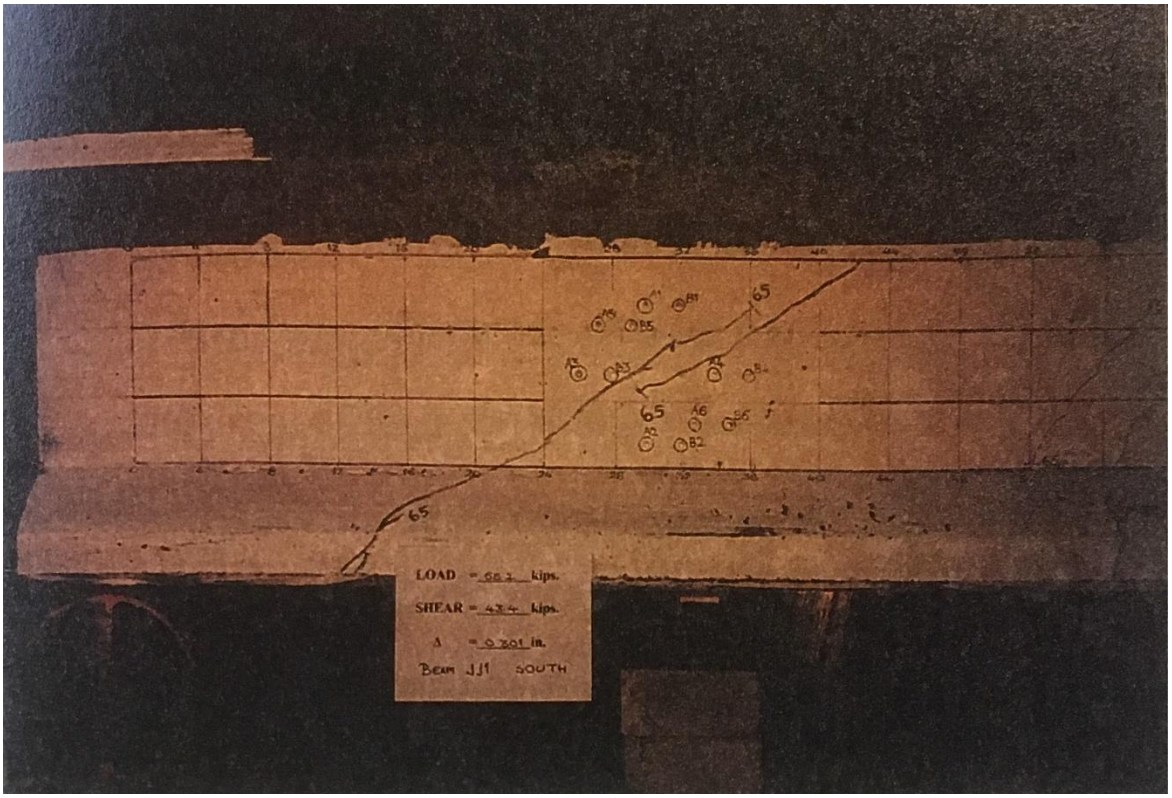

Figure 3.24. Photo of South End of Beam JJ1 Showing First Web Shear Cracking from Jacob (1998)

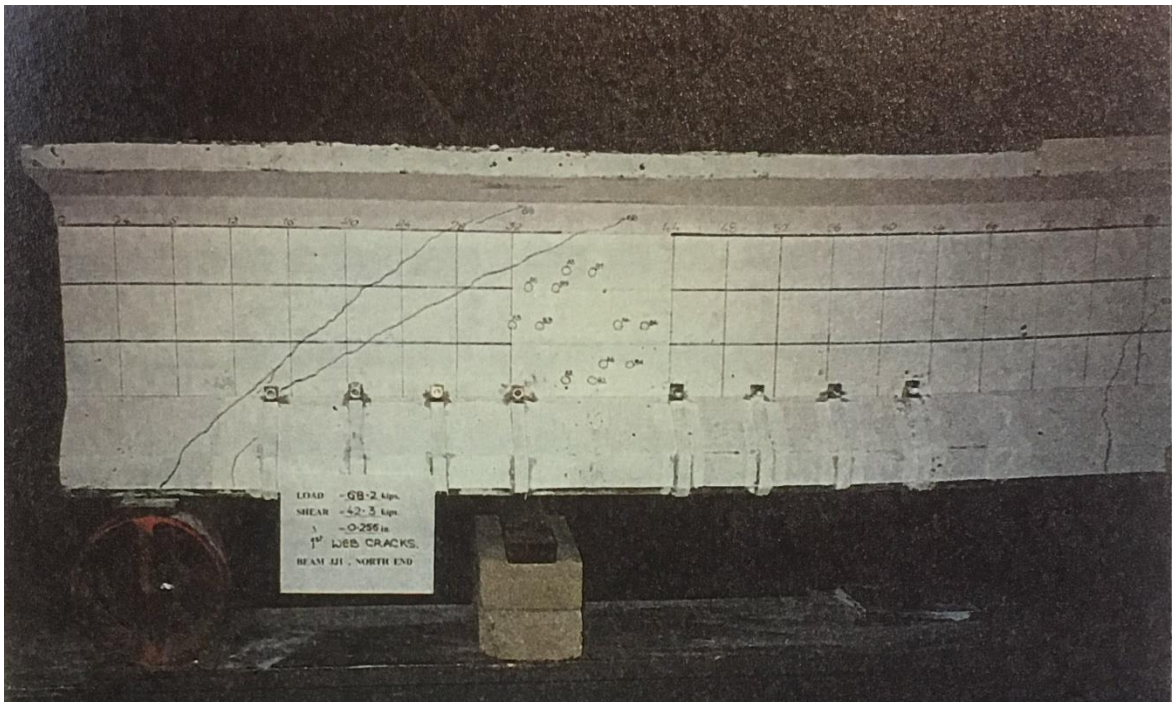

Figure 3.25. Photo of North End of Beam JJ1 Showing First Web Shear Cracking from Jacob (1998)

Provided below in Table 3.13 are the values of the cracking shear force Vcr during testing and from FEA.

Table 3.13. Cracking Shear Force During Testing and from FEA

Beam End	Shear Force V_{cr} from Test (kips)	Shear Force V_{cr} from FEA (kips)	Difference V_{cr} = Test V_{cr} – FEA V_{cr}	Divided V_{cr} (FEA) ÷ V_{cr} (Test)
JJ1 North	43.50	23.27	20.23	0.5349
JJ1 South	42.30	25.23	17.07	0.5965
JJ4 South	38.70	24.30	14.40	0.6279
ID-10-5-1-N	36.40	23.66	12.74	0.6500
ID-10-5-1-S	44.20	26.74	17.46	0.6050
IA-6-6-1-N	33.15	9.78	23.37	0.2950
IA-6-6-1-S	39.50	15.41	24.09	0.3901
IA-6-6-2-N	29.30	22.85	6.45	0.7799
IA-10-6-2-S	48.70	23.38	25.32	0.4801
		Average Difference =	**19.90**	Average = 0.5510 (55.10%)
		Standard Deviation =	**6.12**	
		Reliability =	**65.36%**	

Provided below in Table 3.14 are the values of the deflections under cracking shear force Vcr during testing and from FEA.

Table 3.14. Deflections under Cracking Shear Force During Testing and from FEA

Beam End	Deflection at Cracking from Test (in)	Deflection at Cracking from FEA (in)	Difference of Deflections = Test Deflection – FEA Deflection	Divided Deflection (FEA) ÷ Deflection (Test)
JJ1 North	0.26	0.20	0.06	0.7692
JJ1 South	0.31	0.18	0.13	0.5806
JJ4 South	0.26	0.20	0.06	0.7692
ID-10-5-1-N	1.20	0.15	1.05	0.1250
ID-10-5-1-S	0.48	0.14	0.34	0.2917
IA-6-6-1-N	0.33	0.18	0.15	0.5455
IA-6-6-1-S	0.70	0.18	0.52	0.2571
IA-6-6-2-N	0.50	0.16	0.34	0.3200

IA-10-6-2-S	1.20	0.16	1.04	0.1333
		Average Difference =	**0.41**	Average =
		Standard Deviation =	**0.39**	0.4213
		Reliability =	**65.36%**	(42.13%)

Provided below in Table 3.15 are the values of the strains under cracking shear force Vcr during testing and determined from FEA model at DEMEC strain monitoring locations at 36 in. (DEMEC 1) and 38 in. (DEMEC 2) from the ends of the beams by Jacob (1998), as shown in Figure 3.26. Strain rosettes were centered at 12 in. from the beam bottom. Values of strains were linearly interpolated for values of shear force applied in FEA model required to cause cracking in the web, as shown in Figures 3.27 to 3.29. The values of strains are reported in Tanasap (2015) who reported the strain monitoring data and provided additional analysis to Jacob's (1998) results. Figures 3.27 to 3.29 also provide the shear strain data, and the shear strain data from FEA and from testing is compared in Table 3.16.

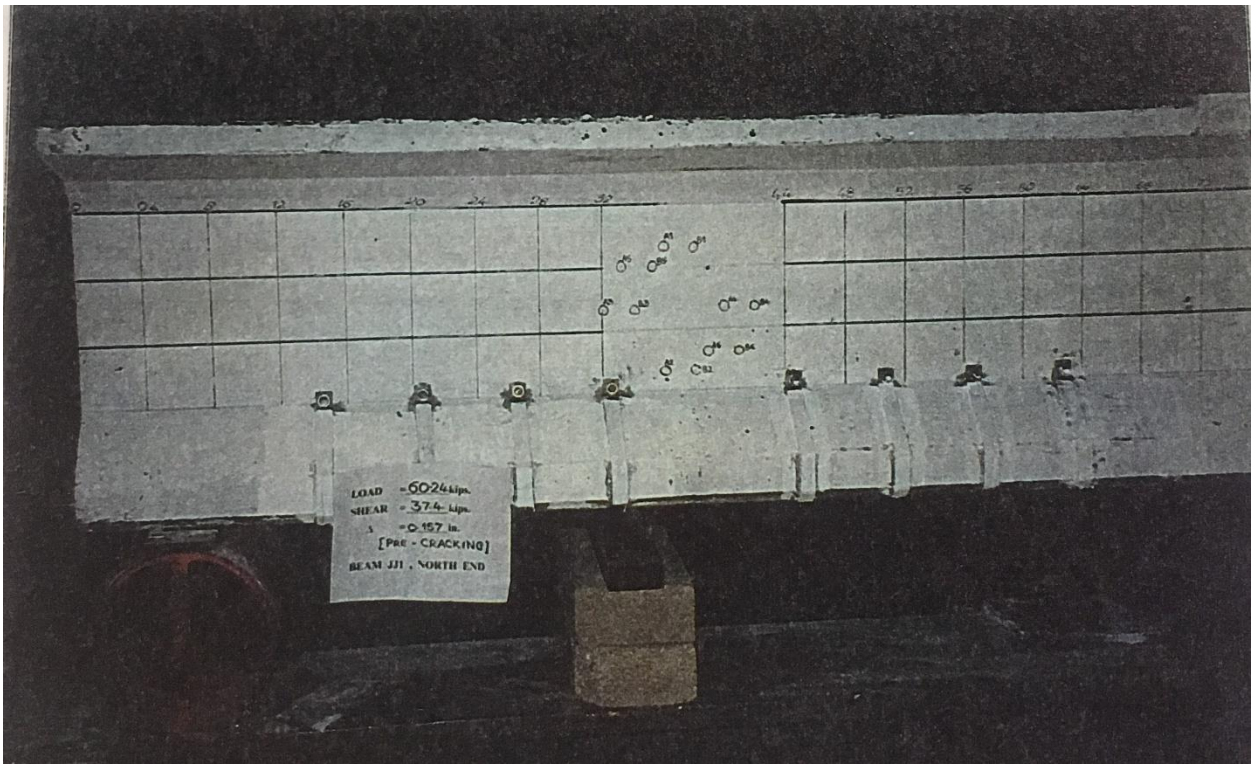

Figure 3.26. Photo of 4 in. Grid on Beam Web Showing DEMEC Target Rosette Pattern from Jacob (1998)

Table 3.15. Principal Strains under Cracking Shear Force during Testing and Determined from FEA Model

Beam End	Principal Strains (FEA) at DEMEC Strain Monitoring Locations	Principal Strains (Testing) at DEMEC Strain Monitoring Locations (Tanasap (2015))	Difference of Strains = Test Strain – FEA Strain	Divided Strain (FEA) ÷ Strain (Test)
JJ1 South DEMEC 1	8.42E-05	8.95E-05	5.25E-06	0.9413
JJ1 South DEMEC 2	8.41E-05	1.06E-04	2.22E-05	0.7913
JJ1 North DEMEC 1	9.31E-05	1.47E-04	5.39E-05	0.6333
JJ1 North DEMEC 2	9.39E-05	2.62E-04	1.68E-04	0.3590

JJ4 South DEMEC 1	8.94E-05	8.53E-05	-4.04E-06	1.0474
JJ4 North DEMEC 2	9.02E-05	7.63E-05	-1.39E-05	1.1826
				Average = 0.6983 (69.83%)

	Shear Force (kips)	Shear Stress (ksi)	At 36 in					At 38 in				
			ε_0 (x10^{-3} in/in)	ε_{90} (x10^{-3} in/in)	ε_{135} (x10^{-3} in/in)	γ_{xy} (x10^{-3})	θ_p (degree)	ε_0 (x10^{-3} in/in)	ε_{90} (x10^{-3} in/in)	ε_{135} (x10^{-3} in/in)	γ_{xy} (x10^{-3})	θ_p (degree)
Pre − Cracking	0.00	0.000	0.000	0.000	0.000	0.000	0.00	0.000	0.000	0.000	0.000	0.00
	4.69	0.083	-0.122	-0.020	0.028	0.199	31.44	-0.126	-0.004	0.020	0.171	27.21
	8.14	0.144	-0.130	-0.016	0.012	0.171	28.12	-0.130	-0.008	0.028	0.195	28.97
	11.96	0.212	-0.126	-0.012	0.045	0.228	31.68	-0.126	-0.008	0.053	0.240	31.87
	15.73	0.279	-0.122	-0.004	0.057	0.240	31.87	-0.118	0.000	0.069	0.256	32.60
	19.76	0.350	-0.122	-0.004	0.057	0.240	31.87	-0.118	0.000	0.077	0.272	33.26
	26.50	0.470	-0.118	0.000	0.097	0.313	34.64	-0.118	0.004	0.113	0.341	35.13
	29.91	0.531	-0.114	-0.008	0.109	0.341	36.36	-0.122	0.004	0.130	0.377	35.75
	33.30	0.591	-0.110	0.000	0.134	0.377	36.87	-0.114	0.004	0.150	0.410	36.95
	35.07	0.622	-0.106	0.008	0.142	0.382	36.67	-0.118	0.012	0.154	0.414	36.26
	36.61	0.649	-0.114	0.004	0.150	0.410	36.95	-0.114	-0.004	0.158	0.434	37.88
	38.21	0.678	-0.102	0.012	0.166	0.422	37.43	-0.114	0.004	0.170	0.450	37.64
	39.76	0.705	-0.106	0.012	0.174	0.442	37.52	-0.110	0.008	0.190	0.483	38.12
	41.33	0.733	-0.102	0.028	0.186	0.446	36.86	-0.110	0.020	0.207	0.503	37.73
	43.49	0.771	-0.094	0.041	0.203	0.458	36.83	-0.098	0.028	0.227	0.523	38.21
Post − Cracking	43.49	0.771	0.611	1.385	1.705	1.414	30.65	0.623	1.320	1.292	0.641	21.29
	45.00	0.798	1.149	2.843	3.815	3.638	32.52	1.162	2.649	3.005	2.200	27.97
	42.06	0.746	1.319	3.281	4.285	3.970	31.86	1.368	3.447	4.196	3.577	29.92
	43.15	0.765	1.542	3.390	4.577	4.221	33.18	1.575	3.617	4.572	3.954	31.34
	42.51	0.754	1.336	3.054	4.119	3.848	32.97	1.360	3.353	4.577	4.440	32.91
	37.93	0.673	1.222	2.977	3.977	3.755	32.48	1.234	3.305	4.022	3.504	29.71
	38.48	0.683	1.226	3.009	4.026	3.816	32.48	1.234	3.353	3.317	2.046	22.00
	38.85	0.689	1.198	3.005	3.985	3.767	32.19	1.206	3.357	3.321	2.078	22.01
	39.47	0.700	1.182	3.001	3.985	3.788	32.17	1.198	3.370	4.046	3.524	29.18

Figure 3.27. Strain Gauge Monitoring Data Reported by Tanasap (2015) for JJ1 South Beam End

	Shear Force (kips)	Shear Stress (ksi)	At 36 in					At 38 in				
			ε_0 (x10^{-3} in/in)	ε_{90} (x10^{-3} in/in)	ε_{135} (x10^{-3} in/in)	γ_{xy} (x10^{-3})	θ_p (degree)	ε_0 (x10^{-3} in/in)	ε_{90} (x10^{-3} in/in)	ε_{135} (x10^{-3} in/in)	γ_{xy} (x10^{-3})	θ_p (degree)
Pre − Cracking	0.00	0.000	0.000	0.000	0.000	0.000	0.00	0.000	0.000	0.000	0.000	0.00
	9.31	0.165	-0.082	0.081	0.101	0.203	25.66	-0.062	0.069	0.130	0.252	31.32
	12.35	0.219	-0.082	0.065	0.105	0.228	28.61	-0.074	0.073	0.219	0.438	35.75
	15.52	0.275	-0.078	0.069	0.117	0.244	29.49	-0.058	0.057	0.231	0.463	38.06
	18.81	0.334	-0.078	0.061	0.122	0.260	30.98	-0.070	0.069	0.243	0.487	37.06
	21.92	0.389	-0.074	0.057	0.142	0.301	33.27	-0.070	0.065	0.255	0.515	37.69
	25.14	0.446	-0.074	0.057	0.154	0.325	34.06	-0.062	0.073	0.271	0.531	37.90
	28.06	0.498	-0.090	0.057	0.162	0.357	33.84	-0.053	0.065	0.296	0.580	39.24
	31.12	0.552	-0.070	0.061	0.174	0.357	34.97	-0.053	0.065	0.296	0.580	39.24
	34.27	0.608	-0.078	0.057	0.190	0.402	35.75	-0.049	0.069	0.304	0.588	39.31
	37.37	0.663	-0.078	0.053	0.203	0.430	36.57	-0.049	0.065	0.324	0.633	39.88
	40.32	0.715	-0.078	0.061	0.223	0.463	36.66	-0.045	0.073	0.344	0.661	39.93
Post − Cracking	42.34	0.751	-0.147	0.069	0.178	0.434	31.80	-0.118	0.085	0.304	0.641	36.20
	40.35	0.716	-0.163	0.053	0.182	0.475	32.79	-0.134	0.077	0.312	0.681	36.38
	35.08	0.622	-0.118	0.065	0.146	0.345	31.03	-0.102	0.077	0.292	0.608	36.80

Figure 3.28. Strain Gauge Monitoring Data Reported by Tanasap (2015) for JJ1 North Beam End

	Shear Force (kips)	Shear Stress (ksi)	At 36 in					At 38 in				
			ε_0 (x10^{-3} in/in)	ε_{90} (x10^{-3} in/in)	ε_{135} (x10^{-3} in/in)	γ_{xy} (x10^{-3})	θ_p (degree)	ε_0 (x10^{-3} in/in)	ε_{90} (x10^{-3} in/in)	ε_{135} (x10^{-3} in/in)	γ_{xy} (x10^{-3})	θ_p (degree)
Pre – Cracking	0.00	0.000	0.000	0.000	0.000	0.000	0.00	0.000	0.000	0.000	0.000	0.00
	4.55	0.081	-0.110	-0.016	0.016	0.159	29.69	-0.139	0.008	0.004	0.139	21.69
	7.19	0.128	-0.110	-0.041	0.024	0.199	35.37	-0.139	0.000	0.012	0.163	24.81
	10.21	0.181	-0.106	-0.024	0.032	0.195	33.63	-0.118	0.000	0.020	0.159	26.66
	13.40	0.238	-0.110	-0.020	0.041	0.211	33.48	-0.143	0.000	0.036	0.215	28.25
	16.90	0.300	-0.106	0.004	0.053	0.207	31.01	-0.139	0.004	0.045	0.224	28.74
	20.11	0.357	-0.106	-0.016	0.061	0.244	34.88	-0.130	0.004	0.053	0.232	29.93
	23.39	0.415	-0.102	0.000	0.081	0.264	34.43	-0.130	0.012	0.073	0.264	30.82
	26.74	0.474	-0.098	0.012	0.097	0.280	34.27	-0.126	0.000	0.085	0.296	33.46
	30.02	0.532	-0.102	0.008	0.105	0.305	35.06	-0.126	0.004	0.097	0.317	33.81
	33.42	0.593	-0.094	0.012	0.122	0.325	35.95	-0.122	0.000	0.109	0.341	35.13
	36.71	0.651	-0.094	0.020	0.150	0.373	36.50	-0.122	0.004	0.126	0.369	35.56
	40.06	0.711	-0.090	0.053	0.170	0.377	34.65	-0.118	0.020	0.150	0.398	35.40
	43.39	0.770	-0.070	0.085	0.203	0.390	34.17	-0.114	0.032	0.186	0.454	36.06
Post – Cracking	43.39	0.770	0.420	1.183	1.337	1.070	27.27	0.060	1.187	1.373	1.499	26.54
	45.36	0.805	0.514	1.438	1.519	1.086	24.80	0.121	1.369	1.571	1.653	26.47
	46.70	0.828	0.732	1.656	1.802	1.216	26.38	0.372	1.519	1.827	1.763	28.47
	48.57	0.861	1.076	2.426	2.442	1.382	22.84	0.708	2.341	2.681	2.313	27.39
	50.02	0.887	1.579	3.329	3.256	1.605	21.26	1.255	3.378	4.038	3.443	29.17
	52.03	0.923	1.757	3.613	4.248	3.127	29.66	1.627	3.722	4.686	4.022	31.25
	53.42	0.947	2.057	3.750	4.706	3.605	32.42	2.077	3.929	5.330	4.654	34.15
	53.79	0.954	2.024	3.714	4.658	3.577	32.36	2.053	3.888	5.257	4.573	34.07
	54.55	0.968	2.040	3.779	4.739	3.658	32.29	2.081	3.981	5.378	4.695	33.98
	54.97	0.975	2.040	3.819	4.783	3.707	32.18	2.089	3.989	5.411	4.743	34.08
	0.00	0.000	0.542	1.523	1.478	0.892	21.14	0.465	1.413	1.624	1.370	27.65

Figure 3.29. Strain Gauge Monitoring Data Reported by Tanasap (2015) for JJ4 South Beam End

Table 3.16. Shear Strains under Cracking Shear Force during Testing and Determined from FEA Model

Beam End	Shear Strains (FEA) at DEMEC Strain Monitoring Locations	Shear Strains (Testing) at DEMEC Strain Monitoring Locations	Difference of Shear Strains = Test Shear Strain – FEA Shear Strain	Divided Shear Strain (FEA) ÷ Shear Strain (Test)
JJ1 South DEMEC 1	2.60E-04	2.99E-04	3.92E-05	0.8691
JJ1 South DEMEC 2	2.62E-04	3.28E-04	6.61E-05	0.7984
JJ1 North DEMEC 1	2.84E-04	3.11E-04	2.74E-05	0.9120
JJ1 North DEMEC 2	2.85E-04	5.22E-04	2.37E-04	0.5455
JJ4 South DEMEC 1	2.76E-04	2.68E-04	-7.25E-06	1.0270
JJ4 North DEMEC 2	2.77E-04	2.73E-04	-4.24E-06	1.0156
				Average = 0.8209 (82.09%)

In addition to these values, the maximum shear stresses at the Neutral Axis (Line 2) calculated by FEA model at the time of cracking, are found to compare well with the values for the equal shear force as reported by Tanasap (2015). These values are compared in Table 3.17.

Table 3.17. Shear Stresses under Cracking Shear Force during Testing and Determined from FEA Model

Beam End	Shear Stress (FEA) (psi)	Shear Stress (Testing) (psi), Reported in Tanasap (2015)	Difference of Shear Stresses = Test Shear Stress – FEA Shear Stress	Divided Shear Stress (FEA) ÷ Shear Stress (Test)
JJ1 South	429.88	447.39	-17.51	0.96
JJ1 North	428.49	412.90	15.59	1.04
JJ4 South	432.30	431.03	1.27	1.00
				Average = 1.00 (100.05 %)

In summary, the FEA model is providing adequate results as confirmed through testing results, including in part the shear force measurements, deflection measurements and strain gauge measurements. No FEA model is perfect and many models have certain shortcomings in matching the experimental program results, due in part that many models can have variations in the inputs that sometimes don't exactly match the verification program variables, whereas the experimental program depends on the variability and quality control in building and testing of the specimens. Based on these results and these multiple comparisons of the experimental programs with the FEA results, it may be said that the FEA model is verified and can be used within a reasonable measure of confidence.

Based on the results of the experimental testing and comparing it with the ANSYS results for experimental testing and at release condition we can better understand the impacts of different variables based on the tensile stresses they impart on the ends of the beams. That was one of the major goals of this study.

Different neoprene pad dimensions were used for the modeling of beams under loading for looking at shear, flexure and deflections, and for beams under release conditions for looking at web test locations. 2-inch long neoprene pad was found to be significantly better match than 6-inch long pad for comparison with real world results and theory applying to 3/8 scale beam model.

CHAPTER IV

RESULTS AND CONCLUSIONS

This chapter describes the results obtained from FEA that incorporate the variables described above. The data will show that the variations in strand patterns and the variations in the bond qualify of prestressing strands affect the stresses in end regions of pre-tensioned, prestressed beams. In general, the results indicate that improving strand bond quality (higher bond values with the ASTM A1081 test, or higher concrete strengths) will generally result in higher tensile stresses in end regions. It was also found when looking into the effects of varying concrete strength that on the average about 55% of the increase in tensile stresses is caused by the increased modulus of elasticity, whereas about 45% of the tensile stress increase is due to the bond effects. Additionally, the results indicate that debonding of some prestressing strands has the effect of reducing tensile stresses near the bottom of the webs of I-shaped beams. The addition of fully-tensioned top strands tended to increase tensile stresses at the N.A., but these effects were mitigated substantially by using fully tensioned top strands together with debonding, or shielding of bottom strands.

Results for all 35 cases analyzed in ANSYS are summarized in the Tables shown below. The results are reported primarily as stresses, and not strains, which is deemed sufficient for the purposes of this study, since tensile stresses close to $f_t' \approx 4\sqrt{fc'}$ are understood to be significant and can cause cracking. Since the FEA modeling is performed in the linear elastic region, Hooke's Law is applicable and it would be very simple to correlate stresses to strains through

Hooke's Law and provided values of modulus of elasticity. Strains computed by using Hooke's Law closely match those computed by the FEA models for various cases at test locations, which is one more proof of the validity of the model. In general tensile strains were not higher than about 118 microstrains. Strains were also used in validating the model by comparing the strains in the FEA model to those for DEMEC gauges reported by Tanasap (2015). This Chapter IV provides some figures of stress results for the purpose of comparison. These and remaining figures are provided also in the Appendix.

Table 4.1 shows the principal stresses in vertical YZ-plane at the Neutral Axis for all 35 studied cases. The maximum tensile strain corresponding to these stresses was 118 microstrains. The ANSYS figures and plots associates with these cases are provided in the Appendix.

Table 4.1. Maximum Principal Stress Results (psi) along Neutral Axis (Line 2) from ANSYS FEA

Ansys Case No.	Strand Size	ASTM 1081	f'ci	"Measured" Transfer Length (in)	Smax, Line 2 (psi) Distance from Beam End, z (in.)				
		(lbs)	(ksi)		2	4	6	8	12
1	0.5	9000	6	29.36	112.34	60.20	37.74	26.39	9.84
2	0.5	12000	6	24.77	172.10	92.45	49.52	23.37	-15.13
3	0.5	18000	6	19.37	249.67	129.81	52.95	0.12	-68.81
4	0.6	14400	6	27.41	202.11	112.58	69.34	45.46	10.52
5	0.6	21600	6	21.41	324.16	176.67	87.30	27.75	-57.32
6	0.6	28800	6	19.30	395.57	207.66	83.41	-3.40	-109.66
7	0.5	9000	10	25.32	185.90	104.49	56.09	25.20	-16.78
8	0.5	12000	10	20.14	246.97	137.26	64.93	14.10	-55.12
9	0.5	18000	10	18.66	312.95	166.61	61.65	-15.65	-100.64
10	0.6	14400	10	24.00	317.89	183.76	99.28	42.09	-37.56
11	0.6	21600	10	19.48	424.77	236.63	105.56	9.33	-112.63
12	0.6	28800	10	18.63	486.58	259.61	94.33	-27.04	-148.99
13	0.5	9000	4	34.64	86.09	45.68	29.62	22.42	13.35
14	0.5	12000	4	27.43	138.92	75.98	44.19	26.40	2.12
15	0.5	18000	4	21.28	225.04	122.87	121.32	16.18	-43.88
19	0.5	9000	4	34.72	159.60	91.91	51.28	26.47	0.77
20	0.5	12000	4	27.56	191.65	106.38	59.39	31.70	-2.96
21	0.6	14400	6	27.53	284.80	160.46	93.05	53.36	1.61
22	0.6	21600	6	22.04	438.66	239.22	114.35	28.93	-88.98
23	0.6	28800	6	19.59	530.17	272.55	101.86	-18.32	-159.32
24	0.6	14400	6	24.35	260.43	157.21	98.65	61.89	10.43
25	0.6	21600	6	16.88	403.86	238.03	128.95	48.83	-69.21
26	0.6	28800	6	11.56	487.08	273.47	125.53	13.95	-130.34
27	0.6	14400	6	24.53	177.68	108.12	72.71	51.91	18.89
28	0.6	21600	6	17.04	289.89	175.96	101.60	47.33	-36.73
29	0.6	28800	6	11.63	353.52	210.55	108.68	29.93	-80.73
21	0.6	14400	6	27.53	284.80	160.46	93.05	53.36	1.61
21A	0.6	14400	6	30.07	223.70	137.38	94.30	68.28	27.94
21B	0.6	14400	6	32.70	163.39	114.25	95.05	82.32	52.39
24	0.6	14400	6	24.35	260.43	157.21	98.65	61.89	10.43
24A	0.6	14400	6	26.89	203.89	131.83	94.85	71.88	34.21
24B	0.6	14400	6	29.52	148.07	106.83	91.28	81.42	56.05
25	0.6	21600	6	16.88	403.86	238.03	128.95	48.83	-69.21
25A	0.6	21600	6	19.42	334.04	211.46	133.37	74.63	-24.24
25B	0.6	21600	6	22.05	260.23	181.02	135.13	98.12	20.48

Table 4.2 shows the principal stresses in vertical YZ-plane at Line 3, for all 35 studied cases. The maximum tensile strain corresponding to these stresses was 104 microstrains. The ANSYS figures and plots associates with these cases are provided in the Appendix.

Table 4.2. Maximum Principal Stress Results (psi) along Line 3 from ANSYS FEA

Ansys Case No.	Strand Size	ASTM 1081	f'ci	"Measured" Transfer Length (in)	Smax, Line 3 (psi) Distance from Beam End, z (in.)				
		(lbs)	(ksi)		2	4	6	8	12
1	0.5	9000	6	29.36	124.01	172.40	167.16	138.82	75.56
2	0.5	12000	6	24.77	169.56	209.69	189.92	146.03	55.60
3	0.5	18000	6	19.37	233.87	246.58	196.45	122.40	-18.45
4	0.6	14400	6	27.41	208.03	272.80	256.62	206.85	101.55
5	0.6	21600	6	21.41	307.18	344.01	291.04	203.68	31.94
6	0.6	28800	6	19.30	369.81	372.01	283.51	160.81	-50.70
7	0.5	9000	10	25.32	169.21	189.18	165.20	124.57	45.83
8	0.5	12000	10	20.14	222.19	221.22	176.09	114.84	-0.54
9	0.5	18000	10	18.66	283.00	238.95	155.22	58.57	-62.46
10	0.6	14400	10	24.00	287.45	300.76	251.46	179.37	44.70
11	0.6	21600	10	19.48	385.01	348.43	252.14	134.41	-66.58
12	0.6	28800	10	18.63	443.17	350.82	205.52	53.21	-85.02
13	0.5	9000	4	34.64	97.87	139.98	138.55	118.00	70.90
14	0.5	12000	4	27.43	137.05	175.06	163.68	132.10	65.93
15	0.5	18000	4	21.28	207.18	223.84	186.86	129.48	18.12
19	0.5	9000	4	34.72	133.61	134.40	116.77	93.15	52.58
20	0.5	12000	4	27.56	170.70	197.66	177.19	139.14	66.06
21	0.6	14400	6	27.53	258.73	305.82	274.91	214.95	99.53
22	0.6	21600	6	22.04	387.75	396.37	320.08	213.89	17.52
23	0.6	28800	6	19.59	468.52	434.97	315.66	166.84	-159.32
24	0.6	14400	6	24.35	233.50	258.50	225.23	169.50	64.31
25	0.6	21600	6	16.88	362.23	330.26	247.60	145.80	-33.58
26	0.6	28800	6	11.56	441.71	352.10	225.37	87.09	-114.68
27	0.6	14400	6	24.53	177.31	224.54	207.83	163.22	68.26
28	0.6	21600	6	17.04	271.97	276.82	220.45	138.51	-17.41
29	0.6	28800	6	11.63	331.41	288.45	195.78	83.77	-89.91
21	0.6	14400	6	27.53	258.73	305.82	274.91	214.95	99.53
21A	0.6	14400	6	30.07	219.29	283.59	267.97	221.41	121.85
21B	0.6	14400	6	32.70	177.02	261.36	261.11	226.17	141.55
24	0.6	14400	6	24.35	233.50	258.50	225.23	169.50	64.31
24A	0.6	14400	6	26.89	193.97	243.26	226.29	182.39	89.32
24B	0.6	14400	6	29.52	155.94	225.76	225.80	193.36	111.70
25	0.6	21600	6	16.88	362.23	330.26	247.60	145.80	-33.58
25A	0.6	21600	6	19.42	307.26	322.36	266.39	183.03	19.45
25B	0.6	21600	6	22.05	249.00	306.59	279.55	215.06	69.93

Table 4.3 shows the shear stresses in vertical YZ-plane at Line 3, for all 35 studied cases. The maximum tensile strain corresponding to these stresses was 105 microstrains. The ANSYS figures and plots associates with these cases are provided in the Appendix.

Table 4.3. Shear Stress Results (psi) along Line 3 from ANSYS FEA

Ansys Case No.	Strand Size	ASTM 1081 (lbs)	f'ci (ksi)	"Measured" Transfer Length (in)	Syz, Line 3 (psi) Distance from Beam End, z (in.) 2	4	6	8	12
1	0.5	9000	6	29.36	189.45	238.64	214.47	181.04	144.19
2	0.5	12000	6	24.77	211.50	269.90	246.65	211.05	165.48
3	0.5	18000	6	19.37	238.38	307.95	282.70	238.67	170.09
4	0.6	14400	6	27.41	279.46	350.90	314.18	264.44	209.13
5	0.6	21600	6	21.41	325.96	416.47	379.80	322.14	236.53
6	0.6	28800	6	19.30	353.46	454.41	412.13	340.81	239.54
7	0.5	9000	10	25.32	173.04	229.16	220.60	198.87	166.86
8	0.5	12000	10	20.14	193.66	258.69	249.96	223.72	174.26
9	0.5	18000	10	18.66	214.33	287.69	272.91	235.38	183.44
10	0.6	14400	10	24.00	258.13	340.83	326.66	292.84	239.21
11	0.6	21600	10	19.48	295.96	394.25	375.71	327.14	243.43
12	0.6	28800	10	18.63	317.78	422.66	392.84	336.28	252.39
13	0.5	9000	4	34.64	158.45	201.49	183.24	156.41	127.21
14	0.5	12000	4	27.43	177.76	229.07	212.37	184.83	151.78
15	0.5	18000	4	21.28	207.29	271.30	255.24	223.16	171.72
19	0.5	9000	4	34.72	102.97	146.63	156.43	155.24	148.60
20	0.5	12000	4	27.56	173.77	229.50	221.67	201.26	173.73
21	0.6	14400	6	27.53	269.85	348.09	326.39	288.81	242.88
22	0.6	21600	6	22.04	324.57	425.45	404.83	358.57	276.80
23	0.6	28800	6	19.59	357.82	471.14	444.51	382.53	278.99
24	0.6	14400	6	24.35	194.96	250.69	230.33	198.65	162.30
25	0.6	21600	6	16.88	215.58	283.68	265.58	230.28	178.44
26	0.6	28800	6	11.56	219.89	293.98	276.09	238.16	193.14
27	0.6	14400	6	24.53	204.58	253.49	218.12	174.29	128.56
28	0.6	21600	6	17.04	216.97	274.70	240.54	193.85	138.18
29	0.6	28800	6	11.63	215.53	277.26	243.71	196.44	153.69
21	0.6	14400	6	27.53	269.85	348.09	326.39	288.81	242.88
21A	0.6	14400	6	30.07	252.94	314.31	293.63	262.79	229.45
21B	0.6	14400	6	32.70	233.32	284.97	260.88	234.58	213.95
24	0.6	14400	6	24.35	194.96	250.69	230.33	198.65	162.30
24A	0.6	14400	6	26.89	195.38	239.67	213.93	182.29	151.36
24B	0.6	14400	6	29.52	191.73	229.27	198.18	165.34	139.15
25	0.6	21600	6	16.88	215.58	283.68	265.58	230.28	178.44
25A	0.6	21600	6	19.42	221.39	274.44	249.46	215.18	171.49
25B	0.6	21600	6	22.05	219.95	264.60	232.66	197.61	162.78

Table 4.4 shows the principal stress angles in vertical YZ-plane at Line 3, for all 35 studied cases. The ANSYS figures and plots associates with these cases are provided in the Appendix.

Table 4.4. Principal Stress Angles (degrees) along Line 3 from ANSYS FEA

Ansys Case No.	Strand Size	ASTM 1081 (lbs)	f'ci (ksi)	"Measured" Transfer Length (in)	θp, Line 3 (degrees) Distance from Beam End, z (in.) 2	4	6	8	12
1	0.5	9000	6	29.36	42.87	32.21	24.62	19.59	14.15
2	0.5	12000	6	24.77	38.70	30.60	23.84	19.12	13.44
3	0.5	18000	6	19.37	34.13	28.83	22.76	18.05	11.92
4	0.6	14400	6	27.41	40.22	30.79	23.57	18.72	13.37
5	0.6	21600	6	21.41	35.17	28.95	22.69	18.07	11.99
6	0.6	28800	6	19.30	32.62	27.94	21.93	17.16	11.34
7	0.5	9000	10	25.32	34.90	29.80	24.19	19.96	14.38
8	0.5	12000	10	20.14	31.38	28.39	23.33	19.15	13.02
9	0.5	18000	10	18.66	21.34	24.73	21.94	18.55	12.51
10	0.6	14400	10	24.00	32.13	28.35	23.13	19.03	13.37
11	0.6	21600	10	19.48	28.57	26.87	22.04	17.80	11.98
12	0.6	28800	10	18.63	26.58	25.85	21.11	17.20	11.50
13	0.5	9000	4	34.64	44.14	33.09	25.39	20.31	14.85
14	0.5	12000	4	27.43	39.71	31.29	24.51	19.82	14.36
15	0.5	18000	4	21.28	34.14	29.14	23.36	18.93	12.90
19	0.5	9000	4	34.72	30.31	30.13	26.72	23.38	17.90
20	0.5	12000	4	27.56	35.57	30.51	25.18	21.19	15.89
21	0.6	14400	6	27.53	35.91	29.97	24.30	20.22	15.08
22	0.6	21600	6	22.04	31.25	28.39	23.68	19.79	13.78
23	0.6	28800	6	19.59	29.12	27.60	23.13	19.05	13.09
24	0.6	14400	6	24.35	31.56	27.49	22.20	18.26	13.53
25	0.6	21600	6	16.88	24.89	24.92	21.13	17.73	12.87
26	0.6	28800	6	11.56	21.57	23.66	20.69	17.66	13.66
27	0.6	14400	6	24.53	37.18	28.53	21.19	16.20	11.10
28	0.6	21600	6	17.04	29.54	25.53	19.63	15.19	10.21
29	0.6	28800	6	11.63	25.35	23.88	18.78	14.74	11.02
21	0.6	14400	6	27.53	35.91	29.97	24.30	20.22	15.08
21A	0.6	14400	6	30.07	38.50	30.56	24.64	20.59	15.71
21B	0.6	14400	6	32.70	42.21	31.52	24.91	20.92	16.43
24	0.6	14400	6	24.35	31.56	27.49	22.20	18.26	13.53
24A	0.6	14400	6	26.89	35.57	28.28	22.18	18.08	13.63
24B	0.6	14400	6	29.52	40.12	29.49	22.26	17.85	13.73
25	0.6	21600	6	16.88	24.89	24.92	21.13	17.73	12.87
25A	0.6	21600	6	19.42	28.70	25.51	20.92	17.43	12.89
25B	0.6	21600	6	22.05	33.23	26.60	20.85	17.10	13.01

Tables 4.2 and 4.4 are illustrated in Figure 4.1 for ANSYS Case 1.

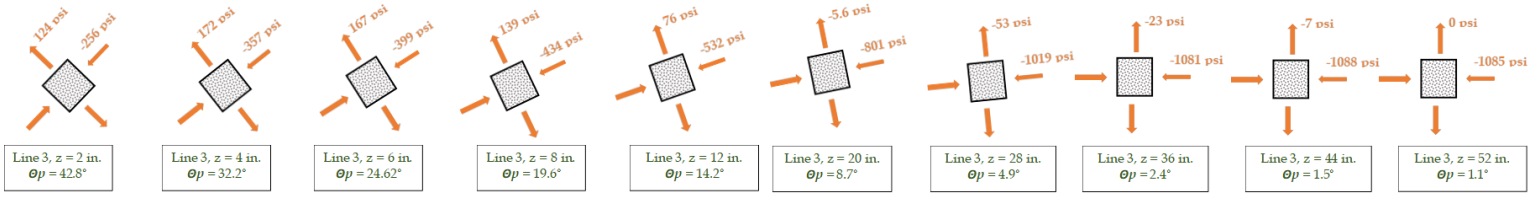

Figure 4.1. Example of Changing Stress Orientations and Magnitudes for ANSYS Case 1

To further address the validity of model here are a few points to make:

- The maximum tensile stresses occur generally within 6 inches from the end of the beam. This is very reasonable, and is a significant and important difference in our analysis.
- One can see that the compressive stress at Line 3 gradually build up from the end of the beam through the transfer zone. This is more like the data that we have observed when measuring concrete surface strains at ends of pre-tensioned members, as we measured transfer lengths in the past. This is the expected result. The "peak" compressive stress is not occurring at the end of the member, but builds through the transfer zone and through the St. Venant's effect.
- The principal angle begins (at the end of the member) at a little less than 45 degrees, which of course is an expected result. This is shown in Figure 4.1. Most interesting will be how much variation occurs in the principal angle when one includes the top strand. The angle will decrease.
- Considering the principal angle and principal stresses at 6 inches from the end of the beam, bottom line is that there is probably insufficient tensile stress to cause cracking on its own.

Due to space limitation in this paper and for sake of clarity, the number of figures displayed in the body of the report are limited. The remaining figures are provided in the Appendix of the report. The following selected FEA model results from ANSYS are displayed to demonstrate the effects of different variables on end-regions in the prestressed concrete beam, and serve to answer the five basic questions:

- Strand Bond Quality: Variations in principal tension for ANSYS cases 1 and 3 to demonstrate effects of variations in strand bond quality;
- Effects of Strand Size: Variations in principal tension for ANSYS cases 2 and 4 to demonstrate effects of strand size;
- Effects of Concrete Strength: Variations in principal tension for ANSYS cases 6 and 12 to demonstrate effects of concrete strength;
- Effects of Fully-Tensioned Top Strands: Variations in principal tension for ANSYS cases 13 and 19 to demonstrate effects of the top strand;
- Effects of Some Bottom Strand: Variations in principal tension for ANSYS Cases 22 and 25 to demonstrate effects of the debonding strand.

4.1 Effects of Improved Strand Bond Quality

It was found that the higher bonding strand results in increased tensile stresses in the concrete in end regions.

Following cases were compared:

- For 0.5-inch strands, 6 ksi concrete strength, no top strand, no debond cases ANSYS 1 (ASTM A1081 = 9,000 lbs) and ANSYS 3 (ASTM A1081 = 18,000 lbs) (Figures 4.2 – 4.6);
- For 0.5-inch strands, 10 ksi concrete strength, no top strand, no debond cases ANSYS 7 (ASTM A1081 = 9,000 lbs) and ANSYS 9 (ASTM A1081 = 18,000 lbs);
- For 0.6-inch strands, 6 ksi concrete strength, no top strand, no debond cases ANSYS 4 (ASTM A1081 = 14,400 lbs) and ANSYS 6 (ASTM A1081 = 28,800 lbs);
- For 0.6-inch strands, 10 ksi concrete strength, no top strand, no debond cases ANSYS 10 (ASTM A1081 = 14,400 lbs) and ANSYS 12 (ASTM A1081 = 28,800 lbs);
- For 0.6-inch strands, 6 ksi concrete strength, with top strand, no debond cases ANSYS 21 (ASTM A1081 = 14,400 lbs) and ANSYS 23 (ASTM A1081 = 28,800 lbs);
- For 0.6-inch strands, 6 ksi concrete strength, with top strand, with debond cases ANSYS 24 (ASTM A1081 = 14,400 lbs) and ANSYS 26 (ASTM A1081 = 28,800 lbs);
- For 0.6-inch strands, 6 ksi concrete strength, no top strand, with debond cases ANSYS 27 (ASTM A1081 = 14,400 lbs) and ANSYS 29 (ASTM A1081 = 28,800 lbs).

Variations in principal tension for ANSYS Cases 1 and 3 are shown in Figures 4.2 – 4.5. From observing the color band display of the results, it is obvious that there are more “red” areas or areas of higher tensile stress in the ANSYS Case 3 (A1081 = 18,000 lbs) than in ANSYS case 1 (A1081 = 9,000 lbs).

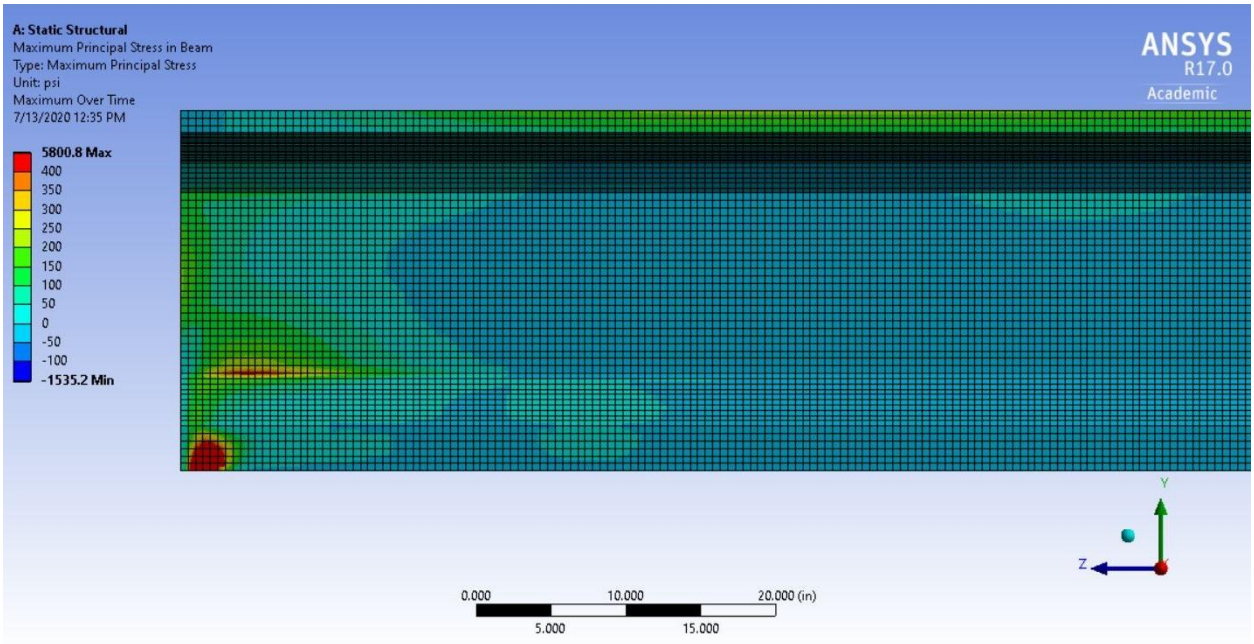

Figure 4.2. ANSYS 1 Principal Tensile Stress, A1081 = 9,000 lbs, 0.5 in. strands, f'ci = 6 ksi, No Top Strand, No Debonding

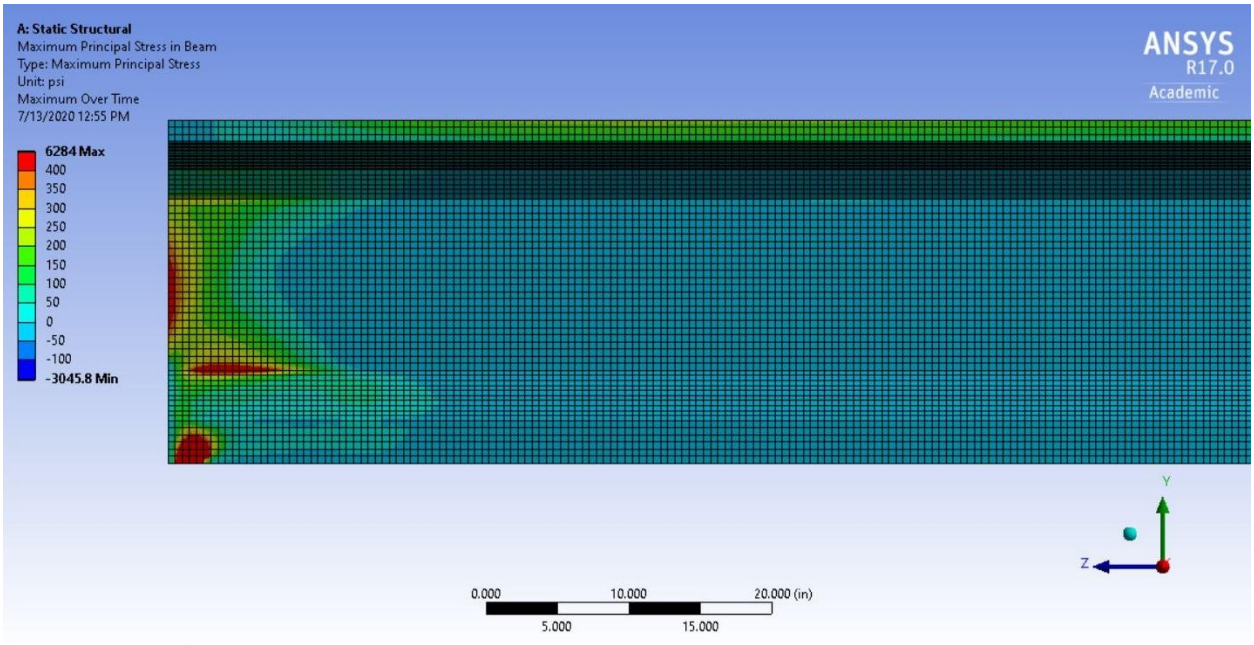

Figure 4.3. ANSYS 3 Principal Tensile Stress, A1081 = 18,000 lbs., 0.5 in. strands, f'ci = 6 ksi, No Top Strand, No Debonding

Figure 4.4 plots the principal tensile stress at the Neutral Axis for ANSYS 1 vs. ANSYS 3. The chart shows that the higher bonding strand generates larger tensile stresses at the N.A. of the pre-tensioned beam. One should note that the transfer lengths for strands in ANSYS 3 case are only 15 in. whereas the transfer lengths for strands in the ANSYS case are 30 in.

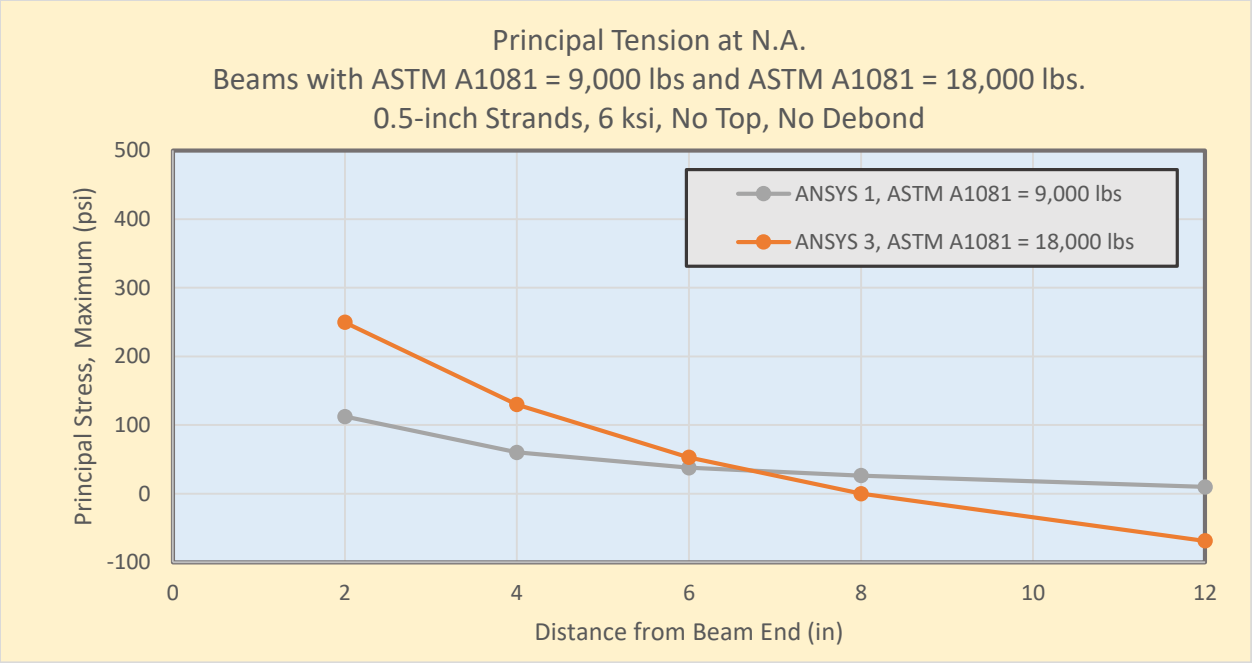

Figure 4.4. Principal Stress (tension) at Line 2, Neutral Axis, ANSYS 1 and ANSYS 3

Figure 4.5 plots the principal tensile stress at "Line 3" for ANSYS 1 vs. ANSYS 3. "Line 3" is located within the web of the I-shaped beam, but very near the bottom flange. The chart shows that the higher bonding strand generates larger tensile stresses at distances within 6 in. of the end of the pre-tensioned beam. One should note that the transfer lengths for strands in ANSYS 3 case are only 15 in. whereas the transfer lengths for strands in the ANSYS case are 30 in.

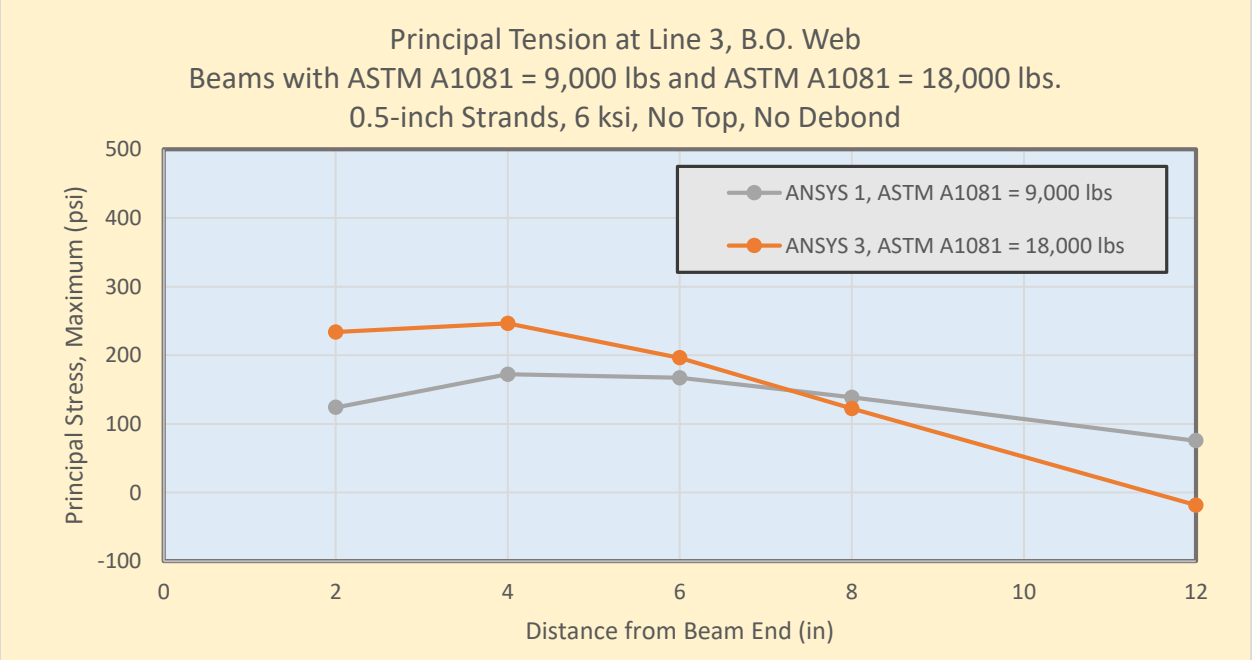

Figure 4.5. Principal Stress (tension) at Line 3, B.O. Web, ANSYS 1 and ANSYS 3

Figure 4.6 plots Syx (the shear stress) at "Line 3" for ANSYS 1 vs. ANSYS 3. "Line 3" is located within the web of the I-shaped beam, but very near the bottom flange. The chart shows that the higher bonding strand generates larger shearing stresses at distances up to 12 in. from the end of the pre-tensioned beam. The higher shear stresses and the higher principal tension stress at Line 3 are a direct result of the strands' prestressing force being transferred to the concrete within a shorter distance from the end of the beam. One should note that the transfer lengths for

strands in ANSYS 3 case are only 15 in. whereas the transfer lengths for strands in the ANSYS case are 30 in.

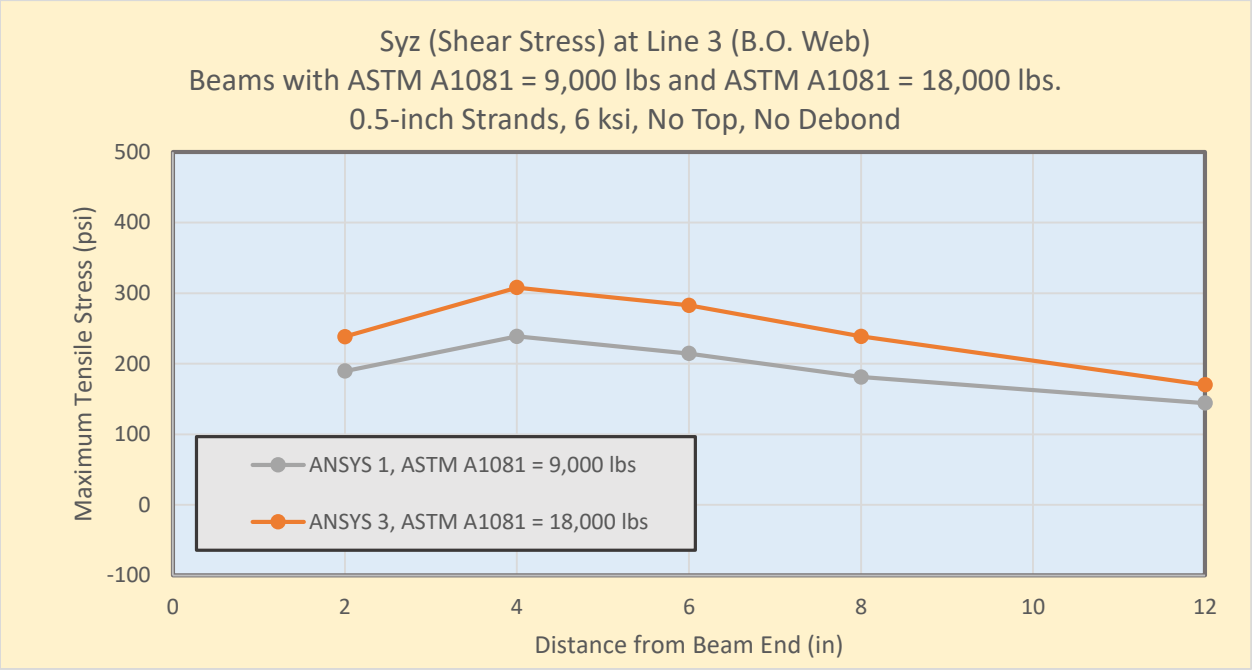

Figure 4.6. Shear Stress at Line 3, B.O. Web, ANSYS 1 and ANSYS 3

4.2 Effects of Strand Size

It was found that larger strand sizes result in increased tensile stresses.

Following cases were compared:

- For 6 ksi concrete strength, no top strand, no debond cases ANSYS 2 (0.5-inch strands, ASTM A1081 = 12,000 lbs) and ANSYS 4 (0.6-inch strands, ASTM A1081 = 14,400 lbs) (Figures 4.7 – 4.11);

- For 10 ksi concrete strength, no top strand, no debond cases ANSYS 8 (0.5-inch strands, ASTM A1081 = 12,000 lbs) and ANSYS 10 (0.6-inch strands, ASTM A1081 = 14,400 lbs);
- For 6 ksi concrete strength, no top strand, no debond cases ANSYS 3 (0.5-inch strands, ASTM A1081 = 18,000 lbs) and ANSYS 5 (0.6-inch strands, ASTM A1081 = 21,600 lbs);
- For 10 ksi concrete strength, no top strand, no debond cases ANSYS 9 (0.5-inch strands, ASTM A1081 = 18,000 lbs) and ANSYS 11 (0.6-inch strands, ASTM A1081 = 21,600 lbs.

Noteworthy, 12,000 lbs pull-out for 0.5-inch strand is the same bond stress as the 14,400 lbs pull-out for 0.6-inch strand. Variations in principal tension for ANSYS cases 2 and 4 are shown in Figures 4.7 – 4.10. From observing the color band display of the results, it is obvious that there are more "red" areas or areas of higher tensile stress in the ANSYS case 4 (0.6-inch strands and A1081 = 14,400 lbs) than in ANSYS case 2 (0.5-inch strands A1081 = 12,000 lbs). Larger size strands are also associated with higher ASTM Bond Test values, which also leads to higher tensile stresses in case of 0.6-inch strands.

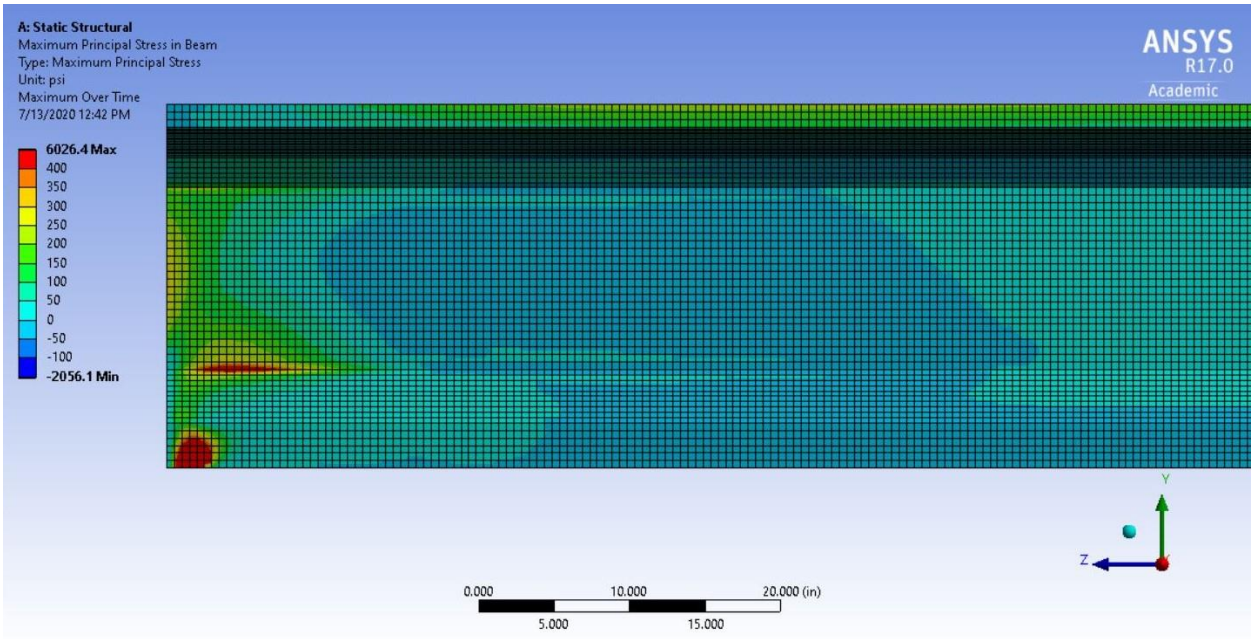

Figure 4.7. ANSYS 2 Principal Tensile Stress, A1081 = 12,000 lbs., 0.5 in. strands, f'ci = 6 ksi, No Top Strand, No Debonding

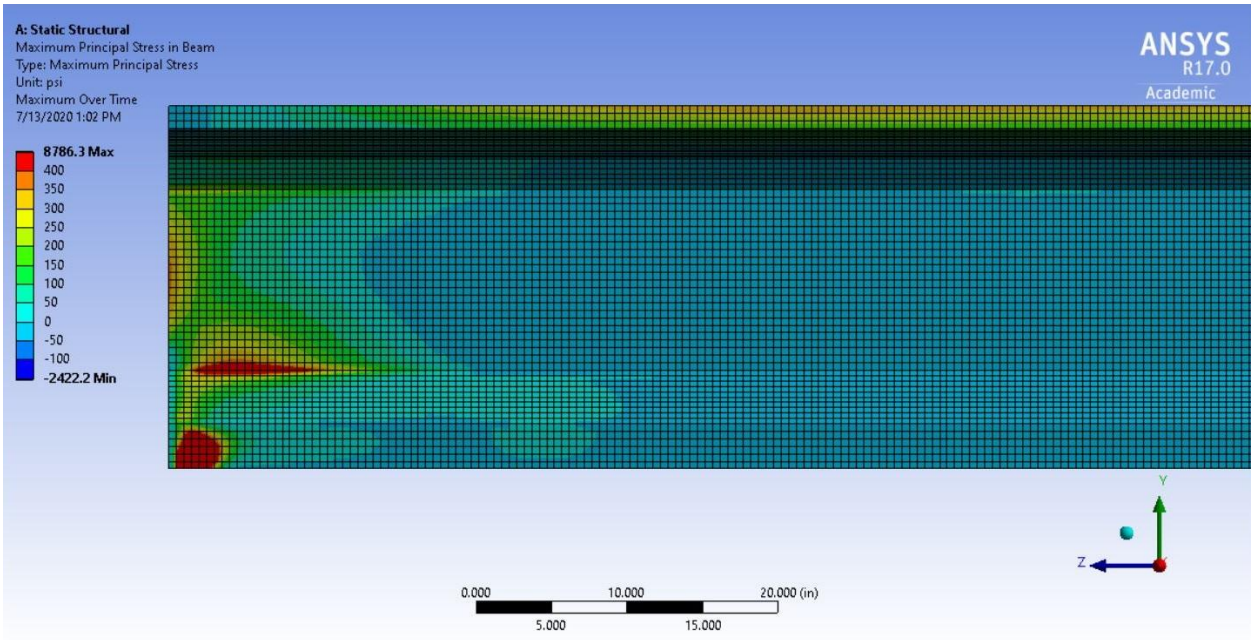

Figure 4.8. ANSYS 4 Principal Tensile Stress, A1081 = 14,400 lbs, 0.6 in. strands, f'ci = 6 ksi, No Top Strand, No Debonding

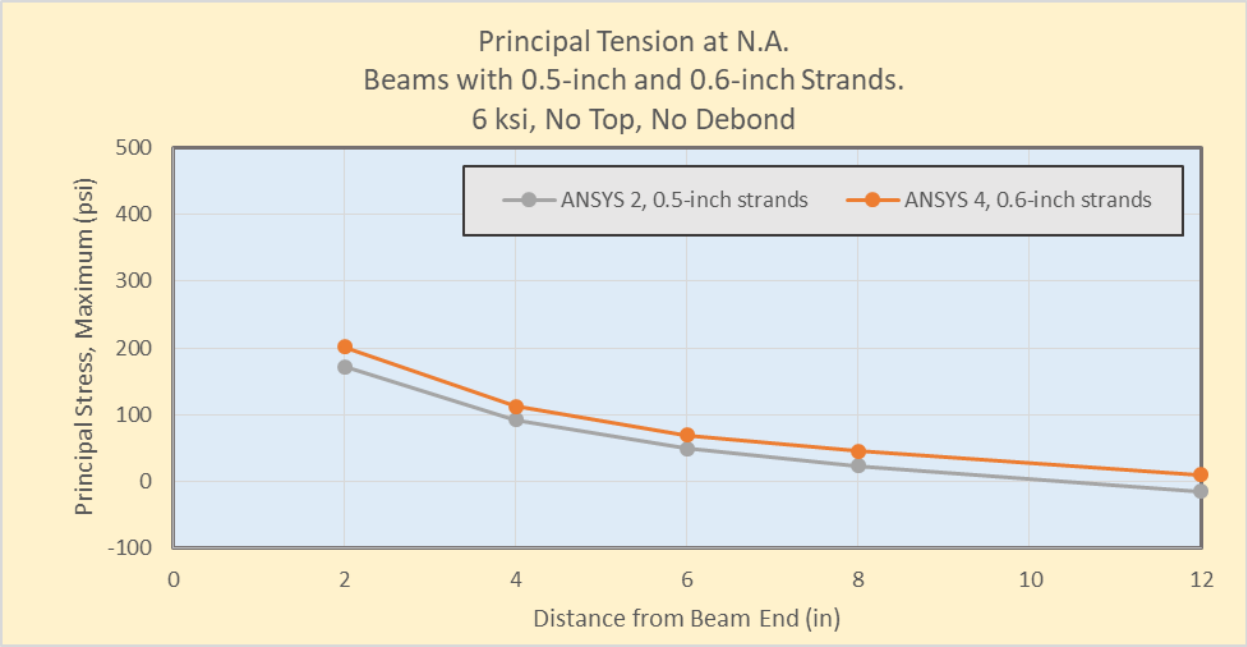

Figure 4.9. Principal Stress (tension) at Line 2, Neutral Axis, ANSYS 2 and ANSYS 4

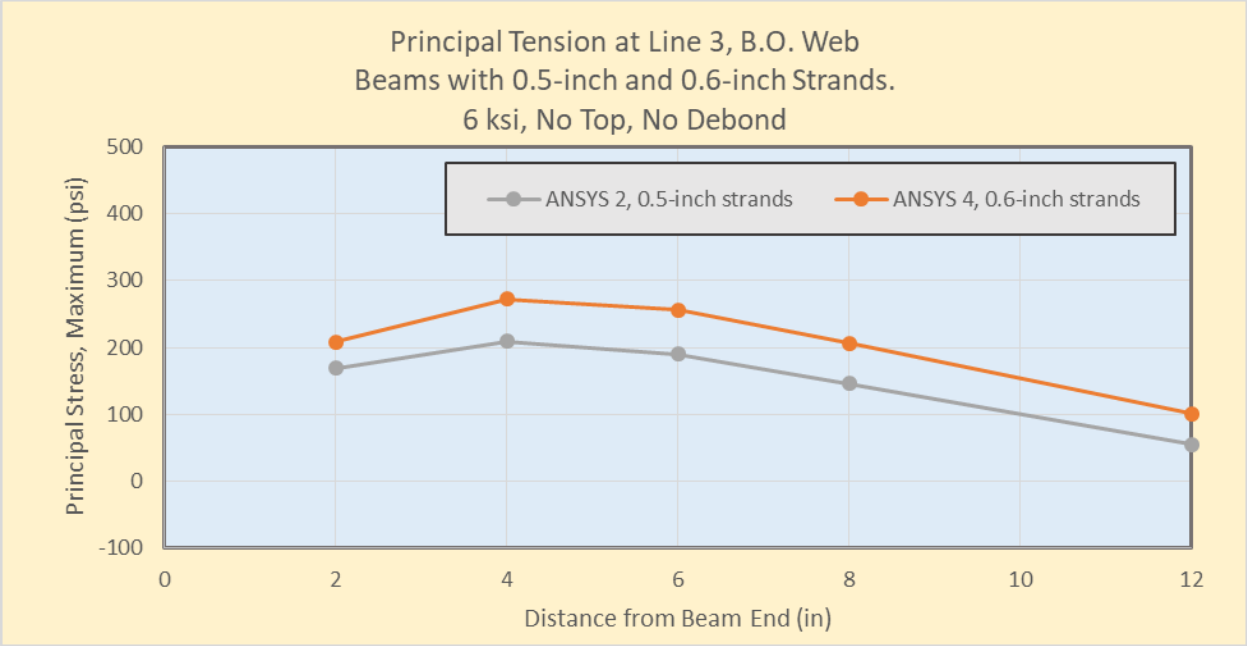

Figure 4.10. Principal Stress (tension) at Line 3, B.O. Web, ANSYS 2 and ANSYS 4

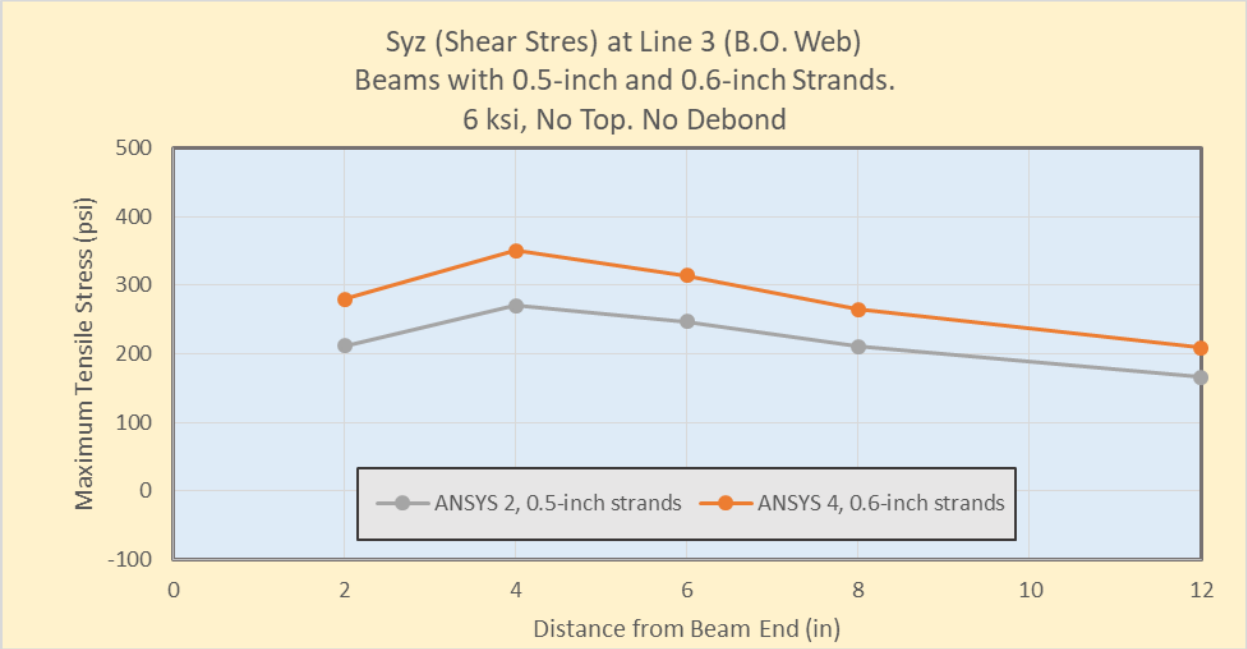

Figure 4.11. Shear Stress at Line 3, B.O. Web, ANSYS 2 and ANSYS 4

4.3 Effects of Concrete Strength

It was found that higher concrete strength results in shorter bond length and increased tensile stresses.

Following cases were compared:

- For ASTM A1081 = 9,000 lbs, 0.5-inch strands, no top strand, no debond cases ANSYS 13 (4 ksi), ANSYS 1 (6 ksi) and ANSYS 7 (10 ksi);
- For ASTM A1081 = 12,000 lbs, 0.5-inch strands, no top strand, no debond cases ANSYS 14 (4 ksi), ANSYS 2 (6 ksi) and ANSYS 8 (10 ksi);
- For ASTM A1081 = 18,000 lbs, 0.5-inch strands, no top strand, no debond cases ANSYS 15 (4 ksi), ANSYS 3 (6 ksi) and ANSYS 9 (10 ksi);
- For ASTM A1081 = 14,400 lbs, 0.6-inch strands, no top strand, no debond cases ANSYS 4 (6 ksi) and ANSYS 10 (10 ksi);
- For ASTM A1081 = 21,600 lbs, 0.6-inch strands, no top strand, no debond cases ANSYS 5 (6 ksi) and ANSYS 11 (10 ksi);
- For ASTM A1081 = 24,000 lbs, 0.6-inch strands, no top strand, no debond cases ANSYS 6 (6 ksi) and ANSYS 12 (10 ksi) (Figures 4.12 – 4.16).

Variations in principal tension for ANSYS cases 6 and 12 are shown in Figures 4.12 – 4.15. From observing the color band display of the results, it is obvious that there are more "red" areas or areas of higher tensile stress in the ANSYS case 12 (10 ksi concrete strength at release) than in ANSYS case 6 (6 ksi concrete strength at release).

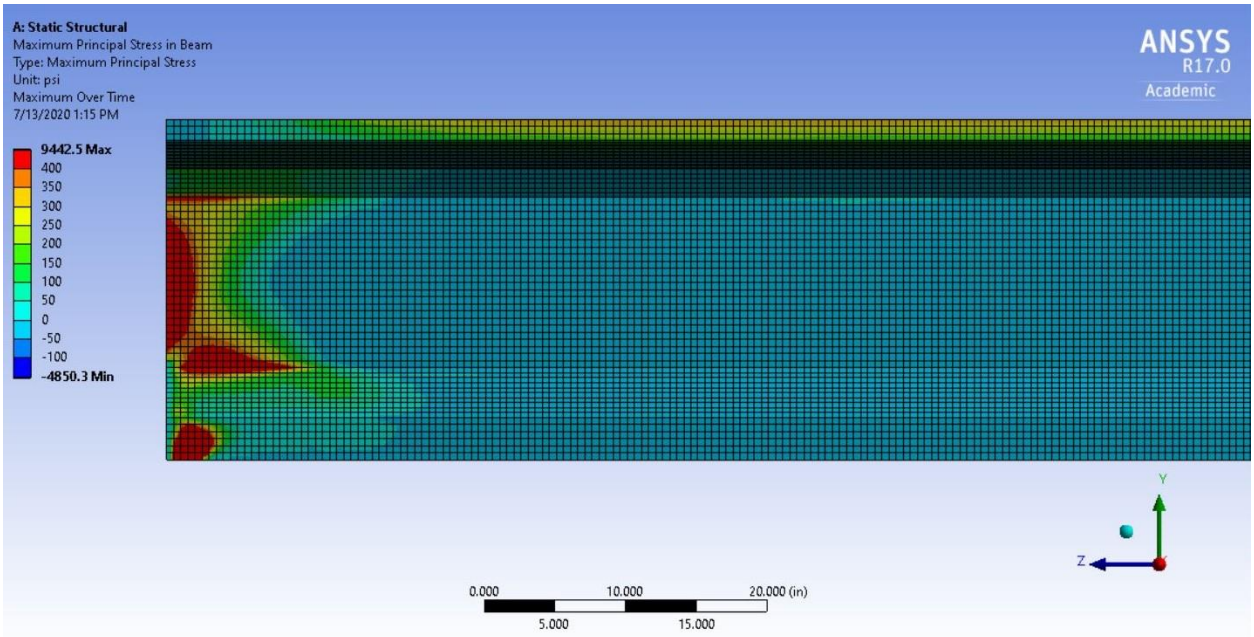

Figure 4.12. ANSYS 6 Principal Tensile Stress, A1081 = 28,800 lbs., 0.6 in. strands, f'ci = 6 ksi, No Top Strand, No Debonding

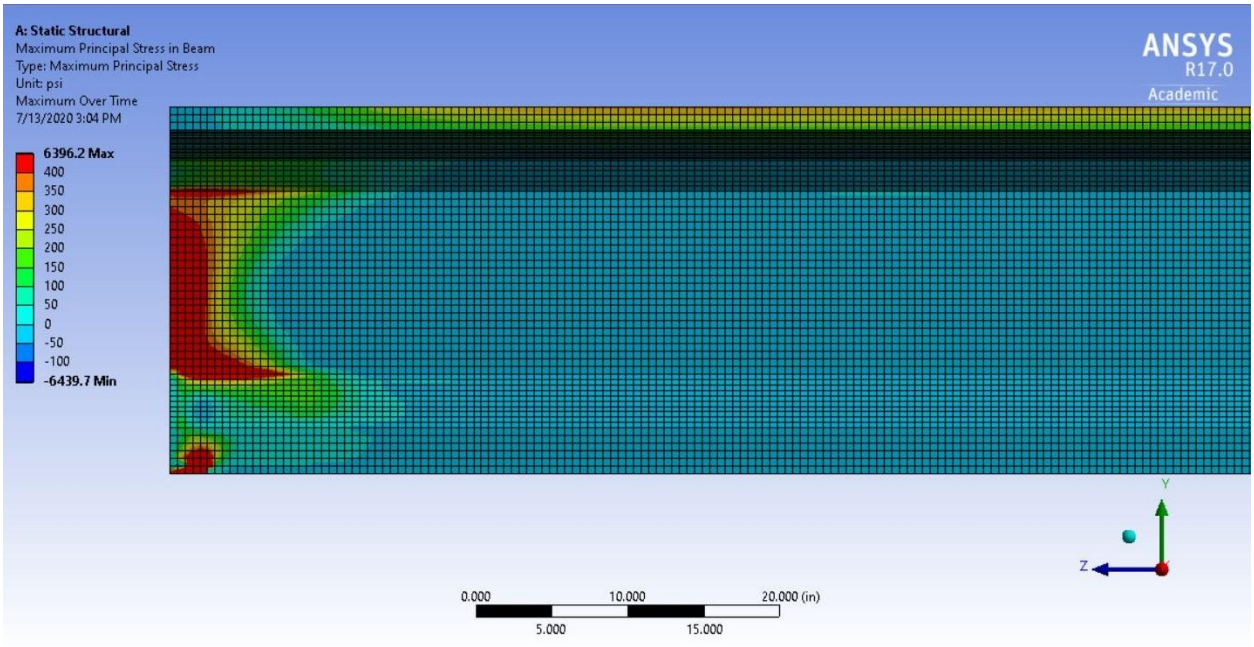

Figure 4.13. ANSYS 12 Principal Tensile Stress, A1081 = 28,800 lbs., 0.6 in. strands, f'ci = 10 ksi, No Top Strand, No Debonding

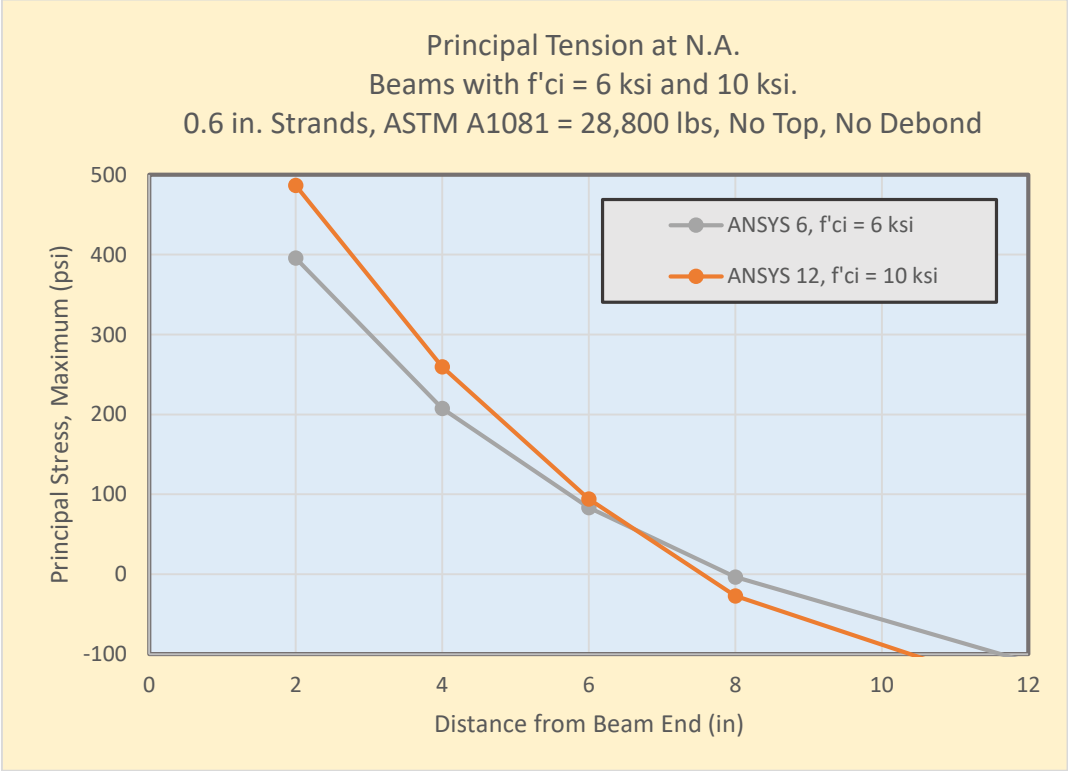

Figure 4.14. Principal Stress (tension) at Line 2, Neutral Axis, ANSYS 6 and ANSYS 12

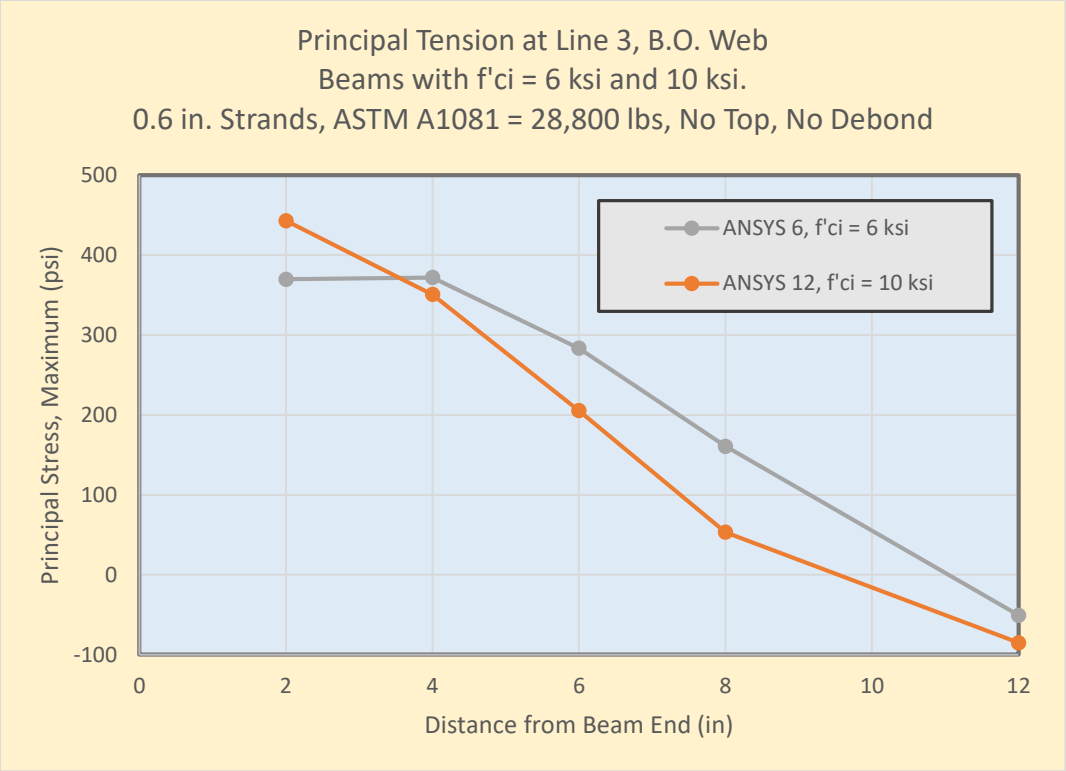

Figure 4.15. Principal Stress (tension) at Line 3, B.O. Web, ANSYS 6 and ANSYS 12

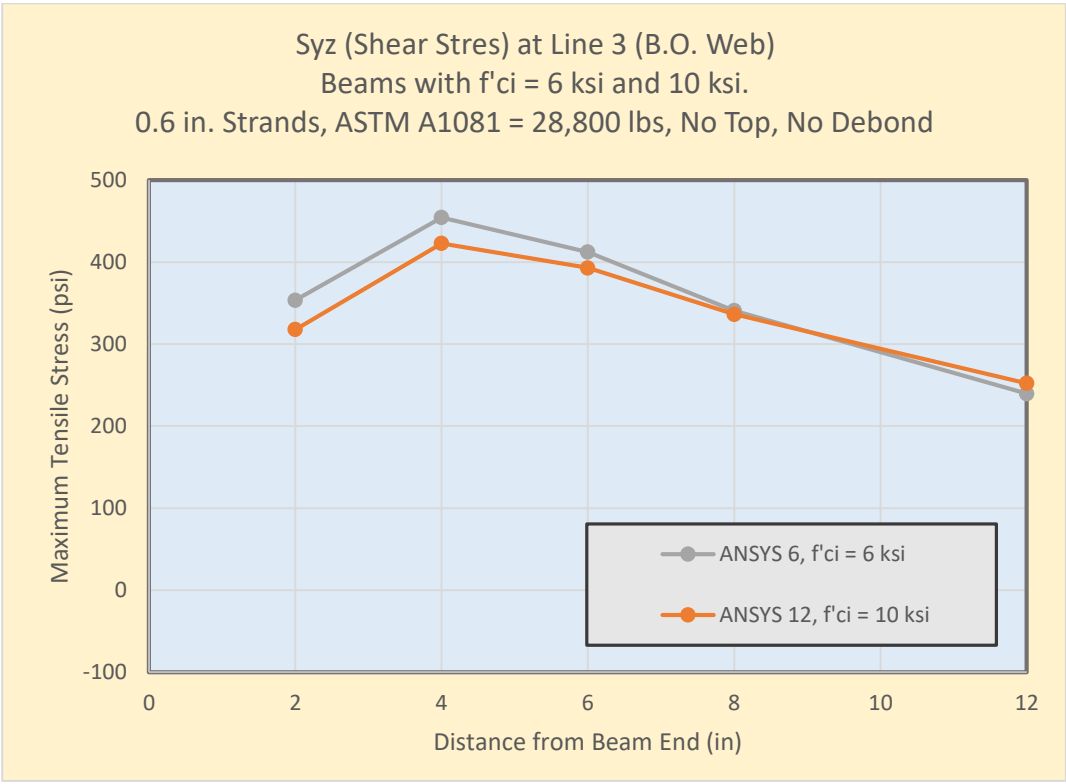

Figure 4.16. Shear Stress at Line 3, B.O. Web, ANSYS 6 and ANSYS 12

4.4 Effects of Top Strand

It was found that the addition of the fully tensioned top strand increases tension stresses at the neutral axis, and tensile stresses at the bottom of the web are higher.

Following cases were compared:

- For ASTM A1081 = 9,000 lbs, 0.5-inch strands, 4 ksi concrete strength, no debond cases ANSYS 13 (no top strand) and ANSYS 19 (with top strand);
- For ASTM A1081 = 12,000 lbs, 0.5-inch strands, 4 ksi concrete strength, no debond cases ANSYS 14 (no top strand) and ANSYS 20 (with top strand);
- For ASTM A1081 = 14,400 lbs, 0.6-inch strands, 6 ksi concrete strength, no debond cases ANSYS 4 (no top strand), ANSYS 21 (with top strand) and all strand debond 4 inches ANSYS 21B (with top strand);
- For ASTM A1081 = 21,600 lbs, 0.6-inch strands, 6 ksi concrete strength, no debond cases ANSYS 5 (no top strand) and ANSYS 22 (with top strand) (Figures 4.17 – 4.21);
- For ASTM A1081 = 28,800 lbs, 0.6-inch strands, 6 ksi concrete strength, no debond cases ANSYS 6 (no top strand) and ANSYS 23 (with top strand).

Variations in principal tension for ANSYS cases 13 and 19 are shown in Figures 4.17 – 4.21. From observing the color band display of the results, it is obvious that there are more “green” areas (compared with lower stress “cyan” areas) or areas of higher tensile stress in the ANSYS case 19 (with top strand) than in ANSYS case 13 (no top strand).

The data shows the following:

- Addition of top strand will increase principal tension at the beam’s neutral axis (NA).
- Addition of top strand increases principal tension at the bottom of (B.O.) beam’s web.

- Addition of top strand has little effect on the shear stress computed at the bottom of (B.O.) beam's web.

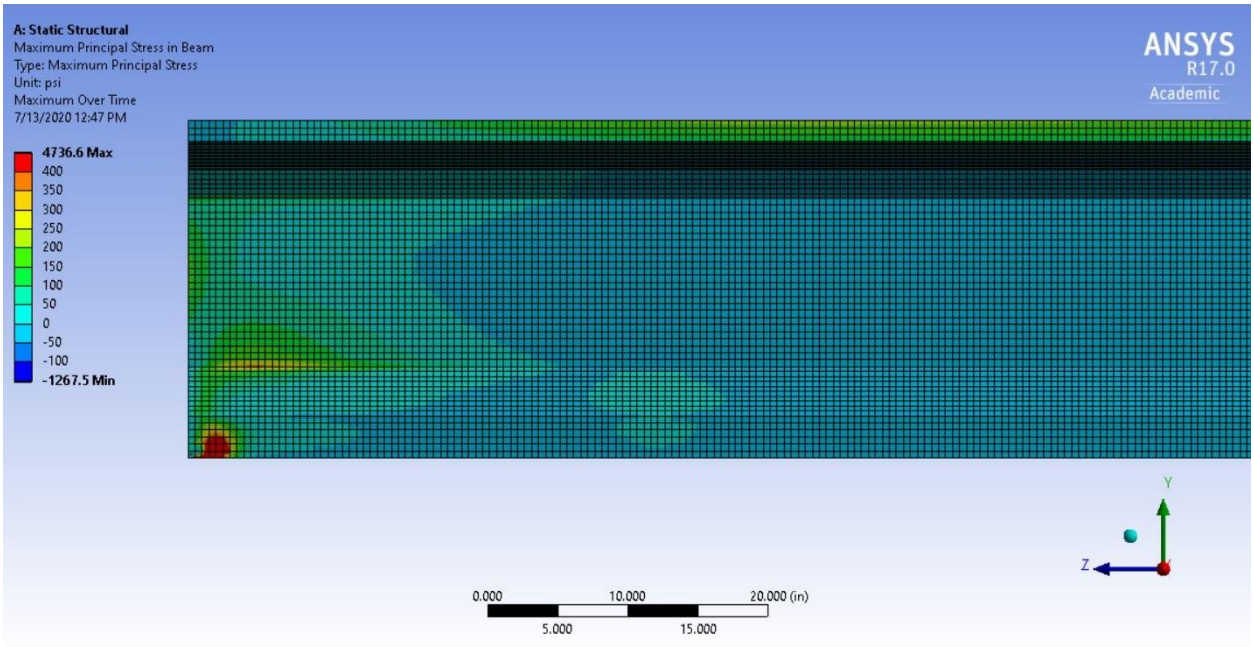

Figure 4.17. ANSYS 13 Principal Tensile Stress, A1081 = 9,000 lbs, 0.5 in. strands, f'ci = 4 ksi, No Top Strand, No Debonding

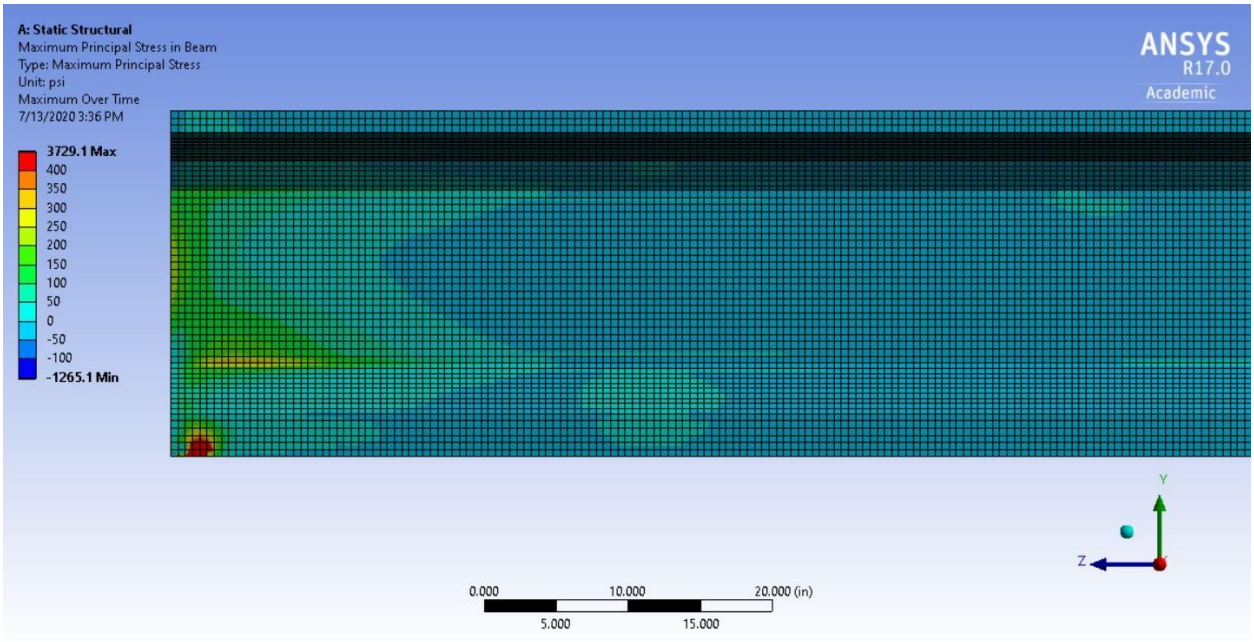

Figure 4.18. ANSYS 19 Principal Tensile Stress, A1081 = 9,000 lbs, 0.5 in. strands, f'ci = 4 ksi, With Top Strand, No Debonding

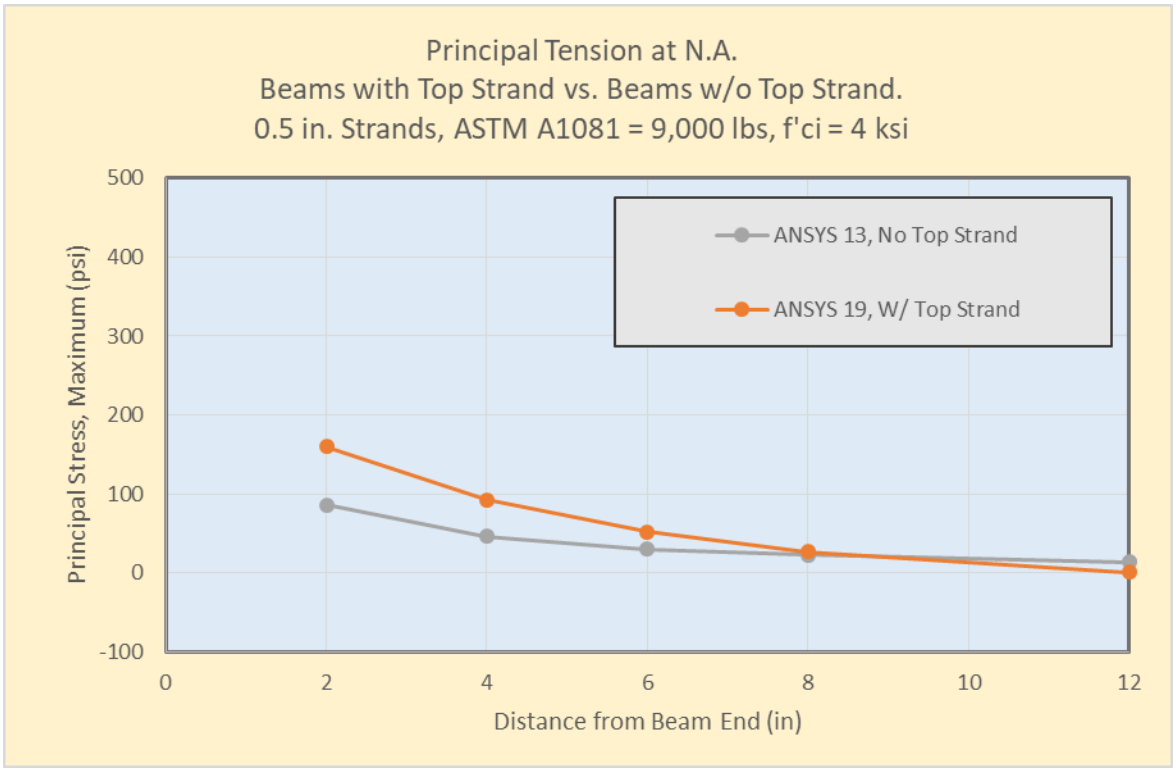

Figure 4.19. Principal Stress (tension) at Line 2, Neutral Axis, ANSYS 13 and ANSYS 19

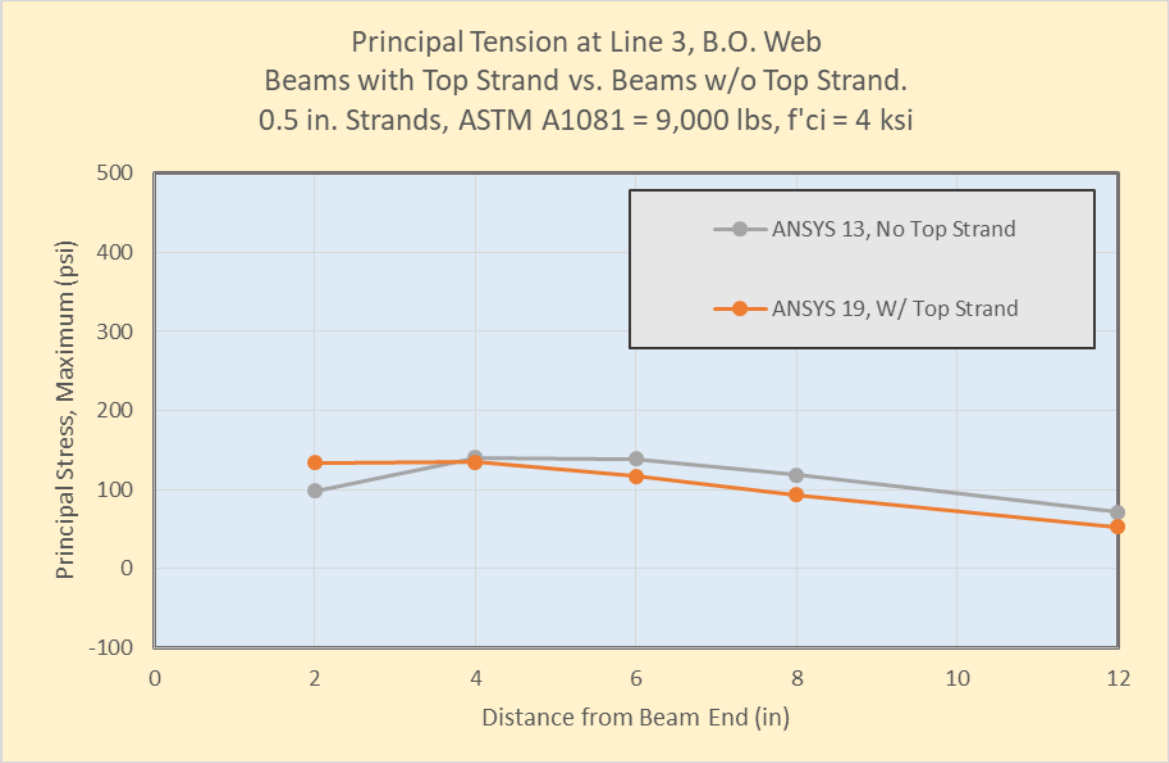

Figure 4.20. Principal Stress (tension) at Line 3, B.O. Web, ANSYS 13 and ANSYS 19

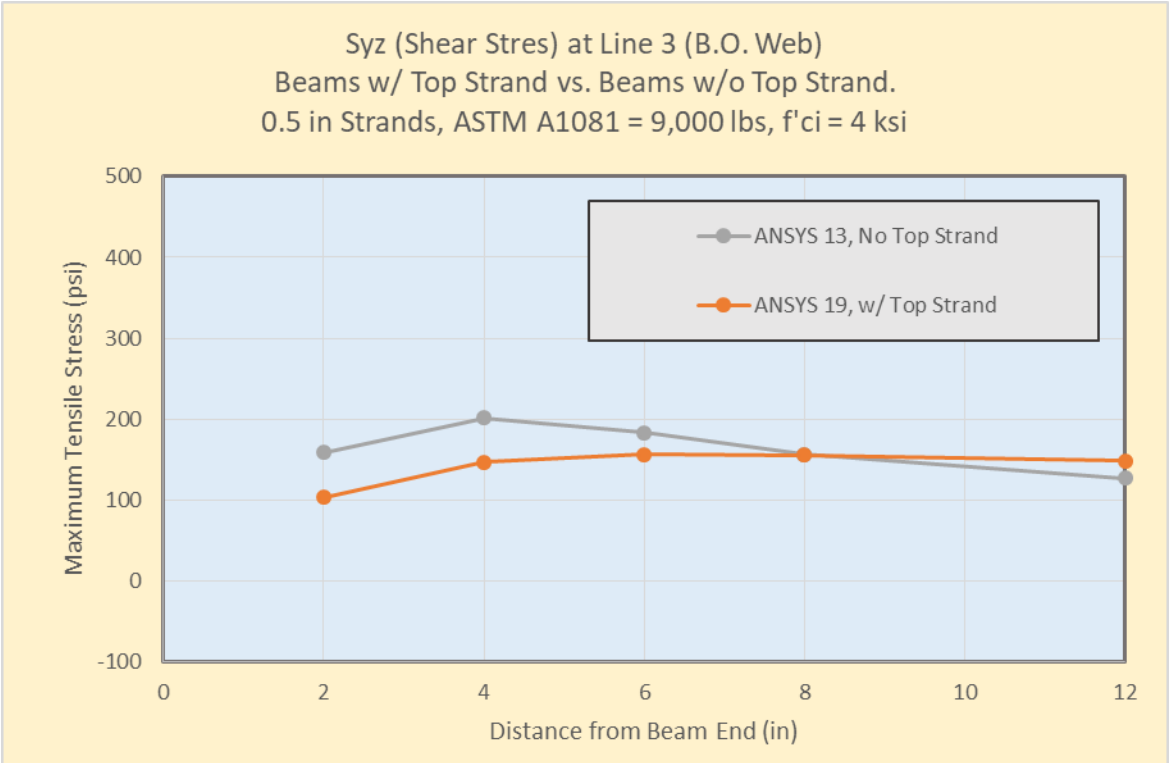

Figure 4.21. Shear Stress at Line 3, B.O. Web, ANSYS 13 and ANSYS 19

4.5 Effects of Debonding Strand

It was found that debonding one strand in four reduces principal tensile stresses.

One strand located at 4 inches from beam bottom was debonded 24 inches from beam end.

Following cases were compared:

- For ASTM A1081 = 14,400 lbs, 0.6-inch strands, 6 ksi concrete strength, with top strand cases ANSYS 21 (no debond) and ANSYS 24 (with one strand debond);
- For ASTM A1081 = 21,600 lbs, 0.6-inch strands, 6 ksi concrete strength, with top strand cases ANSYS 22 (no debond) and ANSYS 25 (with one strand debond) (Figures 4.22 – 4.26);
- For ASTM A1081 = 28,800 lbs, 0.6-inch strands, 6 ksi concrete strength, with top strand cases ANSYS 23 (no debond) and ANSYS 26 (with one strand debond);
- For ASTM A1081 = 14,400 lbs, 0.6-inch strands, 6 ksi concrete strength, no top strand cases ANSYS 4 (no debond) and ANSYS 27 (with one strand debond);
- For ASTM A1081 = 21,600 lbs, 0.6-inch strands, 6 ksi concrete strength, no top strand cases ANSYS 5 (no debond) and ANSYS 28 (with one strand debond);
- For ASTM A1081 = 28,800 lbs, 0.6-inch strands, 6 ksi concrete strength, no top strand cases ANSYS 6 (no debond) and ANSYS 29 (with one strand debond).

Variations in principal tension for ANSYS cases 22 and 25 are shown in Figures 4.22 – 4.25. From observing the color band display of the results, it is obvious that there are more “red” areas

or areas of higher tensile stress in the ANSYS case 22 (no debonding) than in ANSYS case 25 (debonded one strand).

Closer observation of these results reveals:

- Debonding of one strand (20%) 24 inches has little effect on principal tension at the beam's neutral axis (NA).
- Debonding of one strand reduces principal tension at the bottom of (B.O.) beam's web where the reduction in stress is significant in the range of 15%.
- Debonding of one strand reduces the shear stress at the bottom of (B.O.) beam's web where the reductions approach 25%.

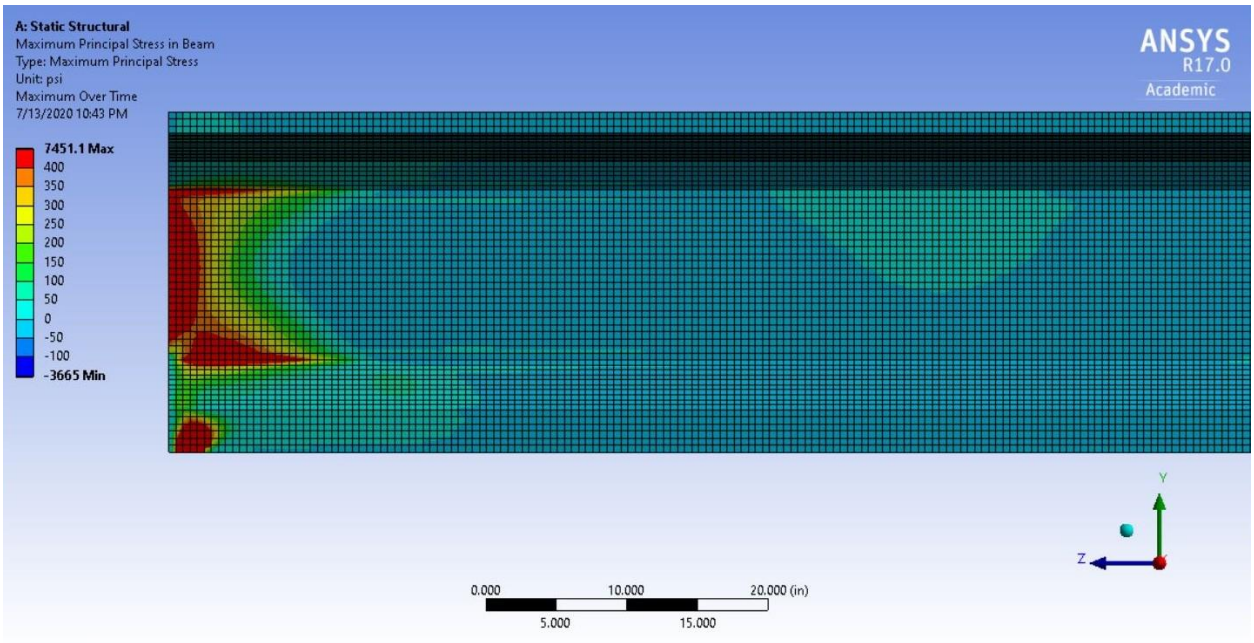

Figure 4.22. ANSYS 22 Principal Tensile Stress, A1081 = 21,600 lbs., 0.6 in. strands, f'ci = 6 ksi, With Top Strand, No Debonding

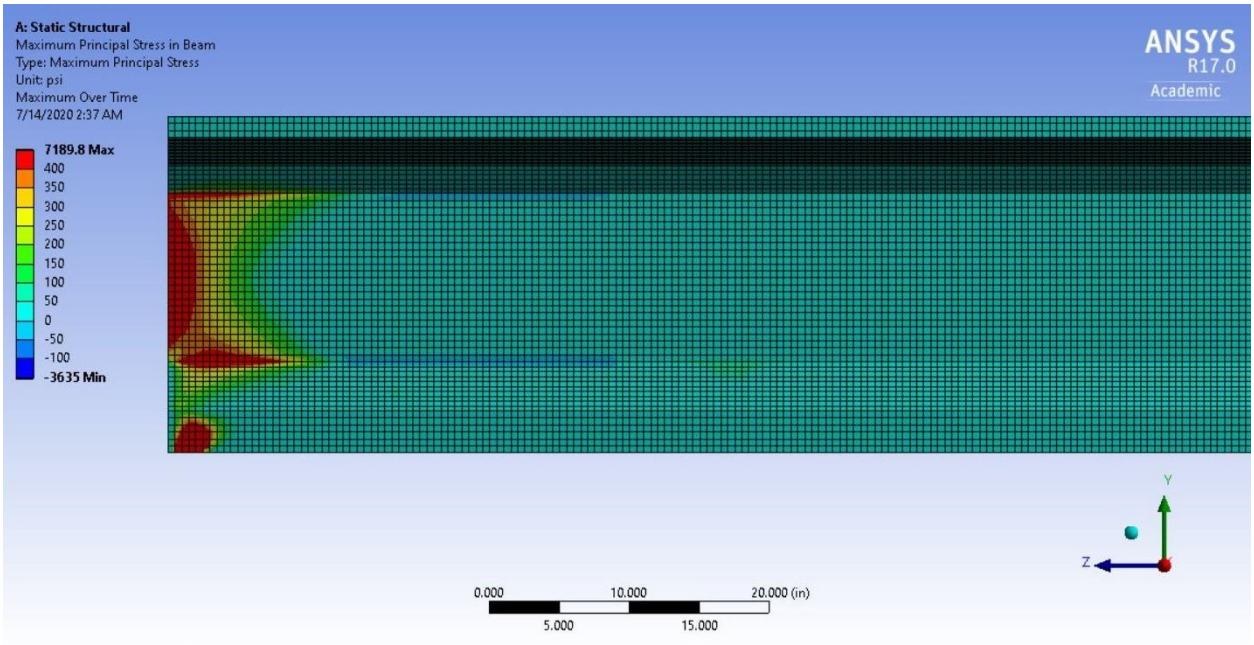

Figure 4.23. ANSYS 25 Principal Tensile Stress, A1081 = 21,600 lbs., 0.6 in. strands, f'ci = 6 ksi, With Top Strand, Debond One Strand

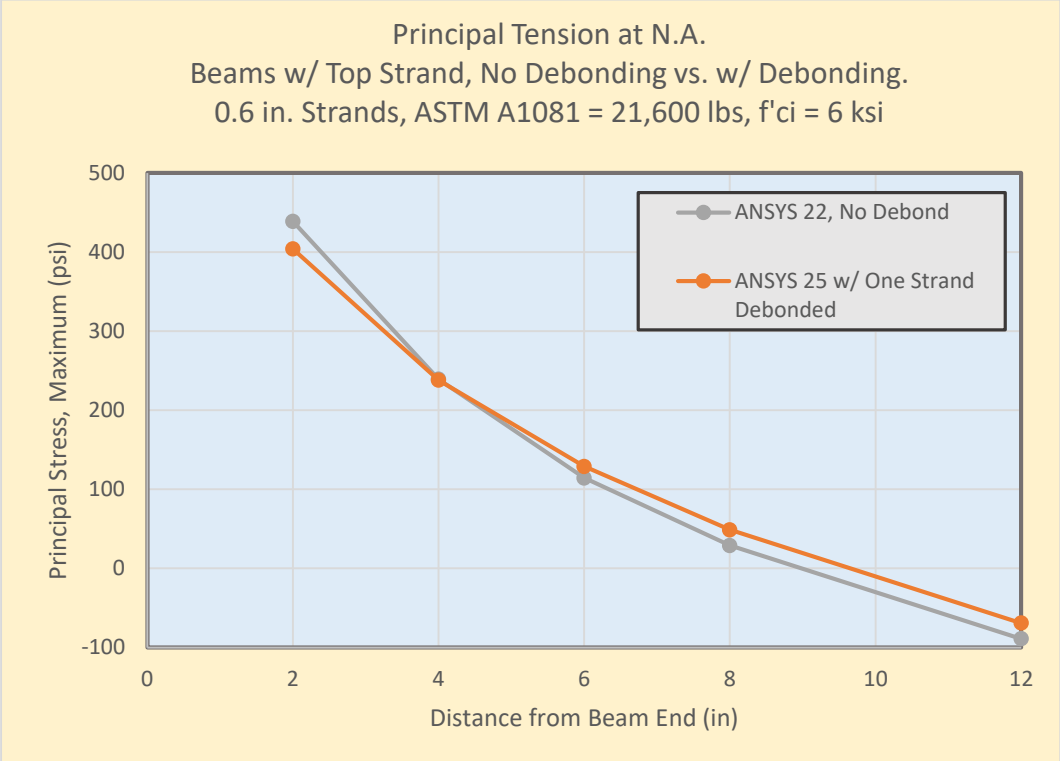

Figure 4.24. Principal Stress (tension) at Line 2, Neutral Axis, ANSYS 22 and ANSYS 25

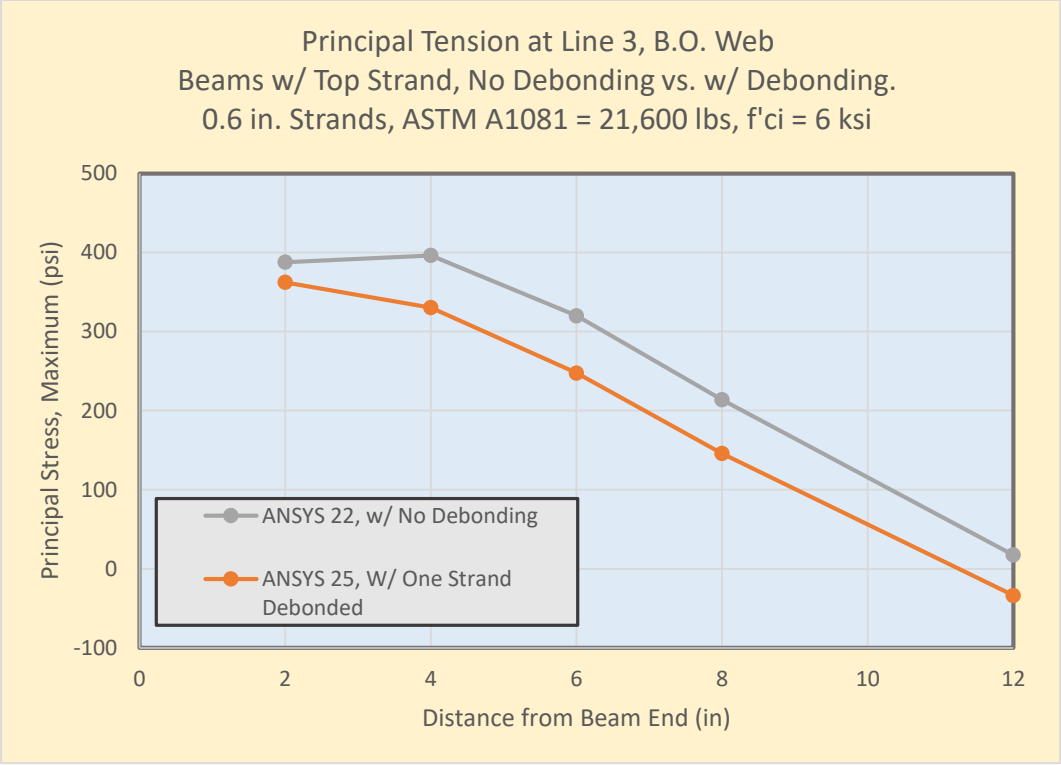

Figure 4.25. Principal Stress (tension) at Line 3, B.O. Web, ANSYS 22 and ANSYS 25

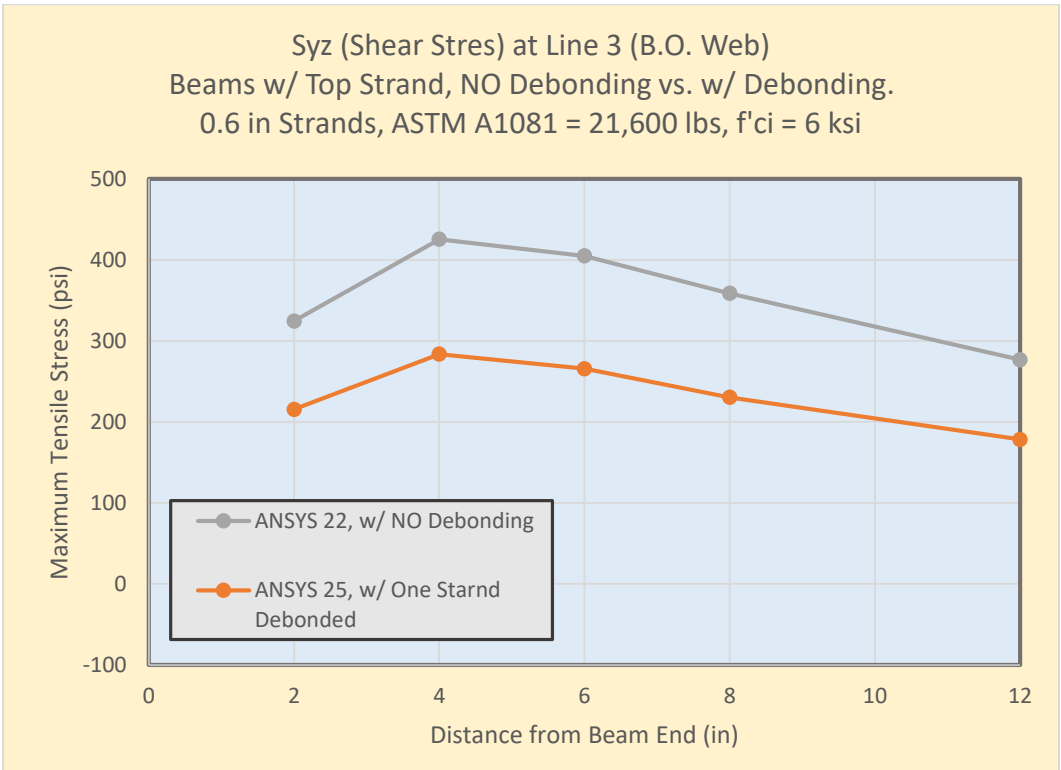

Figure 4.26. Shear Stress at Line 3, B.O. Web, ANSYS 22 and ANSYS 25

Further, when looking into debonding all strands (except the strand located 4 inches from beam bottom which is already debonded 24 inches) 2 inches and 4 inches in cases ANSYS 21A, 21B, 24A, 24B, 25A and 25B it was found that the “measured” transfer length increases a little more than 2 inches in each increment, and that the principal tensile stresses go down significantly (40% at NA and 30% at the B.O. Web). Debonding all strands by 4 inches significantly reduces principal tension from the beam end for several inches, so this strategy (debonding all strands) merits further investigation as results look very promising. See Figures for ANSYS 21, 21A and 21B shown below for comparison.

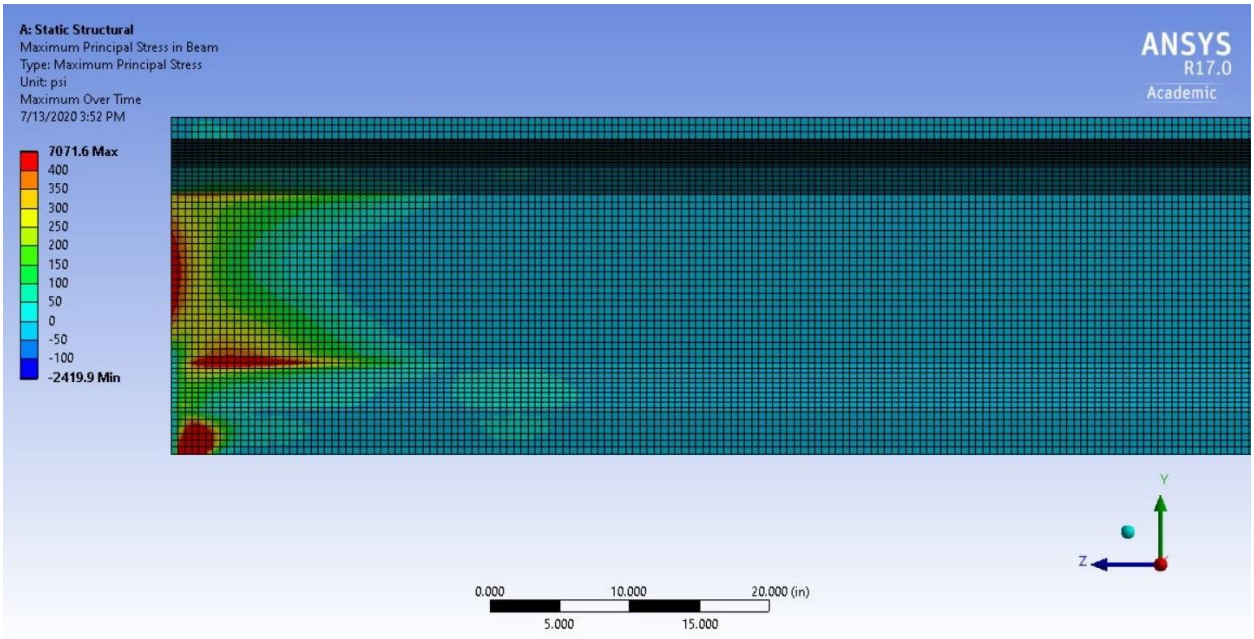

Figure 4.27. ANSYS 21 Principal Tensile Stress, A1081 = 14,400 lbs, 0.6 in. strands, f'ci = 6 ksi, Top Strand, No Debonding

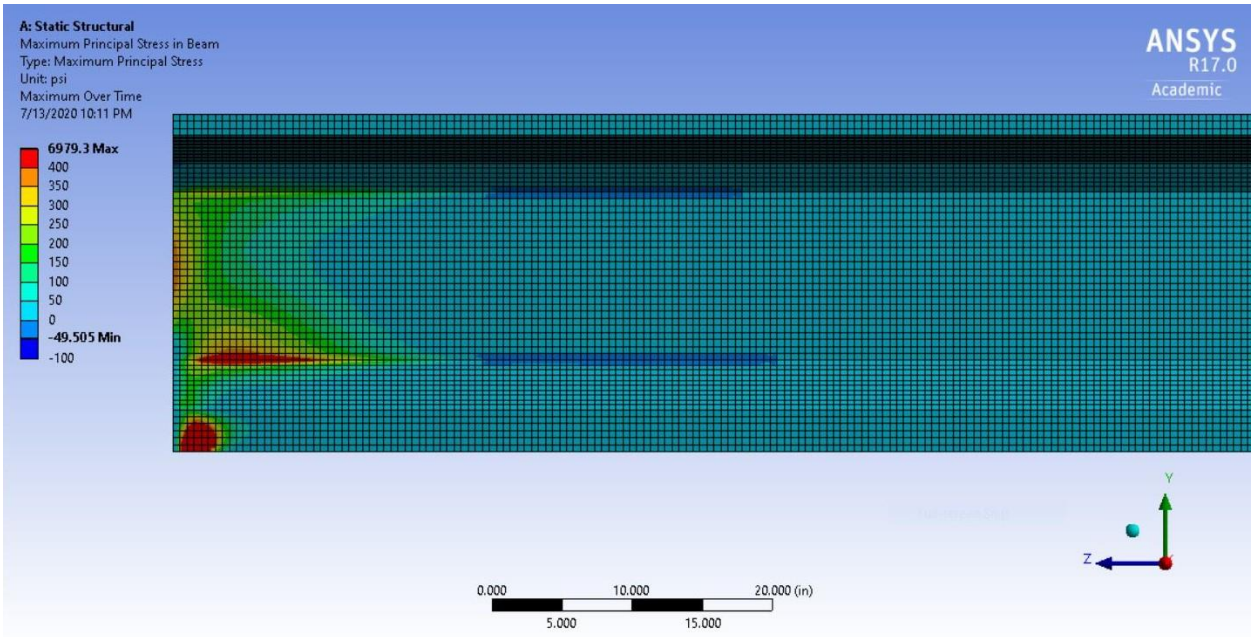

Figure 4.28. ANSYS 21A Principal Tensile Stress, A1081 = 14,400 lbs., 0.6 in. strands, f'ci = 6 ksi, Top Strand, 2" Debond All Strands

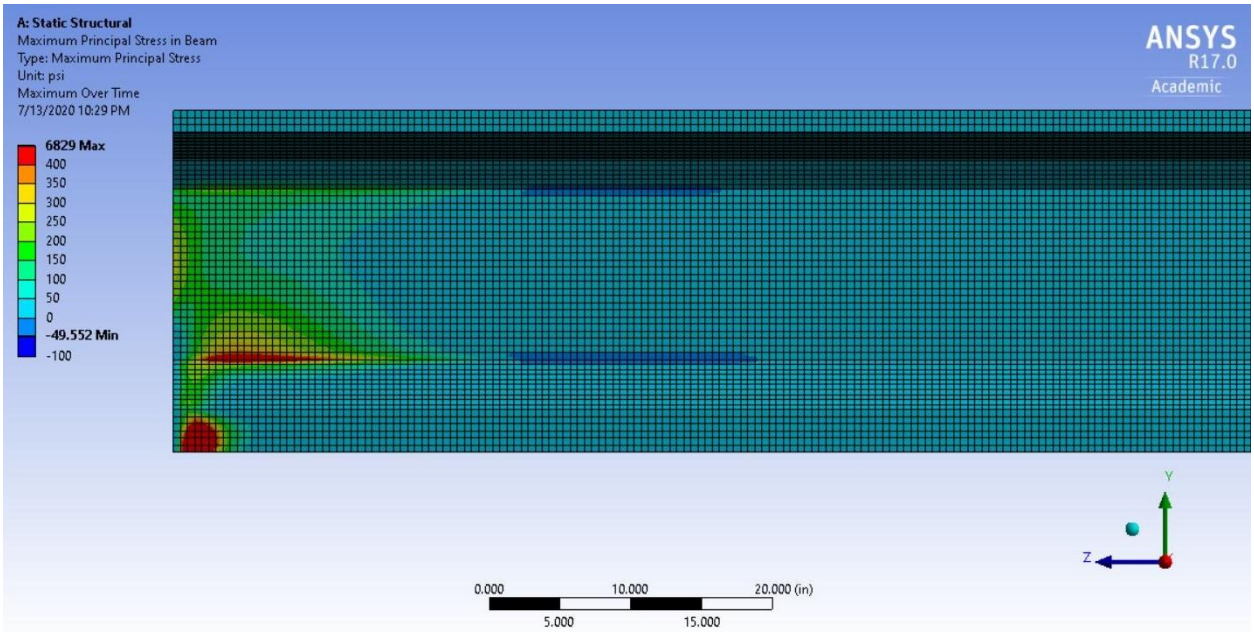

Figure 4.29. ANSYS 21B Principal Tensile Stress, A1081 = 14,400 lbs., 0.6 in. strands, f'ci = 6 ksi, Top Strand, 4" Debond All Strands

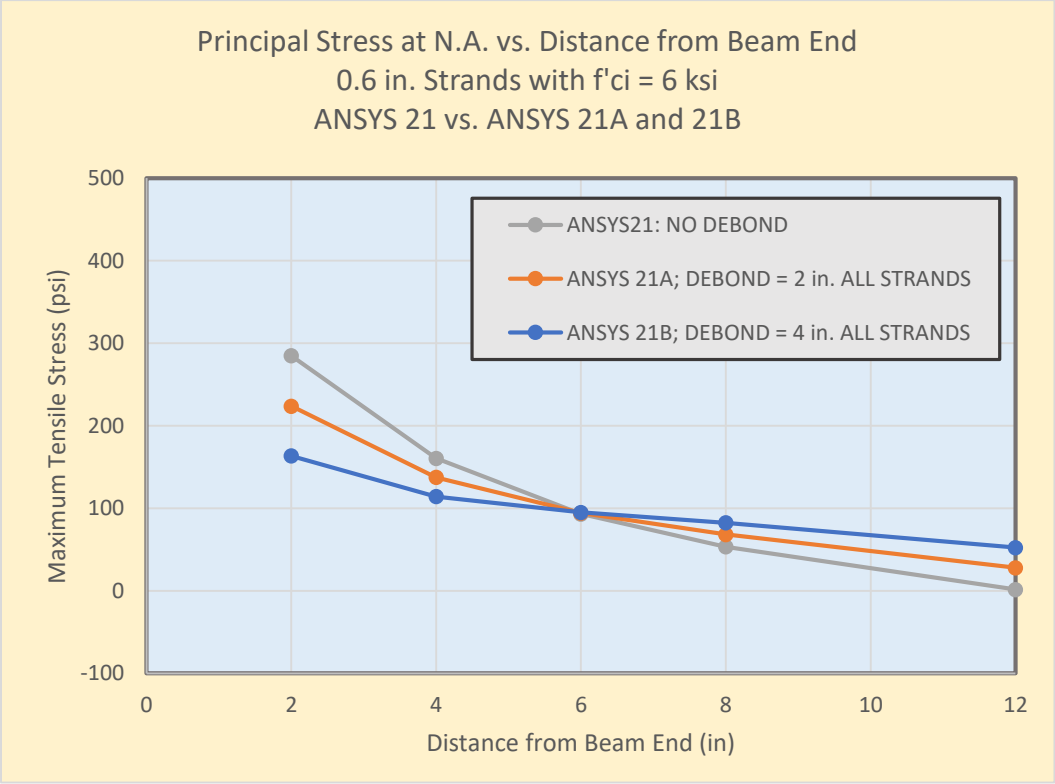

Figure 4.30. Principal Stress (tension) at the N.A., ANSYS 21, ANSYS 21A and ANSYS 21B

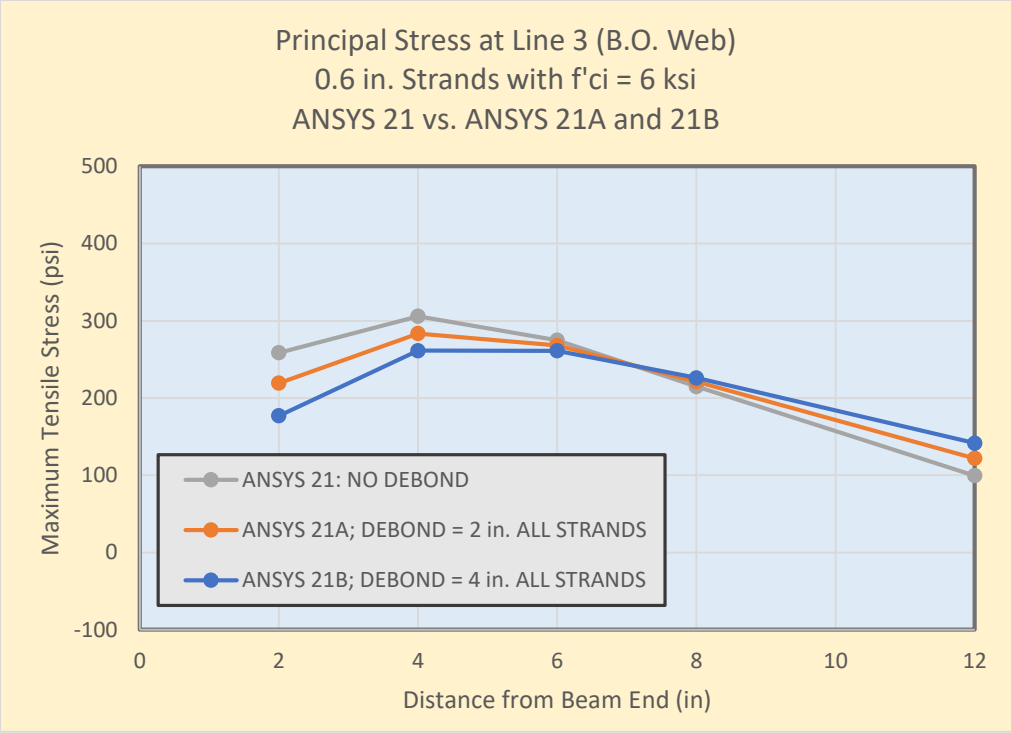

Figure 4.31. Principal Stress (tension) at Line 3, B.O.Web, ANSYS 21, ANSYS 21A and ANSYS 21B

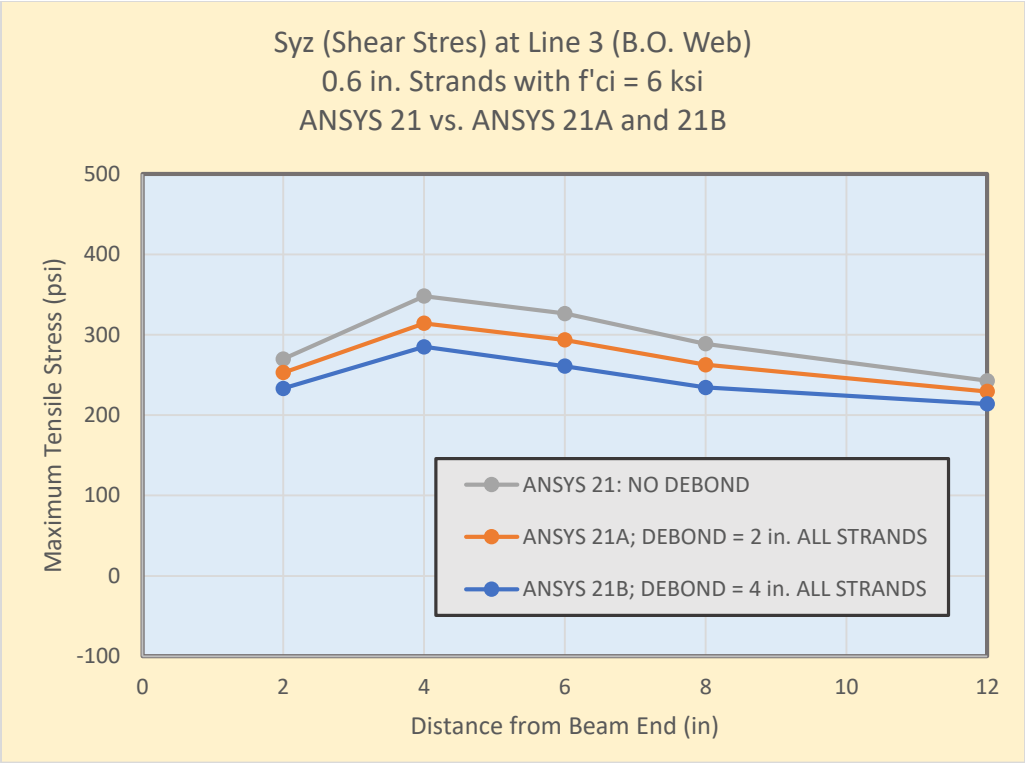

Figure 4.32. Shear Stress at Line 3, B.O. Web, ANSYS 21, ANSYS 21A and ANSYS 21B

4.6 Conclusions

Cracking in the experimental beams would start occurring at tensile stresses of approximately 400 psi on the average. This value of tensile stresses was observed to occur at number of FEA runs in the end regions, indicating that cracking in concrete starts to occur even at the prestress release conditions, and that this issue needs to be mitigated.

In summary, the following findings were observed as a result of the FEA to examine influence of prestressing variables and to find answers to the five stated questions.

1. ***What are the effects of improved strand bond quality (higher ASTM 1081)?***

Answer 1: It was found that the higher bonding strand results in increased tensile stresses in the concrete in end regions.

2. ***What are the effects of strand size (prestressing force) (0.5 vs. 0.6 in. strand)?***

Answer 2: It was found that larger strand sizes result in increased tensile stresses.

3. ***What are the effects of concrete strength?***

Answer 3: It was found that higher concrete strength results in shorter bond length and increased tensile stresses.

4. ***What are the effects of the top strand?***

Answer 4: It was found that the addition of the fully tensioned top strand increases tension stresses at the neutral axis, and tensile stresses at the bottom of the web are higher:

a. Addition of top strand will increase principal tension at the beam's neutral axis (N.A.).
b. Addition of top strand increases principal tension at the bottom of (B.O.) beam's web.

c. Addition of top strand has little effect on the shear stress computed at the bottom of (B.O.) beam's web.

5. What are the effects of the debonding strands?

Answer 5: It was found that debonding one strand in four reduces principal tensile stresses:

a. Debonding of one strand (20%) 24 inches has little effect on principal tension at the beam's neutral axis (N.A.).
b. Debonding of one strand reduces principal tension at the bottom of (B.O.) beam's web. Reduction in stress is significant in the range of 15%.
c. Debonding of one strand reduces the shear stress at the bottom of (B.O.) beam's web. Reductions approach 25%.
d. When looking into debonding all strands 2 inches and 4 inches (except the strand located 4 inches from beam bottom which is already debonded 24 inches) in cases ANSYS 21A, 21B, 24A, 24B, 25A and 25B it was found that the "measured" transfer length increases a little more than 2 inches in each increment, and that the principal tensile stresses go down significantly (40% at N.A. and 30% at the B.O. Web).
e. Debonding all strands by 4 inches significantly reduces principal tension from the beam end for several inches, so this strategy (debonding all strands) merits further investigation as results look very promising.

Overall, based on the FEA data that was produced and the previous considerations, here are some of the further summarized conclusions we can make:

1. Improving the bond quality of strand as measured by ASTM A1081 increases tension in end regions.

2. Increasing the size of the prestressing strands, and the corresponding prestress forces increases tension in end regions.
3. Increasing concrete strength at release improves the bond-ability of strand with concrete, and accordingly, increasing concrete strength increases the tension in end regions.
4. The inclusion of fully tensioned top strand (20% of total) increased principal tension in the webs at the neutral axis (N.A.).
5. The inclusion of fully tensioned top strand does not significantly increase principal tension at the bottom of (B.O.) beam's web.
6. The debonding of 25% of bottom strands reduced principal tension at the neutral axis (N.A.) by 9%.
7. The debonding of 25% of bottom strands reduced principal tension at the bottom of (B.O.) beam's web by 10%. Debonding 25% of bottom strands decreased the shear stress at the bottom of (B.O.) beam's web by 28%.
8. The debonding of all strands significantly reduced tension in the end regions. At the N.A., principal tension decreased 22% by debonding all strands 2 inches. At the N.A., principal tension decreased by 43% by debonding all strands 4 inches.

4.7 Recommendations

The test matrix for FEA was developed to help define the pertinent variables and examine the influence of these variables to the end regions in prestressed concrete beam. The results have implications on the current design practice, since the design practice should have a goal of mitigating cracking and other damage in the end regions of prestressing strands at release, with an ancillary goal of improving performance under external loading.

Following suggested recommendations were produced based on the conducted FEA research:

1. Debond in accordance with the needs for allowable stresses at release (tension and compression) as required by AASHTO.
2. Additionally, debond 50% of the strands at least 4 inches from the end of the beam, or all strands at least 2 inches from the end of the beam to reduce the tension concentrations near the beams' end regions.
3. Debond at least 50% top strands 8 inches, or debond all top strands for 4 inches to help prevent tension stress concentrations near the end regions.

REFERENCES

1. Ganpatye, Amol S., "Recommendations for the Development Length of Prestressing Strands Including the Effects of High Strength Concrete," Master's Thesis, Oklahoma State University, Stillwater, Oklahoma, 2006
2. Mayhorn, Darion, "Investigation of the Effects of End Region Deterioration in Precast, Prestressed Concrete Bridge Girders," Master's Thesis, University of Oklahoma, Norman, Oklahoma, 2016
3. "ANSYS Fundamental FEA Concepts and Applications: A Guidebook for the Use and Applicability of Workbench Simulation Tools from ANSYS, Inc." *<www.cae.tntech.edu/~chriswilson/FEA/ANSYS/ANSYSguide_fea-concepts.pdf> Internet webpage, Downloaded October 2018*
4. Oklahoma Department of Transportation (ODOT), "Oklahoma Department of Transportation Special Provisions for Elastomeric Bearing Pads", 2012
5. Jacob, John, "Improved Shear Reinforcement Details for the End-Regions of Prestressed Concrete Bridge Girders," Master's Thesis, University of Oklahoma, Norman, Oklahoma, 1998
6. American Society for Testing and Materials (ASTM), "Standard Test Method for Evaluating Bond of Seven-Wire Steel Prestressing Strand" (ASTM A1081/A1081M-15)
7. American Society for Testing and Materials (ASTM), "Standard Test Method for Rubber Property – Durometer Hardness" (ASTM D2240-15)

8. Reddy, J.N., “An Introduction to Finite Element Method,” McGraw-Hill, New York, NY, Third Edition, 2006
9. Jiang, Xin. “Bind Performance of High-Capacity Strands in High Strength Concrete.” PhD diss., University of Tennessee, 2013
10. Fjaer, Erling and Ruistuen, Helge. “Impact of the Intermediate Principal Stress on the Strength of Heterogeneous Rock.” Journal of Geophysical Research , Vol. 107, 2002
11. Polydorou, Thomaida.”Determination of Acceptance Criteria for Prestressing Strand in Pre-Tensioned Applications.” PhD diss., Kansas State University, Manhattan, Kansas, 2014
12. Floyd, Royce W., “Investigating the Bond of Prestressing Strands in Lightweight Self-Consolidating Concrete.” PhD diss., University of Arkansas, 2012
13. Carroll, Chris J., Cousing, Thomas E. and Roberts-Wollmann, Carin L., “The Use of Grade 300 Prestressing Strand in Pretensioned Prestressed Concrete Beams.” PCI Journal, January-February, 2017
14. American Society for Testing and Materials (ASTM), “Standard Specification for Steel Strand, Uncoated Seven-Wire for Prestressed Concrete” (ASTM A416/A416M-18)
15. Russell, Bruce W. and Burn, Ned H., “Design Guidelines for Transfer, Development and Debonding of Large Diameter Seven Wire Strands in Pretensioned Concrete Girders. ”Research Report 1210-SF, University of Texas, Austin, 1993
16. Kramer, Steven L., “Geotechnical Earthquake Engineering.” Prentice-Hall, Upper Saddle River, NJ, 1996
17. Shames, Irving H. and Cozzarelli, Francis A., “Elastic and Inelastic Stress Analysis.” Taylor and Francis, Philadelphia, PA, 1997

18. Wight, James K., “Reinforced Concrete: Mechanics and Design.” Pearson Education Limited, England, 2016
19. Schlaich, Jörg and Weischede, Dieter, “Detailing of Concrete Structures.” Bulletin d’Information 150, Comité Euro-International du Béton, Paris, March 1982, pp163.
20. Schlaich, Jörg, Schäfer, Kurt and Jennewein, Mattias, “Toward a Consistent Design of Structural Concrete.” Journal of the Prestressed Concrete Institute, Vol. 32, No. 3, May – June 1987, pp74-150
21. Schlaich, Jörg and Schäfer, Kurt, “Design and Detailing of Structural Concrete Using Strut-and-Tie Models.” Structural Engineer, Vol. 69, No. 6, March 1991, pp13
22. Hasenkamp, Christie J., Badie, Sameh S., Hanna, Kromel E. and Tadros, Maher K., “Proposed Evaluation and Repair Procedures for Precast, Prestressed Concrete Girders with End-Zone Cracking.” PCI Journal, Issue Spring 2012, pp94-119
23. Leonhardt, Fritz, “Cracks and Crack Control in Concrete Structures.” PCI Journal, Issue July-August 1988, pp124-145
24. An, JinWoo, “ Estimation of Beam Prestress by Deflection and Strain Measurements” Master’s Thesis, University of Texas, Austin, Texas, 2012
25. Osborn, A.E.N., Lawler, John Steven, Connolly, James D., “Acceptance Tests for Surface Characteristics of Steel Strands in Prestressed Concrete.” National Cooperative Highway Research Program. Transportation Research Board, 2008
26. Luke, Lance R., “Load Balancing as Design Method for Concrete Prestressed Bridge Girders.” Master’s Thesis, Oklahoma State University, Stillwater, Oklahoma, 2016

27. Vargas, Martí, Rocío, José, Serno, Pedro Ros. And Hale, W.M., “Strand Bond Performance in Prestressed Concrete Accounting for Bondslip.” Technical University of Valencia, Valencia, Spain, 2013
28. Chandran, K., “Assessing the Bond Quality of Prestressing Strands Using NASP Bond Test.” Master’s Thesis, Oklahoma State University, Stillwater, 2006
29. Tessema, E. “The Effect of High Strength Concrete on the Bondability of Prestressing Strands.” Master’s Thesis, Oklahoma State University, Stillwater, 2006
30. Jayaseelan, H., “Prestress Losses in Concrete and the Estimation of Long-Term Deflections and Camber for Prestressed Concrete Bridges.” Master’s Thesis, Oklahoma State University, Stillwater, 2007
31. Carroll, Chris, Cousins, Thomas and Roberts-Wollmann, Carin, “A Practical Approach for Finite-Element Modeling of Transfer Length in Pretensioned, Prestressed Concrete Members Using End-Slip Methodology.” PCI Journal, Summer 2014, pp110-129
32. Ross, Brandon, Willis, Michael, Hamilton, H. and Consolazio, Gary, “Comparison of Details for Controlling End-Region Cracks in Precast, Pretensioned Concrete I-Girders.” PCI Journal, Spring 2014, pp96-108
33. Okumus, Pinar and Oliva, Michael, “Evaluation of Crack Control Methods for End Zone Cracking in Prestressed Concrete Bridge Girders.” PCI Journal, Spring 2013, pp91-105
34. Tuan, Christopher, Yehia, Sherif, Jongpitaksseel, Nipon and Tadros, Maher, “End Zone Reinforcement for Pretensioned Concrete Girders.” PCI Journal, Summer 2004, pp2-16
35. Tanasap, Nuttapong, “Ensuring Shear Strength in I-Shaped Prestressed Concrete Girders.” Master’s Thesis, Oklahoma State University, Stillwater, 2015

36. Oklahoma Department of Transportation (ODOT), "Oklahoma Department of Transportation Specifications", 2009

37. Okumus, Pinar and Oliva, Michael, "Strand Debonding for Pretensioned Bridge Girders to Control End Cracks." ACI Structural Journal 111(1), January 2014, pp201-210

38. American Association of State Highway and Transportation Officials (AASHTO). AASHTO LRFD Bridge Design Specifications. 5th Edition, Washington DC, 2010

39. Hasenkamp, Christie, Badie, Sameh, Tuan, Christopher and Tadros, Maher, "Sources of End Zone Cracking of Pretensioned Concrete Girders." Civil Engineering Faculty Proceedings & Presentations, University of Nebraska, Omaha, 2008

40. Okumus, Pinar, Kristam, Rama and Arancibia, Mauricio, "Sources of Crack Growth in Pretensioned Concrete-Bridge Girder Anchorage Zones after Detensioning." Journal of Bridge Engineering, Volume 21, Issue 10, October 2016

APPENDICES

- A-1: Variations in Principal Tension for ANSYS Cases 1, 2 and 3
- A-2: Variations in Principal Tension for ANSYS Cases 4, 5 and 6
- A-3: Variations in Principal Tension for ANSYS Cases 7, 8 and 9
- A-4: Variations in Principal Tension for ANSYS Cases 10, 11 and 12
- A-5: Variations in Principal Tension for ANSYS Cases 13, 14 and 15
- A-6: Variations in Principal Tension for ANSYS Cases 19 and 20
- A-7: Variations in Principal Tension for ANSYS Cases 21, 21A and 21B
- A-8: Variations in Principal Tension for ANSYS Cases 21, 22 and 23
- A-9: Variations in Principal Tension for ANSYS Cases 24, 24A and 24B
- A-10: Variations in Principal Tension for ANSYS Cases 24, 25 and 26
- A-11: Variations in Principal Tension for ANSYS Cases 25, 25A and 25B
- A-12: Variations in Principal Tension for ANSYS Cases 27, 28 and 29

A-1: Variations in Principal Tension for ANSYS Cases 1, 2 and 3

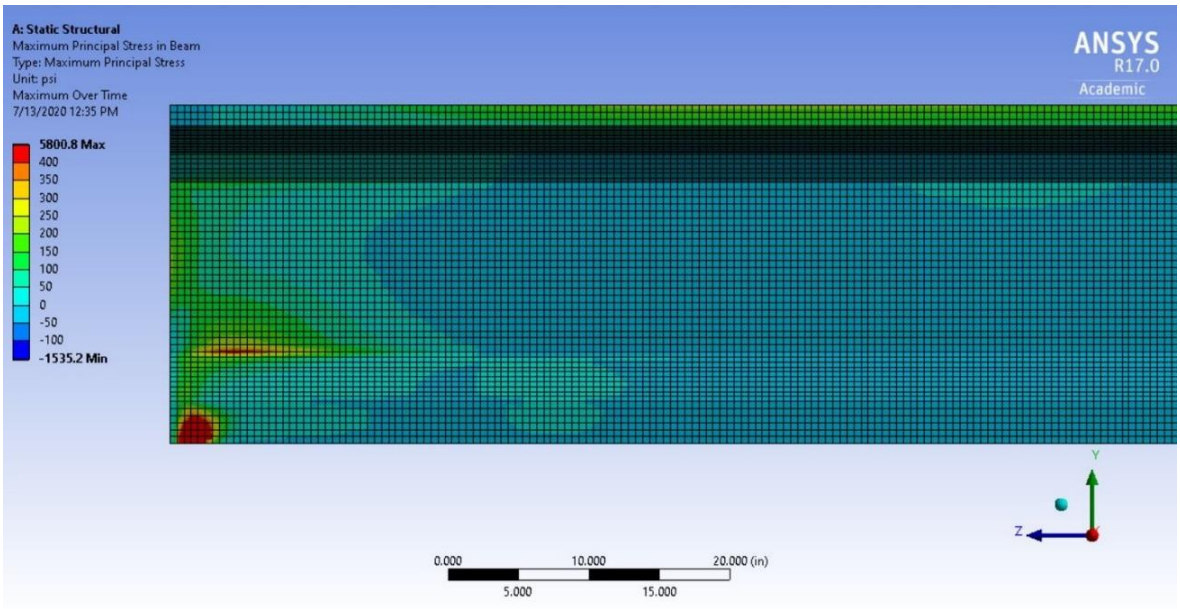

Figure A-1-1. ANSYS 1 Principal Tensile Stress, A1081 = 9,000 lbs, 0.5 in. strands, f'ci = 6 ksi, No Top Strand, No Debonding

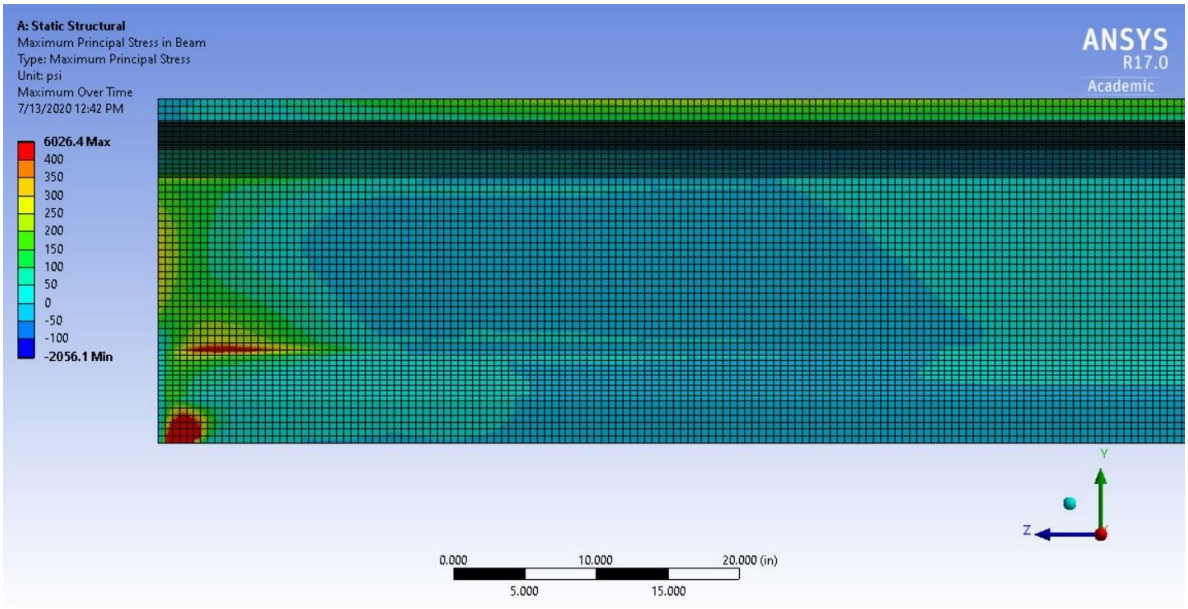

Figure A-1-2. ANSYS 2 Principal Tensile Stress, A1081 = 12,000 lbs., 0.5 in. strands, f'ci = 6 ksi, No Top Strand, No Debonding

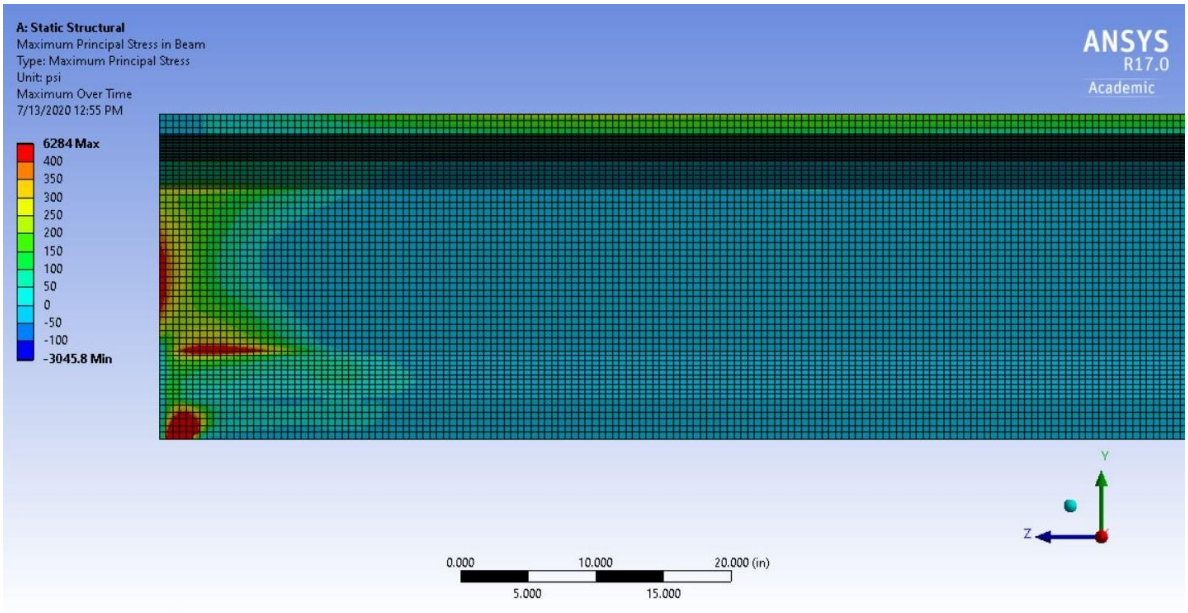

Figure A-1-3. ANSYS 3 Principal Tensile Stress, A1081 = 18,000 lbs., 0.5 in. strands, f'ci = 6 ksi, No Top Strand, No Debonding

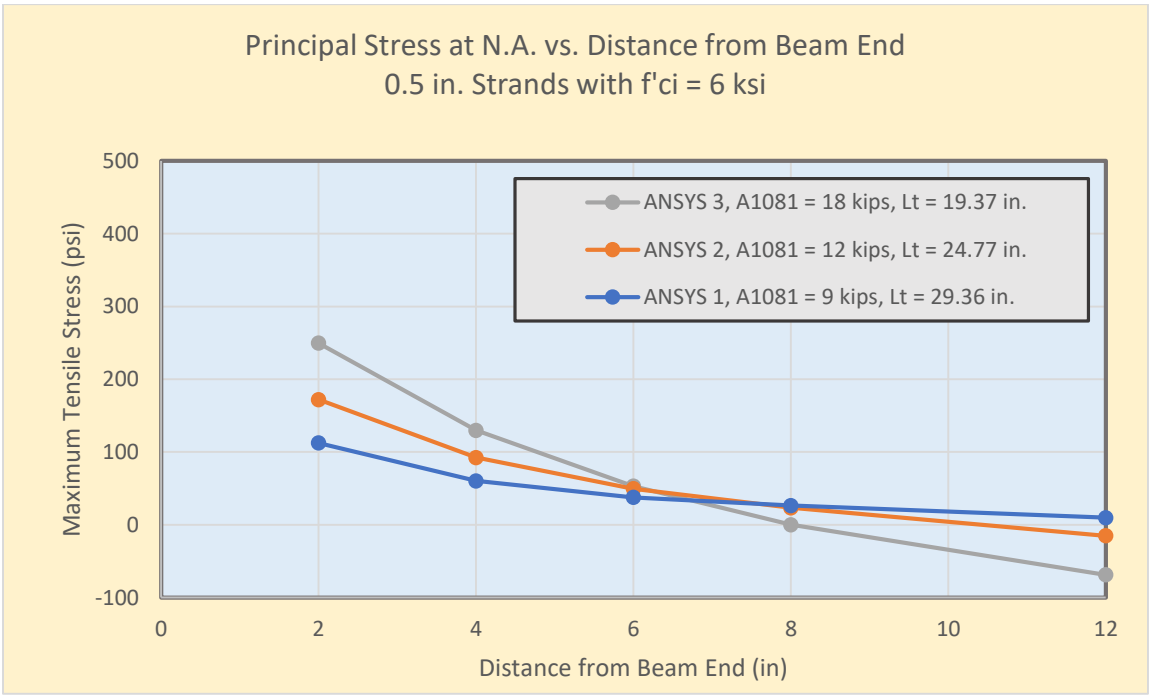

Figure A-1-4. Principal Stress (tension) at the N.A., ANSYS 1, ANSYS 2 and ANSYS 3

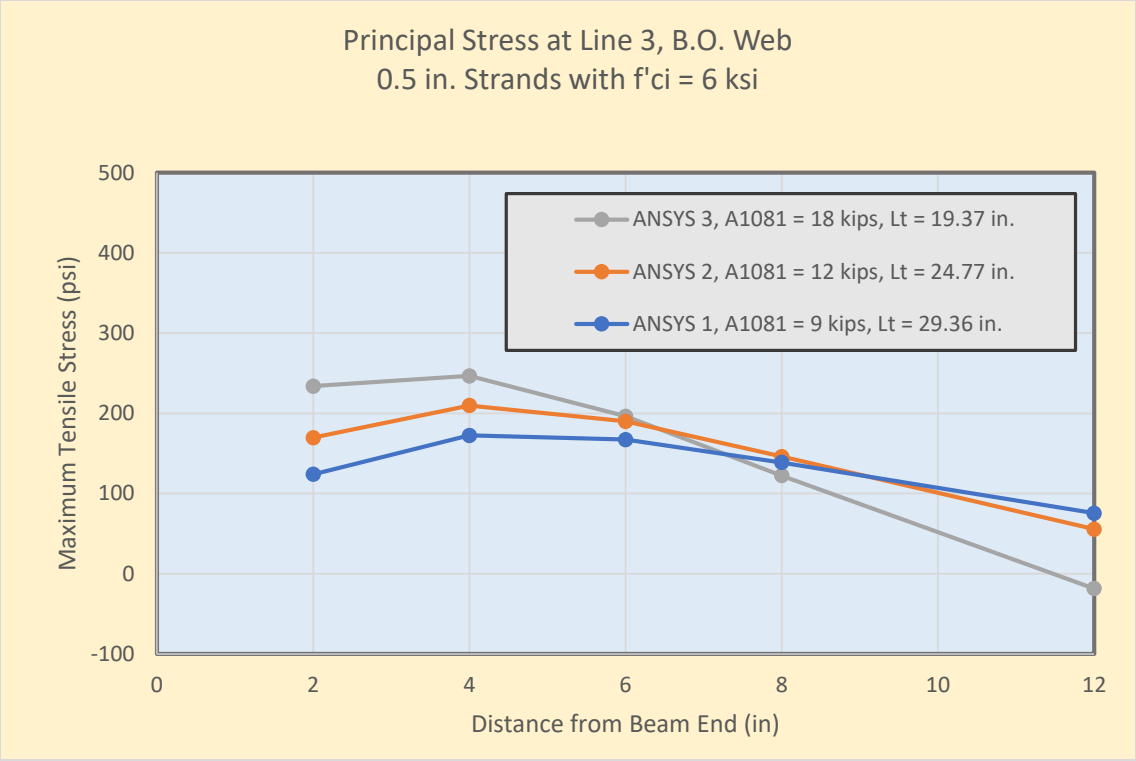

Figure A-1-5. Principal Stress (tension) at Line 3, B.O.Web, ANSYS 1, ANSYS 2 and ANSYS 3

A-2: Variations in Principal Tension for ANSYS Cases 4, 5 and 6

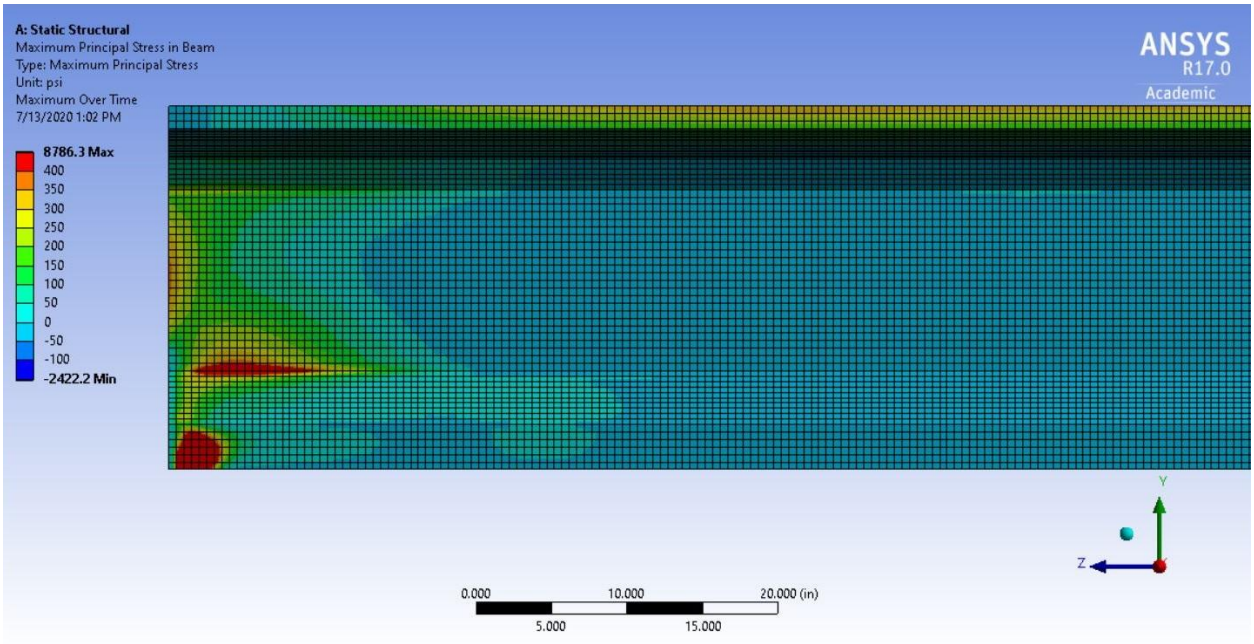

Figure A-2-6. ANSYS 4 Principal Tensile Stress, A1081 = 14,400 lbs, 0.6 in. strands, f'ci = 6 ksi, No Top Strand, No Debonding

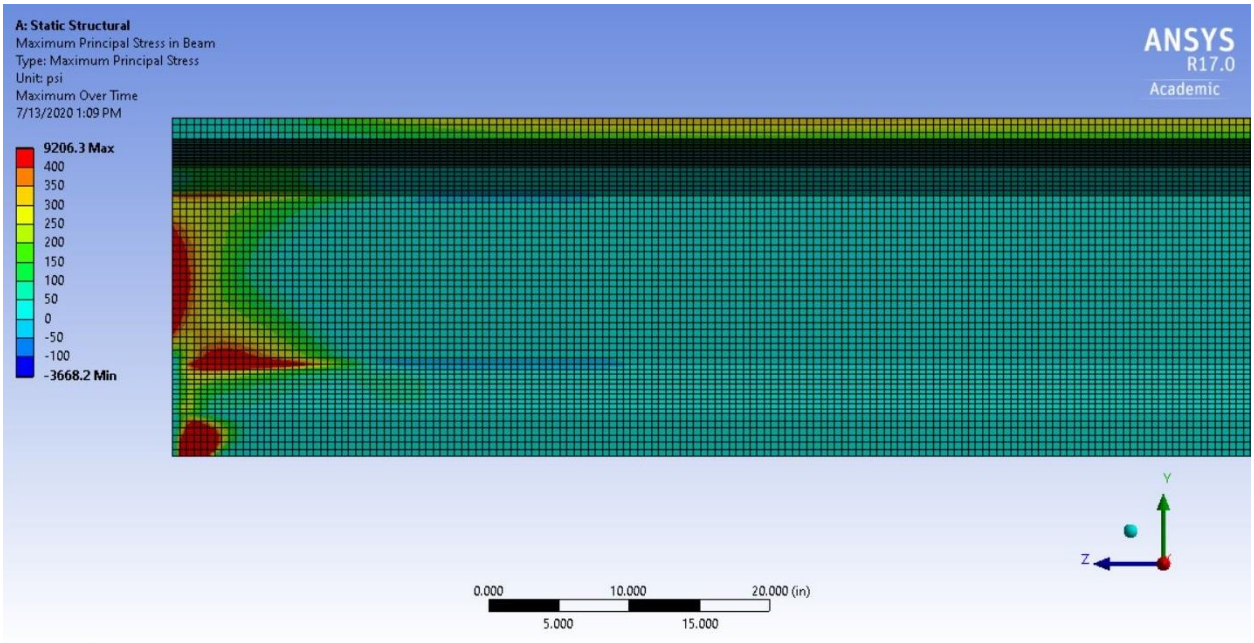

Figure A-2-7. ANSYS 5 Principal Tensile Stress, A1081 = 21,600 lbs., 0.6 in. strands, f'ci = 6 ksi, No Top Strand, No Debonding

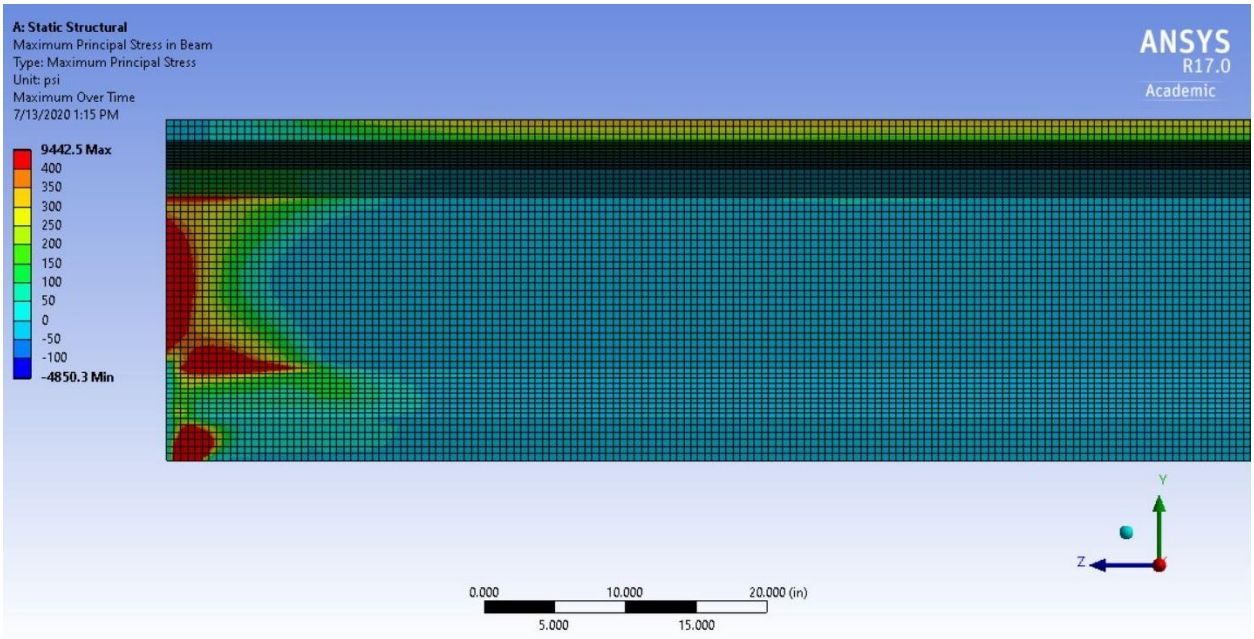

Figure A-2-8. ANSYS 6 Principal Tensile Stress, A1081 = 28,800 lbs., 0.6 in. strands, f'ci = 6 ksi, No Top Strand, No Debonding

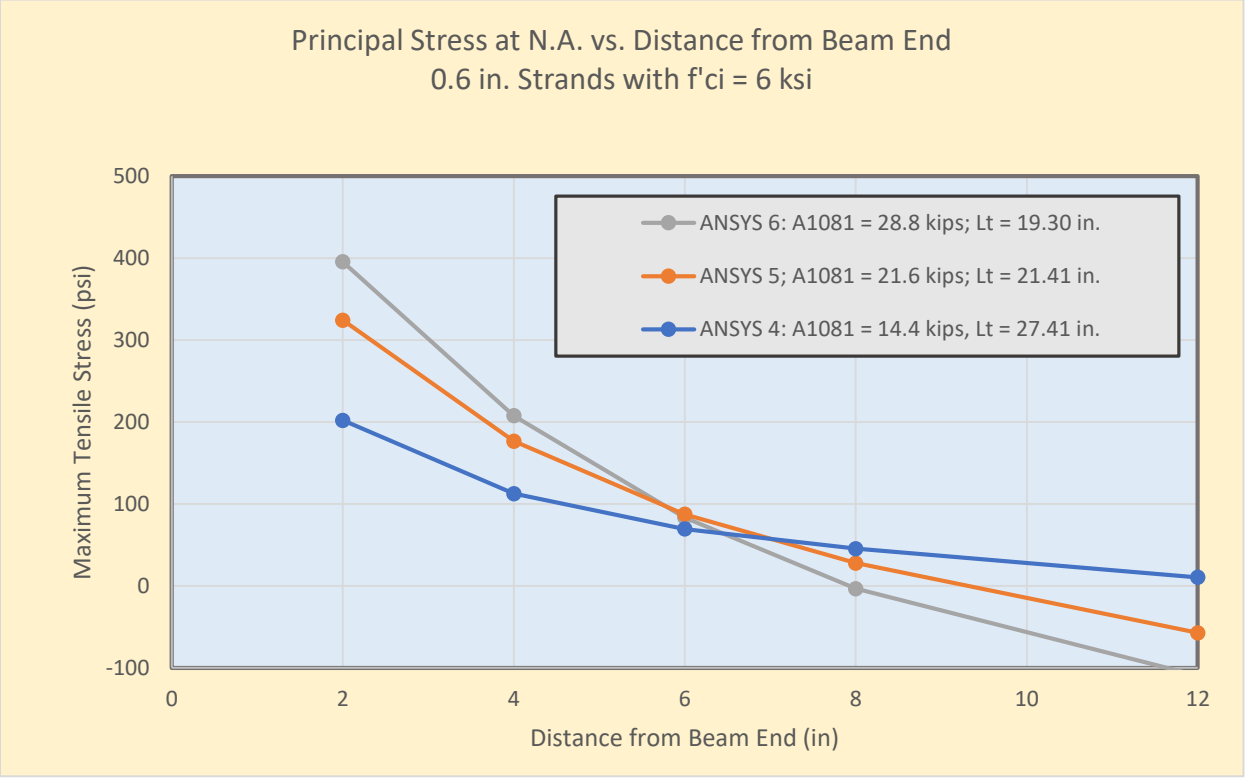

Figure A-2-9. Principal Stress (tension) at the N.A., ANSYS 4, ANSYS 5 and ANSYS 6

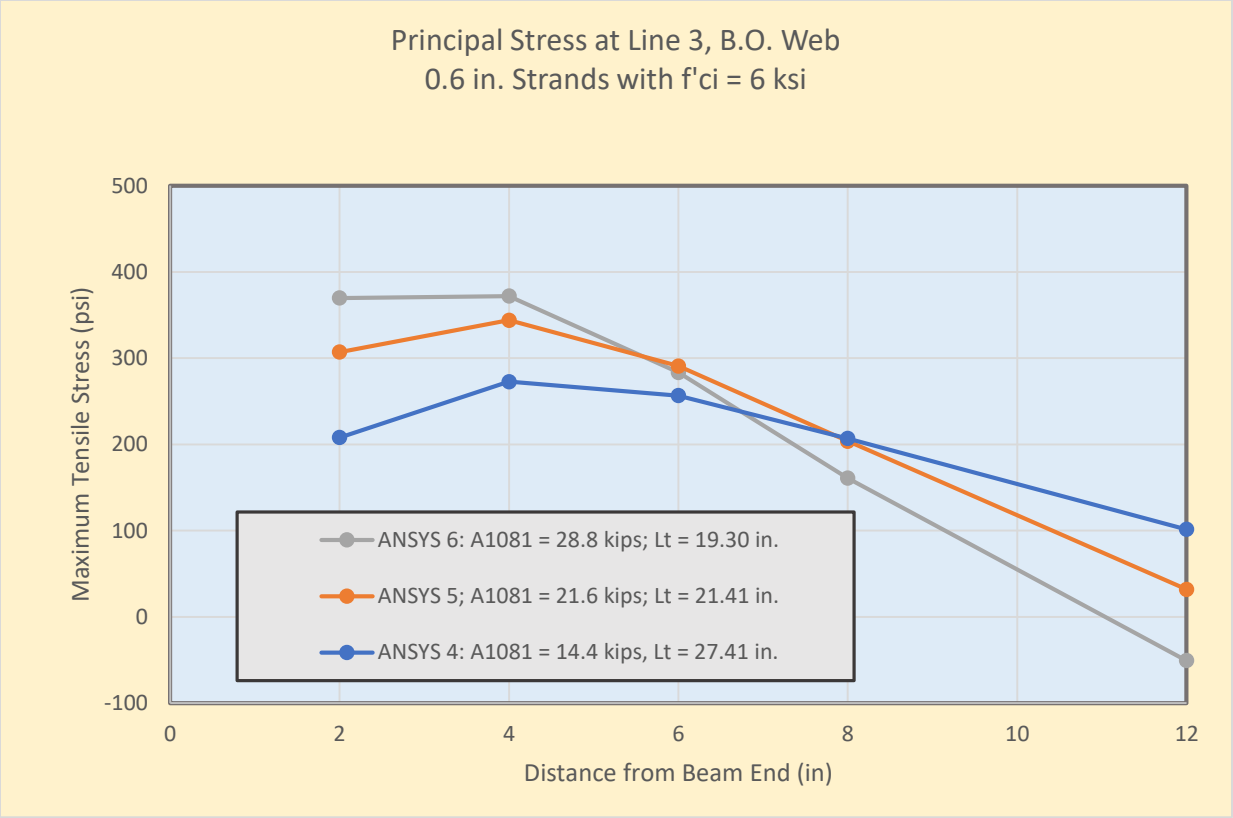

Figure A-2-10. Principal Stress (tension) at Line 3, B.O.Web, ANSYS 4, ANSYS 5 and ANSYS 6

A-3: Variations in Principal Tension for ANSYS Cases 7, 8 and 9

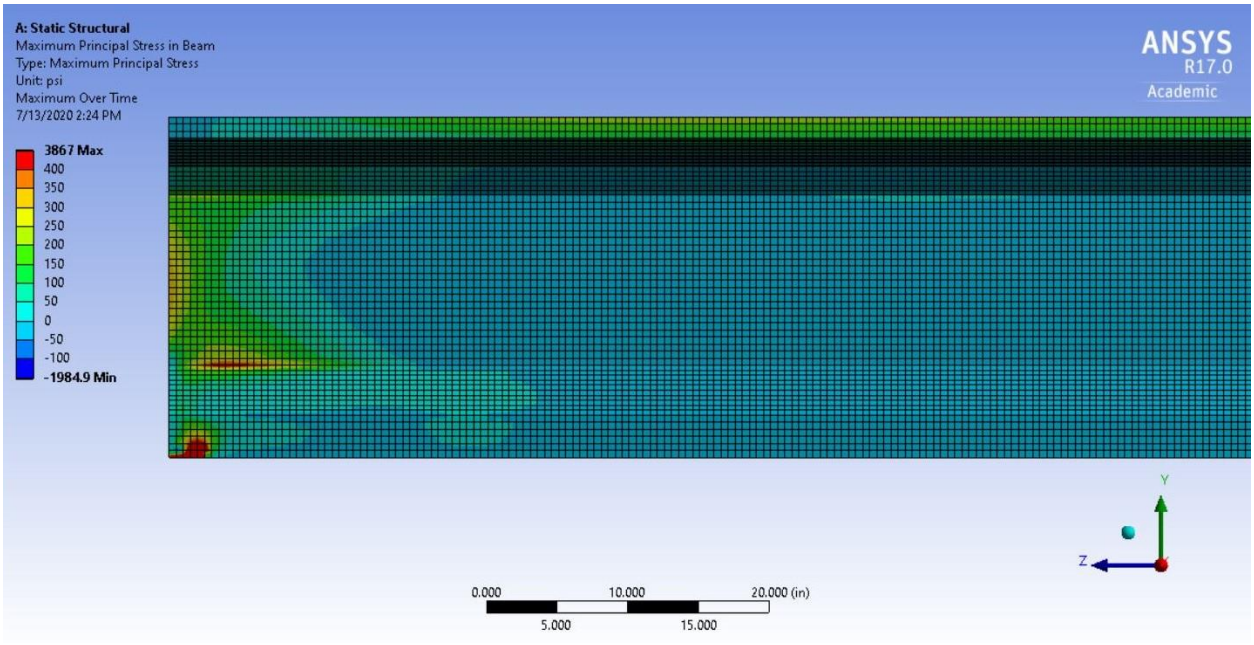

Figure A-3-11. ANSYS 7 Principal Tensile Stress, A1081 = 9.000 lbs, 0.5 in. strands, f'ci = 10 ksi, No Top Strand, No Debonding

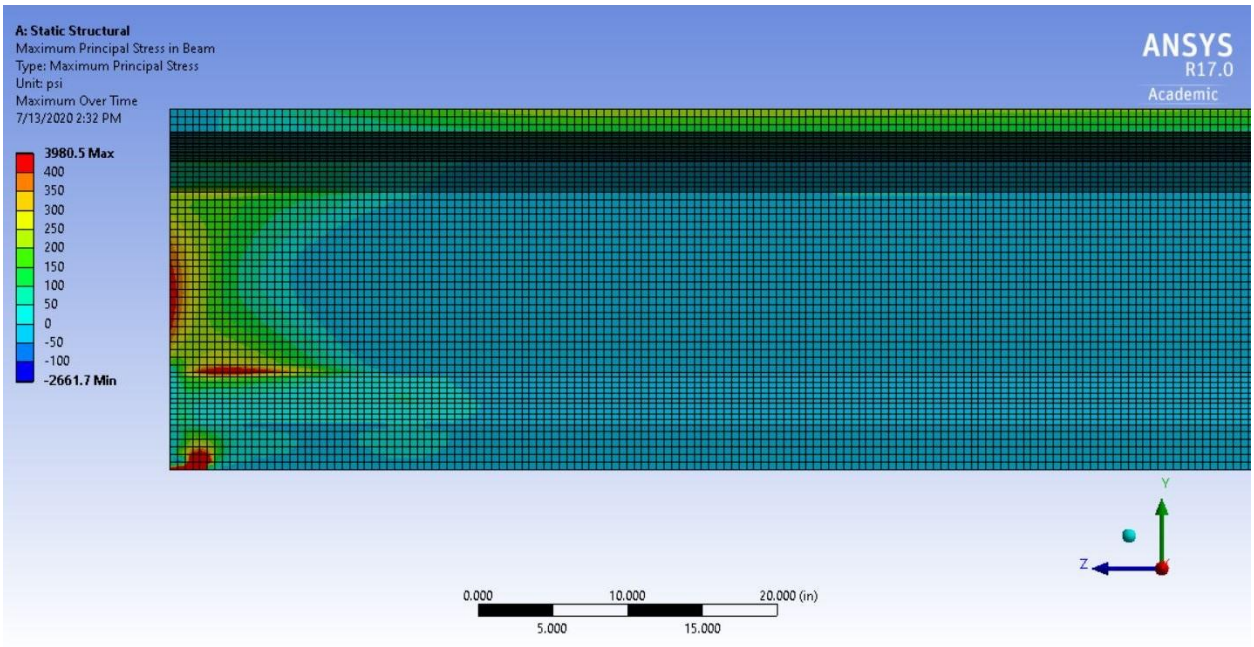

Figure A-3-12. ANSYS 8 Principal Tensile Stress, A1081 = 12,000 lbs., 0.5 in. strands, f'ci = 10 ksi, No Top Strand, No Debonding

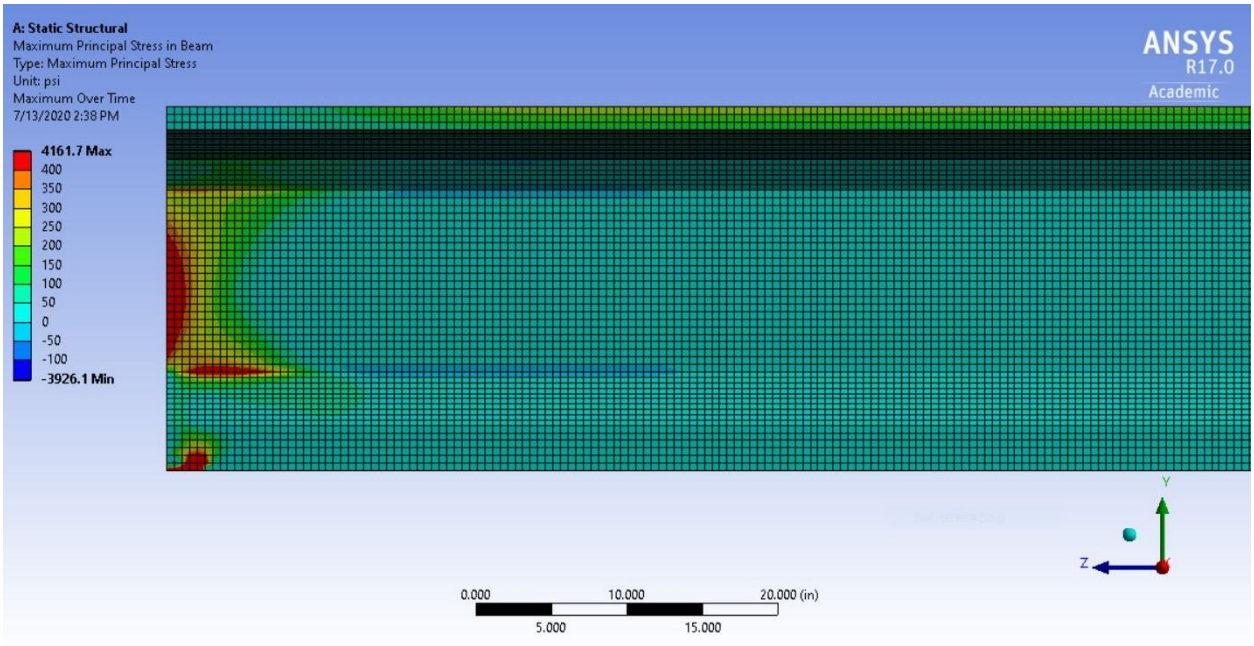

Figure A-3-13. ANSYS 9 Principal Tensile Stress, A1081 = 18,000 lbs., 0.5 in. strands, f'ci = 10 ksi, No Top Strand, No Debonding

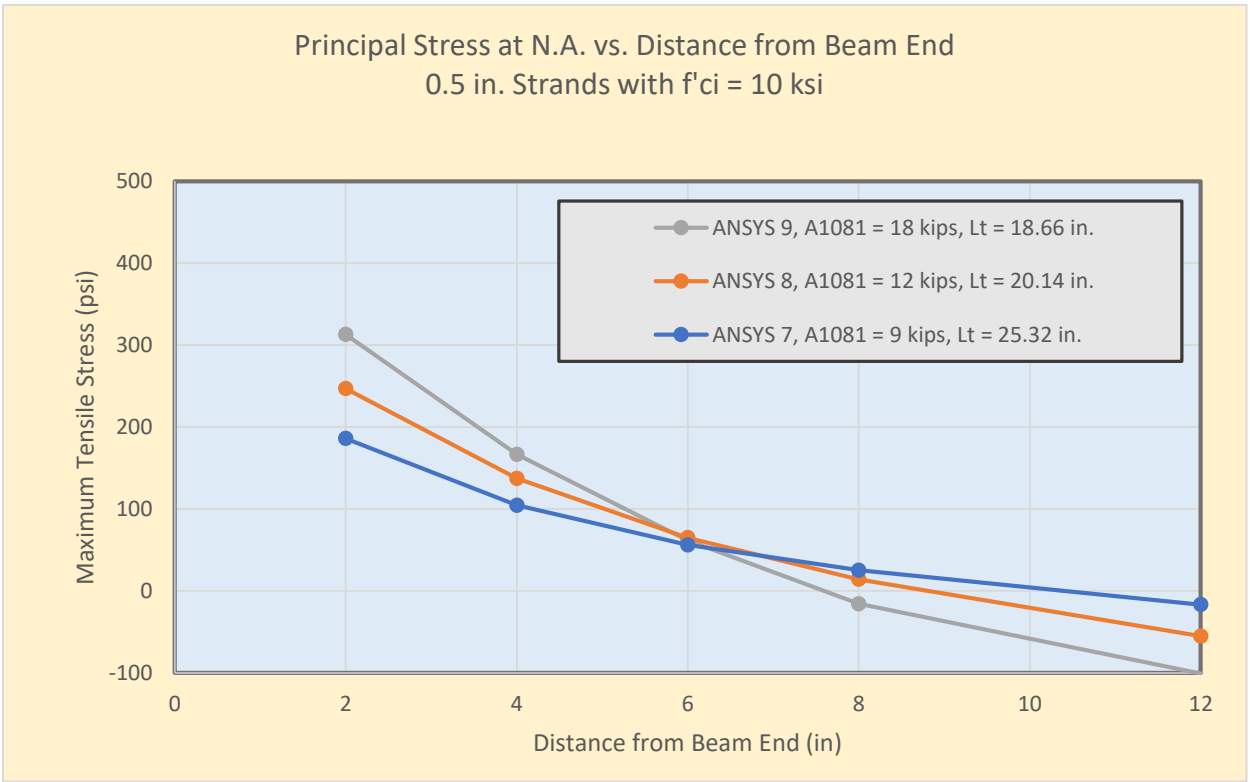

Figure A-3-14. Principal Stress (tension) at the N.A., ANSYS 7, ANSYS 8 and ANSYS 9

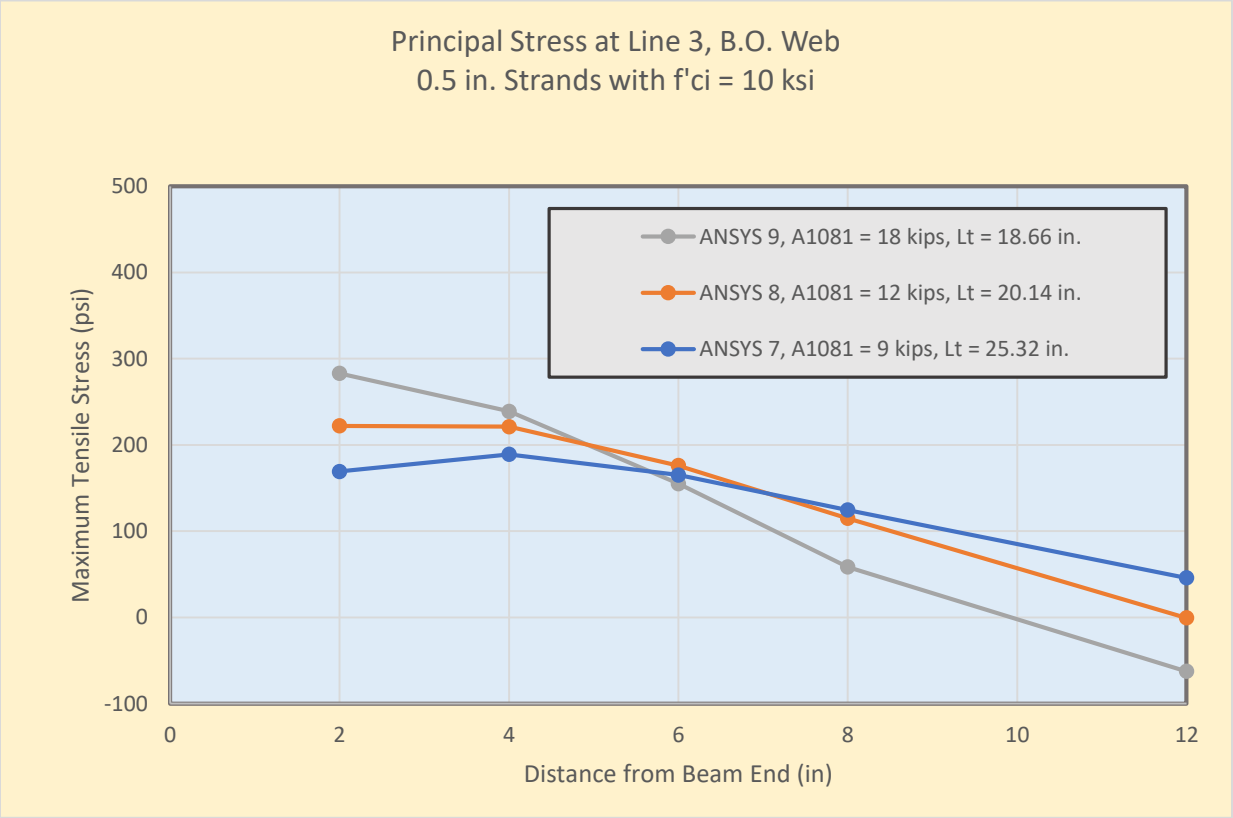

Figure A-3-15. Principal Stress (tension) at Line 3, B.O.Web, ANSYS 7, ANSYS 8 and ANSYS 9

A-4: Variations in Principal Tension for ANSYS Cases 10, 11 and 12

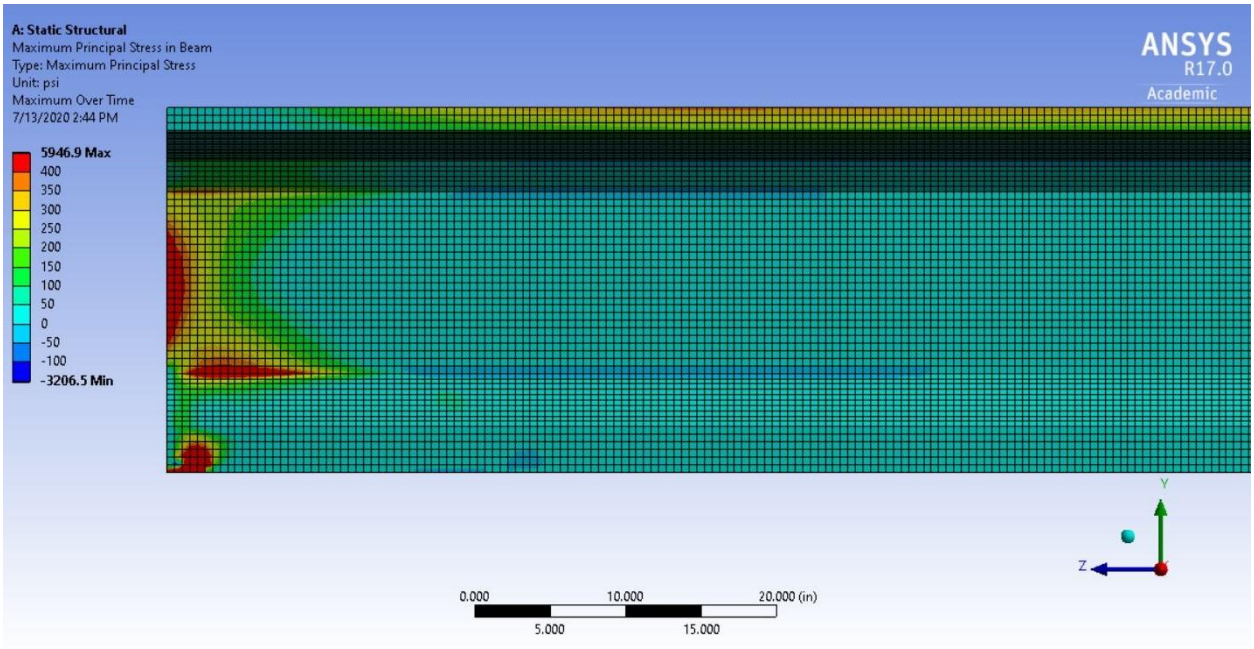

Figure A-4-16. ANSYS 10 Principal Tensile Stress, A1081 = 14,400 lbs, 0.6 in. strands, f'ci = 10 ksi, No Top Strand, No Debonding

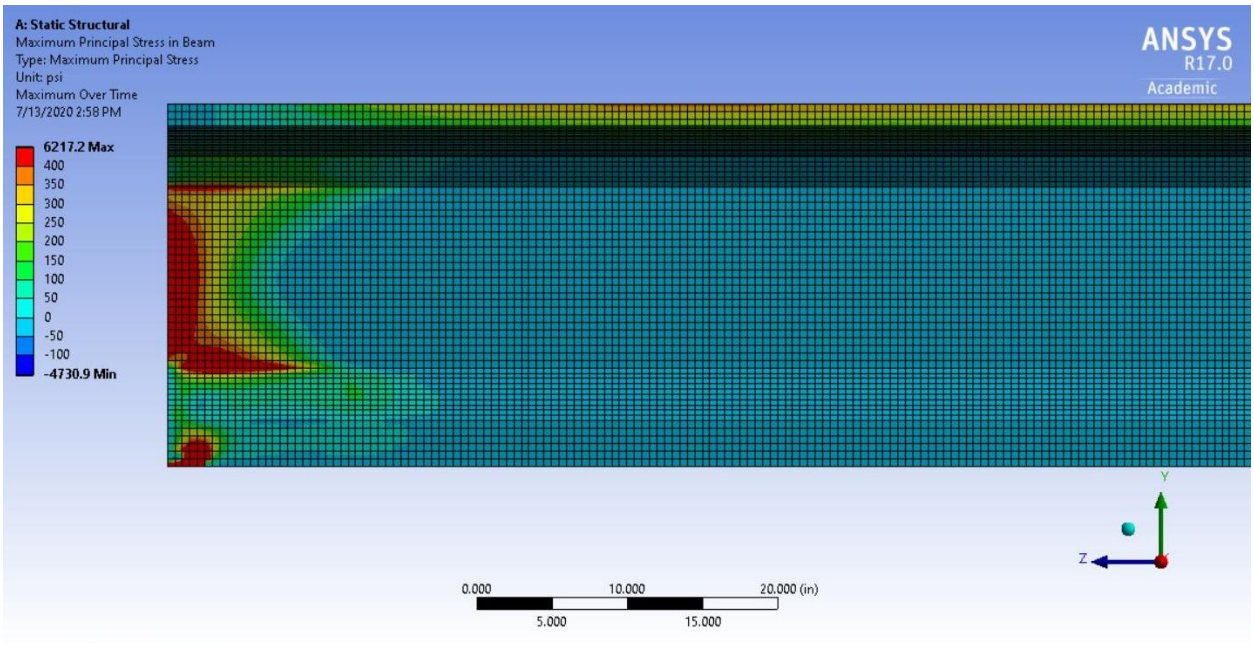

Figure A-4-17. ANSYS 11 Principal Tensile Stress, A1081 = 21,600 lbs., 0.6 in. strands, f'ci = 10 ksi, No Top Strand, No Debonding

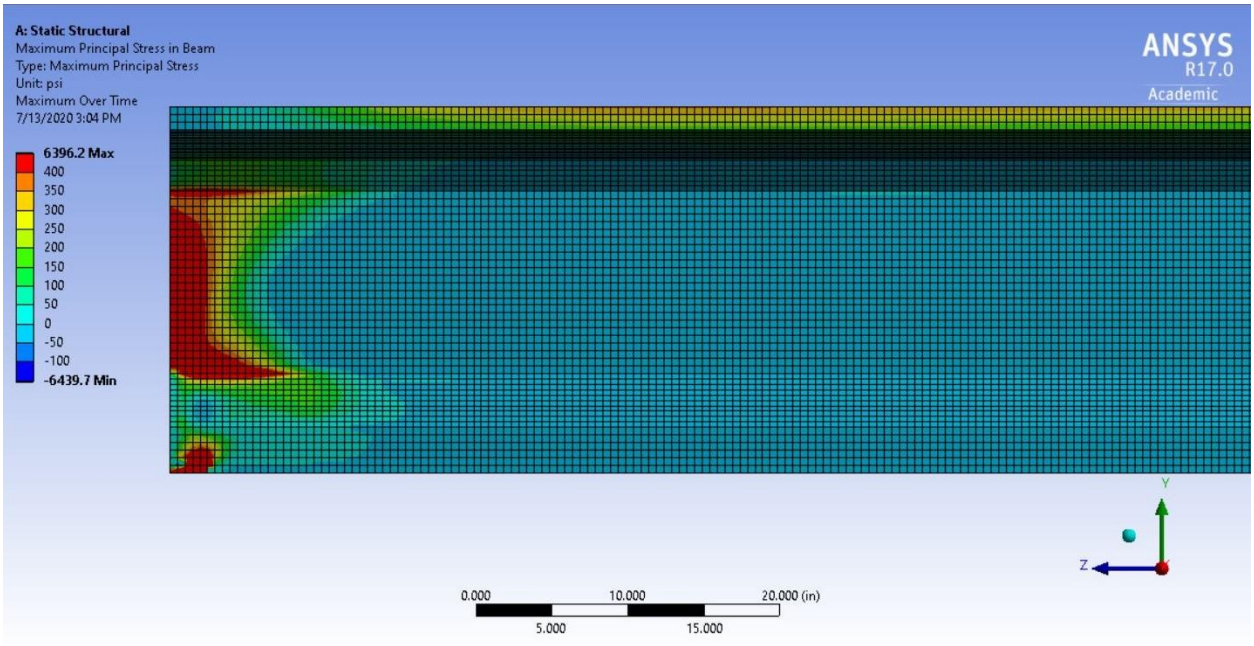

Figure A-4-18. ANSYS 12 Principal Tensile Stress, A1081 = 28,800 lbs., 0.6 in. strands, f'ci = 10 ksi, No Top Strand, No Debonding

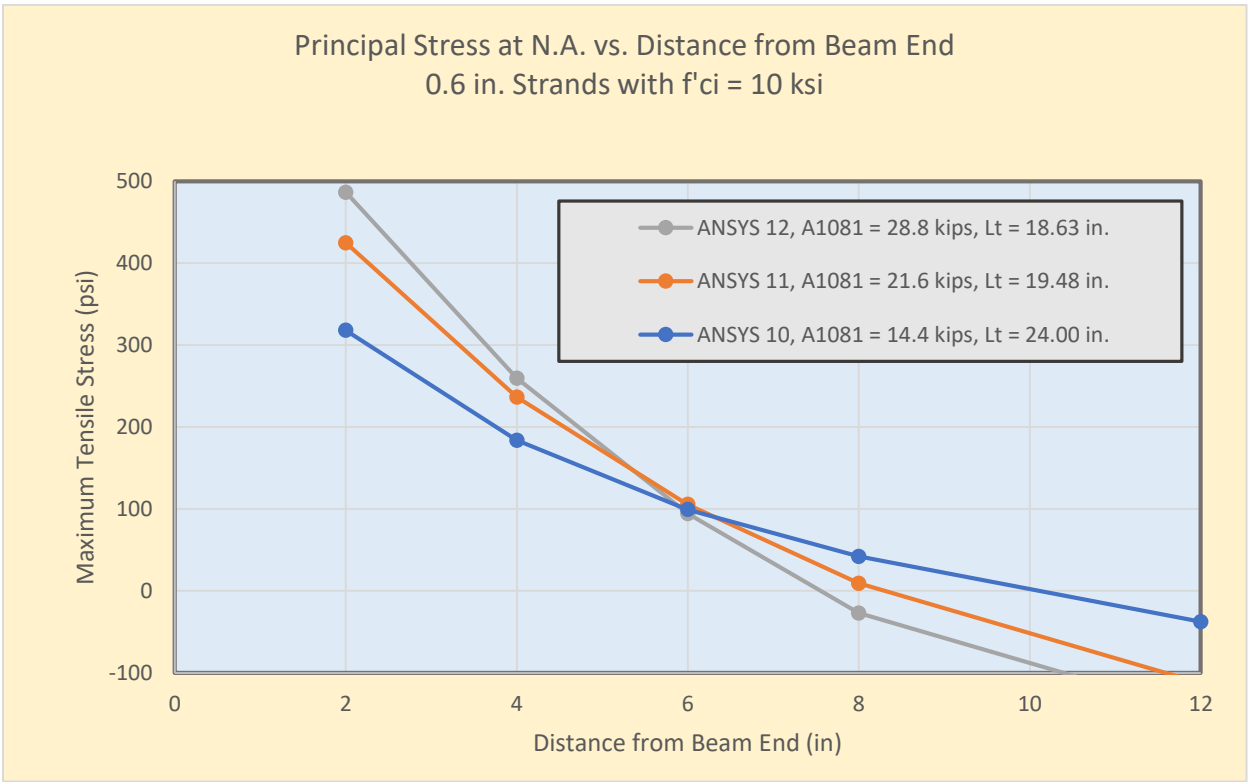

Figure A-4-19. Principal Stress (tension) at the N.A., ANSYS 10, ANSYS 11 and ANSYS 12

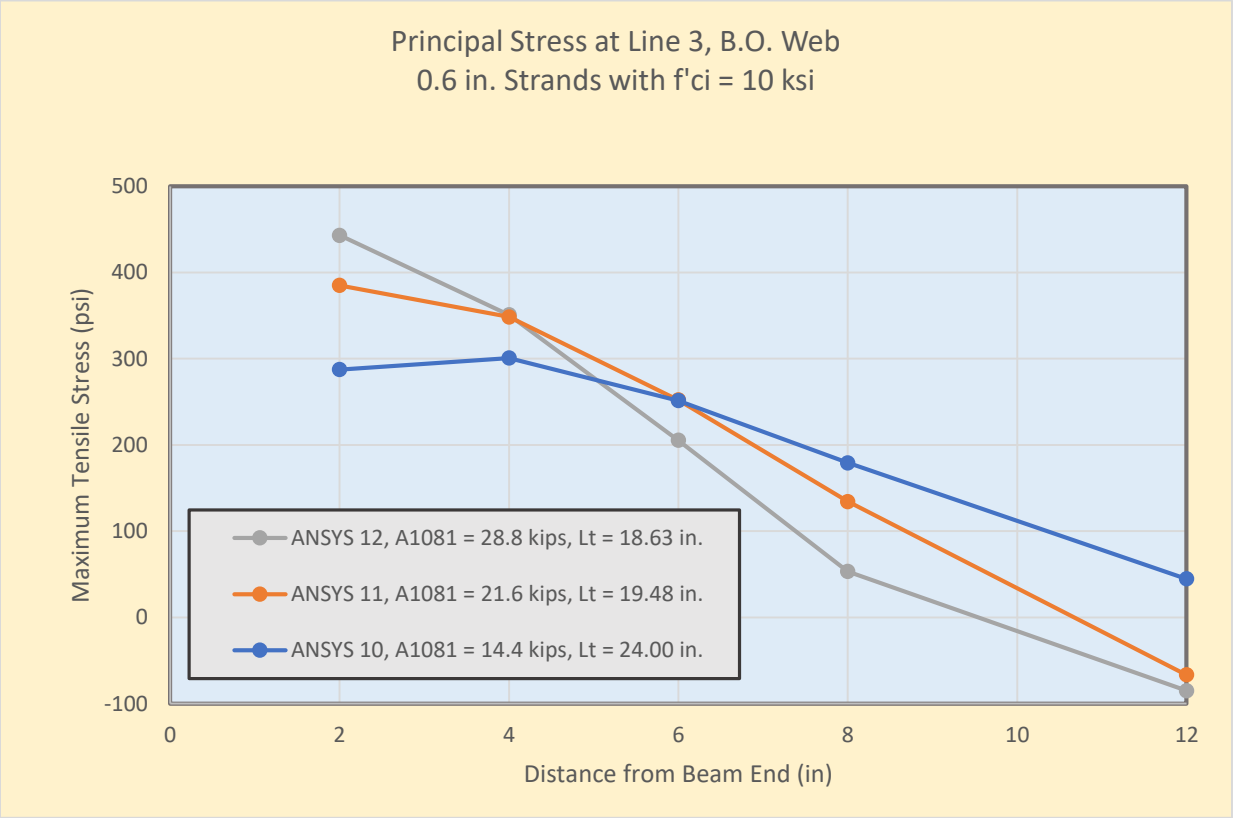

Figure A-4-20. Principal Stress (tension) at Line 3, B.O.Web, ANSYS 10, ANSYS 11 and ANSYS 12

A-5: Variations in Principal Tension for ANSYS Cases 13, 14 and 15

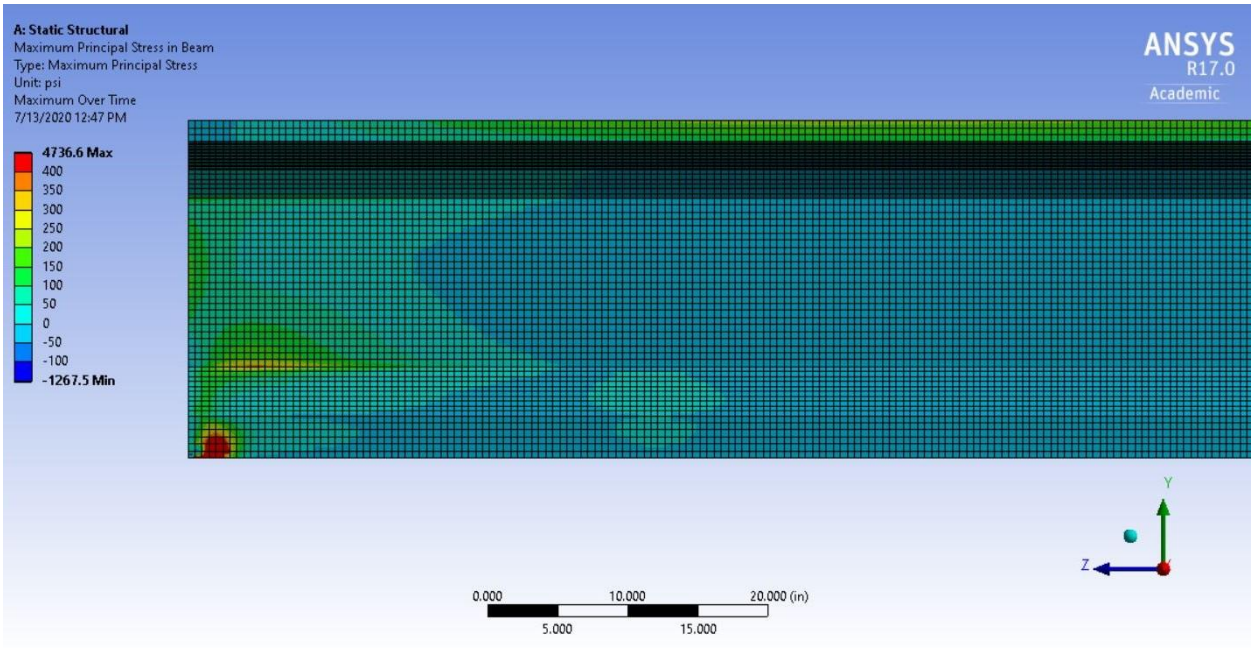

Figure A-5-21. ANSYS 13 Principal Tensile Stress, A1081 = 9,000 lbs, 0.5 in. strands, f'ci = 4 ksi, No Top Strand, No Debonding

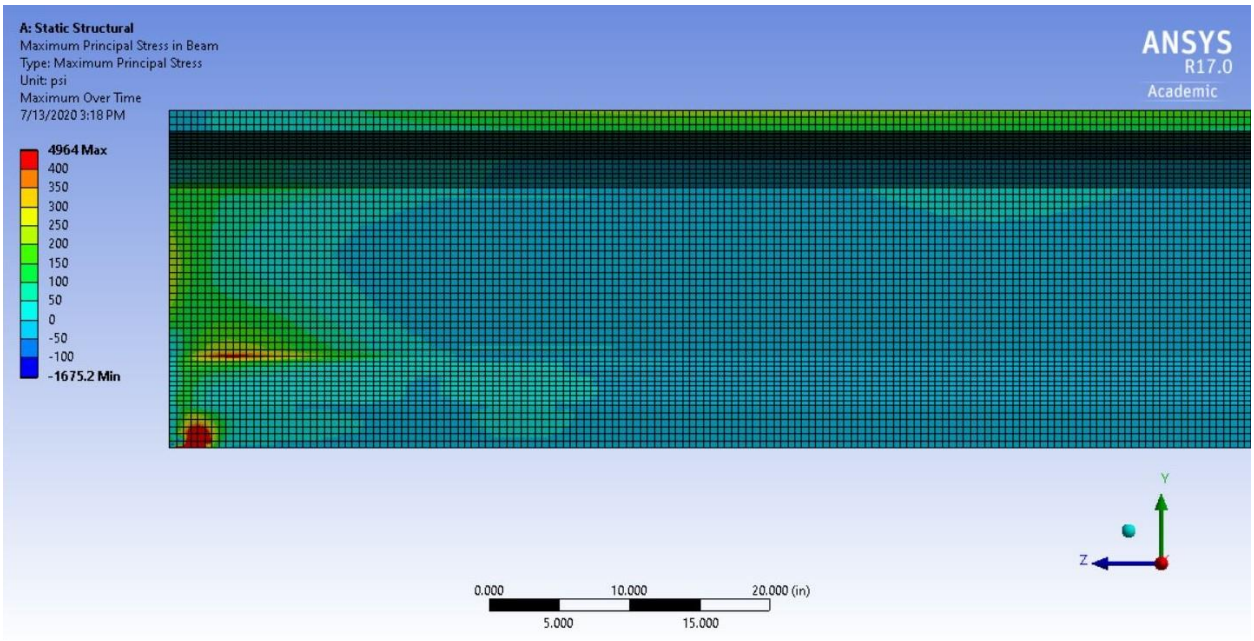

Figure A-5-22. ANSYS 14 Principal Tensile Stress, A1081 = 12,000 lbs., 0.5 in. strands, f'ci = 4 ksi, No Top Strand, No Debonding

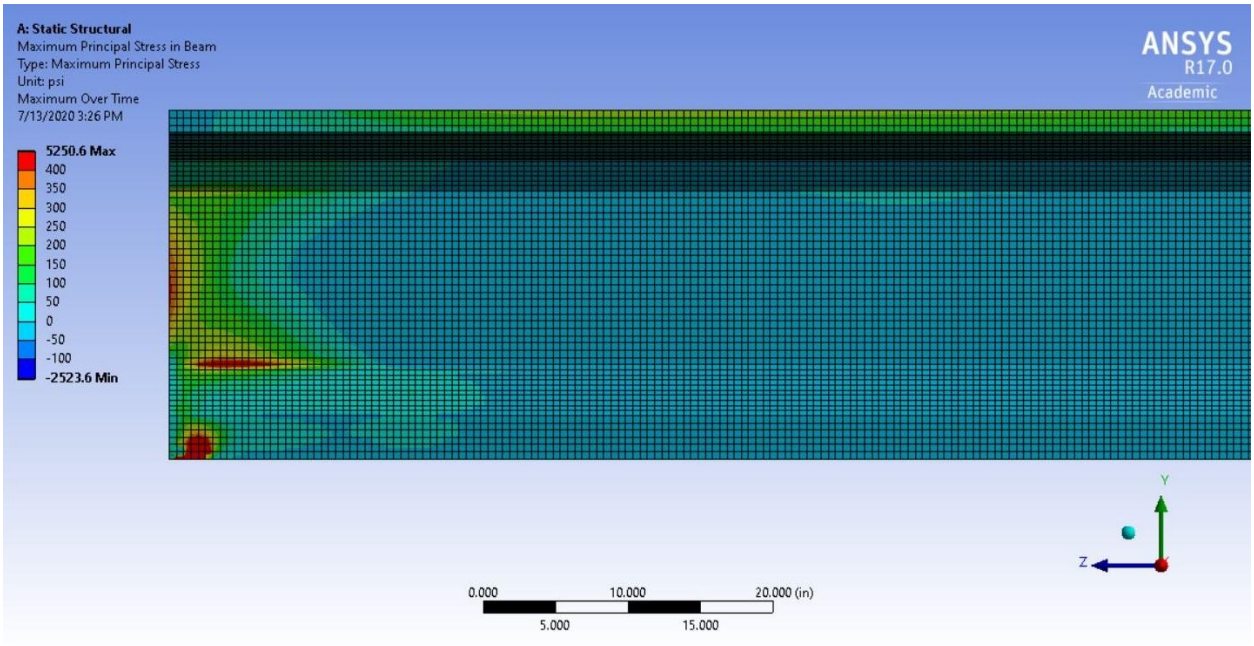

Figure A-5-23. ANSYS 15 Principal Tensile Stress, A1081 = 18,000 lbs., 0.5 in. strands, f'ci = 4 ksi, No Top Strand, No Debonding

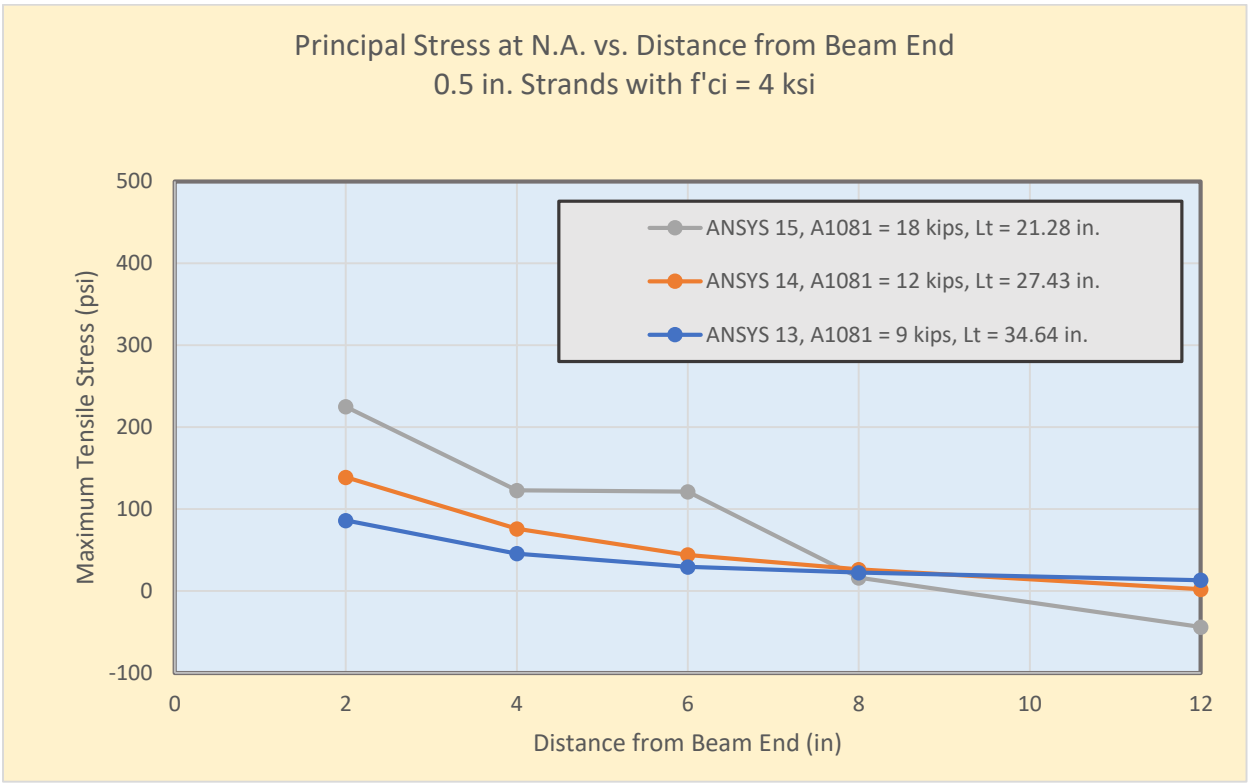

Figure A-5-24. Principal Stress (tension) at the N.A., ANSYS 13, ANSYS 14 and ANSYS 15

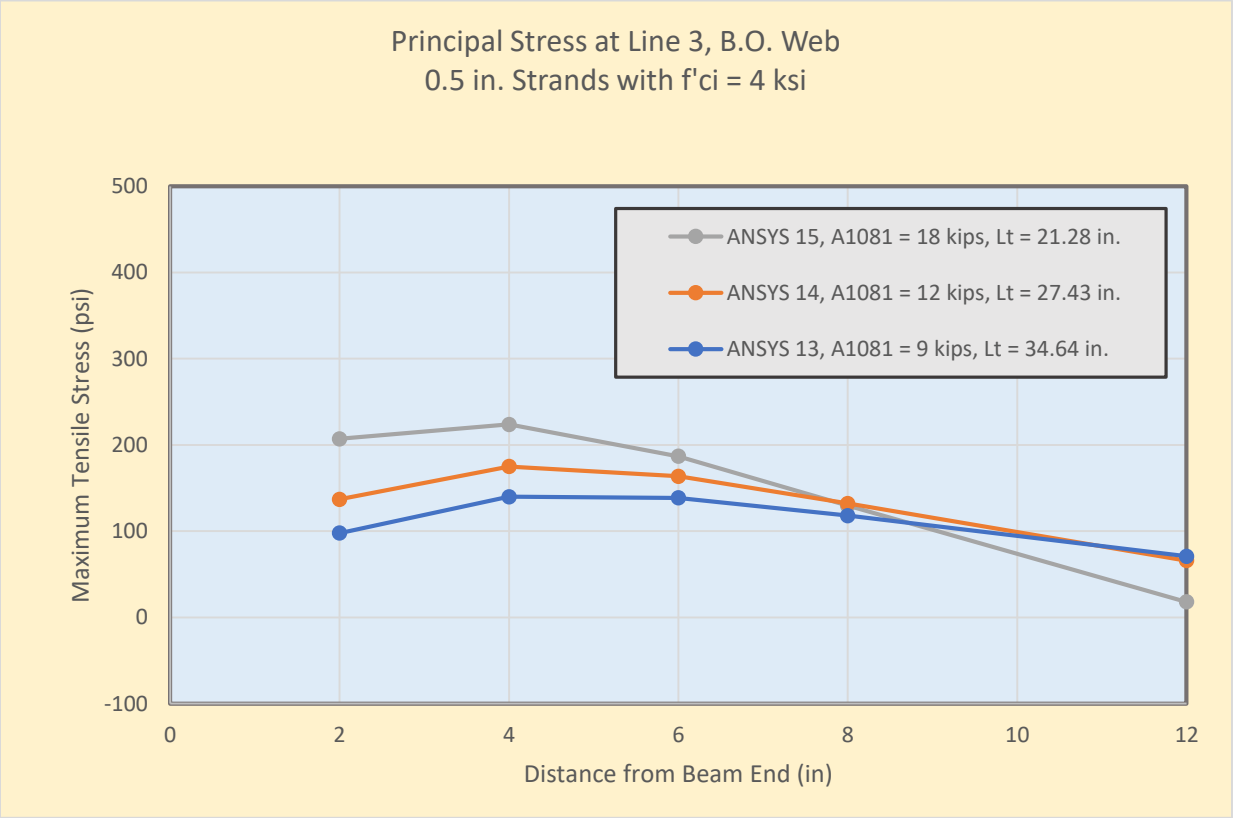

Figure A-5-25. Principal Stress (tension) at Line 3, B.O.Web, ANSYS 13, ANSYS 14 and ANSYS 15

A-6: Variations in Principal Tension for ANSYS Cases 19 and 20

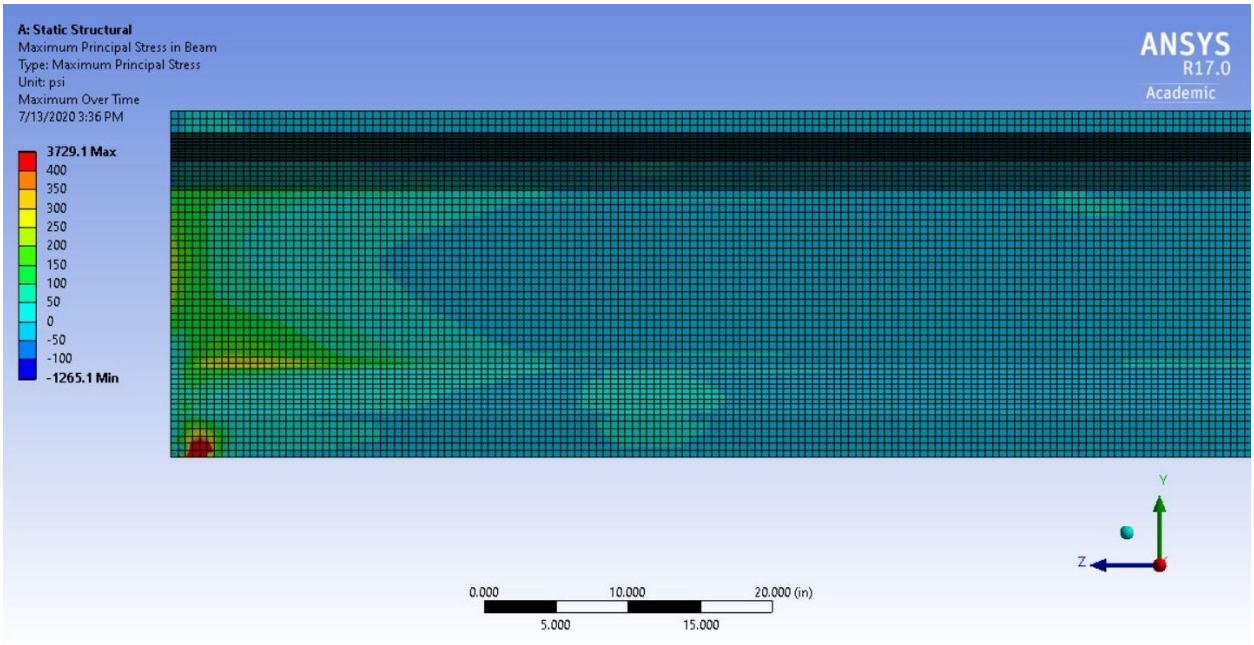

Figure A-6-26. ANSYS 19 Principal Tensile Stress, A1081 = 9,000 lbs, 0.5 in. strands, f'ci = 4 ksi, With Top Strand, No Debonding

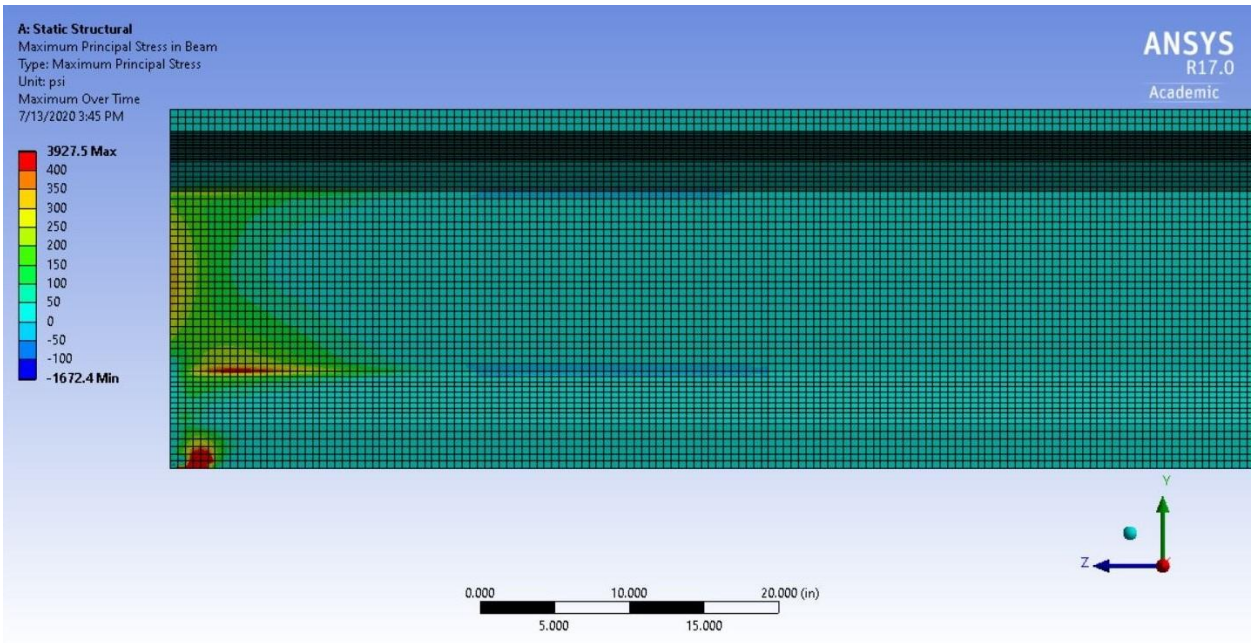

Figure A-6-27. ANSYS 20 Principal Tensile Stress, A1081 = 12,000 lbs., 0.5 in. strands, f'ci = 4 ksi, With Top Strand, No Debonding

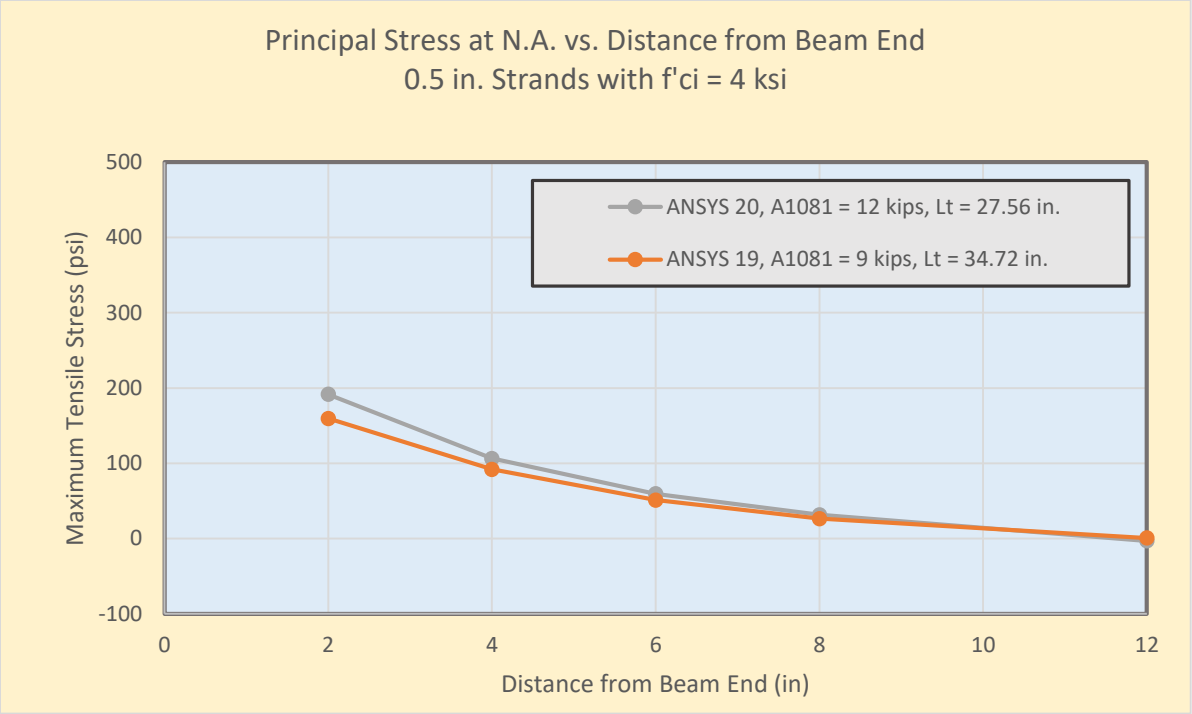

Figure A-6-28. Principal Stress (tension) at the N.A., ANSYS 19 and ANSYS 20

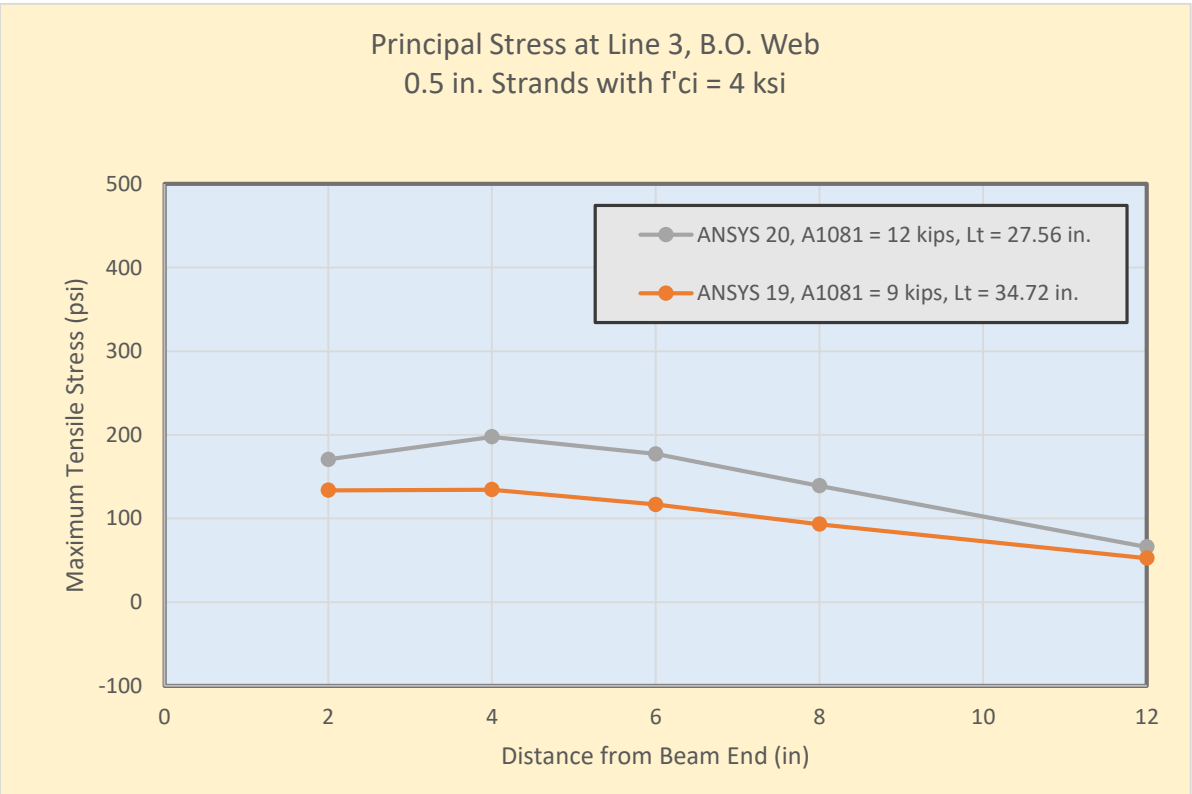

Figure A-6-29. Principal Stress (tension) at Line 3, B.O.Web, ANSYS 19 and ANSYS 20

A-7: Variations in Principal Tension for ANSYS Cases 21, 21A and 21B

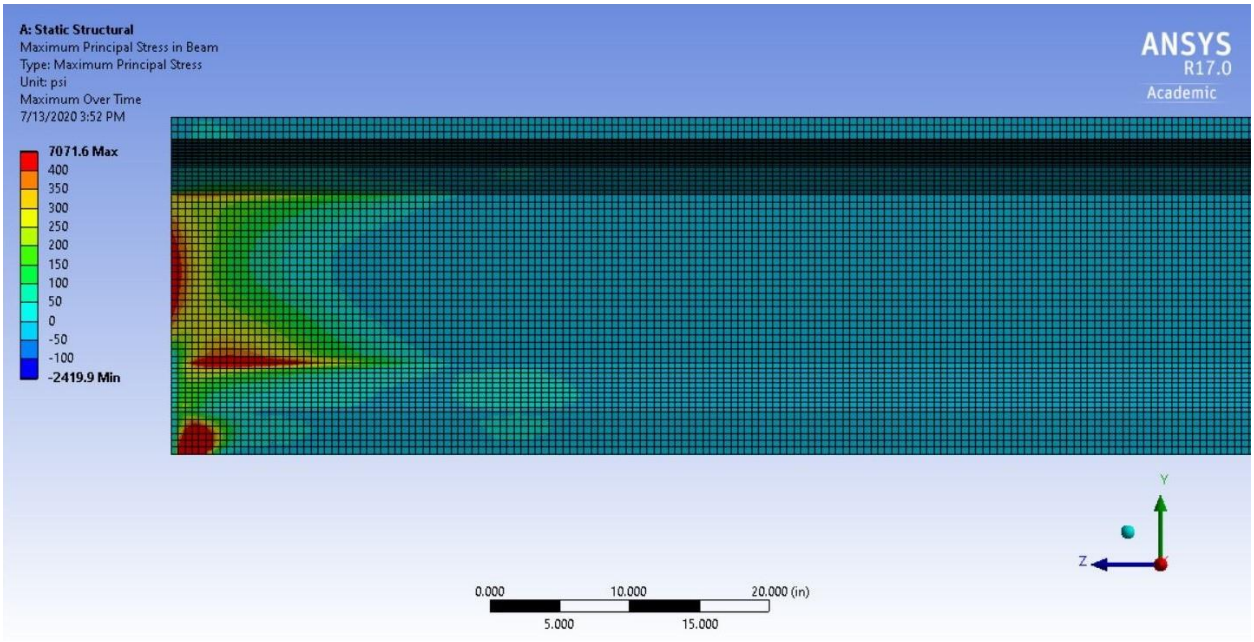

Figure A-7-30. ANSYS 21 Principal Tensile Stress, A1081 = 14,400 lbs, 0.6 in. strands, f'ci = 6 ksi, Top Strand, No Debonding

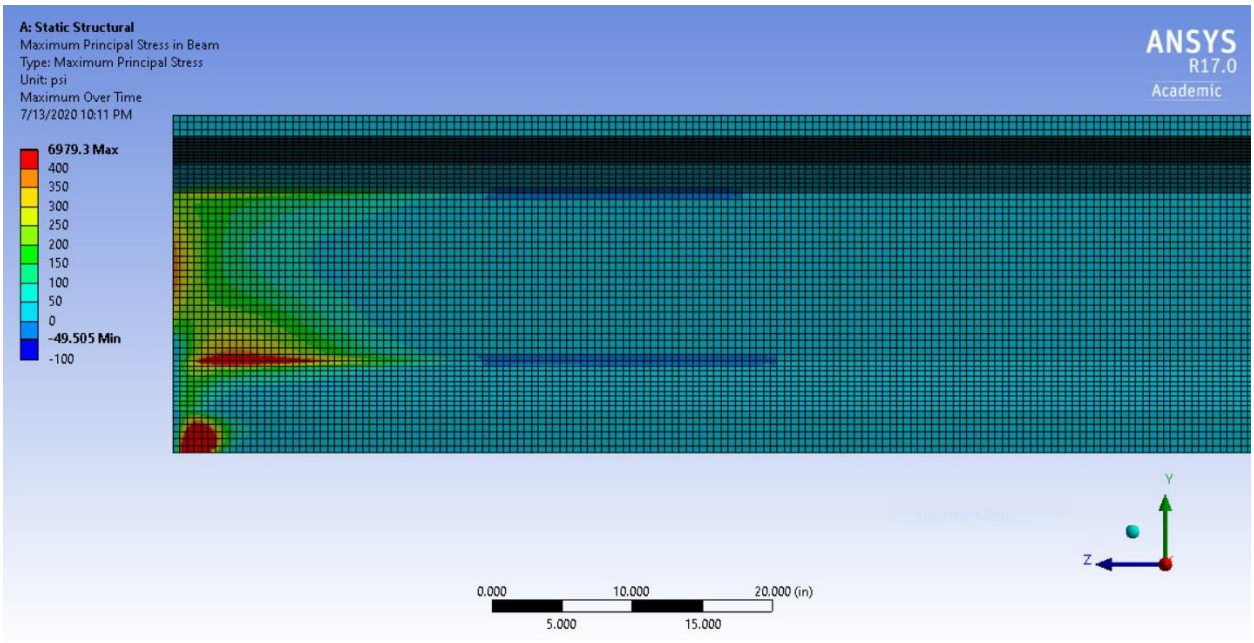

Figure A-7-31. ANSYS 21A Principal Tensile Stress, A1081 = 14,400 lbs., 0.6 in. strands, f'ci = 6 ksi, Top Strand, 2" Debond All Strands

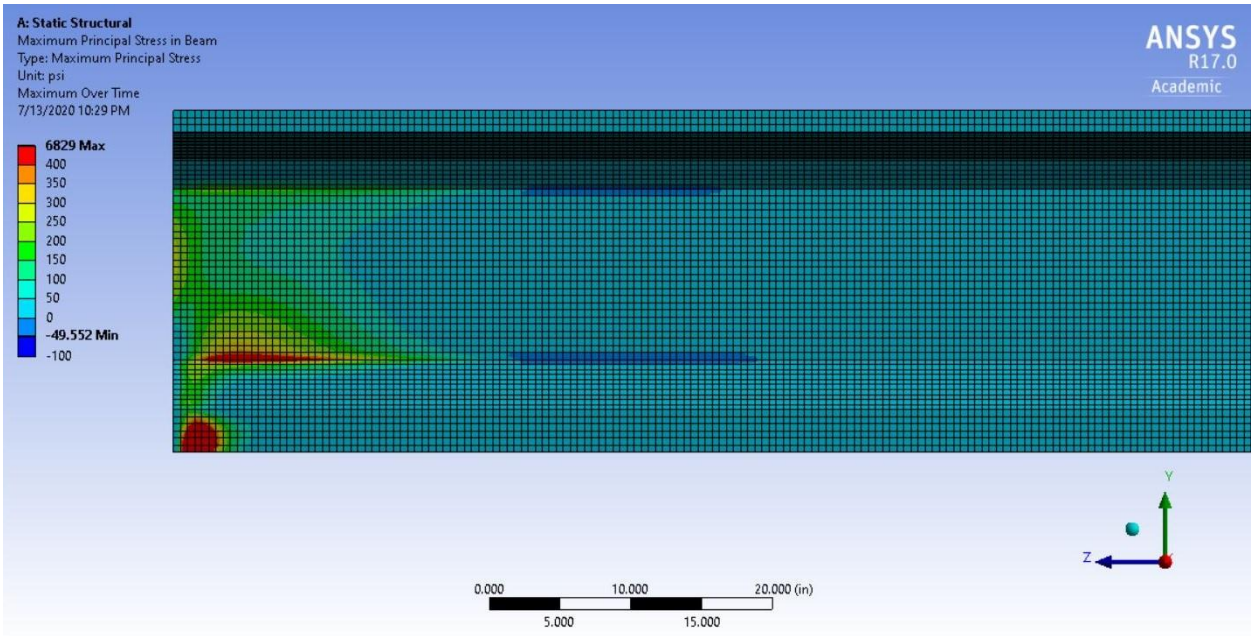

Figure A-7-32. ANSYS 21B Principal Tensile Stress, A1081 = 14,400 lbs., 0.6 in. strands, f'ci = 6 ksi, Top Strand, 4" Debond All Strands

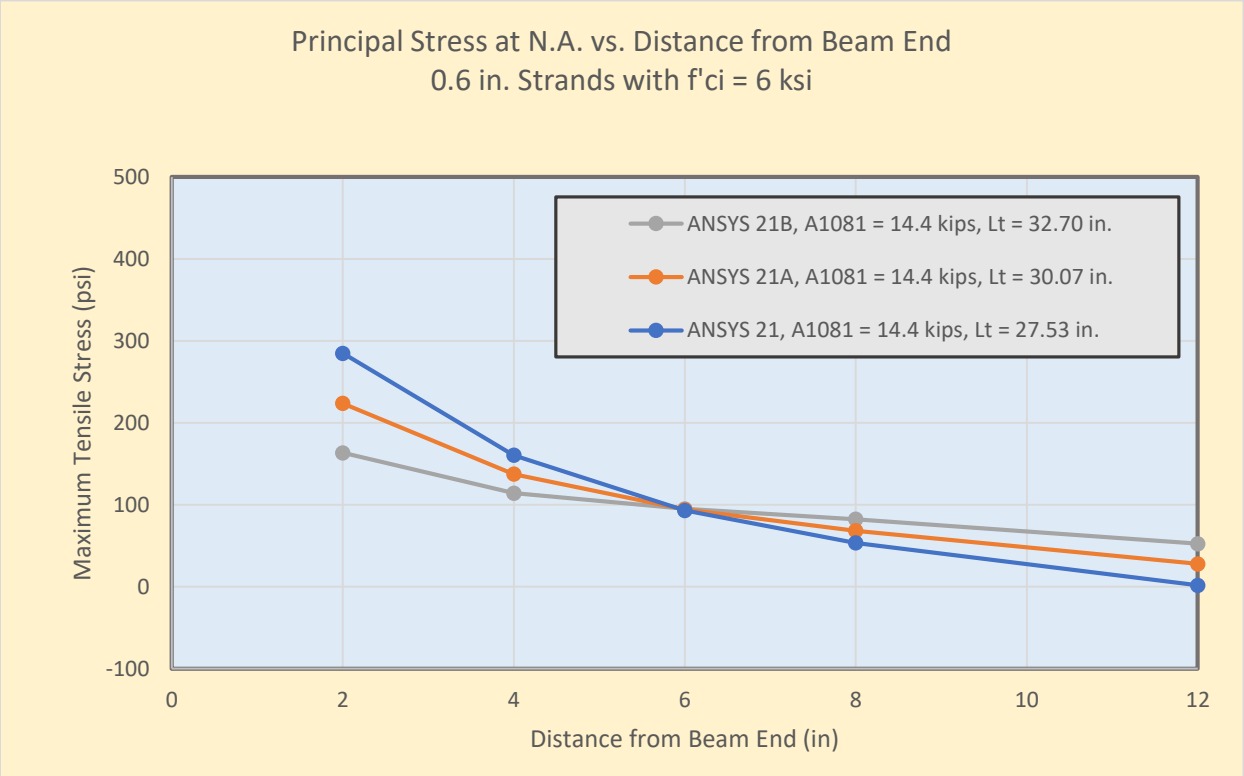

Figure A-7-33. Principal Stress (tension) at the N.A., ANSYS 21, ANSYS 21A and ANSYS 21B

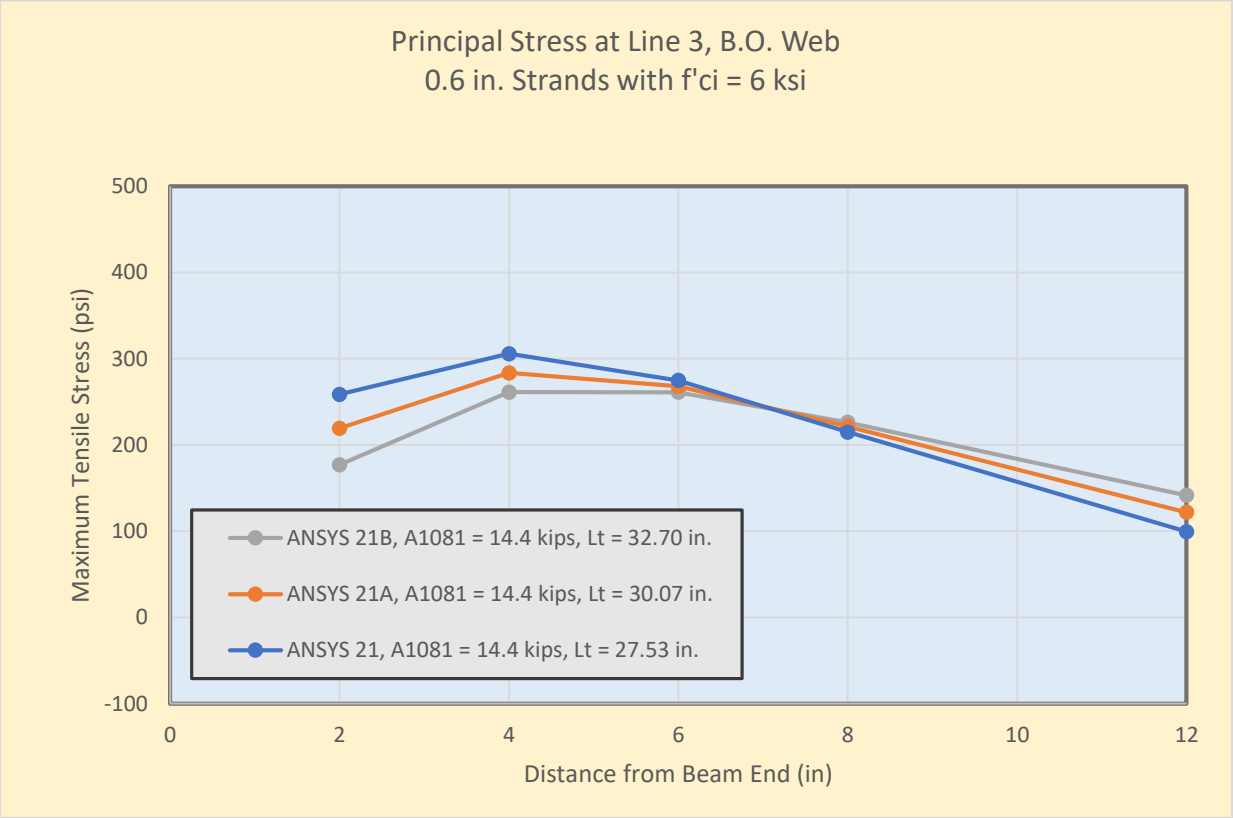

Figure A-7-34. Principal Stress (tension) at Line 3, B.O.Web, ANSYS 21, ANSYS 21A and ANSYS 21B

A-8: Variations in Principal Tension for ANSYS Cases 21, 22 and 23

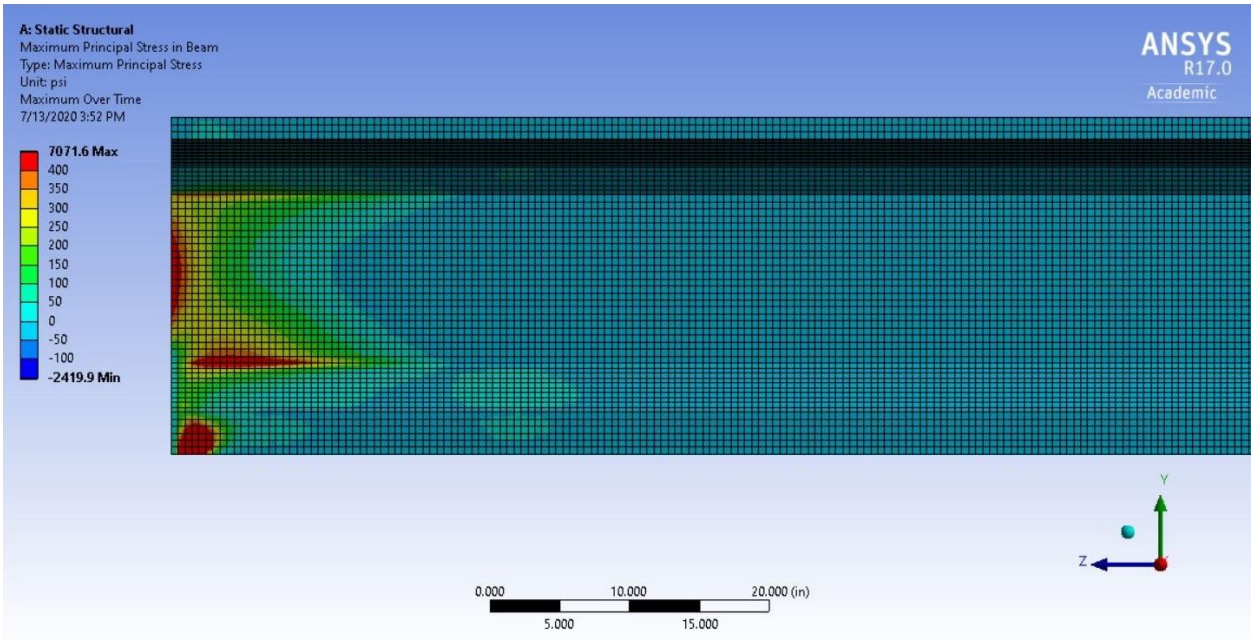

Figure A-8-35. ANSYS 21 Principal Tensile Stress, A1081 = 14,400 lbs, 0.6 in. strands, f'ci = 6 ksi, With Top Strand, No Debonding

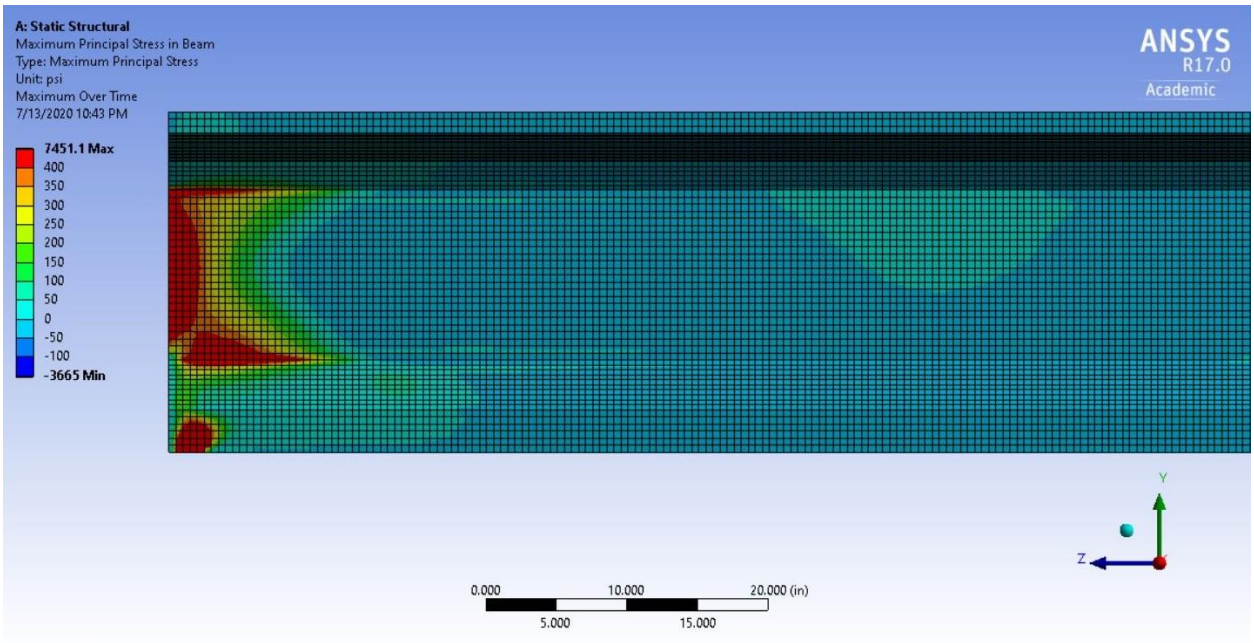

Figure A-8-36. ANSYS 22 Principal Tensile Stress, A1081 = 21,600 lbs., 0.6 in. strands, f'ci = 6 ksi, With Top Strand, No Debonding

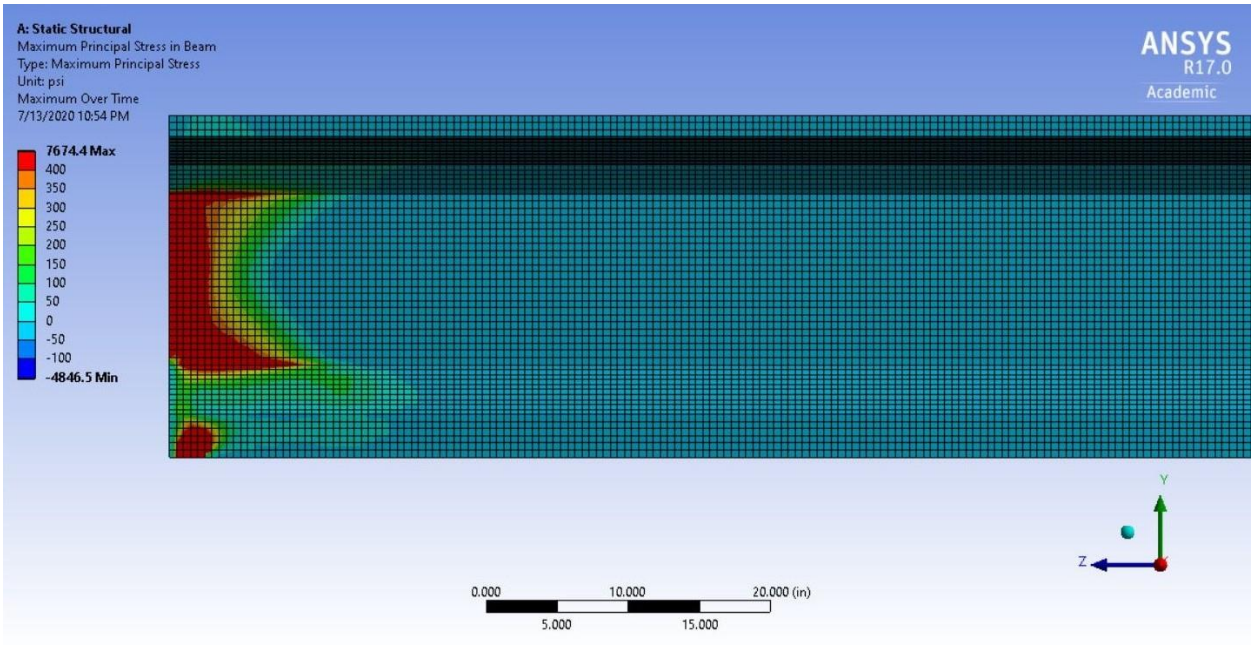

Figure A-8-37. ANSYS 23 Principal Tensile Stress, A1081 = 28,800 lbs., 0.6 in. strands, f'ci = 6 ksi, With Top Strand, No Debonding

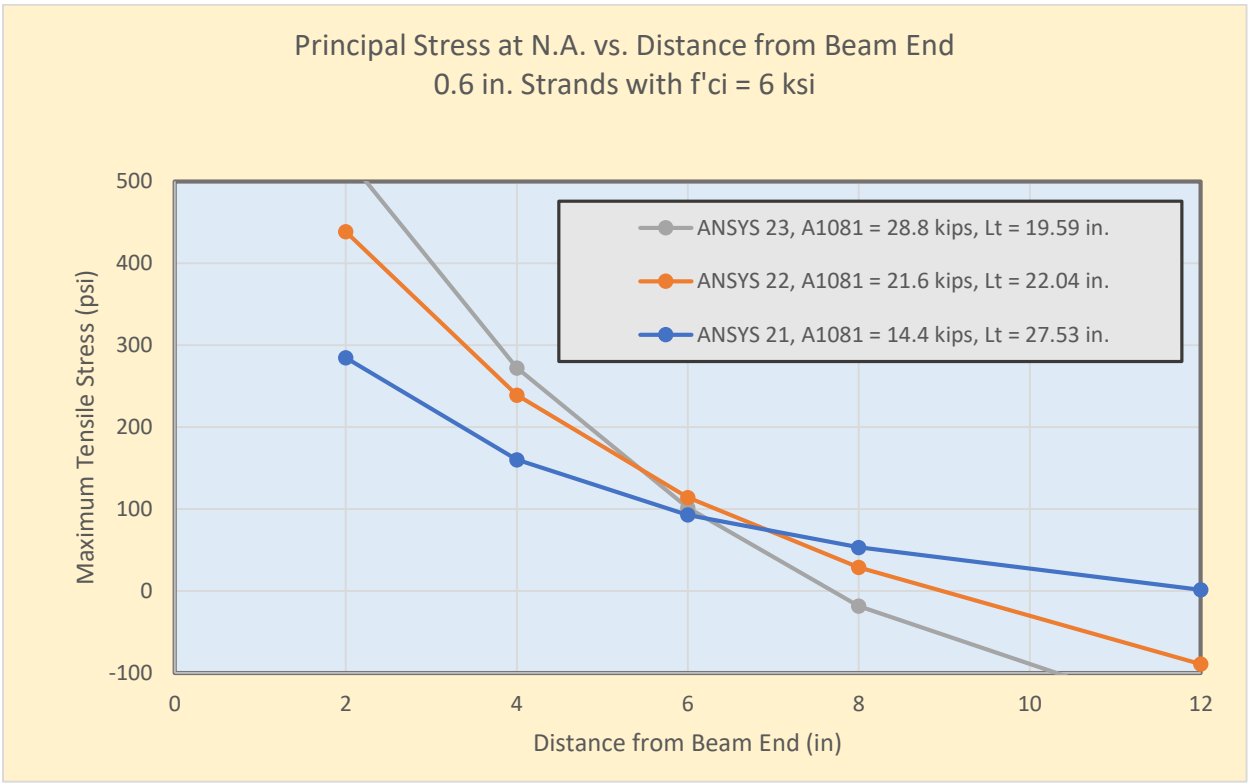

Figure A-8-38. Principal Stress (tension) at the N.A., ANSYS 21, ANSYS 22 and ANSYS 23

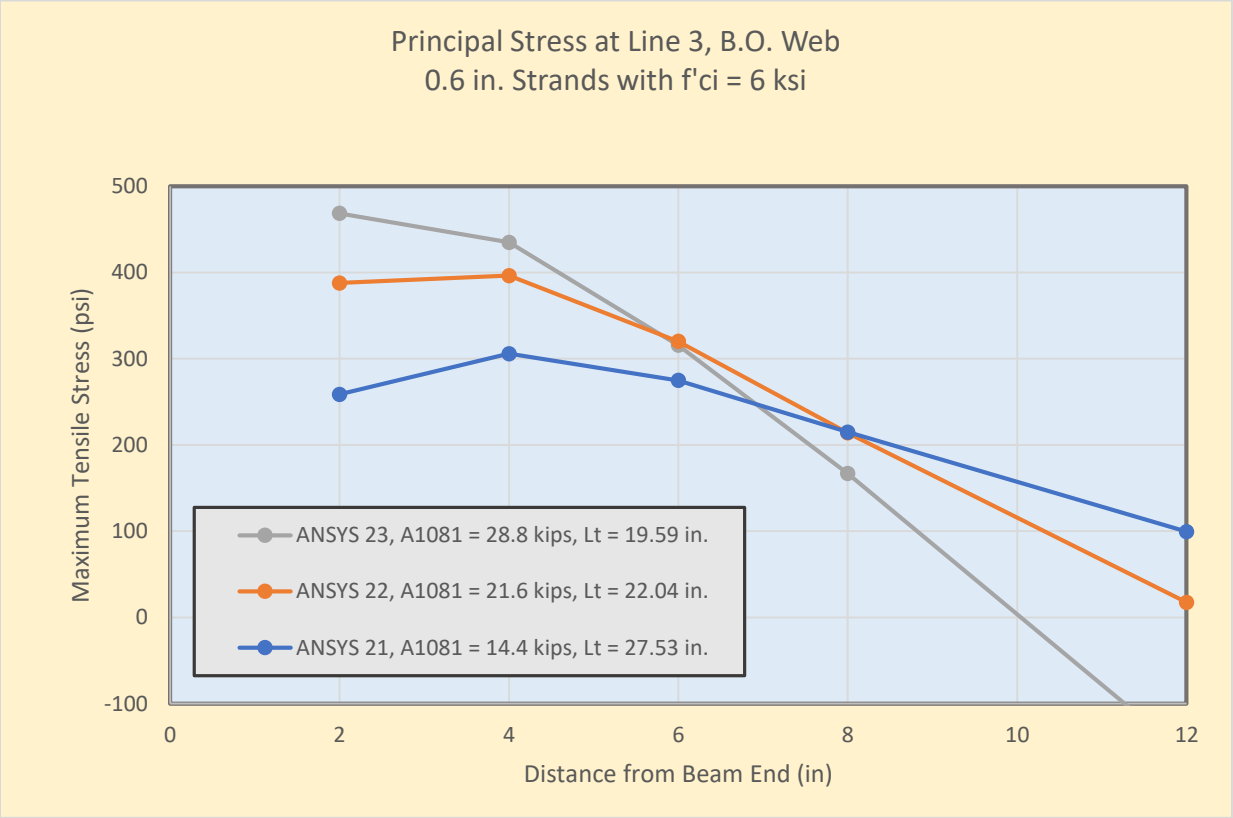

Figure A-8-39. Principal Stress (tension) at Line 3, B.O.Web, ANSYS 21, ANSYS 22 and ANSYS 23

A-9: Variations in Principal Tension for ANSYS Cases 24, 24A and 24B

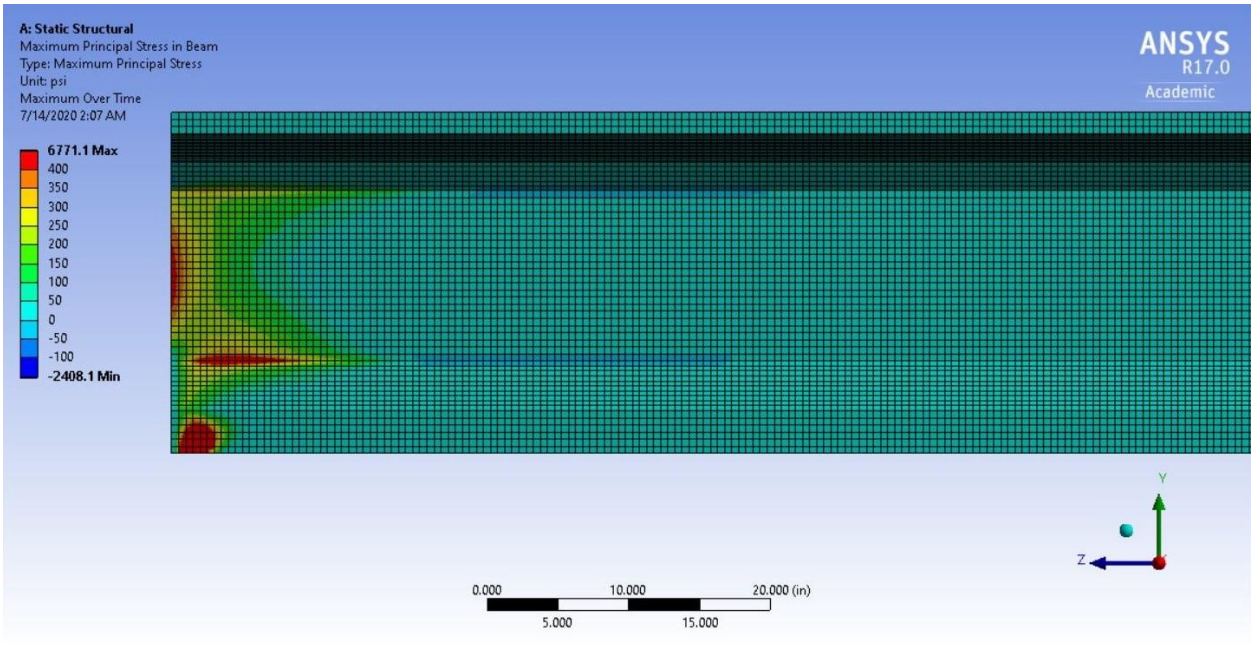

Figure A-9-40. ANSYS 24 Principal Tensile Stress, A1081 = 14,400 lbs, 0.6 in. strands, f'ci = 6 ksi, Top Strand, 24" Debonded Middle Strand

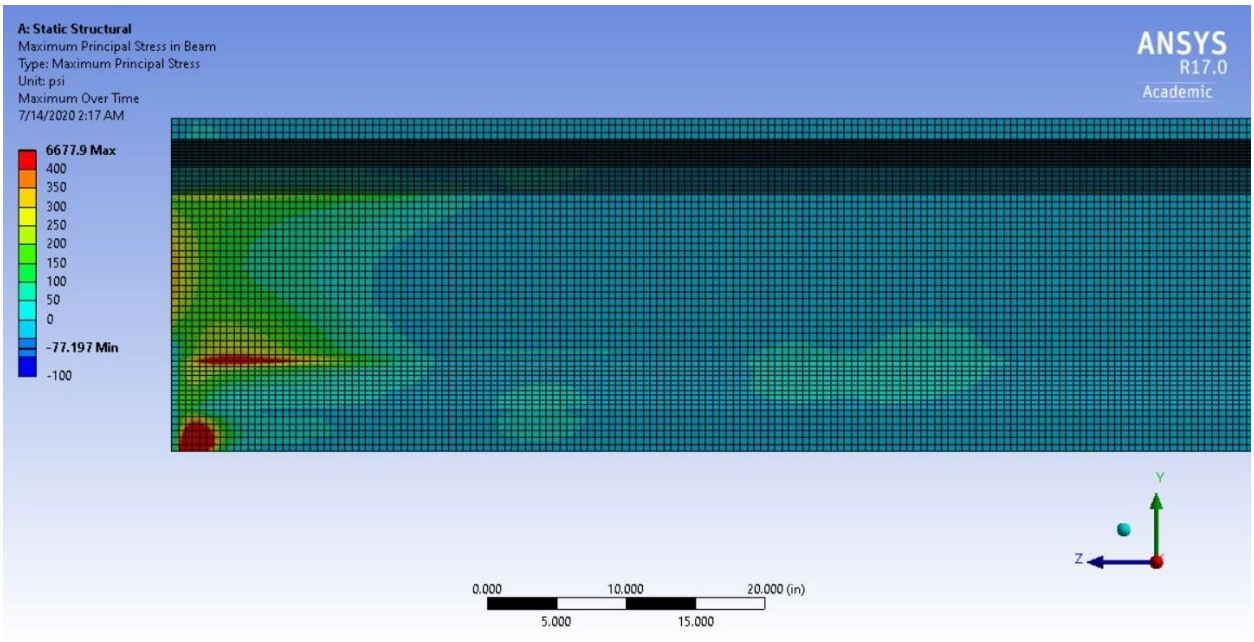

Figure A-9-41. ANSYS 24A Principal Tensile Stress, A1081 = 14,400 lbs., 0.6 in. strands, f'ci = 6 ksi, Top Strand, 24" Debonded Middle Strand, 2" Debonded Top and 3 Bottom Strands

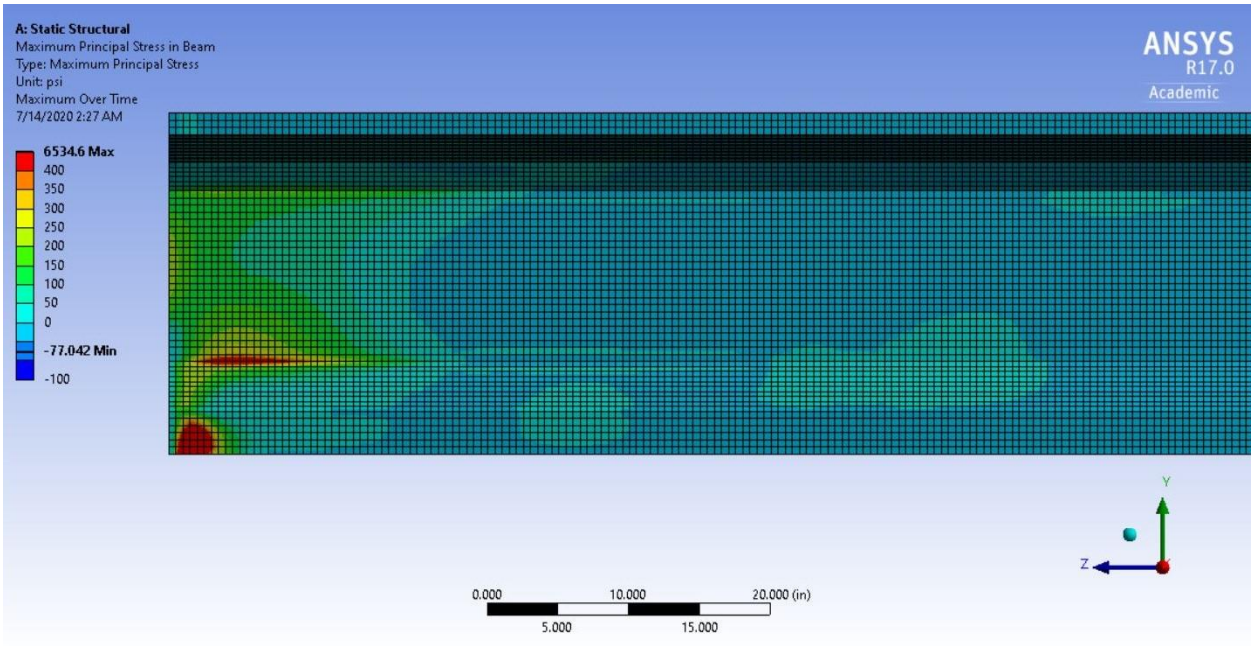

Figure A-9-42. ANSYS 24B Principal Tensile Stress, A1081 = 14,400 lbs., 0.6 in. strands, f'ci = 6 ksi, Top Strand, 24" Debonded Middle Strand, 4" Debonded Top and 3 Bottom Strands

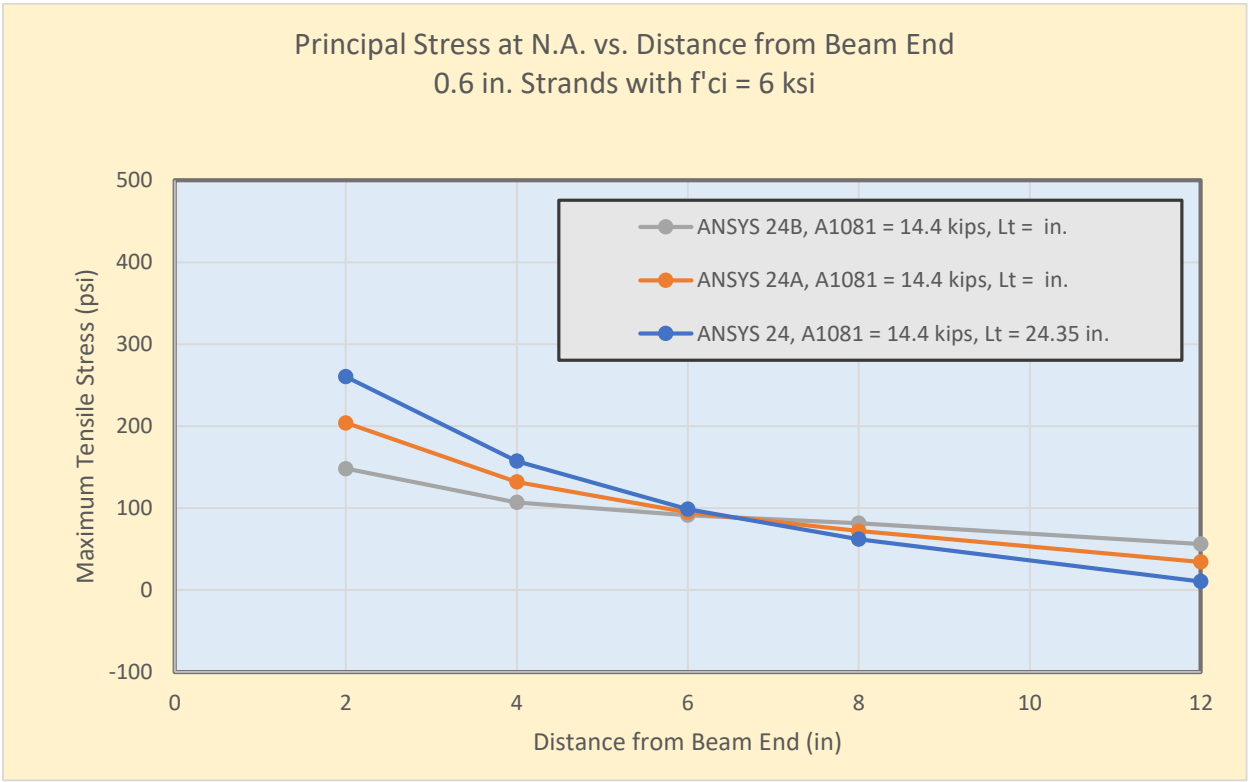

Figure A-9-43. Principal Stress (tension) at the N.A., ANSYS 24, ANSYS 24A and ANSYS 24B

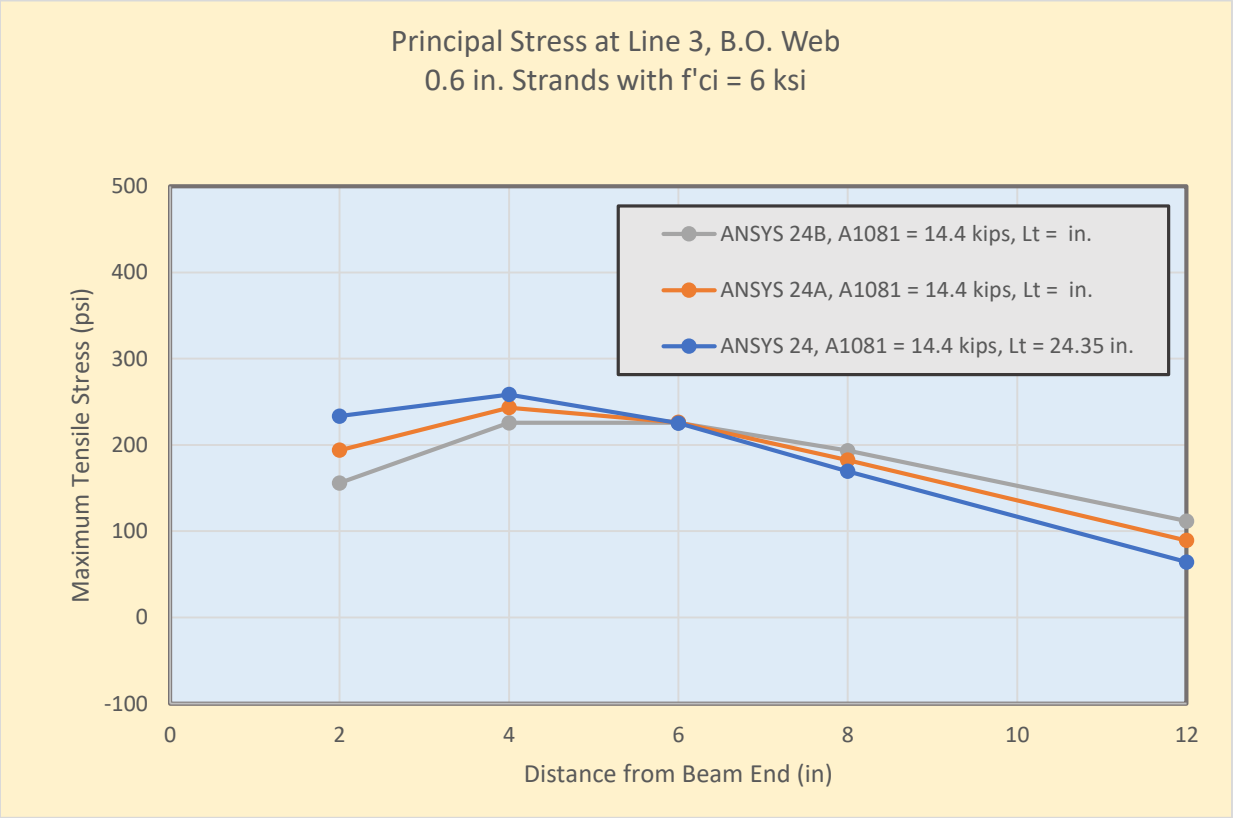

Figure A-9-44. Principal Stress (tension) at Line 3, B.O.Web, ANSYS 24, ANSYS 24A and ANSYS 24B

A-10: Variations in Principal Tension for ANSYS Cases 24, 25 and 26

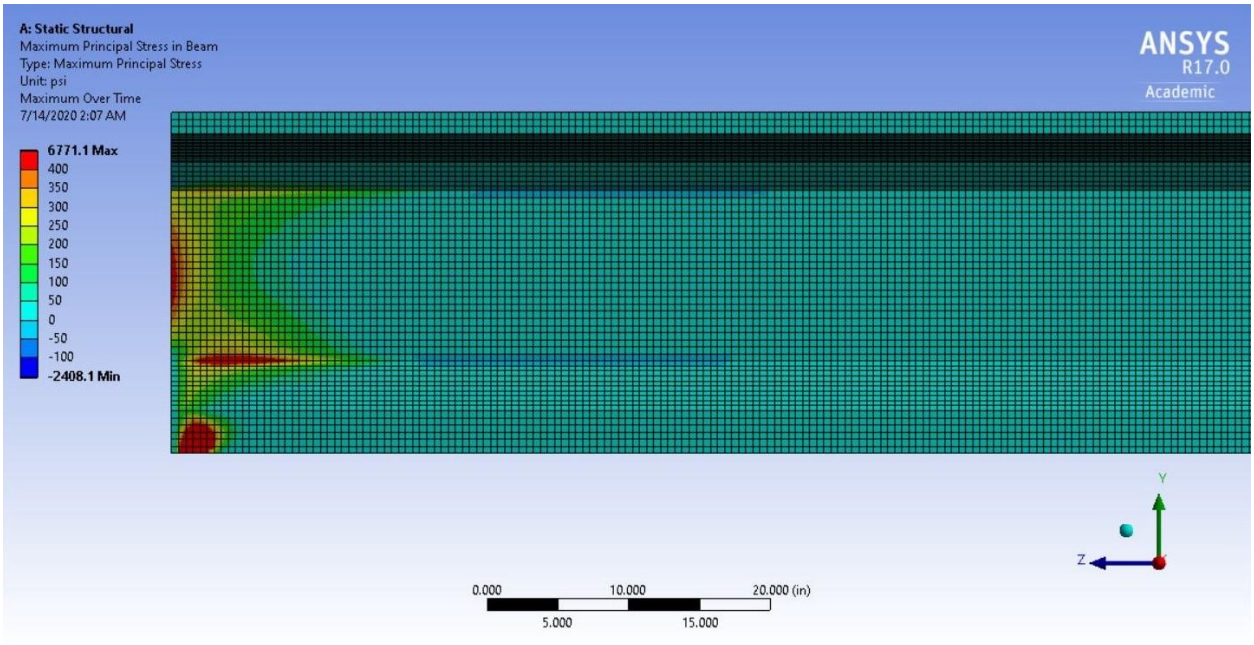

Figure A-10-45. ANSYS 24 Principal Tensile Stress, A1081 = 14,400 lbs, 0.6 in. strands, f'ci = 6 ksi, With Top Strand, Debond One Strand

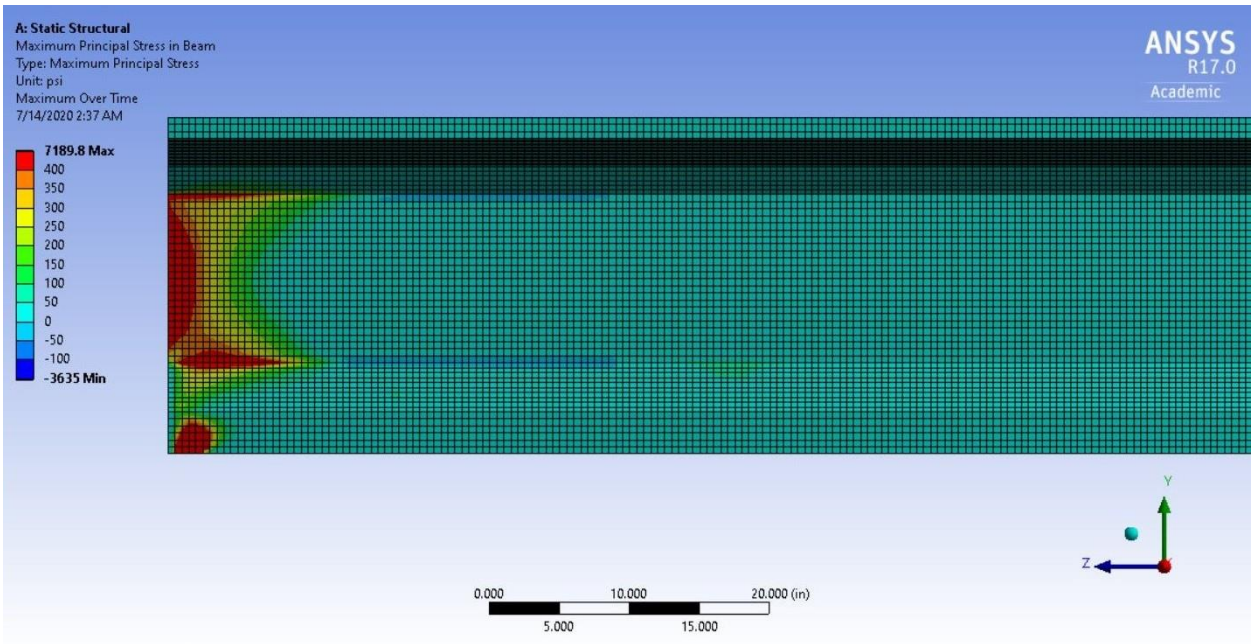

Figure A-10-46. ANSYS 25 Principal Tensile Stress, A1081 = 21,600 lbs., 0.6 in. strands, f'ci = 6 ksi, With Top Strand, Debond One Strand

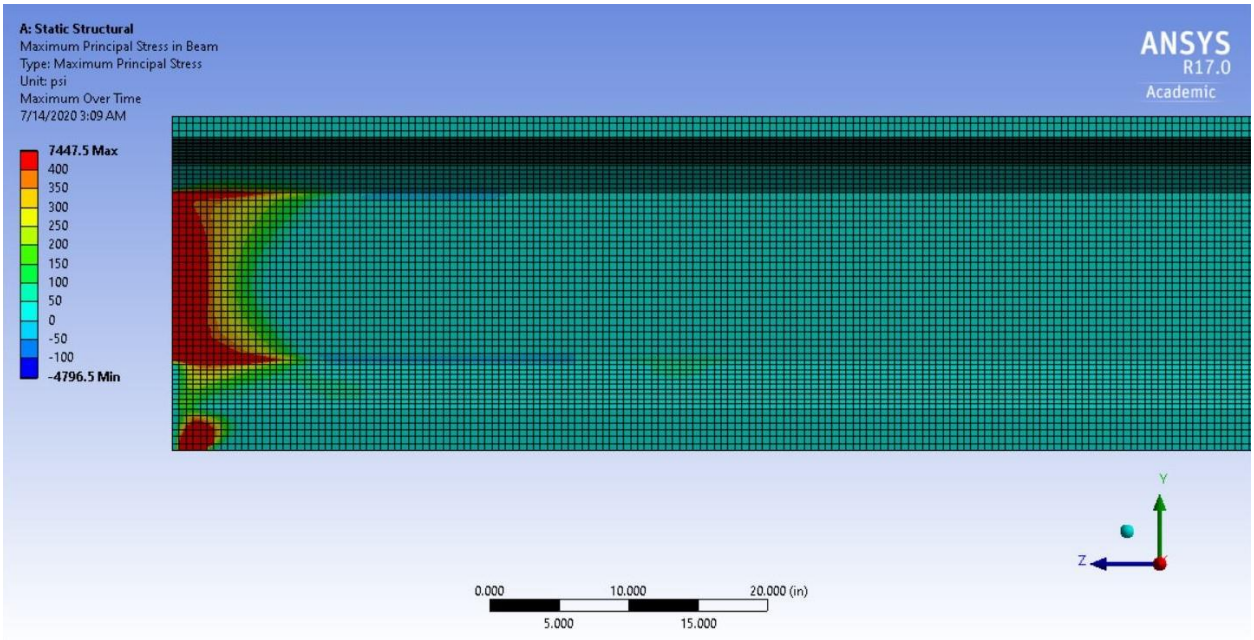

Figure A-10-47. ANSYS 26 Principal Tensile Stress, A1081 = 28,800 lbs., 0.6 in. strands, f'ci = 6 ksi, With Top Strand, Debond One Strand

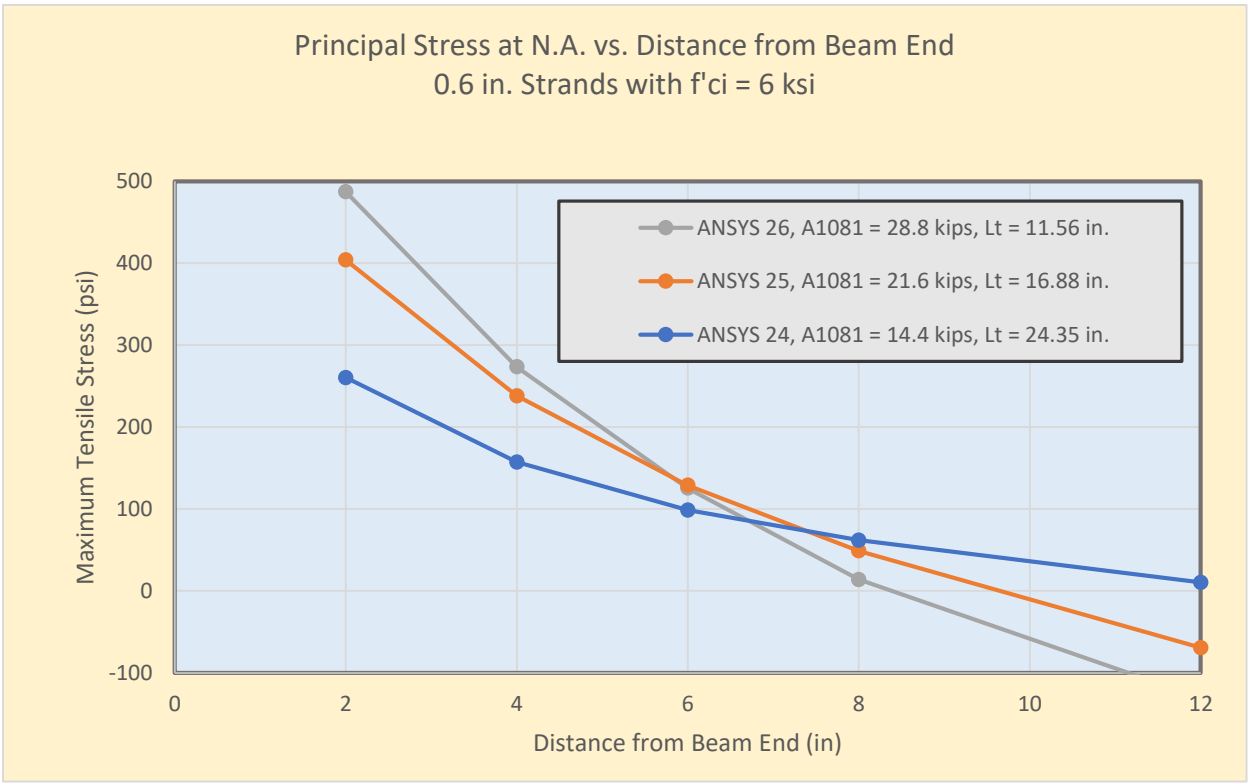

Figure A-10-48. Principal Stress (tension) at the N.A., ANSYS 24, ANSYS 25 and ANSYS 26

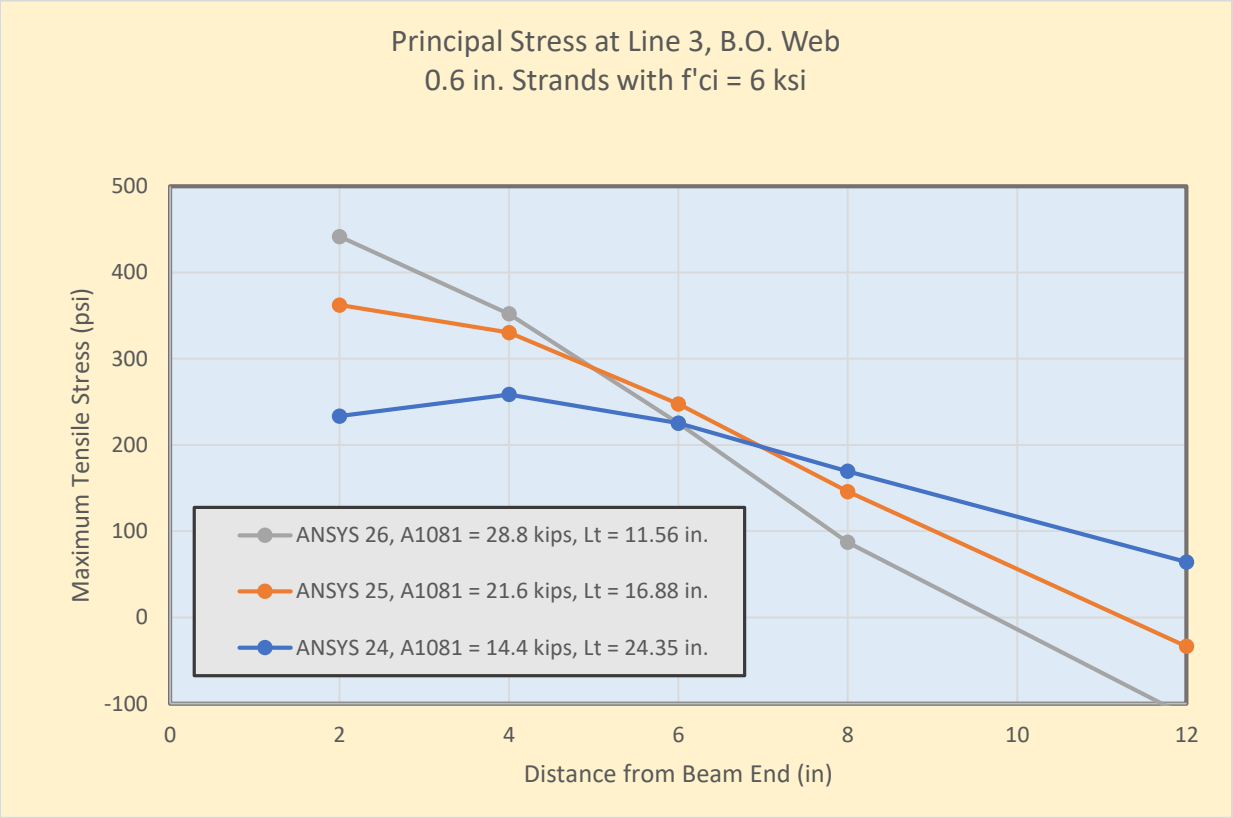

Figure A-10-49. Principal Stress (tension) at Line 3, B.O.Web, ANSYS 24, ANSYS 25 and ANSYS 26

A-11: Variations in Principal Tension for ANSYS Cases 25, 25A and 25B

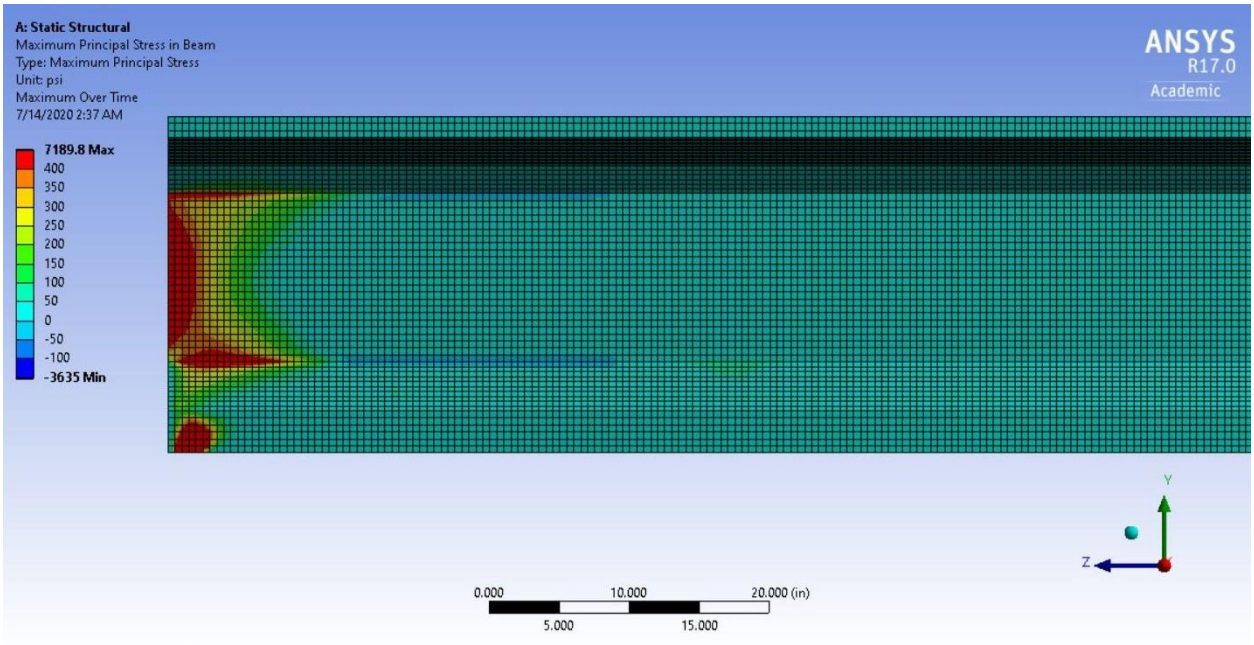

Figure A-11-50. ANSYS 25 Principal Tensile Stress, A1081 = 21,600 lbs, 0.6 in. strands, f'ci = 6 ksi, Top Strand, 24" Debonded Middle Strand

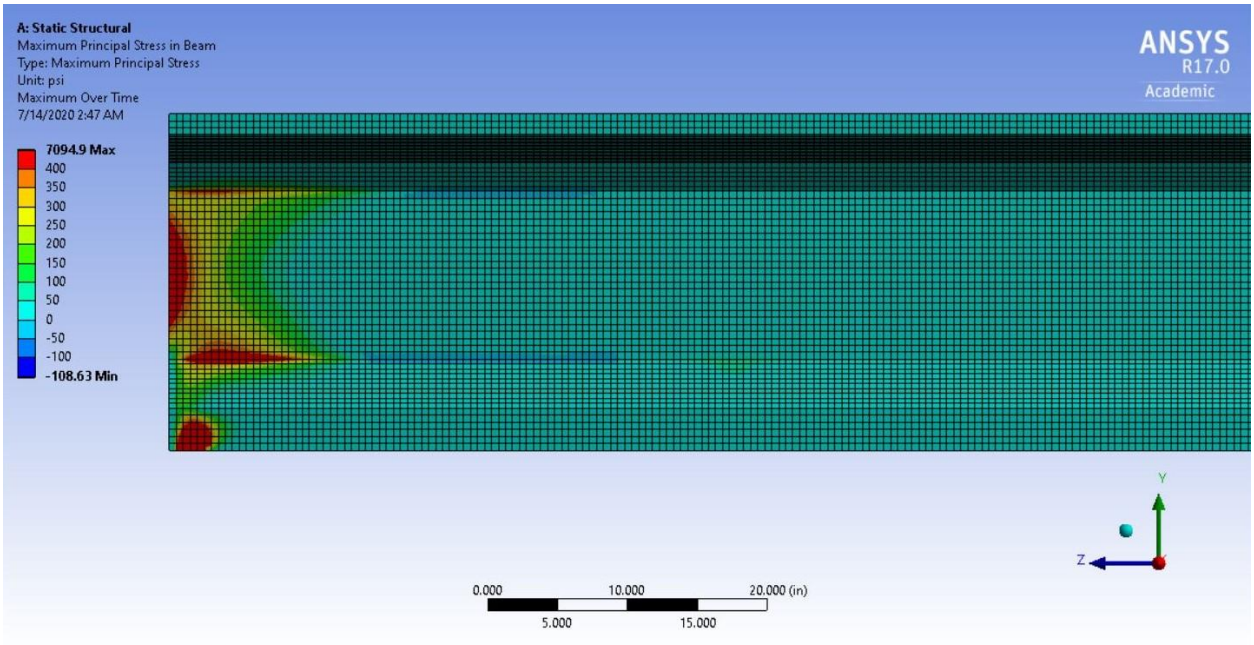

Figure A-11-51. ANSYS 25A Principal Tensile Stress, A1081 = 21,600 lbs., 0.6 in. strands, f'ci = 6 ksi, Top Strand, 24" Debonded Middle Strand, 2" Debonded Top and 3 Bottom Strands

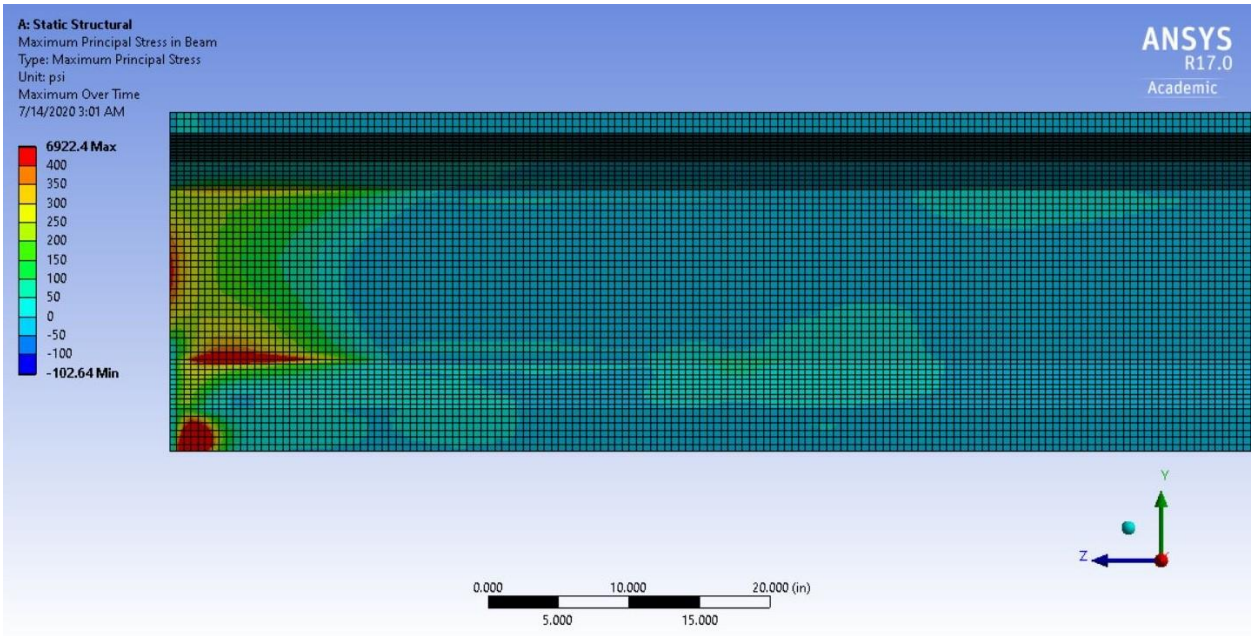

Figure A-11-52. ANSYS 25B Principal Tensile Stress, A1081 = 21,600 lbs., 0.6 in. strands, f'ci = 6 ksi, Top Strand, 24" Debonded Middle Strand, 4" Debonded Top and 3 Bottom Strands

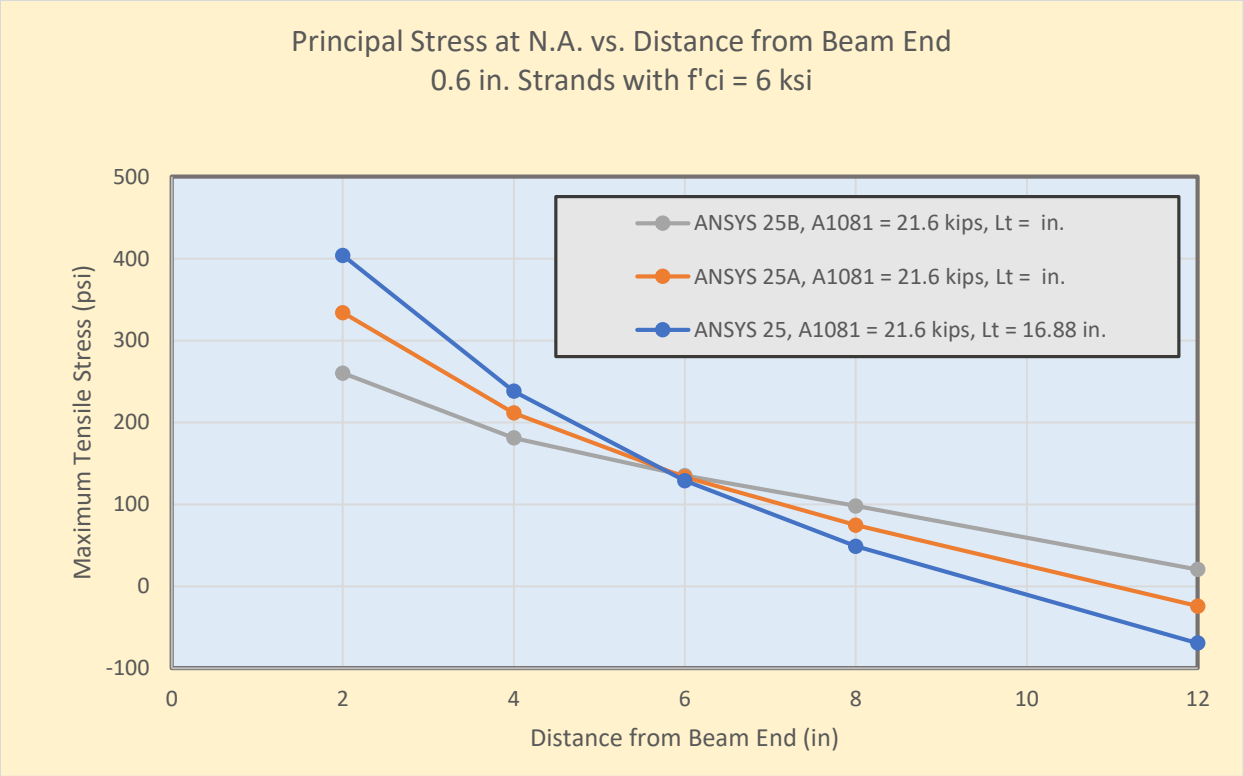

Figure A-11-53. Principal Stress (tension) at the N.A., ANSYS 25, ANSYS 25A and ANSYS 25B

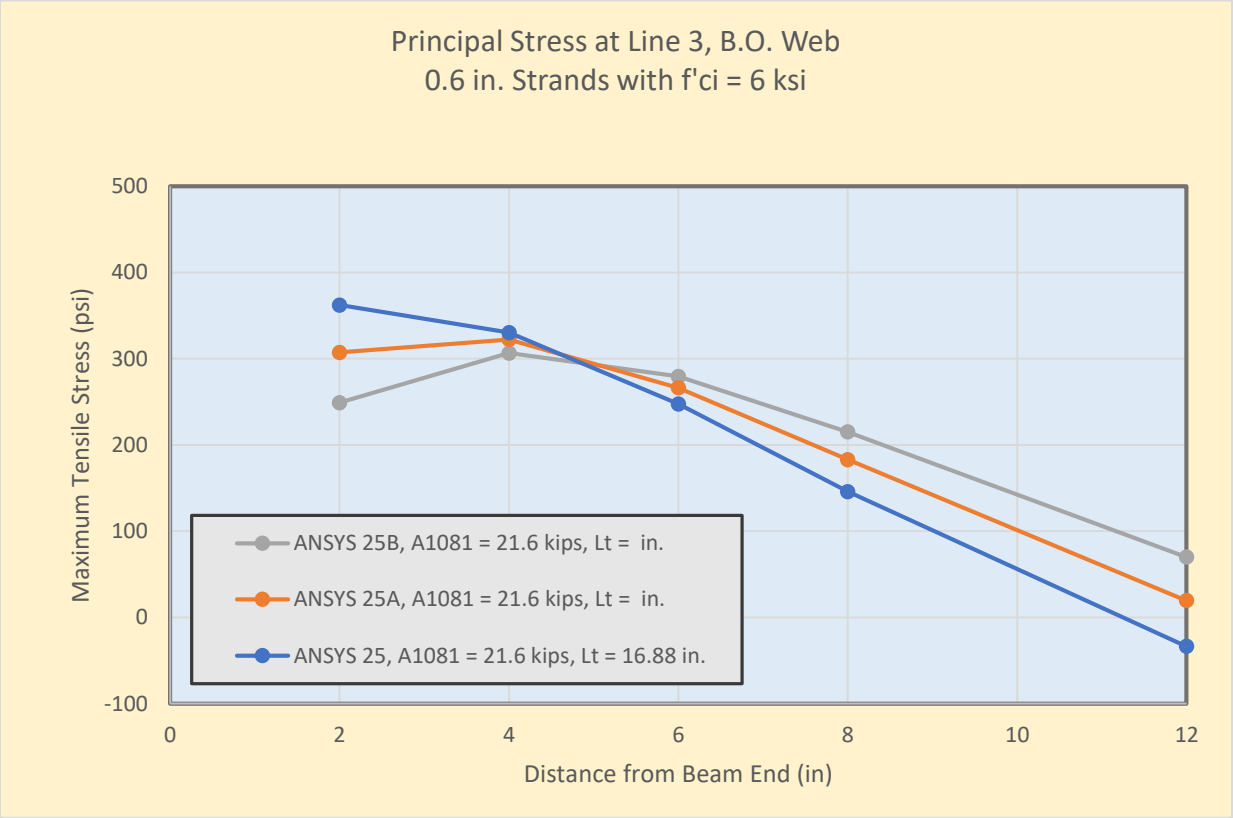

Figure A-11-54. Principal Stress (tension) at Line 3, B.O.Web, ANSYS 25, ANSYS 25A and ANSYS 25B

A-12: Variations in Principal Tension for ANSYS Cases 27, 28 and 29

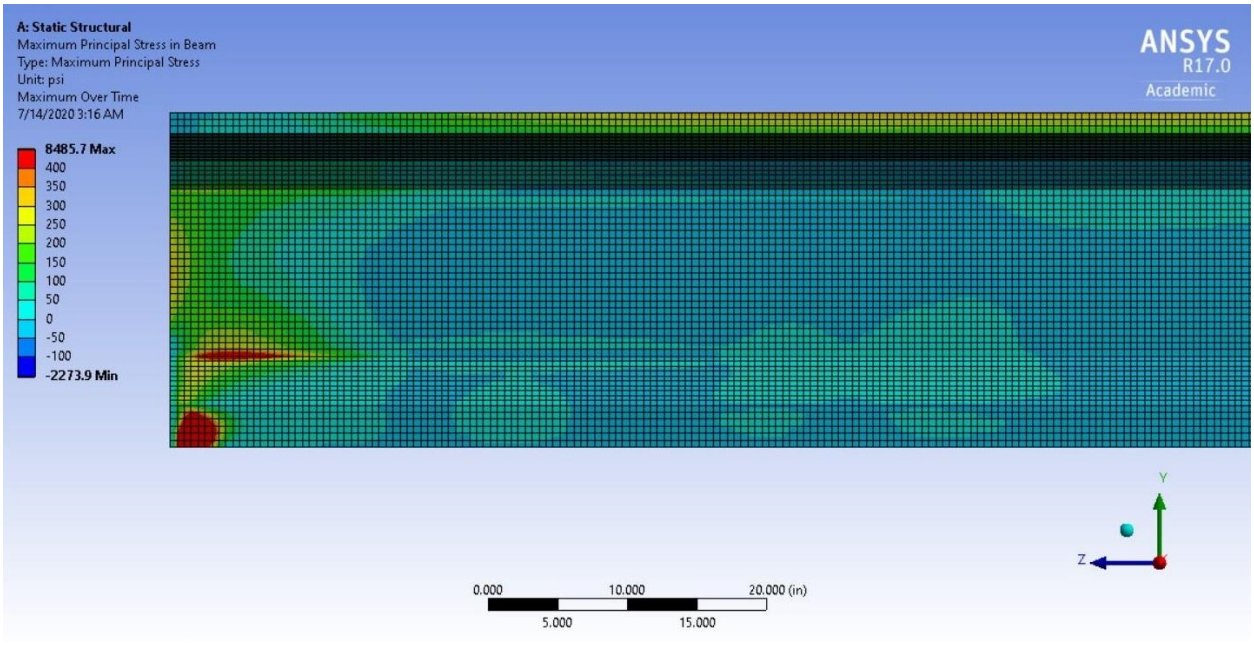

Figure A-12-55. ANSYS 27 Principal Tensile Stress, A1081 = 14,400 lbs, 0.6 in. strands, f'ci = 6 ksi, No Top Strand, Debond One Strand

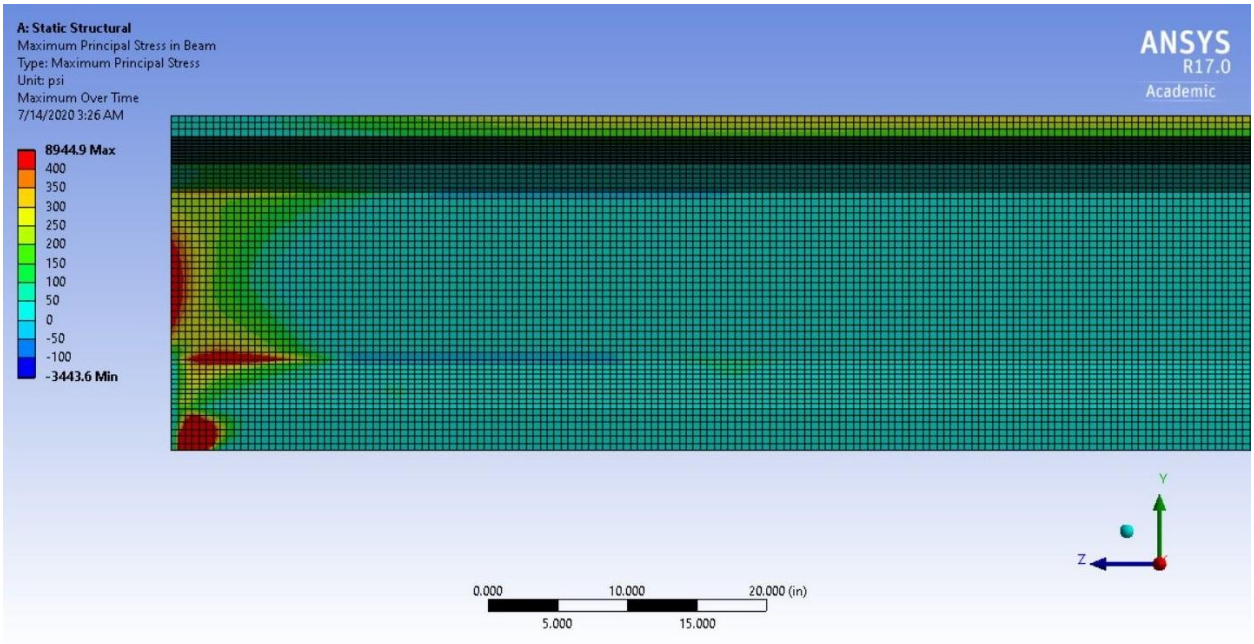

Figure A-12-56. ANSYS 28 Principal Tensile Stress, A1081 = 21,600 lbs., 0.6 in. strands, f'ci = 6 ksi, No Top Strand, Debond One Strand

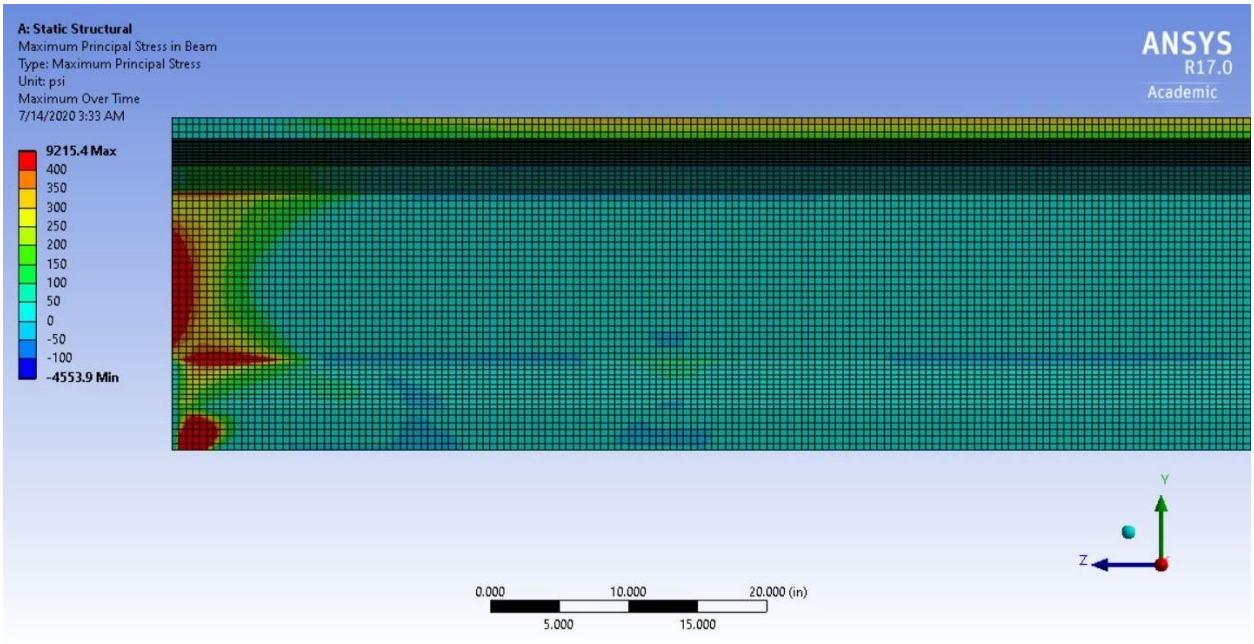

Figure A-12-57. ANSYS 29 Principal Tensile Stress, A1081 = 28,800 lbs., 0.6 in. strands, f'ci = 6 ksi, No Top Strand, Debond One Strand

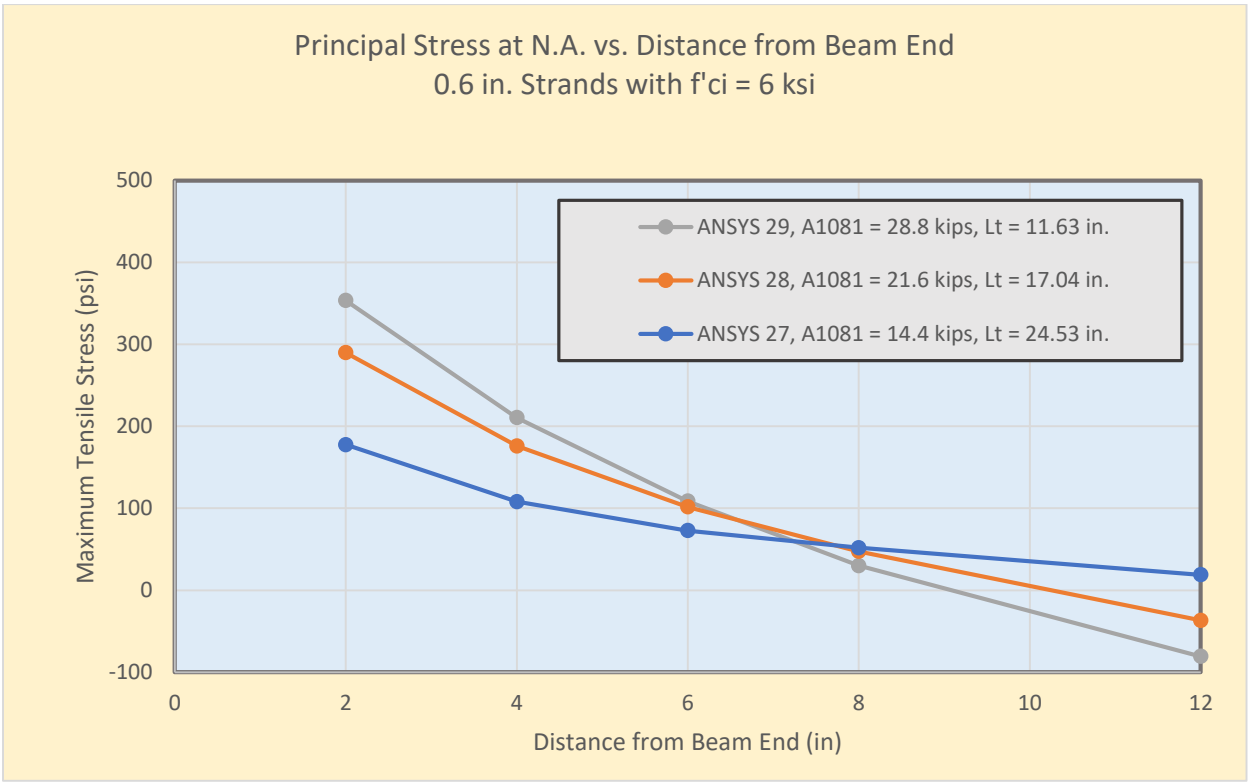

Figure A-12-58. Principal Stress (tension) at the N.A., ANSYS 27, ANSYS 28 and ANSYS 29

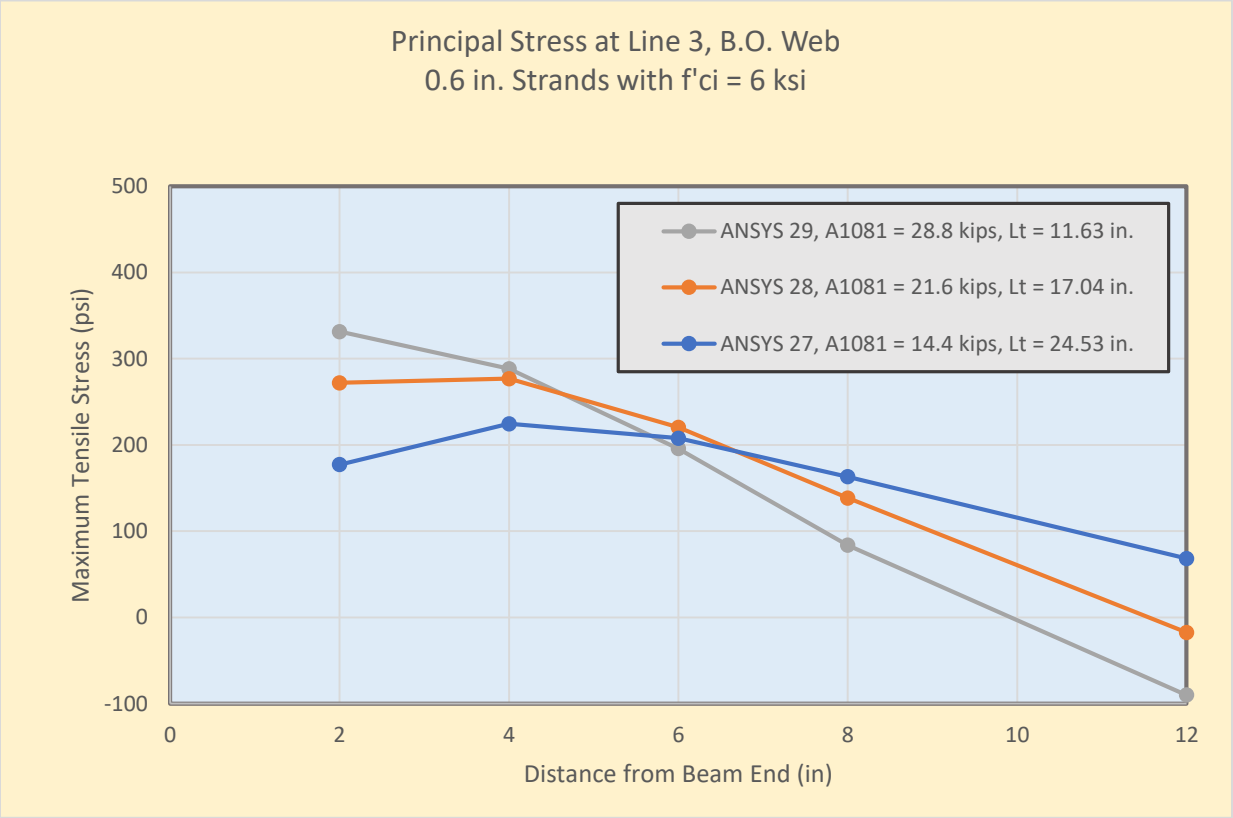

Figure A-12-59. Principal Stress (tension) at Line 3, B.O.Web, ANSYS 27, ANSYS 28 and ANSYS 29

VITA

Goran Radinovic

Candidate for the Degree of

Master of Science

Thesis: FACTORS THAT INFLUENCE END ZONE CRACKING IN PRE-TENSIONED PRESTRESSED CONCRETE BRIDGE BEAMS – A FINITE ELEMENT ANALYSIS

Major Field: Civil Engineering

Biographical:

Education:

Completed the requirements for the Master of Science in Civil Engineering at Oklahoma State University, Stillwater, Oklahoma in May, 2021.

Completed the requirements for the Master of Science in Civil Engineering at University of Oklahoma, Norman, Oklahoma in 2010.

Completed the requirements for the Bachelor of Science in Civil Engineering at University of Oklahoma, Norman, Oklahoma in 2004.

Experience:

Department of Interior – United States Bureau of Reclamation, Oklahoma-Texas Area Office, Oklahoma City, Oklahoma, November 2015 – Present

Oklahoma State - Oklahoma Department of Mines, Oklahoma City, Oklahoma, June 2005 – November 2015

Professional Engineer (PE), State of Oklahoma, December 2012 – November 2022